# NONLINEAR FLUID-STRUCTURE INTERACTION FOR MULTI-DIMENSIONAL SEISMIC ANALYSES OF LIQUID STORAGE TANKS

by

Zühal Özdemir

B.S., Civil Engineering, Istanbul Technical University, 1999

M.S., Civil Engineering, Bogazici University, 2003

Submitted to the Kandilli Observatory and Earthquake Research Institute

in partial fulfillment of

the requirements for the degree of

Doctor of Philosophy

Graduate Program in Earthquake Engineering

Boğaziçi University

2010

# ACKNOWLEDGEMENTS

I would like to express my deepest gratitude to Prof. Erdal Şafak and Prof. Mhamed Souli, my thesis supervisors, and Assist. Prof. Yasin M. Fahjan, for their guidance, continuous encouragement and support during the preparation of this thesis. My sincere gratitude is also due to my advisory committee, Prof. M. Nuray Aydınoğlu, and Prof. Isam Shahrour for their useful suggestions and comments.

I would like to thank my brother Cem Özdemir for his love and continuous help. He always gives me the reason to live and progress. Heartfelt thanks are also due to my mother and father for their endless and invaluable morale support and patience. No words can express my appreciation and gratitude to my family.

My heartfelt thanks extend to Prof. Bilge Siyahi and Assoc. Prof. Bülent Akbaş for their kindness and encouragement. I would also like to thank Hasibe Gül for her exceptional support.

Without support of my dear friends, Ahlem Alia, Ahmad Al-Qadad, Mohammed Amdi, Züleyha Çetkin, Ebru Gündüz, Ebru Sır and Bilgen Sungay, I could not overcome any difficulty in my hard times. The encouragement and kind assistance received from my dear friends, İhsan Engin Bal and Belma Çapa during the preparation of the thesis are gratefully acknowledged.

# ABSTRACT

# NONLINEAR FLUID-STRUCTURE INTERACTION FOR MULTI-DIMENSIONAL SEISMIC ANALYSES OF LIQUID STORAGE TANKS

Real nonlinear behavior of liquid storage tanks includes many complexities which are caused by material yielding, large amplitude free-surface sloshing, non-linear fluid structure interaction, high deformations of tank base and shell, out-off round distortions of the tank shell, soil-tank interaction, successive separation and contact between tank base and foundation and plastic rotations of tank base plate. These nonlinear behavior mechanisms result in different failure modes such as buckling at the tank shell (elephant foot buckling or diamond shape buckling), separation of the junction between the base plate and tank wall due to high joint stresses, uneven settlements at the tank base and rupture of the anchors. The algorithm to be employed for the seismic analyses of tanks should account for these nonlinearity effects for the accurate description of the performance of tanks during earthquakes.

In this thesis, fluid-structure interaction algorithm of finite element method which can take into account the effects of geometric and material nonlinearities of the tank and nonlinear sloshing behavior of contained liquid is utilized to evaluate the actual behavior of steel cylindrical ground supported liquid storage tanks when subjected to realistic base motions. Since seismic design codes generally define ground shaking in the form of an acceleration response spectrum, earthquake ground motions is selected and processed using spectrum matching techniques in time domain to be compatible with the Turkish Seismic Design Code (2007) spectra. In addition to two horizontal components of ground motion, the vertical component is also taken into account in order to determine relative importance of vertical ground motion on the behaviors of anchored and unanchored tanks. In order to clarify the key question of tank problems whether anchoring would prevent earthquake damage to the tank, numerical analyses are carried out on the same tank model

having two different support conditions: anchored and unanchored. The consistency of the provisions presented in current tank seismic design codes and finite element method analysis results are evaluated and recommendations on seismic tank design codes are presented.

# ÖZET

## SIVI İHTİVA EDEN TANKLARIN LİNEER OLMAYAN SIVI-YAPI ETKİLEŞİMİ İLE ÇOK BOYUTLU DEPREM ANALİZLERİ

Sıvı ihtiva eden tankların doğrusal elastic olmayan davranışları, tank malzemesinin akması, sıvı serbest yüzeyinin büyük genlikli çalkalanması, doğrusal elastic olmayan yapı-sıvı etkileşimi, tank tabanının ve cidarının büyük genlikli şekil değiştirmesi, tank cidarının düzgün çembersel kesiti dışındaki deformasyonları, tank-zemin etkileşimi, tank tabanı ve temelinin birbirini takip eden temas ve ayrılması ve tank tabanının plastic dönmesinden kaynaklanan pek çok karmaşık davranış mekanizmasını birlikte içerir. Bu doğrusal elastik olmayan davranış mekanizmaları, depremler esnasında tank cidarının burkulması (fil ayağı ve elmas biçminde burkulma), yüksek gerilmelerden ötürü tank tabanı duvarının ek bölgesinin ayrılması, tank tabanının değişik miktarlarda oturması ve tank tabanını temele bağlayan bağlantı elemanlarının kopması şeklinde değişik hasarlarla ortaya çıkar. Tankların depremler esnasındaki gerçek performanslarının tam olarak belirlenmesi için tankların analizlerinde kullanılacak methodun bahsedilen bütün bu nonlineer etkileri dikkate alması gerekir.

Bu tezde, tankın doğrusal elastik olmayan geometrik ve malzeme davranışlarını ve içerikteki sıvının serbest yüzeyinin lineer olmayan çalkalanmasını dikkate alan sonlu elemanlar methodunun sıvı-katı etkileşimi teknikleri kullanılarak gerçek yer hareketine maruz zemine oturan çelik silindrik sıvı ihtiva eden tankların gerçek davranışları incelenmektedir. Sismik tasarım şartnamelerinde sismik tehlike tasarım ivme spectrumu şeklinde tanımlandığı için analizlerde kullanılmak üzere depremler esnasında alınmış gerçek kayıtlar seçilmiş ve seçilen bu kayıtlar zaman tanım alanında spectrum uyumlu kayıt elde etme yöntemleri kullanılarak Türkiye Deprem Yönetmeliği (DBYBHY, 2007) tasarım ivme spektrumuna uygun olacak şekilde işleme tabi tutulmuştur. Depremin iki yatay bileşenine ilave olarak düşey bileşen de dikkate alınarak, tank modeli üç boyutlu deprem hareketi altında çözülerek düşey bileşenin tankların davranışı üzerindeki göreceli

etkisi belirlenmiştir. Tanklar üzerinde yapılan çalışmaların temel sorusu olan tankın temele bağlanmasının tank üzerindeki deprem hasarlarını engelleyip engelleyemeyeceğini aydınlatmak için analizlerde, tanklar için zemine bağlanmış ve bağlanmamış olmak üzere iki değişik mesnet koşulu kullanılmıştır. Sismik tank tasarım yönetmeliklerinde sunulan değerlerle sonlu elemanlar yönteminden elde edilen sonuçların tutarlılığı değerlendirilmiş ve tank sismik tasarım yönetmeliklerinde verilen kriterler üzerine tavsiyeler sunulmuştur.

# TABLE OF CONTENTS

# LIST OF FIGURES

# LIST OF TABLES

# LIST OF SYMBOLS /ABBREVIATIONS

| | |
|---|---|
| a | A parameter indicating the quality of the construction |
| a | Half length of rectangular tank |
| $A(T)$ | Base shear coefficient |
| $A(T)$ | Spectral acceleration coefficient |
| $A_c(T_{cn})$ | Convective mode base shear coefficient |
| $A_{cn}(t)$ | Base shear coefficient corresponding to convective period |
| $A_g(t)$ | Spectral acceleration |
| $A_g(T_c)$ | Spectral acceleration corresponding to convective period |
| $A_g(T_i)$ | Spectral acceleration corresponding to impulsive period |
| $A_n$ | Coefficient used in velocity potential of harmonically forced 2D rigid tank |
| $A_o$ | Effective ground acceleration coefficient |
| $A_s$ | The cross-sectional area of the shell |
| $A_v(T_v)$ | Base shear coefficient corresponding to breathing mode period |
| b | Body force |
| B | Gradient matrix |
| c | Speed of sound |
| $C_c$ | Convective period coefficient (Malhotra *et al.*, 2000) |
| $C_i$ | Impulsive period coefficient (Malhotra *et al.*, 2000) |
| $C_n$ | Coefficient used in velocity potential of harmonically forced 2D rigid tank |
| D | Amplitude of the harmonic external force |
| D | Tank diameter |
| $d_e$ | Horizontal harmonic displacement |
| Difference | The squared scaled-to-target difference |
| e | Internal energy |
| E | Modulus of elasticity of tank material |
| f | Nodal volume fraction |
| f | Physical property |
| f' | Physical property as function of the reference coordinate |
| $F_{ext}$ | External force vector |
| $F_{int}$ | Internal force vector |

| | |
|---|---|
| g | Gravitational acceleration |
| G | Shear modulus |
| G | Specific gravity of the contained fluid |
| h | Fluid depth |
| H | Height of fluid |
| H | Tank height |
| $h_{convn}$ | Convective mass height |
| $h`_{convn}$ | Convective mass height including base pressure effects |
| $h_f$ | Height of impulsive mass |
| $h_i$' | Height of impulsive mass for rigid tank |
| $h_{impf}$ | Flexible impulsive mass height |
| $h`_{impf}$ | Flexible impulsive mass height including base pressure effects |
| $h_{impr}$ | Rigid impulsive mass height |
| $h`_{impr}$ | Rigid impulsive mass height including base pressure effects |
| $H_s$ | Shell height |
| I | Importance factor |
| I | Moments of inertia of the tank wall about a horizontal centroidal axis |
| $I_0$ | Modified Bessel's functions of order 0 |
| $I_1$ | Modified Bessel's functions of order 1 |
| $I_1, I_1´$ | The modified Bessel function of order 1 and its derivative |
| Id | Identity tensor |
| J | Volumetric strain |
| $J_1$ | Bessel function of the first order |
| k | Number of period steps ($\Delta T$) used to compute the response spectrum |
| $k_f$ | Effective stiffness of the tank-liquid system for impulsive mode |
| $k_f$ | The stiffness of the deformable tank |
| $k_l$ | Effective stiffness of the tank-liquid system for breathing mode |
| $k_v$ | Vertical stiffness of the foundation |
| $k_x$ | Horizontal stiffness of the foundation |
| $k_\theta$ | Rocking stiffness of the foundation |
| $K_h$ | Period coefficient for horizontal mode period |
| $K_n$ | Coefficient used in velocity potential of harmonically forced 2D rigid tank |
| $K_v$ | Period coefficient for vertical mode period |

| | |
|---|---|
| $L_0$ | Distance from the base to the mass center of tank wall |
| $L_R$ | Distance from the base to the mass center of tank roof |
| $m$ | Total mass of the tank wall |
| $M$ | Diagonalized mass matrix |
| $M$ | Momentum |
| $m_0$ | Mass of the foundation |
| $m_{convn}$ | Impulsive convective mass |
| $m_f$ | Impulsive flexible mass |
| $m_i$ | Impulsive mass |
| $m_{impf}$ | Flexible impulsive mass |
| $m_{impr}$ | Rigid impulsive mass |
| $m_l$ | Total mass of the fluid |
| $m_R$ | Total mass of the tank roof |
| $m_s$ | Total mass of the tank including base, support, and foundation |
| $M_{OT}$ | Total design overturning moment |
| $M_t$ | Overturning moment due to tank weight and roof |
| $n$ | Interface normal |
| $n$ | Sloshing mode number |
| $N_{elem}$ | Number of elements |
| $p$ | Pressure |
| $P$ | Equation of state |
| $P$ | Pressure |
| $P$ | The lowest hydrodynamic pressure |
| $P_c\,(r,z,\theta,t)$ | Convective pressure |
| $P_{cb}$ | Convective base pressure |
| $P_{cw}$ | Convective wall pressure |
| $P_i\,(r,z,\theta,t)$ | Impulsive pressure |
| $P_{ib}$ | Impulsive base pressure |
| $P_{iw}$ | Impulsive wall pressure |
| $P_v(z)$ | Pressure due to vertical ground motion |
| $P_{vf}(z)$ | Pressure developed on flexible tank due to vertical ground motion |
| $P_{vr}(z)$ | Pressure developed on rigid tank due to vertical ground motion |
| $Q_{max}$ | Maximum base shear due to hydrodynamic effects |

| | |
|---|---|
| $Q_t$ | Shear force due to tank and roof weight |
| r | Cylindrical coordinate in radial direction |
| r | Radial position |
| R | Radius of tank |
| R | Response modification factor |
| s | A non-dimensional factor |
| S | Source term |
| S(T) | Spectrum coefficient |
| $S_a^{actual}$ | Acceleration spectrum of the given (actual) time history |
| $S_a^{target}$ | Target acceleration response spectrum |
| t | Thickness of tank wall |
| t | Time |
| t | Wall thickness at the base |
| T | Period of oscillator |
| $T_1$ | Fundamental period of structure |
| $T_b$ | Breathing mode period |
| $T_c$ | Sloshing period |
| $T_{c1},\ T_{c2}$ | First and second sloshing mode period |
| $T_f$ | Impulsive mode period |
| $T_F$ | Upper period of scaling range |
| $T_f^*$ | Breathing mode period including soil effects |
| $T_i$ | Impulsive mode period |
| $T_i^*$ | Impulsive mode period including soil effects |
| $T_S$ | Lower period of scaling range |
| $t_s$ | Shell thickness |
| $t_u$ | Equivalent uniform thickness of tank shell |
| $T_{vd}^*$ | Breathing mode period including soil effects for flexible tank |
| $T_{vr}^*$ | Breathing mode period including soil effects for rigid tank |
| u | Fluid particle velocity |
| v | Mesh velocity |
| V | Flux |
| $V_f$ | Volume fraction ratio |
| w | Convective velocity |

| | |
|---|---|
| x | Current Cartesian coordinate |
| x | Apsis of cartesian coordinate system |
| X | Reference (original) coordinate |
| $X_{max}$ | Peak ground acceleration |
| y | Ordinate of cartesian coordinate system |
| z | Liquid level at which wall is investigated measured from base |
| z | Vertical coordinate |
| Z1,Z2,Z3,Z4 | Local site classes defined in Turkish Seismic Code (2007) |
| | |
| $\alpha$ | Time dependent coefficient |
| $\alpha_x$ | Factor convert to static horizontal stiffness values to the dynamic values |
| $\alpha_v$ | Factor convert to static vertical stiffness values to the dynamic values |
| $\alpha_\theta$ | Factor convert to static rocking stiffness values to the dynamic values |
| $\eta$ | Free surface displacement measured from the undisturbed liquid surface at equilibrium |
| $\rho$ | Mass density of fluid |
| $\rho_0$ | Initial density |
| $\rho_s$ | Shell density |
| $\upsilon$ | Poisson's ratio |
| $\omega$ | Circular frequency of the applied motion |
| $\alpha$ | Coefficient for shell imperfections |
| $\delta$ | Maximum imperfection amplitude |
| $\delta_s$ | Sloshing wave height |
| $\gamma$ | A knockdown factor for geometrical imperfections |
| $\lambda$ | A reduction factor for imperfections of an unpressurized shell |
| $\lambda_n$ | The roots of the first derivative of Bessel functions of the first kind and first order |
| $\theta$ | Circumferential angle |
| $\sigma_0$ | Buckling stress of an unpressurized shell with imperfections |
| $\sigma_{bmax}$ | Maximum axial compressive stress |
| $\sigma_{cl}$ | Critical buckling stress |
| $\sigma_m$ | Maximum vertical membrane stress |

| | |
|---|---|
| $\sigma_p$ | Buckling stress of a pressurized shell with imperfections |
| $\sigma_y$ | Yield stress of tank material |
| $\sigma_{Zallowable}$ | Allowable axial compressive stress |
| $\sigma_{\theta max}$ | Maximum hoop stress |
| $\tau_{max}$ | Maximum shear stress |
| | |
| API | American Petroleum Institute |
| ASCE | American Society of Civil Engineers |
| ASD | Allowable stress design |
| EERI | Earthquake Engineering Research Institute |
| MM-ALE | Multimaterial ALE |
| MUSCL | Monotone upwind schemes for conservation laws |
| NZSEE | New Zealand Society of Earthquake Engineering |
| PEER | Pacific Earthquake Engineering Research Center |
| SALE | Single material ALE |
| SLIC | Simple linear interface calculation |
| SRSS | Sum of square roots of squares |
| TSDC | Turkish Seismic Design Code |
| VOF | Volume of fluid methods |

# 1. INTRODUCTION

The vulnerability of tanks to earthquake ground motions were observed in almost every major earthquake. In regions of intense ground shaking, many tanks have been severely damaged and some have failed with disastrous consequences. Earthquake effects on tanks were not extensively evaluated until Alaska Earthquake of 1964. After this earthquake researchers focused on the seismic analysis of tanks to reduce damage and failure risk of such structures in future earthquakes. Although many experimental and analytical studies are available in literature for investigating the behavior of liquid containment tanks under seismic loads so far, the combined effects of various failure modes are rarely considered.

Failure modes of liquid storage tanks which include buckling at the tank shell (elephant foot buckling or diamond shape buckling), separation of the junction between the base plate and tank wall due to high joint stresses, uneven settlements at the tank base and rupture of the anchors are caused by material yielding, large amplitude free-surface sloshing, non-linear fluid-structure interaction, high deformations of tank base and shell, out-off round distortions of the tank shell, soil-tank interaction, successive separation and contact between tank base and foundation and plastic rotations of tank base plate. The algorithm to be employed for the seismic analyses of tanks should account for these nonlinearity effects for the accurate description of the performance of tanks during earthquakes.

This dissertation is focused on the nonlinear response of vertical steel cylindrical storage tanks under earthquake motions. Fully nonlinear fluid-structure algorithm of finite element method which can take into account the effects of complexities associated with the nonlinear tank response  is utilized to evaluate the actual behavior of steel cylindrical ground supported liquid storage tanks when subjected to realistic base motions. Since seismic design codes generally define ground shaking in the form of an acceleration response spectrum, the earthquake ground motion used in the analysis is selected and scaled to be compatible with the Turkish Seismic Design Code (2007) spectra. Real size tank model are analyzed with two different support conditions, anchored and unanchored,

in order to clarify the key question of tank problems whether anchoring would prevent earthquake damage to the tank. The adequacy and consistency of the provisions presented in current tank seismic design codes are evaluated by comparing with finite element method results and the relative importance of vertical component of ground motion on the behaviors of anchored and unanchored tanks is assessed.

## 1.1. Objective of the Work

The main objectives of the dissertation can be summarized as follows:

- Evaluation of non-linear response of the tank-fluid system considering non-linear behavior of tank shell and roof, the effect of fluid sloshing and underlying soil,
- Assessment of the effect of support condition on the overall response of the tank-fluid system,
- Investigation of the nonlinear sloshing response of contained liquid due to lateral and vertical excitation,
- Evaluation of the effect of underlying soil on the response of tank-liquid system by employing simple linear spring soil model,
- Quantification of adequacy of simplified analysis methods for both linear and nonlinear tank-fluid system by emphasizing the limitations of linear approaches and the importance of nonlinear seismic response of liquid containment tanks,
- Investigation of the importance of the second horizontal and vertical ground motion components on the tank response,
- Providing guidance on seismic design of tank-liquid-soil systems.

## 1.2. Scope of the Research

In order to achieve the above listed objectives, the dissertation is split into several stages as follows:

- A review of current practice for seismic design of storage tanks is conducted. The review, which includes all relevant codes of practice and relevant technical papers

from literature, address the description and quantification of the dynamic response of tanks.

- The procedures used in the available codes for the seismic analysis and design of liquid containment tanks are summarized.
- Nonlinear dynamic finite element analyses are performed with finite element program on rigid anchored cylindrical tanks to determine fluid response.
- Tank flexibility and soil effects are integrated into the finite element models in order to evaluate the effects of fluid-structure interaction and underlying soil on the overall system response.
- In order to clarify the key question of tank problems whether anchoring would prevent earthquake damage to the tank, numerical analyses are carried out on the same tank model having two different support conditions: anchored and unanchored.
- In order to assess relative importance of vertical and horizontal components of ground motion, nonlinear dynamic finite element analyses of tank-fluid-soil system are performed under multi-dimensional earthquake loading.

## 1.3. Analysis Platform

During an earthquake, a tank containing liquid can undergo large structural and free surface deformations and high fluid-structure interaction forces causing plasticity and buckling of the tank material. An unanchored tank could lift off the slab, move and come down with considerable impact, generating considerable contact forces as well as material nonlinearity. Since the explicit solution does not need to search for equilibrium at each time step, it could reasonably be expected to cope with problems associated with seismic response of tanks.

LS-DYNA which is an explicit finite element code can be used successfully for various types of dynamic engineering nonlinear problems including fluid-structure interaction. LS-DYNA is chosen over other analysis codes as numerical analysis platform due to its high degree of flexibility and its ability to model the nonlinearities and rapid changes in applied forces to the tank. Moreover, it has a wide range of available material models and equations of state including the ability to model strain rate sensitivity for fluid media and structural materials.

## 2.  PERFORMANCE OF TANKS DURING PAST EARTHQUAKES

In this chapter, categorization of tanks depending on the construction material, support condition and shape is mentioned shortly. General response of tanks to seismic motion is explained along with the tank failure modes. Earthquake observation reports are summarized in order to evaluate performance of tanks during past earthquakes.

### 2.1.  Categorization of Tanks

Liquid storage tanks can be constructed in many configurations: elevated, ground-based, and buried. Cylindrical ground supported tanks made of carbon steel are more numerous than any other type because they are efficient in resisting liquid hydrostatic pressure mostly by membrane stresses, simple in design, and easy in construction. Buried tanks are typically concrete wall construction with concrete roofs. Steel tanks can be fabricated as riveted, welded or bolted (especially for low values of height over radius ratio H/R); in the last decades they have been basically welded world-wide.

Steel ground-based tanks consist essentially of a steel wall that resists outward liquid pressure, a thin flat bottom plate that prevents liquid from leaking out, and a thin roof plate that protects contents from the atmosphere. The tank shell consists of different steel courses with height of approximately one meters and a half; their thickness decreases along the height and rarely exceeds two centimeters in the bottom course. Shell thickness is calculated using empirical formulas (*i.e.* "one-foot-method") according to design guidelines and depends on tank dimensions and content density. Roof can be shaped in many different ways as dome, conical or can be floating. Roofs can be self-supported or columns supported in case of large diameters. The base plate of storage tanks is generally flat or conical shaped.

It is common to classify such tanks in two categories depending on support conditions: anchored and unanchored tanks. Anchored tanks must be connected to large foundations to prevent the uplift in the event of earthquake occurrence. However, anchoring of a tank is not practical to construct and considerably expensive because it

needs a large number of bolts and suitable attachments onto the tank wall and massive foundation. Improperly detailed anchors may damage the shell under seismic loading resulting in a ripped tank bottom. Hence, in practice, it is more common to construct tank shell on a simple ring-wall foundation or directly on the compacted soil due to these disadvantages of anchoring.

## 2.2. General Response of Tanks to Seismic Loadings

The seismic behavior of liquid storage tanks is quite different than that of conventional buildings, since tanks are exposed to hydrodynamic forces under earthquake motion and these forces have to be taken into account in their seismic design. In addition to their hydrodynamic aspects, energy dissipating capacity of these structures is very low and they possess low ductility and redundancy. Moreover, damping associated with tank response is lower than that of other structures. The natural periods of these structures occupy two widely separated ranges. The typical periods of sloshing are very long, up to 6-10 seconds for very large tanks whereas the coupled vibration modes of elastic shell and the contained liquid have periods less than 1 second. So, tanks respond to earthquake motions as two separated system. An earthquake near the tank site containing high frequencies can excite the coupled system, but relatively small first mode sloshing may occur. On the other hand, ground motion resulting from a large earthquake at far distance with low amplitude and long period can generate large amplitude first sloshing mode but not significant coupled vibration modes. These aspects make these structures more vulnerable than the conventional structures against earthquakes.

There are several factors which affect seismic behavior of a tank. Depth of liquid, tank shape, proportions of the tank shell, tank material properties, fixity condition at the base of the shell, and roof type influence the seismic response of tanks. In addition tank and fluid properties, input motion characteristics such as, frequency content, duration and amplitude of excitation control behavior of a tank.

## 2.3.  Tank Failure Modes

Earthquake failure modes of tanks have included buckling of the base of the shell, damage to the roof caused by sloshing of liquid combined with insufficient freeboard, failure of piping or other accessories due to their inability to accommodate the motion of the main tank and differential settlements of the foundation.

### 2.3.1.  Diamond Shape Buckling

Under earthquake loading, overturning is resisted by axial compressive stresses in the wall. Diamond shape buckling is an elastic buckling phenomenon in which, buckling occurs before the plasticity, due to the presence of high axial compressive stresses. The axial membrane stress which causes buckling in a cylindrical shell structure is a function of the amplitude of imperfections, the internal pressure, shell thickness and the circumferential variation of the axial stress. Imperfections tend to reduce the buckling strength of a perfect unpressurized shell while internal pressure exerted by the contained fluids can significantly increase the buckling strength of the tank shell by decreasing the effect of imperfections.

The stabilizing effect of internal pressure may reduce when pressure developed on tank due to vertical component of earthquake motion acts in the reverse direction to both hydrostatic pressure and pressure exerted by the horizontal ground motion component. This reduction in the pressure causes diamond shape buckling. Figure 2.1 illustrates diamond shape buckling developed on wine tanks.

Diamond shape buckling may also occur considerably above the base of the tank where the hydrodynamic pressure is small as compared to its magnitude at the tank base. Figure 2.2 shows the typical example of diamond shape buckling developed at the upper part of the tank shell.

### 2.3.2. Elephant Foot Buckling

Although the internal pressure increases the buckling strength, high internal pressure may lead to severe local bending near the base. This failure mode is an outward bulge just above the tank base and commonly known as "elephant foot buckling".

This problem is an unusual buckling condition, because it involves very high tensile stresses in one direction (hoop stresses), coupled with rather small compressive stresses in the orthogonal direction. Thus, although it is a buckling failure involving considerable plasticity, it occurs at low buckling stresses.

In addition to the combined action of vertical compressive stresses exceeding the critical stress and hoop tension close to the yield limit, Rammerstorfer *et al.* (1990) attributed the formation of elephant foot bulging to a third component which is the local bending stress due to the restraints at the tank base. Figure 2.3 and Figure 2.4 show elasto-plastic (elephant foot) buckling for tanks destroyed by earthquakes.

### 2.3.3. Sloshing Damage

Tanks that are not provided with sufficient freeboard can be damaged by the sloshing waves. Greater impact by sloshing waves can cause the roof to separate from the shell. The sloshing wave motion can also cause roof support columns to be knocked from their support points at the base and can cause roof failure. In Figure 2.5, the roof of an oil tank suffered damage because of sloshing and roof-shell junction leaked during Kern County, California Earthquake of 1952. Figure 2.6 represents a water storage tank which lost its roof and a portion of upper shell during the Long Beach, California Earthquake of 1933.

### 2.3.4. Damage to Piping Connections

Vertical (uplift) and horizontal (sliding) movements of tank base can cause a break in inlet/outlet piping connections which are not designed to accommodate the motion of tank due to lack of enough flexibility. This is one of the most prevalent causes of product loss from storage tanks during earthquakes. Flexible connections can be provided to

prevent this kind damage. Figure 2.7 and Figure 2.8 represent examples of piping damage to tanks.

## 2.3.5. Foundation Failure

Tank storage farms are frequently sited in areas with poor foundation conditions. The liquefaction of materials under the tanks may couple with imposed seismic moments on the tank base from lateral accelerations and may result in base rotation and gross settlements on the order of several meters. In some cases, the loss of liquid from a damaged tank may cause to scour the foundation materials in the vicinity of the tank and may exacerbate the damage by reducing soil support to the tank.



Figure 2.1. Diamond shape buckling developed at the wall of wine tanks

Figure 2.2. Diamond shape buckling at the upper part of the tank shell

(Kocaeli Earthquake of 1999)



Figure 2.3. Elephant foot buckling damage of a water tank

(Landers Earthquake)

Figure 2.4. Elephant foot buckling damage of Santa Clarita Valley tank
(Northridge Earthquake, 1994)



Figure 2.5. Sloshing damage to an oil tank (Kern County, California Earthquake, 1952)
(courtesy of K. V. Steinbrugge)

Figure 2.6. Sloshing damage to a water storage tank

(Long Beach, California Earthquake, 1933. Courtesy of Harold M. Engle)



Figure 2.7. Piping break and shell buckling

Figure 2.8. Broken pipe connections

(Coalinga Earthquake of 1983)

## 2.4. Earthquake Observations

The evaluation and improvement of design criteria for analysis of tanks have relied greatly on observations of tank damages during past earthquakes. Damages to flat-bottom vertical storage tanks in past earthquakes were documented in several post-earthquake investigations. The earthquake reports concerning performance of the steel cylindrical welded roofed aboveground liquid storage tanks are summarized in this section:

- Tokyo Earthquake (M = 8.3, September 1, 1923):

Tanks at the Yokosuka Naval Station failed, allowing drainage of oil to harbor waters, where the oil caught fire causing considerable damage (National Board of Fire Underwriters, 1933).

- El Centro Earthquake (M=6.9, May 18, 1940):

The water supply tanks for the cities of Holtville and Imperial collapsed (Richter, 1958). The epicenter of this earthquake was about 10 km from Holtville and 15 km from Imperial. Both cities were about 8 km from the Imperial Fault.

- Kern County Earthquake (M = 7.5, July 21, 1952):

The magnitude 7.5 Kern County Earthquake occurred on July 21, 1953. Based on the size and location of the epicenter it would be expected that greater tank damage would had occurred, especially considering the extensive damage to older buildings from this earthquake. A possible reason for the minimal damage is that those tanks in close proximity to the epicenter had low levels of oil in the tanks. The catastrophic damage was observed at the Paloma Gasoline Plant; the sloshing of oil or product from the top of a tank at the roof/shell joint was detected in this earthquake (Steinbrugge and Moran, 1954).

- Niigata Earthquake (M = 7.3, June 16, 1964):

This earthquake caused the collapse of number of tanks at a local refinery; a resulting fire caused extensive damage to the refinery (ASCE, 1987).

- Alaska Earthquake (M = 8.6, March 27, 1964):

The Great Alaska magnitude 8.4 earthquake occurred on March 27, 1964. This earthquake caused the first large-scale damage to tanks of modern design and profoundly influenced the research into the vibration characteristics of flexible containers. The epicenter of this earthquake was located in or near Prince William Sound. Damage to tanks and other structures in surrounding cities was extensive. This damaged was caused not only by the strong shaking and ground failure, but also, for many sites, by the tsunami which followed the earthquake.

In Anchorage region, which is located 130 km from the epicenter, damages to larger tanks were minimal while smaller tanks suffered more frequently and more severely for

those tanks situated closer to the water. Tanks at the airport with diameter to height ratio around one were suffered severe elephant foot buckling (including loss of product) as well as shell and roof damages (Rinne, 1967 and Hanson, 1973). Reports on earthquake noted that tanks less than half full did not suffer damage.

This earthquake revealed the vulnerability of tanks at a great distance from the epicenter of a large earthquake. Tanks with diameter to height (D/H) ratio greater than two did not have elephant foot buckling. Those tanks with significantly lower diameter to height ratio experienced elephant foot buckling when full or nearly full. Some tanks had sloshing problems at the roof/shell joint.

- Miyagi-Ken-Oki (Sendai) Earthquake (M = 7.4, June 12, 1978):

Three large tanks failed, the oil overtopped the containment dikes spilling into the refinery and into harbor waters (EERI, 1986). A major oil refinery was located on shore about 10 miles east of the center of the city of Sendai. There were about 87 storage tanks in the facility. The eastern portion of the complex suffered major damage. Three large tanks failed and split their content. Three other tanks suffered but did not fail.

- Imperial Valley Earthquake (M = 6.5, October 15, 1979):

This magnitude 6.5 earthquake provided the opportunity to evaluate the performance of tanks where near ground motions were recorded. Observed damages were similar to those produced by other major earthquakes. It was reported that buckling of the tank shell bottom due to excessive compressive stresses, damage to fixed roofs due to liquid sloshing and failure of attached pipes due to their inability to allow for shell movement, had occurred. It was highly likely that anchorage would had prevented some of the failures. It was observed that tanks with large liquid depth-to radius ratio suffered shell damage (Haroun, 1983).

- Coalinga Earthquake (M = 6.5, May 2, 1983):

The magnitude 6.5 Coalinga Earthquake of 2 May 1983 caused intense ground shaking throughout the epicentral region. This earthquake, which produced large accelerations, showed that large tanks lift off from their foundations and that large tanks are less vulnerable to elephant foot buckling than smaller tanks. Unanchored cylindrical ground supported tanks located at six sites within this oil producing area were damaged in the form of elephant's foot buckling at the base of three moderate sized tanks, joint rupture and top shell buckling in one large old riveted tank, bottom plate rupture of a relatively new welded tank and damage to the floating roofs of 11 tanks. Also oil spilled over the top of many tanks and secondary damages occurred in pipe connections, ladders, etc (Manos and Clough, 1985).

- Loma Prieta Earthquake (M = 7.1, October 17, 1989):

The Loma Prieta Earthquake of a magnitude 7.1 occurred on October 17, 1989 in the Southern Santa Cruz mountains. The earthquake induced incidents of damage to tanks of old and modern design, and even to a retrofitted tank. This earthquake illustrated that tank damage could occur a considerable distance from the epicenter. Uplift of large, unanchored tanks led to the failure of rigidly attached appurtenance such as piping and conduits, and in turn, led to tank rupture and the loss of contents. Damage to tanks was observed in many cities especially Moss Landing (close to the epicenter) and Richmond (far from the epicenter). The damage caused by the uplifting of tank in the Richmond area was most likely associated with sloshing. Damage to a few steel welded raw water unanchored tanks was observed and few tanks leaked their content in the Pacific Gas and Electric Company power generating facility at Moss Landing. Two of tanks which were completely or nearly full at the time of the earthquake suffered buckling at the top course of the shell. A steel welded tank lost several of the vents located on its roof, and evidence of liquid sloshing was clearly seen as the walls of the tank were stained with oil that spilled from the vents. It appears that site amplification of the long period ground motion components was a cause of large amplitude sloshing and the associated damage to tanks built on Bay Mud (Haroun *et al.*, 1991). Damage to tanks during the Loma Prieta Earthquake revealed the need for

redefining the site amplification factor in evaluating both the impulsive and the long-period convective design forces.

- Northridge Earthquake ($M_w$ = 6.7, January 17, 1994):

The Northridge Earthquake ($M_w$ =6.7) of January 17, 1994, caused severe damage to a number of cylindrical liquid storage tanks, and even resulted in the collapse of a tank. Typical modes of tank damage, primarily buckling of the shell, failure at the roof-shell connection, base uplift, anchor failure and elephant-foot buckling near its base, were observed throughout the affected area (Haroun *et al.*, 1997). Nine tanks (capacity 0.5 to 2.5 million-gallon), which were part of the Department of Water and Power's distribution system, suffered damage at the base (tearing and buckling) and at the roof (collapse of the wood trusses). Several others emptied due to inlet-outlet pipe damage from rocking. Several tanks located at the American National Can site in Northridge was subjected to severe forces during the earthquake. An unanchored tank experienced elephant foot buckling in the shell. Tank apparently uplifted during the earthquake and, when dropped, it severed the adjacent piping and released its content (Haroun and Bhatia, 1995).

- Kobe Earthquake (M = 7.2, January, 1995):

The magnitude 6.9 Kobe Earthquake on 17 January 1995 did not provide extensive tank problems which have resulted in prior Japanese earthquakes (Tokyo 1923, Nigata 1964). The closest major refineries were located about thirty-five kilometers from the epicenter at Osaka and Sakai. Acceleration at these three refinery locations was estimated to be about 0.2g. Apparently there was no major damage at these refineries and details of the specific minor damage were not available (EERI, 1995).

A liquid storage tank terminal, about 10 km east of the epicenter and on the waterfront, was damaged from site liquefaction. The terminal was built on reclaimed ground 2-4 km from active faulting and probably experienced peak accelerations of 0.6-0.8g. The damage included principally of tank tilting and loss of foundation supports of piping. Liquefaction was the principle cause of damage at waterfront location. The sparse

of damage to storage tanks in the Kobe Earthquake may be attributed to that few tanks were located in the area of strong shaking.

- Kocaeli Earthquake (M = 7.4, August, 1999):

A great earthquake with a magnitude of $M_w = 7.4$ occurred on 17, August 1999 in the Kocaeli Province of Turkey. Turkey's largest refinery, TUPRAS, experienced major structural collapses and oil spills. Tank farm fires at the refinery burned out of control for several days. The fire initially started at 4 floating roof naphtha tanks. Sloshing of the naphtha in the tanks broke the seals and the fire was ignited from sparks from the metal to metal contact between the roof and tank wall (Johnson, 2002). Six naphtha tanks burned completely and approximately 16 tanks were severely damaged by fire. Five tanks had their floating roofs completely "sink" in the tanks when the seals were damaged and contents sloshed onto the roof. There were 46 tanks with floating roofs and among them 30 tanks were damaged regardless of the size of tanks (Suzuki, 2002). None of the tanks at the refinery were anchored to their foundations, yet no evidence of substantial sliding of the tanks was found. Although hard piping was attached at the base of each tank, there was no evidence of pipe failure in any of tanks not consumed by fire. Estimated economic lost due to tank damages was about US$ 31 million (Sezen and Whittaker, 2004).

### 2.4.1. Summary of Observations

O'Rouke and So (2000) surveyed the seismic performance of 423 on-grade tanks during nine major earthquakes between 1933 and 1994. They found that while less than 4 per cent suffered complete collapse, 40 per cent experienced roof and connection damage and 11 per cent experienced elephant-foot buckling. They estimated an overall probability of 30 per cent that some damage would occur where peak ground accelerations (PGA) were less than 0.5g. This probability increased to 60 per cent for tanks with height to radius ratio greater than 1.4. A similar trend was observed for 50 per cent full tanks. Cooper and Wachholz (1999) also reported on tank performance during six relatively recent earthquakes, for which substantial ground acceleration data existed.

In the light of the reported performance of the liquid storage tanks during past earthquakes, lessons learned from earthquakes and recommendations can be summarized as follows:

- The D/H (tank diameter/tank height) ratio has played a significant role in the reported performance of storage tanks. Assuming identical design and fabrication procedure, tanks with larger aspect ratio tend to suffer less damage.

- Unanchored tanks with D/H (tank diameter/tank height) ratios of 2 and above were not vulnerable to elephant foot buckling. As this ratio decreases, the vulnerability to elephant foot buckling increases.

- Tanks with frangible roof/shell joints and large D/H ratios have suffered failed roof/shell joints with the consequent spillage of oil or product.

- Failure of piping and other accessories was extensively observed. Rigidly-attached piping was familiar reason for the release of tank contents. Piping flexibility at tank connections which allow for relative motion between the tank and its piping, should be provided for both large and small pipe connections.

- Reinforcing pads with no direct attachments to the shell prevent failure of piping attachments and tank shell.

- Large tanks (D>40 m, D/H>2.5) uplifted from its foundation, but shell buckling were not very widespread. Uplift generally caused damage to piping connections. The necessity for anchorage of large tanks should be questioned.

- In many cases, insufficient freeboard led to damage of the roof and due to liquid sloshing. Enough freeboard must be provided to prevent the convective waves from contacting the roof system.

- Long period motion at a distance and soil/foundation conditions are two important conditions which should be paid additional attention and investigated in details.

- Roof/shell damage to tanks was evident in many earthquakes. Due to thermal expansion reasons, the roof rafters to the roof or shell are not welded. However, having continuity between these elements would most likely enhance the earthquake performance of the tanks.

- Examination of damage reports indicates that most of tanks reporting damage were full, or nearly full.

# 3. LITERATURE SURVEY

Numerous theoretical, experimental and numerical investigations have been conducted to seek possible improvements in the design of cylindrical liquid containment tanks to resist earthquakes over the years. Although the liquid storage tanks have highly nonlinear behavior against severe earthquakes, linear theory was extensively used for the seismic analysis of tank shell as well as the fluid domain. Finite element method was widely employed for the seismic analysis of anchored and unanchored liquid storage tanks, however many different simplifications were made in the models in order to facilitate the analyses. In recent years, fully nonlinear fluid-structure interaction algorithms have been developed using finite element method, but their application to tank problems is a missing gap in the literature so far.

## 3.1. Analytical and Numerical Methods

### 3.1.1. Previous Studies of Anchored Tanks

The earlier studies on the evaluation of hydrodynamic pressure developed on a structure due to earthquake motion date back to 1930s. The first solution of such a problem was addressed analytically by Westergaard (1933), who determined the pressures on a rectangular, vertical dam subjected to horizontal acceleration. He proposed that hydrodynamic pressures are exerted by a certain portion of water mass, which was called impulsive mass. This mass moves in unison with the dam structure and actively participates the dynamic response of the coupled system. Jacobsen (1949) developed formulations to compute impulsive fluid pressures, base shear and overturning moment solving Laplace equation under specified boundary conditions for a cylindrical tank containing fluid and for a cylindrical pier surrounded by fluid. Housner (1954, 1957 and 1963) suggested that sloshing motion of the liquid near free surface exerts convective pressures on the tank wall in addition to the impulsive pressures. He represented the liquid response by an equivalent mechanical model capable of producing the same liquid-exerted forces and moments when subjected to the same ground motion and presented values for equivalent masses and their locations that would duplicate forces exerted by liquid on tank.

The impulsive and convective liquid masses were modeled by attaching a rigid mass and a single degree of freedom oscillator, respectively, to the equivalent mechanical model. This concept was constituted the basis for the API 650 standard provisions for vertical cylindrical tanks.

The severe damage to petrochemical tanks during the 1964 Alaska Earthquake led the researchers to investigate seismic behavior of cylindrical steel tanks extensively and it was realized that flexibility of the container was an important factor in determining the response of the coupled system. Therefore, numerical methods had been incorporated into the seismic analysis of tank in order to take into account deformability of tanks.

Edwards (1969) employed finite element method and a refined shell theory to predict seismic stresses and displacements in a vertical cylindrical tank having a height to diameter ratio smaller than one. This investigation treated the coupled interaction between the elastic wall of the tank and the contained liquid. The tank cross section was assumed to be restrained against cross section distortions. Shaaban and Nash (1975) conducted similar research concerned with the earthquake response of cylindrical elastic tanks using the finite element method.

Veletsos (1974) described an approximate method based on the assumption of a prescribed mode of deformation of the tank wall with undistorted cross-section and the use of "added mass" concepts to allow for the inertia of the fluid. The interaction effects between deformable tank shell and sloshing liquid was ignored due to the fact that convective effects are characterized by oscillations of much longer periods than those characterized by the impulsive effects. Convective effects, which are associated sloshing of the liquid, were evaluated by the procedure applicable to rigid tanks. Later, Veletsos and Yang (1977) obtained the natural frequencies of the liquid-tank system applying Flügge's shell theory with a Rayleigh-Ritz type procedure using the natural modes of vibration of uniform cantilever beams. They estimated maximum base overturning moment induced by a horizontal earthquake motion by modifying Housner's model to consider the first cantilever mode of the tank.

In the subsequent studies, the analytical algorithms are coupled with numerical methods in order to find the optimum solution for tank problems with increasing the accuracy while minimizing the time required for the solution. Haroun and Housner (Haroun, 1980, Haroun and Housner, 1981a, 1981b, 1982a, and 1982b, and Haroun, 1983) used boundary integral theory to model fluid region and ring shaped finite elements for tank shell to develop reliable method for analyzing the dynamic behavior of deformable cylindrical tanks. The influence of initial hoop stress due to hydrostatic pressure and the rigidity of the roof on the wall vibrations were investigated. The foundation soil was modeled with spring dashpot elements to take into account the soil flexibility. In order to investigate the effect of the coupling between liquid sloshing modes and shell vibration modes, the quiescent liquid free surface is represented by concentric annular rings restrained in the normal direction by springs. It was found that the coupling effect between liquid sloshing modes and shell vibrational modes is negligible and a spring-mass component added to the simplified mechanical model of Housner (1954) in order to consider the effect of deformability of the tank wall.

Some researchers concentrated on the influence of vertical and rocking motion of an earthquake on the seismic behavior of coupled liquid-tank system. Marchaj (1979) conducted a simplified study that focused attention on the importance of the vertical acceleration in the design of tanks. He proposed that the vertical earthquake ground motions can be translated into radial pulsations of the tank wall-liquid system and result in development of additional stresses in the tank wall in circumferential direction. By neglecting the effect of these stresses tanks may not have sufficient strength to resist earthquake forces. Kumar (1981) carried out a critical study of axisymmetric seismic behavior of tanks in which the radial motion of partly filled tanks was considered but effects of axial deformations were neglected. He reported that for nearly full tanks, such approximation has negligible effects on the accuracy of results, but for nearly empty tanks, axial deformations may influence the response especially for tall tanks. Veletsos and Kumar (1984) presented a design procedure for evaluating the effects of vertical shaking on tanks. Haroun and Tayel (1985a, 1985b and 1985c) reported on a comprehensive study of effects of the vertical component of a ground excitation. The natural frequencies and modes of a flexible tank were evaluated using both numerical and analytical techniques ignoring sloshing liquid and foundation soil flexibility. They calculated tank response

under simultaneous action of both vertical and lateral excitations in order to assess the relative importance of the vertical component of ground acceleration, which had been shown to be important. Haroun and Ellaithy (1985) presented an analytical mechanical model for flexible cylindrical tanks undergoing both a lateral translation and a rigid base rocking motion. The interaction of sloshing modes with shell deformation was assumed to be weak. Using a classical hydrodynamic pressure approach and assuming an approximate deflected shape for the tank walls, the parameters of the model were displayed with graphs. Veletsos and Tang (1986) considered the tank-liquid system to respond as a single-degree-of-freedom system and applied Galerkin's method to evaluate the response of the tank to a vertical component of ground shaking, considering also the flexibility of the supporting medium. Veletsos and Tang (1987) analyzed the dynamic response of upright circular cylindrical tanks to a rocking base motion of an arbitrary temporal variation. He generalized the mechanical model for laterally excited tanks to include the effects of base rocking of both rigid and flexible tanks.

Haroun and Abou-Izzeddine (1992a and 1992b) developed two different mechanical models for flexible cylindrical tanks considering shell-liquid-soil interaction. First model accounted for the effect of rigid-base rocking motion and lateral translation on an elastic cylindrical tank, and the second model represented the tank under vertical ground motion. In both of these models, soil was represented by springs and dashpots with a lumped parameter system of frequency independent characteristics, flexible tank shell was assumed to vibrate in a prescribed form and liquid free surface sloshing was neglected.

The finite element method combined with the boundary element method was used by several investigators, such as Grilli (1988), Huang (1988) and Kondo (1990), to investigate the problem. Hwang and Ting (1987 and 1989) employed the boundary element method to determine the hydrodynamic pressures associated with small amplitude excitations. He obtained frequency-dependent terms related with the natural modes of vibration of the elastic tank and incorporated them into a finite element formulation of an elastic tank in frequency domain. Generalized displacements were computed by synthesizing the complex frequency response using the Fast Fourier Transform procedure.

Mourad (1991) used experimental modal analysis techniques to assess the effects of out-of roundness imperfections on the structure response. He also examined the buckling of the actual tanks. Costley *et al.* (1991) presented a method to determine the critical buckling load of tanks using experimental modal analysis techniques. Rinne (1967) developed a criterion for buckling of the shell due to lateral forces and defined a shell buckling resistance coefficient.

Manos and Clough (1985) evaluated the seismic performance of ground supported cylindrical metal tanks which were damaged during the 1993 Coalinga Earthquake. The ultimate limits specified by the codes for the sloshing wave height which leads to spill of contents over the tank wall and for the overturning moment which causes the buckling at the tank wall were correlated with the damages observed after the earthquake in order to indicate design codes adequacy. They reached to the following conclusions: Although convective mass had only a minor influence on the buckling of the tank shell, the convective sloshing response was the principle contributor to the damages of tanks with floating roofs. The sloshing wave height estimated by the American codes was not consistent with the degree of response that actually occurred. Horizontal inertia forces, which result mainly from the impulsive liquid mass subjected to spectral acceleration, induce base shear forces and overturning moments in the tanks. The uplift with possible damage to buckling of tank shell caused by overturning moment was not adequately addressed by the design standards.

Rammerstorfer *et al.* (1987) discussed three different possibilities for superposing the dynamic pressures due to the horizontal and the vertical earthquake components on the static pressure, and the different modes of wall instabilities. The absolute sum of these three pressure component due to horizontal and vertical ground motion and hydrostatic pressures causes the highest circumferential tensile stresses and leads to plastic buckling of wall at close distance to the base which is called elephant-foot-buckling. The change in the direction of vertical hydrodynamic pressure decreases the stabilizing effect of the pressure and excites elastic (diamond-shape) buckling due to axial compression. The development of hydrodynamic pressure due to both vertical and horizontal ground motion component in opposite direction to the hydrostatic may exert the lowest hydrodynamic pressure on the

tank shell especially near the top of the tank where the shell is rather thin and leads to buckling of this region.

Lay (1993) developed a numerical model for the seismic analysis of tanks with single and double curvatures, which was achieved by transforming the boundary-element equations of the incompressible and inviscid fluid region governed by the Laplace equation into an equivalent finite-element mass matrix, that was combined with the shell finite-element equations of motion. The combined set of equations of motion was solved for the interaction problem. The contributions of tank-wall flexibility and liquid free-surface sloshing to the interaction problem were included.

Fischer and Rammerstorfer (1999) took into account the effect of wall deformation on the sloshing (convective) pressure component of a cylindrical tank in addition to classically considered sloshing pressure component caused by impulsive portion of contained incompressible, non-rotational fluid. Various types of deformation shapes were considered for tank wall. The Laplace equation was solved for fluid domain under dynamic and kinematic free surface boundary conditions and kinematic condition at the container wall. It was observed that the magnitude of the influence of wall deformations on the convective (sloshing) pressure was of minor relevance in comparison to the "classical" sloshing pressure for typical liquid storage steel tanks in the petrochemical industry. It was concluded that for tall tanks the "classical" sloshing pressure should not be estimated by just the fundamental sloshing mode but the contributions from higher modes should also be taken into account.

Chen and Chiang (1999) studied the 2D tank with rigid walls and partially filled with fluid, which was assumed inviscid and incompressible, and solved incompressible Euler equation under fully nonlinear kinematic free-surface condition to analyze the seismic response of sloshing fluid in the tank under rigorous combined surge-heave-pitch motions. The time independent finite-difference method, in which proper coordinate transformations are used to change the time dependent tank boundary to a regular and time-independent square one, was implemented to evaluate the velocity fields and the surface profile of the sloshing fluid, as well as, characteristics of nonlinear sloshing, beating phenomena, occurrence of resonance and the contribution of free-surface convection to its rise.

In order to make the procedure more accurate and more generally applicable, Malhotra *et al.* (2000) had further simplified the tank model of Veletsos (1984) by adding higher mode effects to the first mode for both impulsive and convective components. This procedure was adopted by current version of Eurocode 8.

Lubkowski *et al.* (2000) carried out a series of analyses to assess dynamic soil-structure-pile interaction effects of a steel tank supported by pre-stressed concrete piles and resting on a uniform horizontally layered soil under seismic loading. The entire soil-pile-tank system was modeled using the non-linear, time domain, finite element code LS-DYNA however the tank was represented as mass-spring analogous system.

Virella *et al.* (2003) assessed the influence of a fixed roof on the natural periods of vibrations of thin-walled aboveground steel tanks with clamped boundary conditions at the base. Tanks with open-top, self-supported roofs, and roofs supported by rafters were considered, together with different tank aspect ratios. The roof geometries considered include dome, cone, shallow cone, and flat roofs. It was observed that the free vibration of empty tanks with a fixed roof is governed by either cylinder modes or roof modes. For self-supported roofs predominant roof modes resulted, whereas for tanks with roofs supported by rafters, cylinder modes dominate the dynamic behavior of the tank. Roof dominant modes had natural periods that remain constant regardless of the aspect ratio considered. Cylinder modes, on the other hand, were characterized by natural periods that showed a linear dependence with the aspect ratio of the tank.

Razzaghi and Eshghi (2004) investigated behavior of anchored and unanchored steel cylindrical tanks under near-field and far-field earthquakes. Directivity effect and the angle of source-to-site path with faulting direction of the ground motion were not considered in the nonlinear time-history analyses. Results showed that performances of anchored and unanchored tanks under near-field ground motions were completely different than performances of those excited by far-field earthquakes.

Malhotra (2005) presented a simple method to estimate the roof, shell, and foundation loads arising from insufficient freeboard of cylindrical tank. In this method, the dynamic analysis of the tank-liquid system was based on the exact model of Veletsos and

Yang (1977) and Veletsos (1984) and it was proposed that, in many cases, it may be economical to design a tank for these additional loads than to build a taller tank with sufficient freeboard.

Chen (2005) extended previous study (Chen and Chiang, 1999) adding fluid viscous effects and solved two-dimensional incompressible Navier-Stokes equation using fully nonlinear dynamic free-surface condition in addition to kinematic one. The evolution of the velocity vector and the generation of the vorticity are described. The effects of viscosity and vorticity were studied on the free-surface elevation.

Virella *et al.* (2006) examined the critical horizontal peak ground acceleration which induces the elastic buckling at the top of the anchored cylindrical tank. While the liquid was modeled using an added mass approach, where the fluid mass was obtained from the impulsive pressure distribution given by the analytical methods, convective fluid effects were ignored in order to verify that this buckling mode arises mostly from the impulsive action of the hydrodynamic response of the liquid . They showed that negative pressure developed in the tank close to the free surface of the fluid, where the impulsive hydrodynamic pressure induced by the earthquake excitation exceeds the hydrostatic pressure, induces local compressive hoop stresses which leads to local buckling of the tank.

Xu *et al.* (2006 and 2007) carried out a study to determine the performance of exisitng soil-structure interaction analysis methods by means of computer programs to deeply embedded and/or buried nuclear power plant structures. In order to provide an assessment of the sensitivity of the method to the seismic induced soil pressure calculations, SASSI (Lysmer *et al.*, 1999) and LS-DYNA, which represent two vastly different SSI approaches, were used for the study. SASSI utilizes the wave propagation theory and the principle of superposition to treat the SSI phenomenon. LS-DYNA applies the direct approach to the SSI effect, which treats the near field soil with an explicit FE mesh that is connected to a transmitting boundary to approximate wave propagation in the half-space. Especially for the normal soil pressures, SASSI and LS-DYNA yield comparable results both in shape and magnitude.

Cimellaro *et al.* (2007) worked on a 3D rectangular tank problem to quantify the magnitude of the hydrodynamic pressures acting on the roof due to insufficient freeboard. Analyses were carried out with a commercial 3D nonlinear finite element program. The results showed that high values of hydrodynamic pressures, which were quite underestimated by the simplified method, were generated on the roof from the sloshing waves.

The sloshing behaviors of fluid in 3D rigid cylindrical and rectangular tanks subjected to horizontal harmonic oscillations or recorded earthquake excitations were addressed with a numerical and experimental study by Chen *et al.* (2007). The fully nonlinear kinematic and dynamic surface wave conditions were applied to the fluid domain governed by Laplace equation. In the numerical analysis, 3D Boundary element method and the second-order Taylor series expansion were used as spacial and temporal discretization schemes, respectively, and the boundary of the tank was meshed with isoparametric quadrilateral linear elements.

Mitra *et al.* (2008) carried out a study on partially filled 2D rigid annular, horizontal cylindrical and trapezoidal containers by applying small amplitude (linear) wave theory. The equation of motion of the inviscid and compressible fluid within irrotational flow field was expressed in terms of the pressure variable instead of displacement. Numerical results obtained for simple harmonic oscillation and earthquake excitations were compared with the existing solutions and parametric studies were conducted to show the importance of the nature of excitation, fluid height and the geometry of the container on the free surface displacement, the hydrodynamic pressure and sloshing frequency.

### 3.1.2. Previous Studies on Unanchored Tanks

Many attempts had been made to model the highly nonlinear behavior of unanchored tanks theoretically. Clough (1977) developed a quasi-static relationship between peak overturning moment and rocking displacement of the container with the assumptions regarding distribution of reaction forces and uplift patterns in the tank floor. The response was characterized as a rigid-body rotation of the shell, which lifts off the foundation on one side and rocks up on its toe assuming that rocking of the shell could occur without

considerable distortion of the circular cross-section. The portion of tank base plate which remains in contact was assumed to be circular and to be tangent to the tank shell at its point of contact with the foundation. When the shell rocks, a crescent-shaped region of bottom plate is lifted off the foundation. The weight of liquid acting on this uplifted region is carried by the shell which remains in contact with the foundation. Therefore, it is reacted as a compressive force which was assumed varies linearly from a maximum at the excitation axis to zero value at the edge of the contact line. The overturning moment which causes uplift of the tank was determined from Housner's analog. The two unknowns of the problem are the maximum compressive stress in the tank shell and the central angle of the contact area. These unknowns were found by solving two nonlinear algebraic equations which govern both global vertical force equilibrium and global moment equilibrium. One disadvantage of this model is that it does not take into account the flexibility of either the tank wall or the bottom plate. Furthermore, it neglects the variation of dynamic pressure on the bottom plate and uses a constant value equal to the static pressure.

In 1978, Wozniak and Mitchell (1978) suggested a more realistic model for uplifting by including the flexural stiffness of the bottom plate, and this analysis was introduced in AWWA D100 (2005) and API 650 Standards (2005). It was assumed that the contact area of the bottom plate with the foundation is a segment of an unknown central angle. Flexibility of the tank wall was not considered but the elastic behavior of the bottom plate was taken into account. The base plate was represented by a strip of unit width in the circumferential direction because the relevant uplift region is assumed to be an annular ring of a width much smaller than the radius of the tank. The strip acts as a beam resting on a rigid foundation subjected to a liquid pressure and lifted up by a vertical force at its free end. The maximum value of the force that can be carried by the beam is calculated by invoking two plastic hinges: one at its free end and another at an intermediate point in the uplifted portion of the beam. Because the wall thickness is usually larger than the thickness of the bottom plate, the assumption of a plastic hinge at the edge of the bottom plate is justified. Assuming no restraining effects from the shell and no membrane stress in bottom the plate, relations between thickness of the plate, plastic stress, applied distributed loads and uplifted length can be found explicitly. If the tank experiences uplift, two forces resist such deformation, namely, the weight of roof and shell, and the weight of liquid that will

be lifted up. By writing the equations of equilibrium of vertical forces and moments, the maximum compressive stress and the central angle can be found as in previous model.

Cambra (1982) modified Wozniak and Mitchell's model (1978) by analyzing two elastic beams: one in the uplift region and the other in the contact region. Both beams were subjected to a transverse distributed load which produces longitudinal membrane forces. In contact region, the beam was assumed to be supported on a Winkler foundation. This was considered as improvement since it took into account both the membrane force and the bending moment at the beginning of the uplift region whereas, on a rigid foundation, there were no moments assumed at junction of uplift and contact regions. The membrane force was calculated by considering the strip beam as an extensible string with no longitudinal displacements allowed at its ends, and by assuming that the total load on the strip is carried only by membrane force. This membrane force was later introduced as a given longitudinal force in the linear equation of an elastic beam which is incompatible with the general equilibrium as the total load is already carried through the bending of the beam. In reality, part of the load carried by membrane effects of the plate and the remainder by bending effects. Only the elastic behavior of the plate was considered in contradiction to the valid assumption of the existence of plastic hinges. However, based on this model, it was found that both the wall uplift and the separation of the tank bottom plate occurred at values larger than what design codes anticipate for credible earthquake magnitudes.

Lau (1991 and 1992) adopted a general method for predicting the static tilt performance of a cylindrical liquid storage tank that is free to uplift. The base plate, subjected to both membrane tension and plate bending, was divided into contact and uplifted regions. Deformations of the bottom plate were evaluated by a Ritz-type method using iterations to determine the boundary of the contact region and full continuity was maintained with the tank wall. The cylindrical tank shell was analyzed by using Flugge thin shell theory and its stiffness was cast in a form comparable with that of the base plate for direct stiffness summation. The stiffening effects of the top rim wind girder and the bottom toe ring were also included. Friction exerted along the bottom edge of the shell still in contact with the platform was modeled by lateral support springs of a stiffness that was fine tuned to model frictional forces.

In 1986, Leon and Kausel (1986) proposed some modifications to Wozniak and Mitchell's model. They concluded that this model, which forms the basis of provisions of API 650 Standard (2005), can lead to a significant underestimation of maximum compressive stresses in the shell under the condition of moderate shell uplift, and overestimation of the contribution of fluid weight in resisting lift-off.

Barton and Parker (1987) investigated the seismic response of anchored and unanchored cylindrical storage tanks subjected to only one direction of horizontal excitation by using general purpose finite element computer code. Added mass method and 3D finite elements were employed to model fluid inside the tank and neither material nor geometric nonlinearities were taken into account in the analysis. Response spectrum modal calculations were carried out for anchored tanks, whereas seismic responses of unanchored tanks were evaluated using time history analysis with artificially generated acceleration record. In order to model the contact between ground and tank, spring elements were placed under unanchored tanks. Results of the analysis indicated that due to the impacts between the tank base and floor following the lift-off, stresses in the tank, horizontal displacement at any node on the tank and resultant loads on the floor were considerably greater than for rigidly restraint case, although the vertical displacements were not significantly affected. Added mass models significantly underpredicted the degree of base uplift and maximum reaction forces of unanchored tanks although they gave very consistent results with the realistic 3D fluid models for fully restraint tanks.

El-Zeiny (1995) developed a finite element program to analyze the nonlinear dynamic response of unanchored cylindrical liquid storage tanks subjected to strong base excitation considering both large amplitude liquid sloshing and nonlinear liquid-structure and soil-structure interactions. Liquid region was represented by Laplace equation while the foundation was modeled using tensionless springs. It was observed that the response of unanchored tanks was dominated by uplift mechanism that varied nonlinearly with the intensity and frequency of the input motion. Unanchored tanks supported on flexible foundations exhibited lower compressive stresses and higher uplift displacements than those supported over more rigid foundations (Haroun and El-Zeiny, 1995a, 1995b and El-Zeiny, 2002).

Malhotra and Veletsos (1994a, 1994b and 1994c) and Malhotra (1995) presented a method for evaluation of unanchored cylindrical tank response to horizontal ground shaking. Base plate of the tank was modeled as a uniformly loaded, semi-infinite, prismatic beam that rests on a rigid base and was uplifted by a vertical force at one end. The beam was analyzed considering the effects of continuously varying area of base contact and the nonlinearities associated with membrane action and plastic yielding in the base plate. Because of the difference between the dominant periods of impulsive effects and the dominant periods of convective (sloshing) effects, impulsive and convective actions were considered to be uncoupled. Since the contribution of convective component of the response is usually small, sloshing effects were neglected. For relatively broad tanks, with height-to-radius ratio less than 1.5, the contribution of higher impulsive modes of vibration to the response can also be ignored, therefore the tank-liquid system was considered to respond as a single degree of freedom system with an impulsive mass. It was shown that the ratio of liquid height to tank radius is the most important single parameter governing the uplifting response of tanks.

Koller and Malhotra (2004) compared pushover analyses results with Eurocode 8 recommendations for several tanks with different aspect ratio in terms of plastic rotation of base plate which was the relevant failure mode in all cases. Pushover analyses results gave strong correlation between tank volume and plastic rotation irrespective of H/R ratio whereas Eurocode 8 (2006) results presented strong influence of H/R on plastic rotation. They verified that increase in the foundation stiffness results in increase in the plastic rotation.

Ahari *et al.* (2009) investigated uplift behavior of base plate of unanchored tank by making an analogy with a tapered beam resting on a rigid foundation. The contact effects and geometrical nonlinearity were considered along with the formation of plastic hinge at its end. Analytical equations governing the motion of the beam were solved numerically for non-sliding condition and the results of the presented method were compared with those of existing studies developed for uniform beam. The cross-sectional difference along the beam length caused 5 per cent deviation from the uniform case for uplift response. The increase in the thickness of tank wall affected the initial uplift stiffness slightly but it substantially influenced the uplift resistance after the formation of plastic hinge.

Decreasing the thickness of bottom plate reduced the initial stiffness and consequently caused delay of the formation of plastic hinge. It was observed that the hydrostatic pressure acting on the wall had a significant effect on the initiation of uplift and axial force of the beam while it did not significantly change the uplift force and end moment of the beam.

## 3.2. Experimental Investigations

Several experimental studies had been carried out on tanks, especially for unanchored tanks, because the phenomenon of successive contact and separation between tank base and supporting soil is very complex to model analytically or numerically.

The pioneering experimental work was performed by Clough (1977) on a small scale board tank model to measure the actual behavior of two aluminum cylindrical tank models when subjected to realistic base motions. Special attention was given to the significance of seismic behavior of tanks to the boundary conditions at the foundation and imperfect geometry of cylindrical tank shell. They reported that due to the tank wall flexibility, impulsive hydrodynamic pressure component was amplified beyond the value expected in a rigid tank, and flexibility associated with the uplift mechanism drastically altered the entire tank behavior. Significant out-of-round displacements were observed in both tanks and were believed to be related to initial imperfections of the tank's geometry. It was noted that for the same input acceleration amplitude, shell displacements and stress amplitudes were much higher in unanchored tanks than those in anchored tanks. They also reported that for unanchored tanks, there was a poor correlation between predicted and observed results, and unexpected behavior observed with respect to uplifting kinematics demonstrated the need for additional analytical studies of seismic response of unanchored tanks.

Clough and Niwa (1979) conducted a series of static tilt tests on a tall cylindrical liquid storage tank (7-3/4 ft by 15 ft). The observed behavior was compared with the results of typical design calculations and it was noted that the unanchored tank tilted more and developed much greater axial stresses than were indicated by typical design procedures. Compressive stresses were concentrated on much narrower contact zone than

was expected, leading to amplified peak stress. Kana (1979) measured experimentally wall stresses of a cylindrical flexible tank induced by sloshing and inertial loads.

As a continuation of the experimental work of Clough (1977), Manos and Clough (1982) carried out a series of experiments on the same tank model subjected to 3 different scaled earthquake motions with different boundary and soil conditions. In the case of unanchored tank, response was dominated by the uplift mechanism which varied nonlinearly with the intensity and frequency of input motions. For a rigid foundation, the coupling of uplift mechanism with out-of-round distortions resulted in high compressive axial membrane stresses developed over a narrow contact zone. For more flexible foundations, compressive stresses were smaller due to more widely pressure distribution along the base of the tank wall, on the other hand, larger uplift displacements were accompanied by high levels of compressive hoop stresses on the uplifted part of the tank wall, and correspondingly large bending and membrane stresses in the bottom plate. They concluded that a realistic uplift mechanism prediction, out-of-round distortional response, foundation flexibility and more realistic failure criterion should be incorporated in design procedures.

Niwa and Clough (1982) replicated the tall unanchored tanks damaged during the Greenville-Mt Diablo Earthquake of 24 January 1980 to examine their seismic behavior and buckling mechanism under laboratory conditions. All these damaged tanks were unanchored to their foundation and completely full. The elephant foot buckling were dominant failure mode for broad tanks, while tall tanks suffered a diamond shaped buckling spreading around the circumference. A 9.5 ft diameter by 20 ft high tank was tested under scaled both horizontal and vertical acceleration recorded during this earthquake and buckling patterns similar to those that occurred in the earthquake were observed during tests. The critical buckling stress observed during the development of the diamond-shaped buckle pattern was two thirds of the value predicted from the classical theory. This value was considerably higher than that adopted in the API 650 (2005) and AWWA-D100 (2005) standards. Hence, Niwa and Clough (1982) concluded that the critical buckling stress assumed in current standards for the steel tank design might lead to rather conservative estimates of the buckling strength of free base tank subjected to rocking motions. The actual loading conditions during the uplift response were extremely

different from those provided in static buckling tests of small cylinders under uniform axial compression which are used in design codes for critical buckling stress. Although, high axial compressive stresses was developed at the tank shell, the elephant foot buckling phenomenon was not observed because hoop stresses was only 60 per cent of the yield stress. If membrane stress mechanism developed in the bottom plate is ignored, uplifting stiffness of the bottom plate is considerably underestimated.

Cambra (1982) investigated the earthquake response behavior of an unanchored broad tank model, 12 ft in diameter by 6 ft. in height. The study included axial symmetric lift tests, static tilt tests and dynamic shaking table tests using both rigid mortar as well as flexible rubber foundations. It was concluded that seismic response of tanks was significantly affected by the variation of foundation flexibility. There was strong correlation between the tank shell eccentricities created by fabrication imperfections and/or shell deformations and out-of-round response. An empirical tie element model representing the uplift behavior of the tank base plate was also described in order to improve design procedures for unanchored tanks.

Manos (1986) carried out a series of experiments on broad and tall tanks to determine impulsive mode frequencies and base-overturning moments. It was observed that the predicted frequencies obtained from analytical equations diverged highly from that of measured values.

Sakai *et al.* (1987) presented a static tilt test with a full scale tank model in order to investigate the uplift behavior of large size cylindrical liquid storage tanks. They concluded that the experimental results did not agree with their theoretical analysis around the bottom of the tank. The stress distribution around the shell-base corner and the contact condition between the bottom plate and the foundation should be considered carefully to account for complicated uplift behavior.

Tanaka *et al.* (2000) conducted dynamic tests on small and large scale models under earthquake loading in order to investigate elephant foot buckling and side slipping behavior of cylindrical tanks.

A recent paper of Mathon and Limam (2006) presents the results of a series of experiments which were carried out on thin-walled pressurized cylindrical shells subjected to the bending. The aim of this study was to investigate the diamond shape buckling phenomenon considering the interaction of bending moment with internal pressure.

### 3.3. Previous Investigations on Code Provisions

There are a few studies in the literature that criticizes the tank seismic design codes extensively. One of them was reported by Hamdan (2000) who reviewed the seismic design codes of cylindrical steel liquid storage tanks and correlated their provision with earthquake observations in terms of sloshing wave height. The other response parameters such as base shear, overturning moment, hoop and axial compressive stresses and buckling strength of tanks obtained from different codes were compared and weakness of the codes was addressed.

Jaiswal *et al.* (2007) concentrated on base shear coefficients, idealization approaches of hydrodynamic effects on tanks and response parameters such as pressure and sloshing wave height given in the tank design codes. In code provisions, base shear coefficient is typically specified in terms of design acceleration spectrum, seismic zone factor, soil factor, importance factor, response modification factor, and damping ratio. Jaiswal *et al.* (2007) summarized the effect of such factors given in ten national and international codes for different type of construction material and support conditions and compared the design response spectrum obtained with these parameters. Large variations are obtained between the code spectra because of the lack of unified approaches.

### 3.4. Previous Researches on Fluid-Structure Interaction (FSI)

Due to limitations of analytical methods for the determination of realistic fluid effects on a deformable structure many different numerical fluid-structure interaction algorithms have been developed.

Koh *et al.* (1998) applied a variationally coupled BEM-FEM procedure to analyze dynamic response of 3-D rectangular liquid storage tanks subjected to horizontal ground

excitation including sloshing effects. The tank structure was modeled using finite element method and the fluid region using indirect boundary element method. Results were verified with shaking table test results.

Hwang and Ting (1989) studied the dynamic response of liquid storage tanks, including the hydrodynamic interactions, subjected to earthquake excitations employing the combinations of boundary element method and finite element procedure. The tank wall and inviscid fluid domain were treated as two substructures of the total system-coupled through the hydrodynamic pressures. The boundary element method was employed to determine the hydrodynamic pressures associated with small amplitude excitations and negligible surface wave effects.

Tosaka *et al.* (1989) used a Lagrangian approach to handle the position of the free surface in a two-dimensional container with prescribed motion. The fluid was modeled as potential flow, and Boundary Elements were used to solve Laplace's equation. Examples of motion in rectangular and cylindrical containers were presented.

Nakayama and Tanaka (1990) considered the problem of a circular cylindrical container and nonlinear sloshing with large displacements. The domain was discretized using boundary elements. The solution procedure was particularized for horizontal motion of the containers only.

Kock and Olson (1991) developed a finite element method for analyzing non-linear and linear fluid-structure interaction problems by using a variational indicator based on Hamilton's principle. Irrotational flow of inviscid fluid was considered. The effectiveness of the developed procedure for both linear and non-linear finite element formulations in analyzing a variety of fluid-structure interaction problems was represented.

Souli *et al.* (2000) and Souli and Zolesio (2001) established a procedure for fluid-structure interaction problems based on Arbitrary Lagrangian Eulerian (ALE) algorithm of finite element method. A two-steps procedure based on operator split method was employed in a time step. First step solves the governing equations of structure and fluid in a Lagrangian manner. In the second step, advection of fluid material across element

boundaries was carried out during fictitious time. Explicit time integration scheme was used to advance the solution in time. The applicability of the procedure for sloshing tank problems was validated by analytical method.

Tallec and Mourob (2001) modeled viscous flows inside structures with large deformations as a unique continuous medium considering fluid-structure effects. Lagrangian algorithm was used for structure while fluid domain was treated with arbitrary Lagrangian Eulerian (ALE) formulation. An implicit algorithm was employed, by solving successively the fluid and the structural part of the problem in each time step.

Czygan and von Estorff (2002) coupled Finite Element Method for structure and Boundary Element Method for fluid domain in order to model fluid-structure interaction problems that can take into account material nonlinearities and large deformations in the structure. The derived methodology was applied to a dam subject to earthquake excitation and a fluid-filled tank and it yielded reliable results.

For FSI problems with large structure deformations and violent free surface motions, Aquelet *et al.* (2005) developed a methodology using penalty method to couple Lagrangian structure and Eulerian fluid formulations. In order to prevent fluid penetrations through the structure, spring elements were employed. Penalty forces were determined as proportional to penetration depth. High oscillation due to relative motion between fluid and structure was prevented by defining additional damping to the spring elements.

# 4.  ASSESSMENT OF SEISMIC TANK DESIGN CODES

Seismic tank design codes are used to limit the possibility of the damage to tanks during earthquakes depending on the performance criteria selected. There is a wide variety of code guidelines for the earthquake resistant design of above-ground steel cylindrical liquid storage tanks that specify principles and application rules for the seismic design of the structural aspects of such tanks.

The methodology of tank design code recommendations can be applied in three steps:

- The first step covers the definition of seismic forces corresponding to design level earthquake and their loading on tanks shell and foundation. The impulsive and convective masses representing the fluid effects and their locations are determined and the base shear and overturning moments due to these masses are quantified considering the soil-structure interaction effects.

- The second step comprises the computation of tank seismic response parameters; such as the level of hoop, axial, shear and bending stresses and displacements; induced by loads and pressures which are estimated in the previous step. In addition, sloshing wave height has to be quantified to provide necessary freeboard in order to prevent spilling of liquid and possible damage to the tank roof due to sloshing. Uplift and rotation of the base plate should be determined to avoid the development of high stresses at the tank base and wall and to provide stability of the tank. Pressure on the tank roof due to sloshing waves is computed to prevent tank damage and separation of wall roof junction.

- In the third step, tank response parameters are assessed by comparing with allowable limits to judge whether the design is adequate or whether modifications must be made. A most critical performance criterion is the peak axial stress at the base of the shell. This stress is compared with an allowable value, which is based on a theoretical buckling condition, to prevent elastic and elasto-plastic buckling modes of

tank shell. Moreover, hoop stresses, which are very effective in the development of the elasto-plastic (elephant foot) buckling, have to be limited with material yield strength. The base shear is checked against friction to determine whether tank slides over its foundation.

API-650 (2005), NZSEE (1986) and Eurocode 8 (2006) standards are the most commonly referred ones among the seismic tank design codes in current practice. API 650 document published by the American Petroleum Institute is one of the earliest codes to develop a systematic approach for treating the seismic design of liquid storage tanks. The provisions given in API 650 (2005) are constructed on the method developed by Housner (1954) with modifications of Wozniak and Mitchell (1978) to estimate the loads induced on tanks during earthquakes. The latest addendum of API 650 (2005) refers to ASCE 7-05 document ("Minimum Design Loads for Buildings and Other Structures") for seismic parameters and loads to be taken into account for earthquake resistant design of steel tanks. The most comprehensive guidelines available for the seismic design of storage tanks are supplied by NZSEE (1986) document which were originally developed by Priestley and co-workers. The design basis used in this document assumed no yield or damage being permitted to tanks under the design earthquake loading, and therefore led to some conservatism in the design of large steel storage tanks. Another document of relevance is the 4$^{th}$ Chapter of the Eurocode 8 (2006) standard which addresses specifically the seismic response of pressure vessels and tanks and provides an overview of the various simplified procedures used to quantify the response for tanks/vessels of various configurations.

The common feature of all these codes is that the hydrodynamic forces in a liquid-tank system exerted by seismic loads are converted into equivalent mass-spring system which develops the same forces and moments on tank when subjected to same ground motion (Housner, 1954). The rigid mass component attached on this analog represents the hydrodynamic pressures generated by the liquid part which moves unison with the tank wall and is called as impulsive component. The other one which undergoes sloshing motion near the fluid free surface is named convective component and the convective effect is modeled by placing a series of single degree of freedom oscillator on the simplified system. The properties of this mechanical analog are obtained from tank dimensions and fluid properties.

The most general categorization for these codes can be done by separating them into two groups regarding their tank wall flexibility considerations. API 650 employ mechanical model of Housner (1954) therefore the flexibility of the tank is ignored when calculating the hydrodynamic pressures. NZSEE (1986) and Eurocode 8 (2006) define mechanical analogue properties not only for rigid tanks but also for flexible tanks. NZSEE (1986) guidelines use mechanical model of Veletsos and Yang (1977) for rigid circular tanks and that of Haroun and Housner (1981a) for flexible tanks. Eurocode 8 (2006) mentions mechanical model of Veletsos and Yang (1977) as an acceptable procedure for rigid circular tanks. For flexible circular tanks, models of Veletsos (1984) and Haroun and Housner (1981a) are described along with the procedure of Malhotra *et al.* (2000).

The different design methodologies cause deviations in the response parameters obtained from the codes. For example, API 650 (2005) is based on the allowable (working) stress design (ASD) methods, whereas NZSEE (1986), and Eurocode 8 (2006) specify seismic design forces at the strength design level. In strength design, factored loads are used and they correspond to ultimate level. In this study, in order to compare the seismic response parameters of tanks obtained API 650 (2005) and NZSEE (1986), and Eurocode-8 (2006), a scaling factor of 1.4 (Jaiswal *et al.* (2007) is used to convert seismic design forces from allowable stress design level to strength design level, whereas Whittaker and Saunders (2008) suggested a scaling factor of 1.1.

In API 650 (2005), tanks are categorized according to base support as self anchored and mechanically anchored tanks. NZSEE (1986) guidelines and Eurocode 8 (2006) concentrate on the seismic design of both unanchored and anchored steel tanks and detailed methods for analyzing the seismic behavior of anchored or unanchored tanks are included.

## 4.1. Simplified Analysis Methods Employed in Tank Seismic Design Codes

Simplified methods for the seismic analysis of liquid storage tanks have been widely used for many years since they are straightforward and practical. These methods were initially developed to only determine the fluid generated forces acting on tanks neglecting interaction effects between tank and contained liquid. Yet, extensive tank damages

observed after many major past earthquakes led researchers to obtain more accurate models for the seismic analysis of tanks by relaxing some approximations used in these methods, such as taking into account fluid-tank interaction effects. In all of these methods with either flexible or rigid tank assumption, fluid generated effects are represented by mechanical analog (equivalent spring-mass system) which yields the same base shear and overturning moment with the actual tank-fluid system.

The main assumption underlying the configuration of the mechanical analog is that impulsive and convective effects are uncoupled, since natural periods of these two effects occupy two widely separated ranges. Therefore, the convective and impulsive effects can be represented as independent components on this equivalent simplified model. General structure of the mechanical analog for ground supported cylindrical tanks which are rigidly fixed at its base and subjected to only one component of horizontal ground motion is illustrated in Figure 4.1. In this mechanical analog, the mass $m_{impr}$ simulates the hydrodynamic effects associated with the rigid-body or uniform component of wall motion, whereas $m_{impf}$ represents the effects due to the deformable or flexural impulsive component. The mass $m_{convn}$ characterizes the fluid portion that participates to each natural mode of the sloshing action. The attachment technique of these masses on the mechanical analog reflects the manner how they respond to the seismic motion. Thus, impulsive rigid mass, $m_{impr}$, is connected rigidly to the mechanical analog at a distance $h_{impr}$ from the base, while the impulsive flexible, $m_{impf}$, and convective, $m_{convn}$, masses are attached through pairs of horizontal flexible springs, located at distances $h_{impf}$ and $h_{convn}$ from the base, respectively. If the overturning moment developed due to pressure acting on the base plate is taken into account, the location of the impulsive and convective masses are rearranged to excite the same overturning moment as the actual system. New positions of the impulsive and convective masses are represented with $h`_{impr}$, $h`_{impf}$ and $h`_{convn}$.

The studies carried out to obtain a simplified representation of anchored tank-liquid system using mechanical analogue are summarized in Table 4.1 along with details of their methodology. The provisions presented in the current seismic tank design codes employ these simplified methods for the earthquake resistant design of such structures.
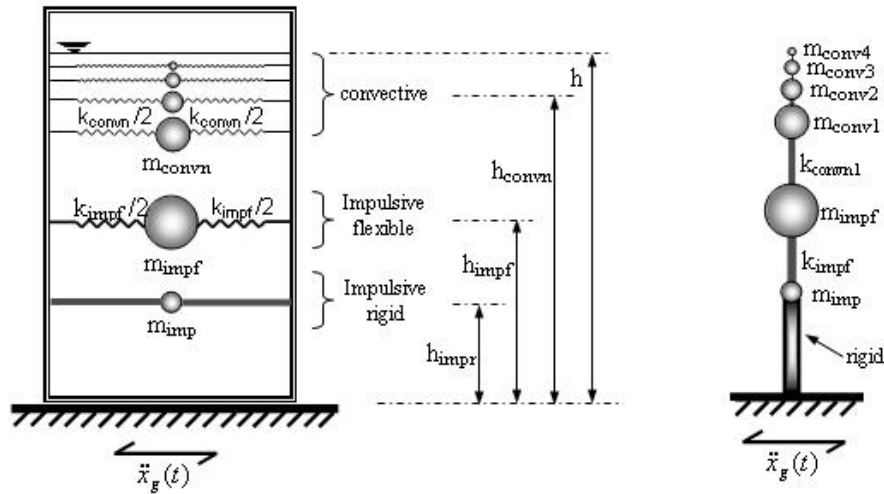
Figure 4.1. Equivalent spring-mass model for ground supported cylindrical tanks subjected to horizontal ground motion

## 4.2. Seismic Demand Parameters of Tanks

Seismic demand parameters of tanks include impulsive and convective mode periods and seismic forces developed at the tank base. Base shear coefficient which is typically specified in terms of design acceleration spectrum, seismic zone factor, soil factor, importance factor, response modification factor, and damping factor is used in order to computed earthquake induced base shear and overturning moment forces on tanks.

### 4.2.1. Impulsive Mode Period

Impulsive mode refers to lateral mode of tank-liquid system and lateral seismic forces exerted on a tank depend on period of this mode. In contrast with the assumption originally made by the Housner (1954) that tank is rigid so the impulsive mode period is zero, current design practice computes the period of impulsive mode depending on the value of impulsive mass and on the stiffness of the tank shell even though code uses Housner's method (such as, API 650). The mass density of tank wall is not included in any of impulsive period expressions given in codes; instead, mass density of fluid is used since mass of the wall is usually quite small as compared to fluid mass for steel tanks. The first impulsive mode period of a flexible anchored tank is around 0.5 seconds or less.

Table 4.1. Details of the simplified methods developed for the seismic analysis of anchored cylindrical tanks subjected to uniaxial loading

| | | Housner (1954) | Yang and Veletsos (1977) | | Haroun and Housner (1981) | Malhotra *et al.* (2000) |
|---|---|---|---|---|---|---|
| Methodology | Fluid | Approximate method for fluid flow | Mathematical solution of Laplace Equation | Mathematical solution of Laplace Equation | Boundary solution techniques | Mathematical solution of Laplace Equation |
| | Structure | - | - | SDOF System vibrate in a prescribed mode | Ring shaped finite elements | SDOF System vibrate in a prescribed mode |
| Tank wall flexibility | | Not considered | Not considered | considered | considered | considered |
| Impulsive rigid component | | considered | considered | considered | considered | - |
| Impulsive flexible component | | - | - | considered | considered | considered |
| Higher tank-fluid system mode effects | | - | - | | Fundamental mode only | included into the 1st mode effects |
| Convective effect is evaluated from rigid tank assumption | | yes | yes | yes | yes | yes |
| Convective effect | | considered | considered | considered | considered | considered |
| Higher Sloshing Mode Effects | | First mode only | First mode only | First mode only | First mode only | included into the 1st mode effects |
| Combination rules (impulsive and convective) | | SRSS | SRSS | SRSS | SRSS | Numerical sum |
| Tank inertia effects | | no | no | no | included | considered |

In the case of anchored tank, a reasonable estimate can be made of the effective shell stiffness, and thus of the impulsive period of vibration. For unanchored tanks, the nonlinear uplift mechanism causes the stiffness to vary significantly with the amplitude of input motion and there is no true impulsive period of vibration. However, it is clear that any apparent period of vibration will be longer than the period of the anchored tank. Although impulsive period of anchored and unanchored tanks may be different, design codes do not give any expressions for unanchored tanks.

For fixed base circular tanks, NZSEE (1986) guidelines have adopted the formula from Haroun and Housner (1981a) for the evaluation of impulsive mode period. Eurocode 8 (2006) has followed the expression given by Scharf (1990). The expression suggested by Malhotra *et al.* (2000) is also given in Eurocode 8 (2006) document. API 650 (2005) gives an expression for the computation of impulsive period of a flexible tank taken from Malhotra *et al.* (2000).

The impulsive mode periods are affected by the soil behavior beneath the tank. In order to take into account the soil effects on impulsive period of tank, NZSEE (1986) and Eurocode 8 (2006) define coefficients to modify the impulsive period of flexible tank resting on rigid foundation. These coefficients include the horizontal and rocking stiffness of the foundation ($k_x$ and $k_\theta$, respectively), effective stiffness of the tank-liquid system ($k_f$) and factors for converting static stiffness values to dynamic values ($\alpha_x$ and $\alpha_\theta$). Impulsive mode period expressions presented in tank design codes are summarized in Table 4.2.

### 4.2.2. Axisymmetric Vibration Period

Axisymmetric vibrations of tank-fluid system are generated under vertical seismic motions. These modes are also called breathing modes. Expression for exact time period of axisymmetric mode of a flexible circular tank is quite involved in the literature. However, considering certain approximations like, mass of tank wall is quite small as compared to fluid mass, some simple closed form expressions have been given by Veletsos (1984) and Haroun and Tayel (1985a and b).

The NZSEE (1986) and Eurocode 8 (2006) documents require that the lowest frequency vertical mode of vibration to be considered to act concurrently with horizontal mode. Eurocode 8 (2006) has used expression from Haroun and Tayel (1985a and b). NZSEE (1986) guidelines give formula derived by Veletsos (1984). The evaluation of vertical time period of a flexible tank is not involved in API 650 (2005).

The breathing modes are influenced by the soil conditions under the tank. NZSEE (1986) and Eurocode 8 (2006) supplied expressions for the evaluation of periods of these modes not only for flexible tanks but also for rigid tanks which includes the values of

coefficient Kv are given in graphical form. Table 4.2 gives details of the expressions used in various codes to evaluate the impulsive and axisymmetric mode periods of cylindrical tanks resting on rigid and soft soil. In this table, $\rho$, E, t, R, D, $t_u$, H, g, $h_f$, $h'_i$ , $m_s$, $m_l$, $m_0$ and $k_f$ represent mass density of fluid, modulus of elasticity of tank material, thickness of tank wall, radius of tank, diameter of tank, equivalent uniform thickness of tank shell, height of fluid, acceleration due to gravity, height of impulsive mass, height of impulsive mass for rigid tank, total mass of the tank including base, support, and foundation, total mass of the fluid, mass of the foundation and the stiffness of the deformable tank, respectively.

### 4.2.3. Convective Mode Period

The period of fundamental sloshing mode depends mainly on the diameter of the tank and to a lesser extent on the depth of liquid. Typical periods of convective mode are very long (up to 6-10 seconds for large tanks) and are more influenced by the level of seismic ground displacements rather than ground accelerations. Since the convective (sloshing) response is practically insensitive to both the tank wall and the foundation flexibility due to its long period of oscillation, all codes give expression of convective mode period for only rigid tank. API 650 (2005) recommends the expression derived by Housner (1954) and defines only first sloshing frequency whereas NZSEE (1986), and Eurocode 8 (2006) have adopted the formula from Veletsos and Yang (1977) and permit the computation of higher sloshing mode periods. The expressions for the computation of sloshing period defined in these codes are summarized in Table 4.3. In this table, n, R, D, g, H and $T_c$ represent mode number, radius of tank, diameter of tank, acceleration due to gravity, liquid height and sloshing period, respectively. No expression is given in the corresponding code. Figure 4.2 represents the variation of convective mode period ratio with H/R ratio. According to this figure, for a given tank radius, convective mode period is insensitive to increase in fluid depth after fluid depth exceeds tank radius. Also, it can be observed from this figure that, convective mode period decreases with the decrease in mode numbers.

Table 4.2. Equations for impulsive time period given in tank seismic design codes

| Support Condition | Code | Resting on rigid foundation | Resting on soft soil including SSI effects |
|---|---|---|---|
| Anchored | API 650 | | |
| | Horizontal mode | $T_i = \dfrac{C_i H}{\sqrt{\dfrac{2 t_u}{D}}} \sqrt{\dfrac{\rho}{E}}$ <br><br> (Malhotra *et al.*, 2000) | No expressions are given |
| | Vertical mode | Evaluation of vertical time period is not described. | No expressions are given |
| | Eurocode 8 | | |
| | Horizontal mode | $T_i = \dfrac{R(0.157(H/R)^2 + (H/R) + 1.49)}{\sqrt{\dfrac{E\,t(z/H = 1/3)}{\rho H}}}$ <br><br> (Scharf, 1990) <br><br> $T_i = \dfrac{C_i \sqrt{\rho H}}{\sqrt{\dfrac{t_u E}{R}}}$ <br><br> (Malhotra *et al.*, 2000) <br> $C_i$ is a coefficient given as function of H/D in graphical form. | For rigid tank: <br> $T_i^* = 2\pi \sqrt{\left( \dfrac{m_i + m_o}{k_x\,\alpha_x} + \dfrac{m_i\,h_i'^2}{k_\theta\,\alpha_\theta} \right)}$ <br> For deformable tank: <br> $T_f^* = T_f^{\,0} \sqrt{\left( 1 + \dfrac{k_f}{k_x\,\alpha_x}\left[ 1 + \dfrac{\alpha_x k_x\,h_f^2}{k_\theta\,\alpha_\theta} \right] \right)}$ <br><br> $k_f = 4\pi^2 \dfrac{m_f}{T_f^2}$ <br><br> $k_x, k_\theta, \alpha_x, \alpha_\theta$ (*Gazetas*, 1983) |
| | Vertical (breathing) mode | $T_b = 4R \sqrt{\dfrac{\pi \rho H (1 - \nu^2) I_0(\pi R/(2H))}{2 E I_1(\pi R/(2H)) t(H/z = 1/3)}}$ <br><br> $I_0$, $I_1$ are respectively modified Bessel's functions of order 0 and 1 | For rigid tank: <br> $T_{vr}^* = 2\pi \sqrt{\left( \dfrac{m_s}{k_v\,\alpha_v} \right)}$ <br> For flexible tank: <br> $T_{vd}^* = T_{vd}^{\,0} \sqrt{\left( 1 + \dfrac{k_l}{k_v\,\alpha_v} \right)}$ <br><br> $k_l = 4\pi^2 \dfrac{m_l}{T_{vd}^2}$ <br><br> $k_v, \alpha_v$ (*Gazetas*, 1983) |
| | NZSEE | | |
| | Horizontal mode | $T_i = \dfrac{5.61 \pi H \sqrt{\rho/E}}{K_h}$ <br> $K_h$ is given in graphical form as a function of H/R and t/R. | The same expression given in Eurocode 8 for deformable tank |
| | Vertical (breathing) mode | $T_b = \dfrac{5.61 \pi H \sqrt{\rho/E}}{K_v}$ <br> $K_v$ is given in graphical form as a function of H/R and t/R. | The same expression given in Eurocode 8. |
| Unanchored | API 650 | | |
| | Eurocode 8 | No expressions are given | No expressions are given |
| | NZSEE | | |

Table 4.3. Equations for convective mode period ($T_c$) given in seismic design codes

| Support Condition | Code | Resting on rigid foundation | Resting on soft soil including SSI effects |
|---|---|---|---|
| Anchored | API 650 (2005) <br><br> (Housner, 1954) | $T_c = \dfrac{1.04}{\sqrt{\tanh\left(\dfrac{3.68\,H}{D}\right)}}\sqrt{D}$ | * |
| | Eurocode 8 (2006) <br><br> (Veletsos and Yang, 1977) | $T_c = \dfrac{2\,\pi\,\sqrt{R/g}}{\sqrt{\lambda_n \tanh\left(\dfrac{\lambda_n H}{R}\right)}}$ <br><br> $\lambda_1 = 1.841,\ \lambda_2 = 5.331, \lambda_3 = 8.536$ | * |
| | (Malhotra, 2000) | $T_c = C_c \sqrt{R}$ <br> ($C_c$ are given in graphical form as a function of H/R) | * |
| | NZSEE (1986) <br><br> (Veletsos and Yang, 1977) | $T_c = \dfrac{2\,\pi\,\sqrt{R/g}}{\sqrt{\lambda_n \tanh\left(\dfrac{\lambda_n H}{R}\right)}}$ | * |
| Unanchored | API 650 (2005) <br> Eurocode 8 (2006) <br> NZSEE (1986) | * | * |



Figure 4.2. Comparison of convective mode period ratios for a rigid tank given in different codes

### 4.2.4. Hydrodynamic Pressure Distribution

Stresses developed in the tank wall depend on distribution of hydrodynamic pressure along the wall height. Housner (1954) was derived the expressions for distribution of hydrodynamic pressure on a rigid tank wall and base due to lateral base excitation. Both impulsive and convective components of hydrodynamic pressure were considered. Veletsos and Yang (1977) also obtained the distribution of hydrodynamic pressure on rigid as well as flexible tank. Veletsos (1984) separated the hydrodynamic pressure exerted on the flexible tank due to lateral seismic forces into three different components. First component takes into account the movement of the liquid assuming the tank shell to be rigid (impulsive-rigid). The pressure generated by the movement of the liquid due to the flexibility of the tank was taken into account by the impulsive-flexible component. The movement of the liquid due to free surface sloshing generates the convective pressure part. Impulsive and convective pressure distributions along the tank wall have different pattern which is curvilinear. Since the flexibility of tank wall does not influence the convective pressure distribution, all the codes compute convective component considering tank to be rigid.

Expressions for distribution of impulsive and connective hydrodynamic pressure on the tank from various codes are given in Table 4.4, in which, z, r, H, $\rho$, $I_1$, $I_1^{'}$ and $J_1$ denote liquid level at which wall is investigated measured from base, radial position, height of liquid surface, mass density of fluid, the modified Bessel function of order 1 and its derivative and Bessel function of the first order, respectively. Although API 650 (2005) uses the Housner's method, it does not specify expressions for the hydrodynamic pressure distribution on the tank wall and base. Only the formulations to compute properties of mechanical analogue are involved in the code. Both NZSEE (1986) guidelines and Eurocode 8 (2006) use approach of Veletsos (1984) to obtain hydrodynamic pressure distribution in rigid and flexible circular tanks. In NZSEE (1986) guidelines, expressions of pressure distribution at tank wall and base are not given explicitly, however graphically distribution of that is shown. Simplified linear pressure distribution is also described in NZSEE (1986). Eurocode 8 (2006) provides expressions of Veletsos (1984) to obtain distribution of impulsive and convective hydrodynamic pressures for flexible tanks as well as rigid tanks. All of the codes recommend that the hydrodynamic pressure acting on the

base of tank as well as walls is included in the analysis of tank support system and soil foundation.

Table 4.4. Expressions for distribution of impulsive and convective hydrodynamic pressure due to horizontal excitation given in various codes

| Code | | Distribution of hydrodynamic pressure due to horizontal excitation |
|---|---|---|
| API 650 | | Distribution of hydrodynamic pressure is given neither with equations nor graphically. But since method of Housner (1954) is used in API 650, the equations derived for a rigid tank in this method are given here. |
| | Impulsive | Wall $\quad p_{iw} = \rho\,H\,\sqrt{3}\left(1 - \dfrac{z}{H} - \dfrac{1}{2}\left(1 - \dfrac{z}{H}\right)^2\right)Tanh\left(\sqrt{3}\,\dfrac{R}{H}\right)Cos\,\theta\,A_g(T_i)\,g$ |
| | | Base $\quad p_{ib} = -\rho\,H\,\dfrac{\sqrt{3}}{2}\,\dfrac{Sinh\left(\sqrt{3}\,\dfrac{r}{H}\right)}{Cosh\left(\sqrt{3}\,\dfrac{R\,Cos(teta)}{H}\right)}Cos\,\theta\,A_g(T_i)\,g$ |
| | Convective | Wall $\quad p_{cw} = \rho\,\dfrac{9}{8}\,R\left(\dfrac{Cosh\left(\sqrt{\dfrac{27}{8}}\,\dfrac{z}{R}\right)}{Sinh\left(\sqrt{\dfrac{27}{8}}\,\dfrac{H}{R}\right)}\right)\left(1 - \dfrac{Cos^2\theta}{3}\right)Cos\,\theta\,A_g(T_c)\,g$ |
| | | Base $\quad p_{cb} = \rho\,\dfrac{9}{8}\,R\,\dfrac{1}{Cosh\left(\sqrt{\dfrac{27}{8}}\,\dfrac{H}{R}\right)}\left(\dfrac{r}{R} - \dfrac{1}{3}\left(\dfrac{r}{R}\right)^3\right)Cos\,\theta\,A_g(T_c)\,g$ |
| Eurocode8 | | |
| | Impulsive | $p_i(r,z,\theta,t) = \rho\,H\,Cos(\theta)A_g(t)\displaystyle\sum_{n=0}^{\infty}\dfrac{(-1)^n\,8\,I_1\left[(2n+1)\dfrac{\pi}{2}\dfrac{r}{H}\right]}{(2n+1)^2\,\pi^2\,I_1'\left[(2n+1)\dfrac{\pi}{2}\dfrac{R}{H}\right]}Cos\left[(2n+1)\dfrac{\pi}{2}\dfrac{z}{H}\right]$ |
| | Convective | $p_c(r,z,\theta,t) = \rho\,R\,Cos(\theta)\,A_{cn}(t)\displaystyle\sum_{n=1}^{\infty}\dfrac{2\,J_1\left[\lambda_n\dfrac{r}{R}\right]}{J_1[\lambda_n]}\dfrac{Cosh\left[\lambda_n\dfrac{z}{R}\right]}{Cosh\left[\lambda_n\dfrac{H}{R}\right]}$ |
| NZSEE | | |
| | Impulsive Convective | Explicit expressions are not given, however graphically distribution of hydrodynamic pressure is shown. Pressure distribution is taken from Veletsos and Yang (1977) for rigid circular tanks and Haroun and Housner (1981) for flexible tanks. |

**4.2.5.  Response to Vertical Base Excitation**

Under the influence of vertical excitation, liquid exerts axisymmetric hydrodynamic pressure on tank wall. The evaluation of pressure generated by the vertical component of earthquake motion is essential in properly assessing the safety and strength of tank wall against buckling.

The provisions on inclusion of effect of vertical excitation are covered in all codes. API 650 (2005) does not supply any expression for the hydrodynamic pressure distribution due to vertical ground motion. It recommends a base shear coefficient for vertical acceleration which is 14 percent of that of lateral acceleration. However, vertical acceleration effects need not be combined concurrently for determining loads, forces and resistance to overturning in the tank shell. Vertical seismic effects should be considered in the computation of shell hoop tensile stresses, shell membrane compression, anchorage design, fixed roof components, sliding and foundation design.

For tanks with rigid wall, NZSEE (1986) and Eurocode 8 (2006) define linearly distributed hydrodynamic pressure the same as hydrostatic pressure which act perpendicular to tank wall in outward direction. The formulations for the hydrodynamic pressure distribution due to vertical ground motion defined in the codes are given in Table 4.5. In this table, z, H, $\rho$, g and $A_v$ denote liquid level at which wall is investigated measured from base, height of liquid surface, mass density of fluid, acceleration due to gravity, and vertical base shear coefficient, respectively.

Distribution of hydrodynamic pressure due to vertical excitation is influenced by wall flexibility. The effect of wall flexibility on distribution of hydrodynamic pressure is not considered in NZSEE (1986) guidelines. Eurocode 8 (2006), however, has incorporated the effect of wall flexibility on distribution of hydrodynamic pressure using the expression defined by Fischer and Seeber (1998).

**4.2.6. Base Shear and Overturning Moment**

Seismic excitation of a cylindrical tank produces hydrodynamic pressure at the shell-liquid interface and tank base and this pressure imposes a resultant shear force and overturning moment on the structure. The most crucial factors in computing the seismic design of tanks are these two quantities because they are used for judging the safety of tanks against shell buckling and uplift. For an anchored tank, the base shear is mainly resisted by sliding friction between the tank base plate and the supporting foundation material with negligible resistance from bolts, whereas overturning moment is mainly resisted by compression in the tank wall and tension in anchor bolts. An unanchored tank withstand the overturning moment by the weight of the tank wall and by the weight of a portion of the tank contents adjacent to the shell.

In tank design codes, base shear and overturning moment are obtained using mechanical analogue properties. Comparisons of variation of mechanical analogue properties such as, impulsive and convective masses ($m_i$ and $m_c$, respectively), and their height from the tank base ($m_i$ and $m_c$, respectively), with H/R obtained from API 650 (2005), NZSEE (1986) and Eurocode 8 (2006) documents are plotted in Figure 4.3 to Figure 4.6. In these figures, m and H represents total mass of liquid and fluid depth, respectively. The portion of tank contents that acts in a convective fashion decreases as tank aspect ratio (H/R) increases, with the impulsive mode becoming more dominant. Conversely, for tanks of very low aspect ratio, only about 30 per cent of tank contents acts with the walls, with the remainder responding in various sloshing modes. Impulsive and convective masses and their locations obtained from different code provisions are very consistent for all H/R values.

Table 4.5. Expressions for distribution of hydrodynamic pressure due to vertical excitation given in various codes

| Code | Distribution of hydrodynamic pressure due to vertical excitation | |
|---|---|---|
| API 650 | Rigid Tank | Distribution is not described. |
| | Flexible tank | Distribution is not described. |
| Eurocode 8 | Rigid Tank | $P_{vr}(z) = (1 - z/H)\,\rho\,g\,H\,A_v(T_v)$ |
| | | $P_{vf}(z) = 0.815\,f(H/R)\,\rho\,H\cos(\pi\,z/(2\,H))\,A_v(T_{vf})$ |
| | Flexible tank | $f(H/R) = 1.078 + 0.274\ln(H/R)\quad for\ 0.8 \le H/R < 4$ |
| | | $f(H/R) = 1.0\quad for\ H/R < 0.8$ |
| NZSEE | Rigid Tank | $P_v(z) = A_v(T = 0)(1 - z/H)\,\rho\,g\,H$ |
| | Flexible tank | $P_v(z) = A_v(T_v)(1 - z/H)\,\rho\,g\,H$ |
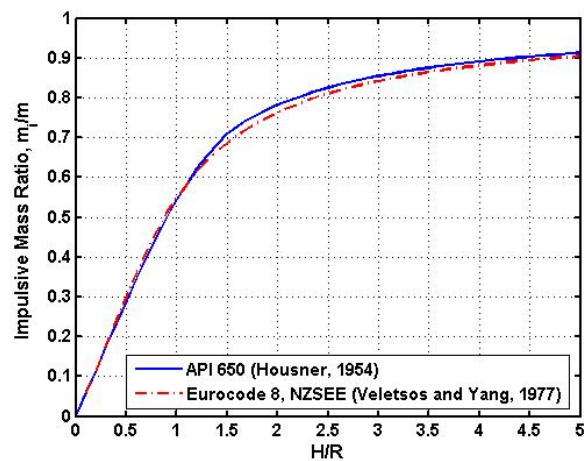


Figure 4.3. Comparison of impulsive mass ratios for a rigid tank given in different codes
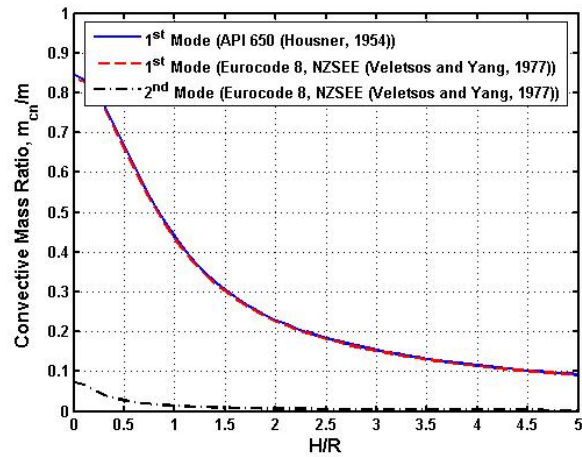
Figure 4.4. Comparison of convective mass ratios for a rigid tank given in different codes
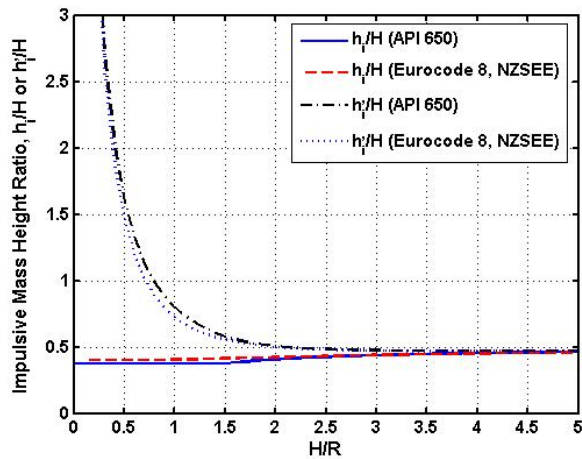


Figure 4.5. Comparison of impulsive mass height ratios for a rigid tank given in different codes
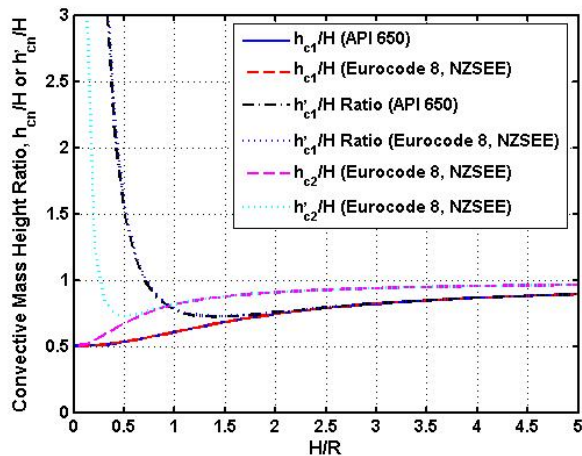


Figure 4.6. Comparison of convective mass height ratios for a rigid tank given in different codes

In Figure 4.7 to Figure 4.9, base shear and overturning moment obtained by provisions given in tank design codes are plotted as a dimensionless parameters in terms of fluid mass, m, fluid wave height, H, base shear coefficient, A(T), and gravitational acceleration, g. Base shear and overturning moment developed due to impulsive and convective effects are almost the same for all code provisions.

Since the hydrodynamic pressures generated by vertical excitation is axisymmetric, this hydrodynamic pressure does not produce a shear force or moment resultant at any horizontal level of the tank, or immediately above or below the base.

### 4.3. Response Parameters of Tanks

The most important response parameters of tanks include maximum free surface wave height, uplift displacement of tank base and shell stresses. The free surface wave height has to be quantified to provide necessary freeboard in order to prevent spilling of liquid and possible damage to the tank roof due to sloshing. The maximum base uplift is important to provide suitable flexibility in the design of any piping that is attached to the tank wall. Tank shell stresses should remain under certain limit in order to provide safety of tanks against buckling.
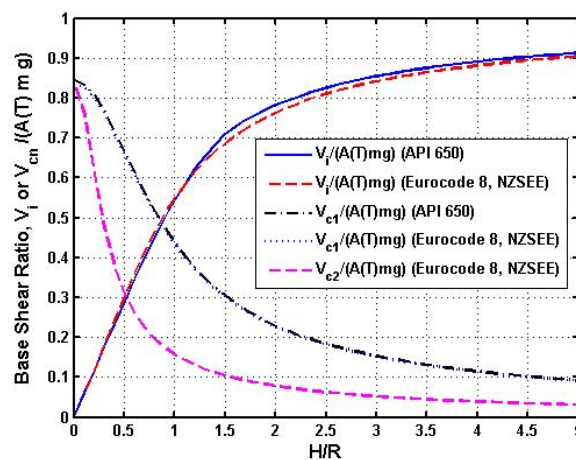


Figure 4.7. Comparison of base shear ratios for a rigid tank given in different codes
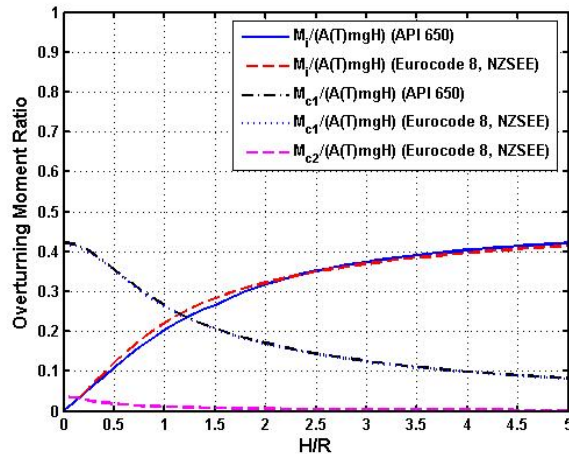
Figure 4.8. Comparison of overturning moment ratios at base of tank wall for a rigid tank given in different codes (excluding pressure at the tank base)
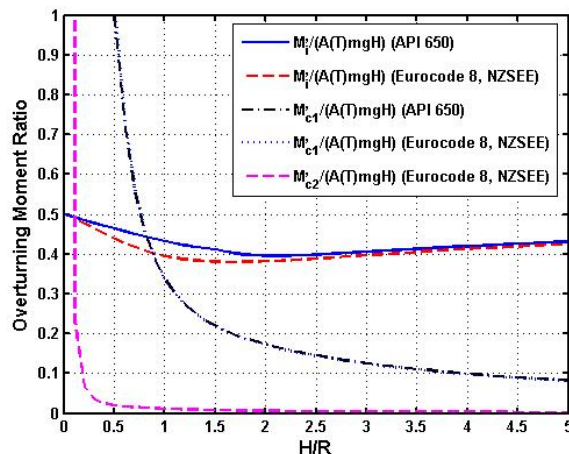


Figure 4.9. Comparison of overturning moment ratios at base of tank for a rigid tank given in different codes (including pressure at the tank base)

### 4.3.1. Sloshing Wave Height

API 650 (2005), NZSEE (1986) guidelines and Eurocode 8 (2006) give explicit expressions to evaluate maximum sloshing wave height which is derived with the assumption of small amplitude wave motion. These expressions are given in Table 4.6. In this table, D, $T_{c1}$, $T_{c2}$ and $A_c(T_{cn})$ represent diameter of tank, first sloshing period, second sloshing period, and convective mode base shear coefficient, respectively. All API 650 (2005), NZSEE (1986) guidelines and Eurocode 8 (2006) define maximum sloshing wave

height as a function of tank diameter and the convective mode base shear coefficient, $A_c(T_{cn})$ which includes the effects of sloshing period, sub-soil classification and peak ground acceleration. According to these expressions, the maximum magnitude of the wave height is assumed to occur at $\theta=0°$ and at the tank circumference where $\theta$ is the circumferential angle.

In contrast to the other codes, NZSEE (1986) recommends that the contribution of the first two antisymmetric sloshing modes is considered in the evaluation of sloshing wave height and to be combined with SRSS rule. NZSEE (1986) and Eurocode 8 (2006) do not consider the presence of two horizontal earthquake components which may lead to higher wave heights. The same approach is adopted in the API 650 (2005).

All of these codes assume that the base boundary condition and soil flexibility do not affect the maximum sloshing wave height. But maximum sloshing wave height obtained from codes may give unconservative results for unanchored tanks resting on both rigid and flexible foundations (Hamdan, 2000).

Table 4.6. Expressions for maximum sloshing wave height given in various codes

| Code | Sloshing wave height |
|---|---|
| API 650 | $\delta_s = 0.5\,D\,A_c(T_{c1})$ |
| Eurocode 8 | $\delta_s = 0.42\,D\,A_c(T_{c1})$ |
| NZSEE (1986) | $\delta_s = 0.5\,D\,\sqrt{0.84\,A_c(T_{c1}) + 0.07\,A_c(T_{c2}) + .......}$ |

**4.3.2. Base Uplift and Plastic Rotation of Base Plate**

Eurocode 8 (2006) presents graphs for uplift width and uplift height as functions of normalized overturning moment and H/R ratio. However, in some cases, the range of these charts does not cover the relevant overturning moment ranges. These figures are based on purely static finite element analyses of Scharf (1990). NZSEE (1986) employs a formula to

compute uplift displacement of the unanchored tank base depending on overturning moment exerted by hydrodynamic effects, radial membrane forces in the tank base plate, uplift width, yield stress of the tank base plate material, base plate thickness, foundation stiffness and hydrodynamic pressure acting on the tank base plate. This equation was obtained by modifying the equation derived by Cambra (1982) assuming that base plate material will yield. API 650 (2005) presents uplift displacement as a function of yield stress of the tank base plate material, base plate thickness and uplift width. Although uplift is caused by overturning moment at the tank base, API 650 (2005) evaluates uplift independently from overturning moment.

Both NZSEE (1986) and Eurocode 8 (2006) recommend the computation of plastic rotation of the base plate depending on the uplift displacement and width of the base plate with the same formulation. The maximum allowable plastic rotation is limited with 0.20 radian (11.5 degrees) assuming a maximum allowable steel strain of 5 per cent and a length of the plastic hinge of 2 times thickness of the base plate. But for some cases, the plastic rotation of unanchored tank base could not be evaluated according to Eurocode 8 (2006) since uplift width and height can not be obtained according to this code. API 650 (2005) does not present any recommendation for the plastic rotation of the base plate.

### 4.3.3. Tank Stresses

Although seismic damages in tanks are due to many causes, the principle design consideration in seismic design codes is the buckling of the tank wall due to axial compressive and hoop stresses. The maximum hydrodynamic pressures evaluated from equivalent spring mass assumption are used to compute the maximum seismic overturning moment at the tank base. The axial and hoop stresses in the wall required to resist this moment may be evaluated from a static analysis procedure by making use of the ordinary beam theory for design purposes.

Maximum axial stress due to overturning moment at a section immediately above the base generated by the hydrodynamic forces and self weight of the tank is expressed with following equation for a cylindrical tank by ordinary beam theory:

$$\sigma_{b\max} = \frac{M_{OT}}{I}R + \rho_s\, g\, H_s = \frac{M_{OT}}{\pi\, R^2\, t} + \rho_s\, g\, H_s \qquad (4.1)$$

where, $M_{OT}$ is total design overturning moment, $t$ is the wall thickness at the base, $I$ is the moment of inertia of the tank wall about a horizontal centroidal axis, $R$ is the tank radius, $\rho_s$ is the shell density and $H_s$ is the shell height. The first part of the this formula represents the axial stresses due to overturning moment and the second part gives the axial stresses due to self weight of the tank shell and roof.

The axial shell stresses developed due to tank inertia may be added to the total axial stresses by adding the overturning moment $M_t$ to the $M_{OT}$ given in Equation 4.1:

$$M_t = (m\, L_o + m_R\, L_R)\, \ddot{x}_{\max} \qquad (4.2)$$

in which $m$ and $m_R$ are the total masses of the tank wall and roof, respectively and $L_o$ and $L_R$ are the distances from the base to the respective mass centers. $\ddot{x}_{\max}$ is the peak ground acceleration.

Tensile hoop forces due to the integrated effects of hydrostatic and hydrodynamic pressures acting normal to the tank wall are effective on the development of the elasto-plastic buckling of the tank shell. Tensile hoop force resists radial displacements and base plate increases this resistance. Therefore maximum hoop force in the shell occurs above the shell-base junction. The maximum value of the circumferential and hoop stress in the tank wall is given by:

$$\sigma_{\theta\max} = \frac{\bar{p}_{\max}\, R}{t} + \rho_s\, R\, \ddot{x}_{\max} \qquad (4.3)$$

in which $\bar{p}_{\max}$ is the maximum value of the total wall pressure, $t$ is the wall thickness, $\rho_s$ is the tank shell density. The second part of this equation takes into account the horizontal inertia forces of the tank itself.

The maximum shear stress due to hydrodynamic effects on the tank is computed by following formulation:

$$\tau_{max} = 2\frac{Q_{max}}{A_s} = \frac{1}{\pi}\frac{Q_{max}}{R\,t} \tag{4.4}$$

in which, $A_s$ and $Q_{max}$ represent the cross-sectional area of shell and maximum base shear due to hydrodynamic effects, respectively. The horizontal tank inertia effect may be added to the base shear value according to following formulation:

$$Q_t = (m + m_R)\ddot{x}_{max} \tag{4.5}$$

NZSEE (1986) employs ordinary beam theory to specify the maximum axial compression stresses in the tank shell. API 650 (2005) design procedure offers a concise way of determining the maximum applied axial stresses for anchored as well as unanchored tanks depending on the minimum anchorage ratio. Eurocode 8 (2006) does not present any procedure for computation of design tank shell stresses.

NZSEE (1986) employs graphs for the normalized hoop force and bending moment distributions along the tank height developed due to hydrostatic, impulsive-rigid and convective pressure components as a function of H/R and R/t ratio. API 650 (2005) provides distribution of hoop stresses along the tank wall proportional to pressure distribution throughout the tank height which is obtained by Housner's method. According to NZSEE (1986) design procedure, the tension from combined hoop stresses has to be less than the yield stress of the tank material. API 650 (2005) specifies 0.9 times yield stress of the tank material to limit hoop stresses.

Codes employ different procedures to determine the axial compressive stresses of unanchored tank. Eurocode 8 (2006) presents a graph to compute axial compressive stress in the unanchored tank wall as functions of normalized overturning moment and H/R ratio, but, in same cases, the range of the graph is not sufficient to cover normalized overturning moments of tanks. API 650 (2005) design procedure determines the maximum applied axial stresses for unanchored tanks depending on the minimum anchorage ratio considering

a portion of the tank contents used to resist overturning moment. In NZSEE (1986), portion of the tank shell which remains in contact with the ground carry the resisting force caused by the weight of the liquid above the uplifted part of the tank and shell stress is computed using this resisting force.

At the moment there are no design guidelines regarding the effect of uplifting on the distribution of the hoop stress. This stress is considered unaltered by the uplift mechanism of the tank.

NZSEE (1986) advices to take into account the inertia effects of tank for the computation of maximum tank shell stresses. The formulation for the axial compressive stress calculation given in API 650 (2005) includes the inertia effects. Eurocode 8 (2006) recommends that "for steel tanks, the inertia forces acting on the shell due to its own mass are small in comparison with the hydrodynamic forces, and can normally be neglected".

### 4.4. Capacity of Tanks for Buckling Modes

In seismic tank design codes, the axial compressive stresses in the tank wall are limited with an allowable stress value in order to prevent elastic (diamond shape) and elasto-plastic (elephant-foot) buckling failure modes. Diamond shape buckling is an elastic buckling phenomenon in which, buckling occurs before the plasticity, due to the presence of high axial compressive stresses, whereas elephant foot buckle mechanism is caused by the combined action of vertical compressive stresses exceeding the critical stress, hoop tension close to the yield limit and the local bending stresses due to the restraints at the tank base and material plasticity and buckling almost occur at the same time.

### 4.4.1. Buckling in Membrane Compression (Elastic Buckling)

The axial membrane stresses to cause buckling in a cylindrical shell structure is a function of the amplitude of imperfections, the internal pressure, shell thickness and the circumferential variation of the axial stress. Imperfections are the radial errors in the perfect circular position of wall and tend to reduce the buckling strength of a perfect unpressurized shell which is defined by classical theory (Timoshenko and Gere, 1961). The

buckling strength of the perfect shell is reduced due to imperfections depending on a ratio of maximum imperfection amplitude to wall thickness. Also quality of the construction is effective on tank imperfections. A slight internal pressure has a strengthening effect on the buckling stress, which tends to approach the classical stress. An increase in the buckling strength due to the axial stresses being induced by bending action rather than uniform axial loading is also considered. Circumferential variation of buckling stress reduces the probability of coincidence of the maximum axial stress with the maximum imperfection amplitude, and therefore increases the buckling strength. Thus, the buckling load associated with membrane compression induced by bending exceeds that where the compression is induced by axial load. Both NZSEE (1986) and Eurocode 8 (2006) apply this procedure to check buckling at the tank shell of anchored tanks.

In API 650, the allowable axial compressive stress at the tank shell is defined by the following equation:

$$\sigma_{Zallowable} = 41.5 \cdot 10^9 \, \frac{t}{R} \qquad if \qquad \frac{G \, H \, R^2}{t^2} \geq 11 \cdot 10^6 \tag{4.6}$$

otherwise;

$$\sigma_{Zallowable} = 16.6 \cdot 10^9 \, \frac{t}{R} + 7.5 \cdot 10^6 \sqrt{G \, H} \, < 0.5 \, \sigma_y / 10^6 \tag{4.7}$$

where, G is the specific gravity of the contained fluid. These formulations include the effect of internal pressure.

Another methodology for the computation of allowable buckling design stress in diamond shape buckling mode is given by NASA SP-8007 standard (1968) for the cylindrical shells which experience locally a compressive stress:

$$\sigma_{zallowable} = (0.6 \, \gamma + \Delta \gamma) \frac{E \, t_s}{R} \tag{4.8}$$

$$\gamma = 1 - 0.73 \left[ 1 - \exp\left( -\frac{1}{16}\sqrt{\frac{R}{t_s}} \right) \right] \quad \text{(for Pure bending)} \tag{4.9}$$

$$\gamma = 1 - 0.901 \left[ 1 - \exp\left( -\frac{1}{16}\sqrt{\frac{R}{t_s}} \right) \right] \quad \text{(for Pure Axial Compression)} \tag{4.10}$$

$$\Delta\gamma = 0.24 \left[ 1 - \exp\left( -3\frac{P}{E}\left(\frac{R}{t_s}\right)^2 \right) \right]^{0.75} \tag{4.11}$$

where, $\gamma$ is a knockdown factor for geometrical imperfections, $\Delta\gamma$ is an increase factor of $\gamma$ for pressurised shells. $t_s$ is the minimum thickness of tank shell in the lowest 10 per cent of the shell height.

### 4.4.2. Elasto-Plastic Buckling

The bottom of the tank wall is usually subjected to a bi-axial stress state consisting of axial membrane compression and circumferential hoop tensile stress therefore, this region of the tank is more vulnerable against elasto-plastic buckling. In contrast to the case of elastic buckling, internal pressure reduces the elasto-plastic buckling strength of tanks. In this case the hydrodynamic pressure due to all the components of the earthquake excitation must be considered to get a conservative design.

Both NZSEE (1986) and Eurocode 8 (2006) address the same procedure for the computation of buckling strength of tank shell against elasto-plastic buckling. Yet, elasto-plastic buckling is not account for in API 650 (2005).

### 4.5. Design Properties of Tanks

Tank design codes specify damping level of tanks, combination rule not only for impulsive and convective effects but also for accumulation of seismic responses due to horizontal and vertical ground motion components. The procedures for soil-structure

interaction effects and tank inertia effects are also presented in order to compute tank response accurately.

### 4.5.1. Damping

While there is a consensus in the codes (API 650 (2005), NZSEE (1986), and Eurocode 8 (2006)) on the damping level of convective mode which is recommended as 0.5 per cent, impulsive mode damping has generally been assumed to be of the order of 2-5 per cent. API 650 recommends damping factor of 5 per cent whereas Eurocode 8 (2006) assumes 2 per cent damping for anchored and unanchored tanks resting on rigid foundation. NZSEE (1986) defines distinct levels of damping depending on the soil type and tank support condition for horizontal and vertical loading conditions (Table 4.7).

NZSEE (1986) and Eurocode 8 (2006) take into account the effect of not only material damping of both the tank and the soil foundation but also radiation damping (*i.e.* energy lost into the foundation). Effective damping ratio of the tank-foundation system is provided for both rigid and flexible tanks subjected to horizontal and vertical excitations.

### 4.5.2. Soil-Structure Interaction Effects

Soil-structure interaction is effective not only on response of horizontal motion but also on that of vertical motion. Soil flexibility enhances the impulsive time period of both its rigid and flexible components and the total damping of the structure increases by the effect of radiation damping of the soil. In seismic design codes, effect of soil flexibility on tank behavior is taken into account by modifying the impulsive mode periods for both lateral and vertical motions and damping values of tanks. NZSEE (1986) guidelines and Eurocode 8 (2006) provide expressions for period of lateral and vertical mode of tank including the soil-structure interaction effects along with expressions for the equivalent damping of a tank including the radiational damping of soil derived by Veletsos (1984). API 650 (2005) does not take into account the tank-soil coupling.

### 4.5.3. Combination Rule

An important point while using a mechanical model pertains to combination rule used for adding the impulsive, convective and vertical forces. Except Eurocode 8 (2006), all the codes suggest SRSS (square root of sum of squares) rule to combine horizontal impulsive, convective and vertical impulsive forces. Eurocode 8 (2006) recommends use a direct superposition of the impulsive and convective effects, but SRSS rule is employed to combine rigid and flexible components of hydrodynamic pressures generated vertical ground motion.

NZSEE (1986) recommends direct sum of impulsive rigid and impulsive flexible components while obtaining maximum impulsive response. However, because of low probability of coincident response of maximum impulsive, convective and vertical actions, the SRSS rule is suggested to combine these response quantities.

API 650 (2005) suggests SRSS Method to obtain combined effect of impulsive and convective components. This method is also applied for the addition of the vertical and horizontal hydrodynamic pressures.

### 4.5.4. Ground Motion Components

API 650 (2005), NZSEE (1986), and Eurocode-8 (2006) do not account for the presence of two orthogonal horizontal earthquake components, simultaneous effect of one horizontal and vertical earthquake components are considered in the analysis.

### 4.5.5. Tank Inertia Effects

NZSEE (1986) and Eurocode 8 (2006) advice to include shell inertia effects of tank wall and the roof in the analysis of the stresses developed in the tank shell and the foundation.

Table 4.7. Impulsive mode damping factors (NZSEE, 1986)

| Tank Description | % Damping Soft Soil | | % Damping Firm Soil and Rock | |
|---|---|---|---|---|
| | Horizontal Direction | Vertical Direction | Horizontal Direction | Vertical Direction |
| Anchored rigid and flexible tanks | 5 | 7.5 | 2 | 5 |
| Unanchored flexible tanks where significant uplift is expected for horizontal earthquake loads | 15 | 7.5 | 10 | 5 |

# 5. NONLINEAR FLUID-STRUCTURE INTERACTION ALGORITHM

Fluid-structure interaction has fundamental interest in many application area of civil engineering. Common fluid-structure interaction problems include seismic analysis of fluid containing structures such as, fuel or water tanks and pressure vessels, dam-reservoir systems and nuclear vessels. The dynamic interaction problem between a structure and a fluid has been investigated with different procedures such as, Finite Element Method, coupled BEM–FEM approach, Finite Difference Method and coupled Finite-Infinite Element Method. However, Finite Element Method has been more widely used over the other methods because of its flexibility.

## 5.1. Fluid-Structure Interaction with FEM

The conventional finite element procedure for the solution of engineering and academic problems including fluid-structure interaction effects are usually based on a purely Lagrangian algorithm because of easy implementation of this algorithm. But, these problems generally involve large deformations and construction of new free surfaces and can not be handled by the same Lagrangian mesh during the entire simulation since severely distorted elements have low accuracy and their stable time step sizes are small for explicit time integration algorithms to continue the simulation (Belytschko *et al.*, 2000). In this case, a new mesh must be generated and the old solution must be transferred from the old mesh onto the new mesh. This remeshing process can be achieved by a rezoning method where automatic mesh generators are called internally to create a new mesh with a new topology (Benson, 1992). In the rezoning methods, the dependent variables, such as velocity, pressure, internal energy, stress components and plastic strain, are updated on the new mesh by using a remap algorithm. The other alternative to construct undistorted mesh is to use ALE algorithm which control mesh geometry independently from material geometry. ALE algorithm which contains both pure Lagrangian and pure Eulerian approaches was developed in an attempt to combine the advantages of the Lagrangian and Eulerian kinematical descriptions, while minimizing their respective drawbacks as far as possible. Unlike a rezoning method, the topology of the mesh is fixed in an ALE algorithm where only the mesh nodes are relocated to obtain a homogeneous and undistorted mesh.

The accuracy of an ALE calculation is often superior to the accuracy of a rezoned calculation because the algorithms used to remap the solution from the distorted to the undistorted mesh is a second order accurate for the ALE formulation when using second order advection algorithms, while the algorithm for the remap in the rezoning is only first order accurate. Figure 5.1 represents the movement of the material nodes with respect to mesh nodes in Lagrangian, Eulerian and ALE algorithms.
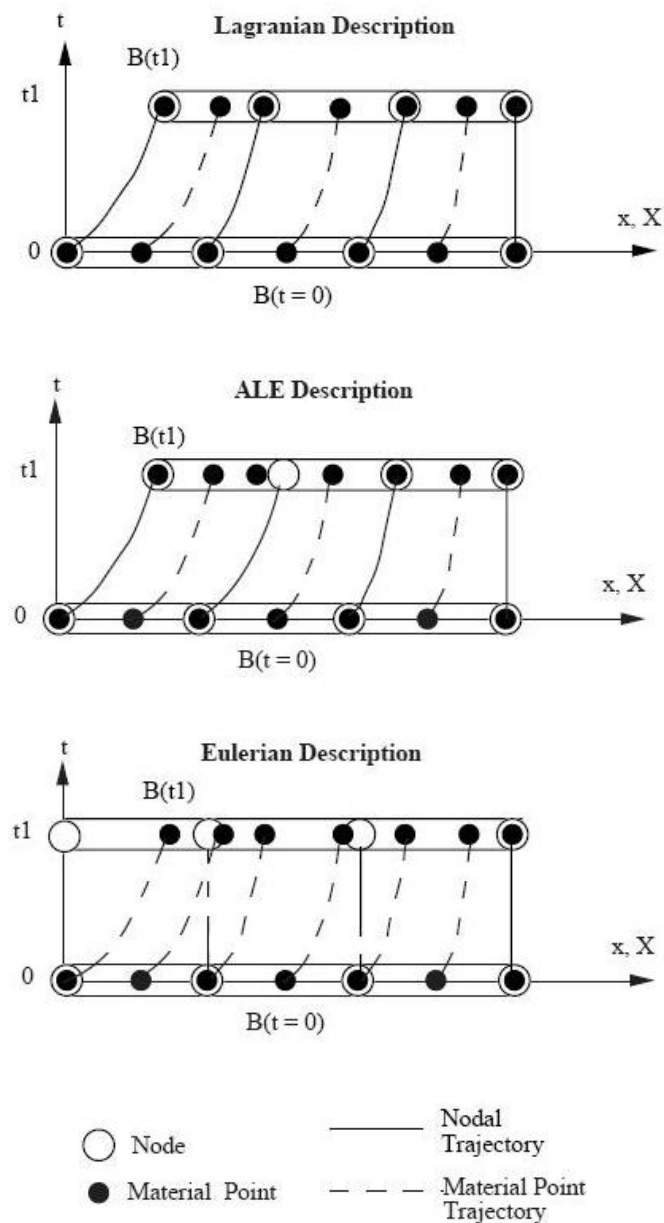


Figure 5.1. Space time depiction of a one dimensional Lagrangian, Eulerian, and ALE (Arbitrary Lagrangian Eulerian) elements (Courtesy of Belytschko *et al.*, 2000)

## 5.2. ALE Algorithm

ALE algorithm is based on the arbitrary movement of a referential domain, which is introduced as a third domain in addition to the common material (Lagrangian) domain and spatial (Eulerian) domain (Hughes, 1981). Total material time derivative of a physical property, f, at fixed initial (Lagrangian) coordinate is decomposed into a local derivative at fixed referential coordinate, describing the change of f with respect to this referential (ALE) configuration, and in a convective part that considers the relative motion of the referential (ALE) configuration with respect to the initial configuration. This relation can be formulized as follows:

$$\dot{f} = \frac{\partial f^r}{\partial t} + \vec{w}_i \frac{\partial f}{\partial x_i}$$

(5.1)

where, $f^r$ represents the function of the reference coordinate and $w$ is the convective velocity which is the relative motion of the velocity of the fluid particles $u$, and to the velocity of the reference coordinate (mesh) $v$:

$$\vec{w} = \vec{u} - \vec{v}$$

(5.2)

It should be remarked that both Lagrangian and Eulerian algorithms are a particular case of ALE algorithm. The Eulerian algorithm is derived by assuming that the reference coordinate (mesh) velocity is zero, therefore the relative velocity between the material and the reference configuration is the material velocity. The Lagrangian algorithm is obtained when the reference coordinate (mesh) velocity equals to material velocity which means convective velocity is null.

### 5.2.1. Governing equations for Fluid in ALE Algorithm

In order to compute interaction forces between fluid and structure, balance equations of both materials are defined with one of the kinematical description of continuum mechanics (Lagrangian, Eulerian and Arbitrary Lagrangian Eulerian) and solved utilizing boundary conditions and constitutive relations of materials. The balance equations for fluid

and structure are formulated with three conservation equations of mass, momentum and energy. Although fluid and structure are governed by the same balance equations, the constitutive equations, which describe material behavior and relate stress to a measure of deformation, of two materials are different. The conservation equations of mass, momentum and energy of fluid are formulated with Navier–Stokes equations which are solved to compute the fluid properties such as density, velocity and pressure.

Since material passes between elements of the computational mesh in ALE algorithm, the density has to be balanced explicitly to account for the conservation of mass during the non-Lagrangian deformation. The equation of mass conservation for a compressible Newtonian fluid in the ALE form is given by:

$$\frac{\partial \rho^r}{\partial t} + \rho \frac{\partial u_i}{\partial x_i} + w_i \frac{\partial \rho}{\partial x_i} = 0 \tag{5.3}$$

The conservation of momentum equation is expressed as:

$$\rho \frac{\partial u_i^r}{\partial t} + \rho w_j \frac{\partial u_i}{\partial x_j} = (\sigma_{ij,j} + \rho b_i) \tag{5.4}$$

The conservation of total energy equation for the ALE algorithm can be written by:

$$\rho \frac{\partial e^r}{\partial t} + \rho w_j \frac{\partial e}{\partial x_j} = (\sigma_{ij} u_{i,j} + \rho b_i u_i) \tag{5.5}$$

where $\rho$ is the density, e is the internal energy per unit volume, b is the body force and t is time. Total Cauchy stress, $\sigma$, is defined as the summation of the pressure and deviatoric terms:

$$\sigma = -P.Id + 2\mu \dot{\varepsilon} \tag{5.6}$$

where Id is the identity tensor, P is the pressure, $\dot{\varepsilon}$ is the strain rate tensor and $\mu$ is the dynamic viscosity of the fluid. The pressure term is obtained from equation of state which

relates pressure to density and internal energy, whereas constitutive equations are used to compute deviatoric part.

The term in Equations 5.3, 5.4 and 5.5 related to the convective velocity is usually referred as the advection term, and accounts for the transport of the material past the mesh. These additional terms in the equations make solving the ALE equations much more difficult numerically than the Lagrangian equations, where the relative velocity is zero. In the Eulerian form of Navier-Stokes equations, although the velocity of the reference coordinate (mesh), u, is zero, the Navier-Stokes Equations (Equations 5.3, 5.4 and 5.5) are not simplified, only the remeshing and smoothing processes are eliminated.

## 5.2.2. Governing Equations for Structure in ALE Algorithm

Although any of the Lagrangian, Eulerian or ALE algorithms can be used to model the fluid motion for fluid-structure interaction problems, the structure is always discretised with Lagrangian approach. Since in Lagrangian algorithm computational mesh nodes always follow the associated points of the material domain during motion, advection term does not exist. Mass conservation equation for structure is satisfied spontaneously. Momentum and energy conservation equations for Lagrangian algorithm can be given as follows respectively:

$$\rho \frac{d u_i}{d t} = \sigma_{ij,j} + \rho b_i \qquad (5.7)$$

$$\rho \frac{d e}{d t} = \sigma_{ij} u_{i,j} + \rho b_i u_i \qquad (5.8)$$

where σ is the total Cauchy stress given by:

$$\sigma = -P.Id + 2G\varepsilon \qquad (5.9)$$

In this formulation, G represents shear modulus and, ε symbolizes shear strain.

**5.2.3. Solution of Navier Stokes Equations in ALE Form**

There are two ways to solve Navier–Stokes equations in ALE form. In the first method, these equations with fully coupled form are solved by integrating forward in time which is very time consuming (Ghosh and Kikuchi, 1991 and Donea, 1983). The more widely favored approach is to employ operator split method, which breaks the governing partial differential equations into a series of simpler ones that are solved sequentially by splitting these equations in two distinct phases namely, Lagrangian and advection phases, in each time step.

Equations 5.3, 5.4 and 5.5 can be rewritten as follows in order to illustrate how splitting is applied to the ALE formulation:

$$\frac{\partial \phi}{\partial t} + w \frac{\partial \phi}{\partial x} = S(x,t) \qquad (5.10)$$

where $w$ is the convective velocity defined in Equation 5.2, $\phi$ are solution variables which are $\rho$, $\rho u$ and $\rho e$ and S is a source term.

Using operator splitting, the equation is re-written as two equations:

$$\frac{\partial \phi}{\partial t} = S(x,t) \qquad (5.11)$$

$$\frac{\partial \phi}{\partial t} = -w \frac{\partial \phi}{\partial x} \qquad (5.12)$$

The first equation has the form of the Lagrangian formulation (w = 0) and its solution is advanced with the Lagrangian step. The second equation includes only the term associated with the convection of the solution variable, and its solution is commonly referred to as the Eulerian step. The schematic view of the operator splitting is given in Figure 5.2.
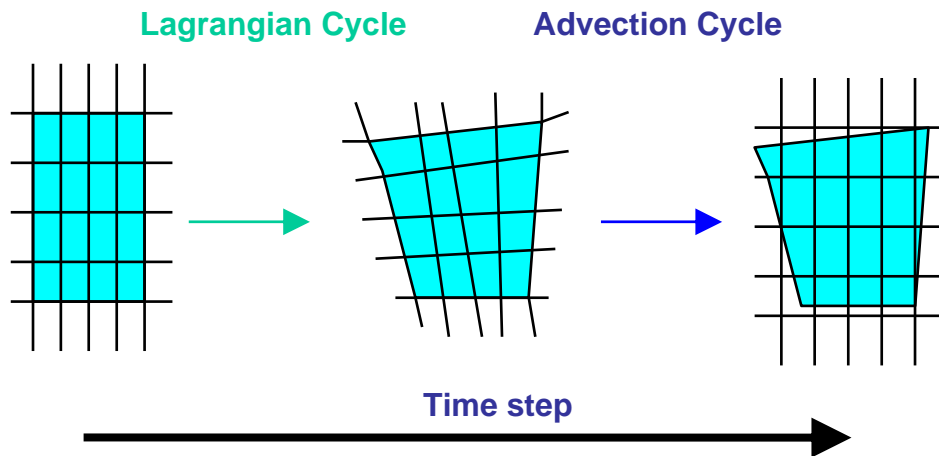
Figure 5.2. Schematic view of operator splitting

The overall flow of an ALE time step can be summarized as follows:

1. Perform a Lagrangian time step.
2. Perform an advection step.
   a. Decide which nodes to move.

   b. Move the boundary nodes.

   c. Move the interior nodes.

   d. Calculate the transport of the element-centered variables.

   e. Calculate the momentum transport and update the velocity.

**5.2.3.1. <u>Lagrangian Phase of Operator Splitting.</u>** In the first phase, all advective effects are neglected and the reference system is forced to follow the material flow as a Lagrangian manner. The physical material deformations are determined according to the equilibrium equations of Lagrangian phase (Equations 5.7 and 5.8) and the constitutive equations. The changes in velocity, displacement, pressure and internal energy due to the internal and external forces are calculated. Transport of material between elements is considered in advection phase. All the physics of the problem is carried out in the Lagrangian phase while the advection phase is purely computational.

From a discretization point of view, Equation 5.7 is computed using one integration point for efficiency and in order to eliminate locking (Benson, 1997). The zero energy modes are controlled with an hourglass viscosity (Flanagan and Belytschko, 1981). Although the continuity equation in partial differential equation form can be used to obtain current density in Lagrangian phase, its integrated form (Equation 5.1) which is more accurate is employed (Belytschko, 2000):

$$\rho J = \rho_0 \tag{5.13}$$

where $\rho$ is the current density, $\rho_0$ is the initial density and J is the volumetric strain given by the Jacobian:

$$J = \det\left(\frac{\partial x_i}{\partial X_j}\right) \tag{5.14}$$

where, $x$ denotes the current Cartesian coordinate, while $X$ is the reference (original) coordinate.

Central difference method, which is derived from Taylor series expansion, is employed to advance the position of the mesh in time using an explicit method in which the solution progresses without any iteration between consecutive time steps. In order to have a second order accurate scheme in time, the velocity must be staggered with respect to the displacement:

$$x^{n+1} = x^n + \Delta t \, u^{n+1/2} \tag{5.15}$$

The internal nodal forces which are a function of stresses and external forces associated with body forces and boundary conditions (boundary forces, non-reflection boundary forces and contact forces) are used to update the velocity in time:

$$u^{n+1/2} = u^{n-1/2} + \Delta t^n . M^{-1} . (F_{ext}^n + F_{int}^n) \tag{5.16}$$

where $F_{int}$ is the internal force vector and $F_{ext}$ is the external force vector and M is the diagonalized mass matrix. For each element of the mesh, the internal force is computed as follows:

$$F_{int} = \sum_{k=1}^{Nelem} \int_k B^t .\sigma .dv \qquad (5.17)$$

where B is the gradient matrix and $N_{elem}$ is the number of elements.

Since the central difference method is explicit, a finite stable time step size which is necessary for a sound wave to cross an element in the mesh must be below a critical value to provide numerical stability (Courant condition (Benson, 1992)):

$$\Delta t \le \frac{\Delta x}{c} \qquad (5.18)$$

where $\Delta x$ is the length of the smallest element in the mesh, c is the speed of sound in the material. For a solid material, the speed of sound is:

$$c^2 = \frac{\frac{4}{3}G + k}{\rho_0} \qquad (5.19)$$

$$k = \rho_0 \frac{\partial P}{\partial \rho} + \frac{P}{\rho} \frac{\partial P}{\partial e} \qquad (5.20)$$

where $\rho$ is the material density, G is the shear modulus, and P ($\rho$, e ) is the equation of state. In Equation (5.17), the second term on the right hand side accounts for the stiffening effect due to the increase of internal energy as the material is compressed. For a fluid material, $k = \rho_0 c^2$ in which $\rho_0$ is the mass density and c is the speed of sound. The viscosity of the fluid material is generally ignored in the calculation of the speed of sound. For sloshing problems the pressure component of stress is much greater than the deviatoric

part of the stress due to low the viscosity of the fluid, and the deviatoric stress is sometimes ignored.

**5.2.3.2. Mixture Theories for Multi-Material Elements.** ALE algorithm allows the finite element mesh to contain more than one material within the same element as well as each element can be restricted to contain a single material. For the single material ALE (SALE) case, the material interfaces are resolved directly by the finite element mesh as in the Lagrangian sense and no material fluxes over element boundaries have to be considered during the advection process.

Mixture theories are required to handle elements containing more than one material, which are commonly called mixed or multi-material elements (Benson 1992 and 1997). The interactions between the adjacent materials in a multi-material element are handled by the mixture theories. The mixture theory distributes the strain increment of an element among the materials in an element and calculates the element stress from the stresses in the materials. The simplest mixture theory gives each material the mean strain rate of the element. The limitation of this mixture theory is the error it introduces when an element contains a very soft material and a very hard material because both materials are forced to accept the same amount of strain. The mean stress mixture theory partitions the strain rate among the materials in the element so that all the materials have the same stress. Problem associated with mean stress mixture theory is that the response is overly soft. For example, in an element containing steel and vacuum, the stress will always be zero in the steel since the vacuum must have zero stress. For most problems, the linear distribution based on volume fraction of the volumetric strain during the Lagrangian phase also leads to incorrect results. The volume distribution should be scaled by the bulk compression of the materials in the element.

**5.2.3.3. Interface Tracking.** In multi-material ALE (MM-ALE) formulations, the interfaces between materials aren't required to follow the mesh lines. Lagrangian methods, level set methods and volume of fluid (VOF) methods can be used for tracking interfaces. Lagrangian methods use particles that are connected by line segments. Level set methods define a level set function that has a value of zero on the interface. The volume of fluid

(VOF) methods use the volume fraction of each material in an element and its surrounding neighbors to construct the interfaces within the element.

The most popular method to track interfaces between multi-materials are the volume of fluid method (VOF) (Hirt and Nichols, 1981) or the Young method (Young, 1982) which is attractive for solving a broad range of non-linear problems in fluid and solid mechanics such as, sloshing and explosion applications (Aquelet, 2003), because it allows arbitrary large deformations and enables free surfaces to evolve. Moreover, the Lagrangian phase of the VOF method is easily implemented in an explicit ALE finite element method. In this method, different material occurrences are considered by their respective volume fractions on the element level. For multi-material elements, the volume fraction of one fluid satisfies:

$$V_f \leq 1 \qquad (5.21)$$

The total stress by σ is weighed by volume fraction to get the fluid stress fields, as:

$$\sigma_f = \sigma \, V_f \qquad (5.22)$$

The Young or volume of fluid (VOF) method is originally developed to track an interface in elements containing two materials for two-dimensional problems. But, this method can be adapted for the three-dimensional problems. The material layout is described solely by the volume fraction repartition of the fluid material in the ALE elements. Specifically, a straight line using the simple linear interface calculation (SLIC) technique of Woodward and Collela (1982) approximates the interface in the cell. Interfaces are initially drawn parallel to the element faces. Then nodal volume fraction is computed to each node based on the fraction volumes of elements that share the same node. This nodal volume fraction repartition determines the slope of the material interface inside the element. The normal vector to the interface inside the element is defined by

$$\vec{n} = \frac{\overrightarrow{grad\,f}}{\left|\overrightarrow{grad\,f}\right|} \qquad (5.23)$$

where f is the nodal volume fraction. The position of the interface is then adjusted so that it divides the element into two volumes, which correctly matches the element volume fraction. The interface position is used to calculate the volume of the fluid flowing across cell sides. As the X-advection, Y-advection and Z-advection are calculated in separate steps, it is sufficient to consider the flow across one side only.

For the single material and voided element case, the same procedure is applied. For voided elements, the stress is zero. In the computational process, the elements loop goes only through elements that are not voided. For free surface problems, the elements that are partially filled ($V_f < 1$) define the free surface. The location of free surface in a sloshing problem is defined with interface-tracking algorithm.

**5.2.3.4. Advection Phase of Operator Splitting.** Tracking of interfaces of different materials in an element is followed by an advection phase in which the solution on the displaced mesh at the end of the Lagrangian phase is mapped into its original position for an Eulerian formulation or arbitrary position for an ALE formulation. In the advection phase, the hyperbolic transport equation (Equation 5.12) is solved successively for the history state variables with initial condition, $\Phi_0(x)$ which is the solution from the Equations 5.7 and 5.8 of Lagrangian phase at the current time. The total number of solution variables, including the velocity, is at least six and depends on the material models. For elements that are modeled with an equation of state, only the density, the internal energy, and the shock viscosity are transported. When the elements have strength, the six components of the stress tensor and the plastic strain must also be advected, for a total of ten solution variables. Kinematic hardening, if it is used, introduces another five solution variables, for a total of fifteen. The nodal velocities add an extra three solution variables that must be transported, and they must be advected separately from the other solution variables because they are centered at the nodes and not in the elements. In addition, the momentum must be conserved.

In advection phase, the time t is a fictitious time. Time step is not updated when solving for the transport equation. Lagrangian and advection phases are carried out within the same time step. There are different ways of splitting the Navier–Stokes problems. In

some split methods, each of the Lagrangian phase and advection phase is solved successively for half time step.

The two most desirable qualities in a transport algorithm are conservation and monotonicity. Conservation requires that the integral of the transport variable over the domain remain unchanged by the transport. Applying this requirement to the density, for example, is equivalent to requiring the conservation of mass. Not all the solution variables, however, are governed by physical conservation laws, *e.g.*, stress isn't conserved, but they are transported as if they are. Monotonicity requires that the transport not introduce any new maxima or minima in the solution or amplify existing ones. This means that no numerical oscillations will be introduced into the solution by the transport algorithm. From a practical standpoint, a minimum of second order accuracy is a third requirement. First order accuracy diffuses the solution excessively unless a very fine mesh is used in the calculation. Since the Lagrangian step generally is no better than second order accurate, third order or higher accuracy in the transport doesn't improve the overall accuracy of the solution.

For the solution of Equation 5.12, the Donor Cell algorithm, a first order upwind method and the second-order Van Leer MUSCL algorithm (Van Leer, 1977) can be used. In the Donor Cell algorithm, history state variables being transported, $\phi$, are piecewise constant with one-point integration. Although this algorithm is stable, conservative, simple and monotonic, it diffuses the solution very rapidly throughout the mesh due to constant representation of $\phi$ within the elements. Better accuracy is obtained by replacing the constant distribution of $\phi$ by a linear function, a quadratic function (PPM (Colella, 1984)), or a more general polynomial (*e.g.*, ENO (Harten 1989 and 1997 and Shu and Osher, 1988)). Any function that is introduced must satisfy two important conditions: 1) its integral over the element must equal the mean value located at the integration point times the element volume, and 2) its maximum and minimum values must be bounded by values in the surrounding elements to avoid introducing or amplifying maxima and minima.

Ideally, both momentum and kinetic energy should be conserved by the transport. Unfortunately this isn't possible while maintaining the monotonicity of the solution. As a consequence, the usual choice is to conserve momentum and accept some loss in the

kinetic energy. In general, momentum is advected instead of velocity to guarantee the conservation of momentum, and the velocities are calculated by dividing the values of the momentum at the nodes by the associated masses. The momentum advection is carried out after the element centered mass advection because the new masses are needed to calculate the new velocities from the momentum.

Momentum is a product of the node-centered velocity and the element-centered density. This imposes a constraint on how the momentum transport is performed that is unique to the velocity field. Two different approaches have been developed to modify element-centered transport algorithms to transporting the momentum. The first constructs a staggered mesh that has the nodes of the original mesh at the centroid of the dual mesh elements, and the staggered mesh nodes are defined as the centroids of the original mesh (Benson, 1992). The second constructs additional solution variables that are transported using a standard element centered transport method (*e.g.*, MUSCL-monotone upwind schemes for conservation laws) then reconstructs the velocity field after the transport.

A cell centered advection algorithm is applied to the staggered mesh for the momentum advection. The data necessary for the advection algorithm are the cell volume before and after the Lagrangian phase, nodal velocities, nodal masses and fluxes between cells. All the data are ready on the staggered mesh except for the fluxes. The new flux values on the staggered mesh are defined using a regular distribution of the fluxes from the original mesh element faces to the new element faces. Once the new flux on the staggered mesh is computed, the momentum advection is performed according to the following algorithm:

$$V^+ M^+ = V^- M^- + \sum_{j=1}^{Nbedges} V_j^- M_j^- \qquad (5.24)$$

where the superscripts '-' and '+' refer to the solution values before and after the transport. Values that are subscripted by j refer to the boundaries of the elements, through which the material flow, and the $V_j^-$ are the fluxes transported through the adjacent elements, these fluxes are computed using the staggered mesh. The flux is positive if the element received material and negative if the element is loosing material.

For the energy advection either internal energy or total energy can be used. If internal energy is advected, total energy can not be conserved and usually decreases with time because momentum advection does not conserve kinetic energy. The decrease in kinetic energy corresponds to the diffusion of velocity through the mesh. In order to solve this problem total energy is advected and the internal energy in an element is calculated as the difference between the total energy and kinetic energy.

### 5.3. Advantages of ALE formulation for Tank Problems

In order to solve complex tank-fluid interaction problems, an appropriate numerical simulation method, which can cope with large deformations of fluid free surface and the structure and accurately predicts the hydrodynamic forces due to impulsive fluid motion effects and the high-speed impacts of sloshing liquid on a tank wall and roof, is required. The nonlinear finite element techniques with either Lagrangian and/or Eulerian formulations may be employed as a numerical method to analyze tank problems. But, most of the Lagrangian formulations used to solve such problems fails due to high mesh distortion of the fluid and Eulerian formulation sacrifices some accuracy when interacted with structure. The Arbitrary Lagrangian Eulerian techniques with or without multi-material formulations are capable of keeping mesh integrity during the motion of the tank.

# 6. NUMERICAL MODELING OF 2D AND 3D SCALED TANKS

Numerical techniques in simulation of tank-fluid interaction problems are the most efficient tool to evaluate the dynamic response of system, since they can minimize the number of experimental tests that are time consuming, very costly and performed only for specific boundary and excitation conditions. Yet, before using numerical techniques for design purposes for the evaluation of different configurations of the fluid-tank systems when subjected to several earthquake ground motions, they should be validated by experimental results.

In this chapter, existing experimental studies carried out on 2D and anchored and unanchored cylindrical tanks are utilized for the verification of the applicability of the numerical procedure detailed in Chapter 5for tank problems when subjected to harmonic and earthquake ground motions. The response parameters of tanks such as, free surface sloshing wave height, pressure time histories, base uplift and shell stresses, obtained by numerical simulations are correlated with those of experimentally observed.

## 6.1. Sloshing in 2D Rigid Tank

The sloshing event inside a 2D rigid tank subjected to resonant and non-resonant harmonic motions is investigated with nonlinear fluid-structure interaction algorithm based on ALE algorithm defined in Chapter 5. Time histories of the free surface wave height obtained at specific locations by numerical method are compared with results of an existing experimental study and analytical solution. Experimental study carried out by Liu and Lin (2008) is considered as reference solution for the evaluation of the numerical findings. The tank dimensions and material properties of the numerical model are determined in accordance with this reference model. Moreover, analytical solution of sloshing problem which is based on the linear potential flow theory is used to compare the nonlinear effects of fluid sloshing with those of linear.

### 6.1.1. Analytical Solution of Rigid 2D Rigid Tank Problem

Motion of irrotational flow of an inviscid and incompressible fluid in a rigid tank is analytically represented by Laplace equation (Rodriguez and Graham, 1952). For a two-dimensional rigid rectangular tank when subjected to horizontal harmonic motion, $d_e = -D \, Sin(\omega \, t)$, at the base, the solution of Laplace equation under kinematic and free surface boundary conditions and kinematic boundary condition at the tank wall gives velocity potential $\Phi$ of the fluid (Faltinsen, 1978):

$$\Phi(x,y,t) = \sum_{n=0}^{\infty} Sin\left\{\frac{(2n+1)\,\pi}{2\,a}x\right\} Cosh\left\{\frac{(2n+1)\,\pi}{2\,a}(y+h)\right\}\left(A_n \, Cos(\omega_n \, t) + C_n \, Cos(\omega \, t)\right) \quad (6.1)$$
$$-\omega \, D \, Cos(\omega \, t)\, x$$

where;

$$A_n = -C_n - K_n / \omega \quad (6.2)$$

$$C_n = \frac{\omega \, K_n}{\omega_n^2 - \omega^2} \quad (6.3)$$

$$K_n = -\frac{\omega^2 \, D}{Cosh\left\{\frac{(2\,n+1)\,\pi}{2\,a}h\right\}} \frac{2}{a}\left(\frac{2\,a}{(2\,n+1)\,\pi}\right)^2 (-1)^n \quad (6.4)$$

Here, the origin of the Cartesian co-ordinate system (x, y) is defined at the centre of the free surface of the fluid. In these formulations, $2\,a$ is the length of tank and $h$ is fluid depth. D and $\omega$ is amplitude and circular frequency of the motion, respectively.

The free surface displacement, $\eta$, measured from the undisturbed liquid surface at equilibrium, and pressure, p, can be defined in terms of velocity potential function as follows:

$$p(x,y,t) = \rho \frac{\partial \Phi}{\partial t} \quad (6.5)$$

$$\eta(x,t) = \frac{1}{g}\frac{\partial \Phi}{\partial t} \qquad (6.6)$$

If Laplace equation is solved for free vibration of tank, the circular frequencies, $\omega_n$, of the sloshing modes can be obtained as:

$$\omega_n^2 = g\frac{(2n+1)\pi}{2a}\tanh\left(\frac{(2n+1)\pi}{2a}h\right) \qquad (6.7)$$

where, n is the mode number.

## 6.1.2. Numerical Modeling of 2D Rigid Tank Problem

In the numerical model, a three-dimensional rigid rectangular tank with a width of 0.57 m, breath of 0.31 m and total height of 0.30 m is filled with water ($\rho = 1000$ kg/m$^3$) up to a height of 0.15 m. In the numerical analyses, the fluid region is treated on a moving mesh using an ALE formulation whereas the structure is characterized with a mesh using a Lagrangian formulation. Nodes of fluid and structure at their interface are merged. The interior liquid is discretized with uniform mesh (Figure 6.1). The sizes of the Lagrangian shell and ALE solid elements are 0.01 m. The model is fixed at its base and harmonic motion is applied as displacement. Natural periods and frequencies of the sloshing obtained by Equation 6.7 are listed in Table 6.1.

Two loading cases are considered as resonance and non-resonance motions. In view of the first fundamental sloshing frequency, $\omega_0$, the excitation frequency of the first case is considered as $\omega = 0.583\ \omega_0$. The second loading is intended to simulate sloshing phenomenon under resonant frequency, therefore the excitation frequency is taken as the same as the first fundamental frequency. The amplitudes of the horizontal harmonic excitations are 0.005 m for both cases. Hydrostatic pressure field is generated increasing gradually until 1 sec. In order to optimize the fluid mesh, a moving ALE mesh that follows the structure motion is employed in the numerical analyses. The time step size is $1.0 \times 10^{-4}$ sec throughout the simulation.

In the experimental study (Liu and Lin, 2008), the time history response of free surface elevation is measured at three locations which were near left (*i.e.* x=-0.265) and right (*i.e.* x=0.265) ends of tank and at the middle of the free surface (*i.e.* x=0). Figure 6.2 and Figure 6.3 present the time history response of free surface elevations at three measurement locations that are extended to 20 s. For non-resonant frequency motion, the numerical solution of sloshing by the proposed method is in a quite acceptable agreement with both the reference solution and the analytical formulation in terms of elevation of free surface (Figure 6.2). For negative (downward) wave amplitudes, numerical results are more consistent than those of analytical, since numerical method takes into account nonlinear sloshing behavior. As it is expected, the wave height is almost zero at the middle of the free surface for each method.

For the resonant frequency case, the wave height increases continuously over time for all solution types at the near left and right end of the tank. The comparison of three solution methods reveals that analytical study overestimates negative surface amplitudes, whereas it underestimates the positive ones (Figure 6.3). Numerical and experimental results are highly consistent in terms of peak level timing, shape and amplitude of sloshing wave. The free surface displacement time histories obtained from numerical and experimental studies show that the positive (upward) sloshing wave amplitudes are always larger than the negative (downward) ones. This phenomenon is a classical indication of a nonlinear behavior of sloshing and caused by suppression effect of the tank base on the waves with negative amplitude. Although the gravity effects exist for both upward and downward fluid motion, the downward motion of fluid is blocked by the tank bottom. The ratio of positive amplitude to absolute negative amplitude increases as the fluid depth decreases. This phenomenon can not be observed from analytical solution because it is derived under linearized assumptions. This verifies that analytical method is not reliable for resonant frequencies where nonlinear sloshing behavior is extremely dominant. On the other hand, the present numerical algorithm can be used for the analysis of sloshing problems in practice for every frequency range of external excitation.

Table 6.1. Sloshing periods and frequencies of the tank model

| Mode Number | Circular Frequency | Frequency (Hz) | Period (sec) |
|:---:|:---:|:---:|:---:|
| 1 | 6.06 | 0.96 | 1.04 |
| 2 | 12.65 | 2.01 | 0.50 |
| 3 | 16.44 | 2.62 | 0.38 |
| 4 | 19.45 | 3.10 | 0.32 |
| 5 | 22.06 | 3.51 | 0.28 |
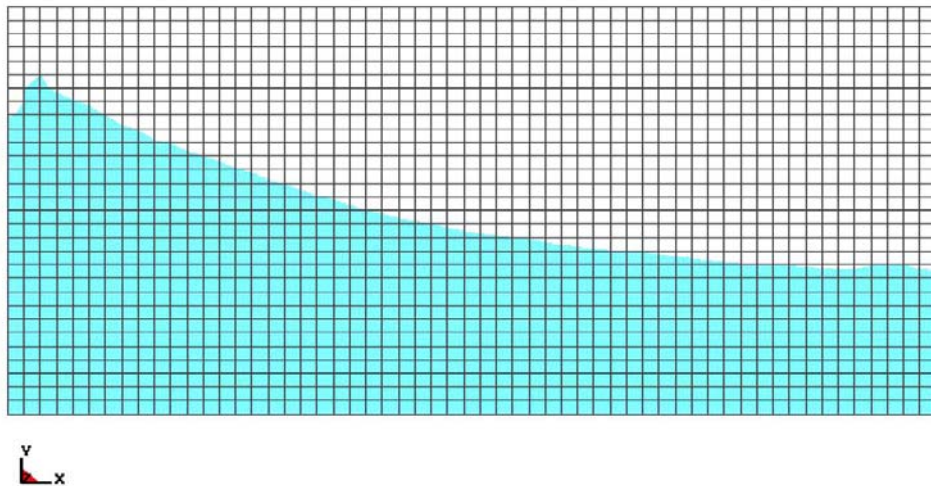


Figure 6.1. Finite element model of the rigid tank with fluid

The Fourier amplitude spectrum of the free surface wave height of resonant frequency case is given in Figure 6.4. It is observed that at the lower frequencies, three distinct peaks are clearly visible within the frequency range 0 to 3.0 Hz. The first peak occurs at approximately 1.02 Hz and has a significantly higher magnitude than at the other excitation frequencies. Secondary peaks are observed at 1.96 and 2.93 Hz. The first peak pertains to the first sloshing frequency of the fluid. The dominant frequency, corresponding to the first sloshing frequency of the tank, is analytically obtained as 0.96 Hz from Equation 6.7. The FE model and the analytical formulation provide similar results for fundamental sloshing frequency.
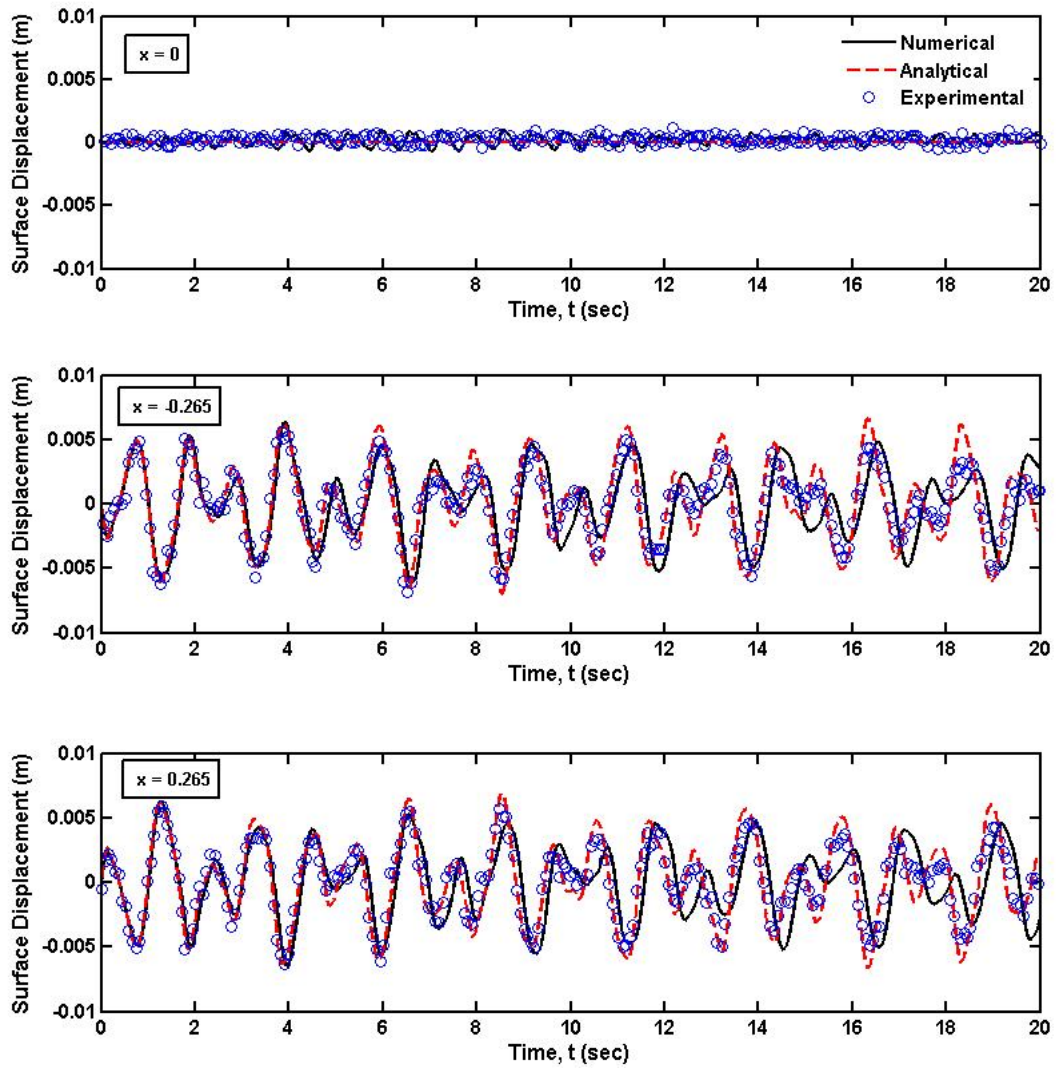
Figure 6.2. Comparisons of the time histories of surface elevation for the present numerical method, the analytical solution and experimental data (non-resonant case)
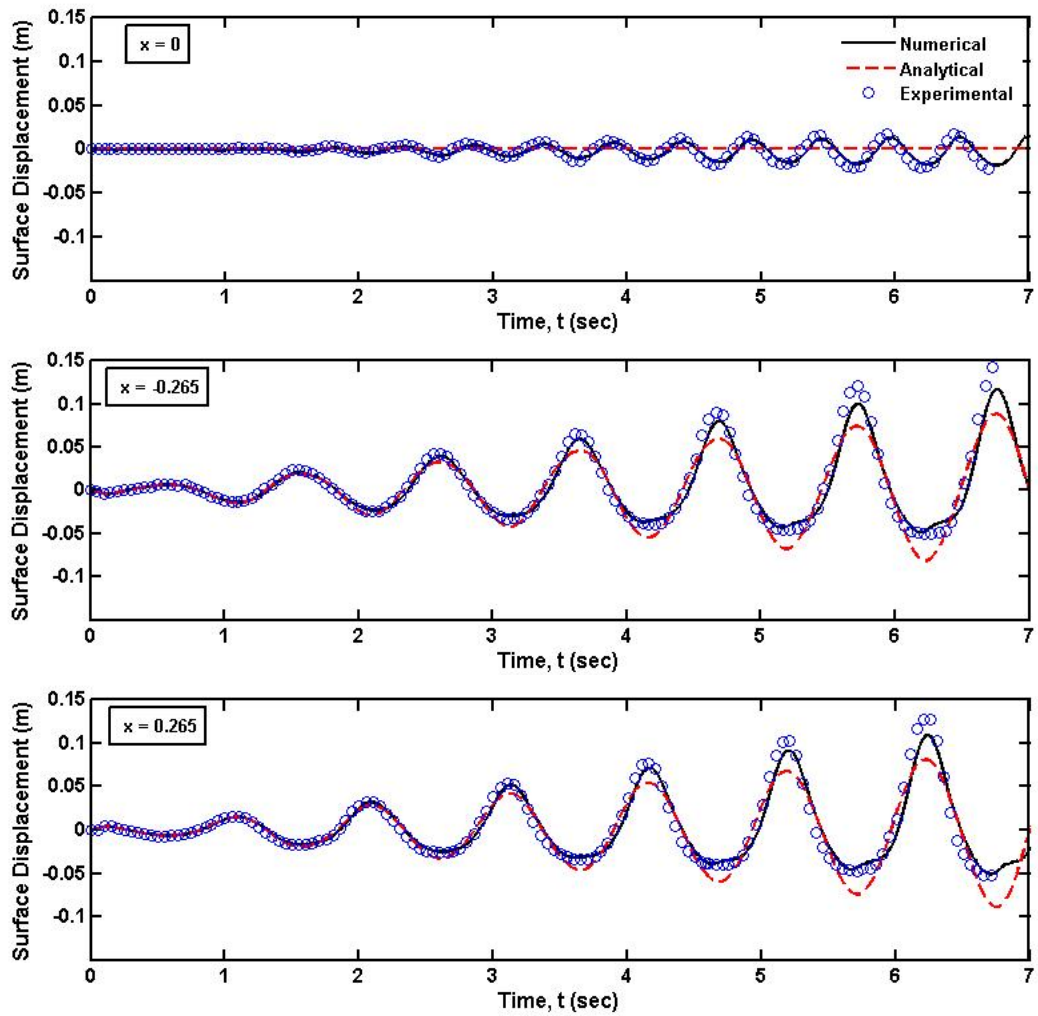
Figure 6.3. Comparisons of the time histories of surface elevation for the present numerical method, the analytical solution and experimental data (resonant case)
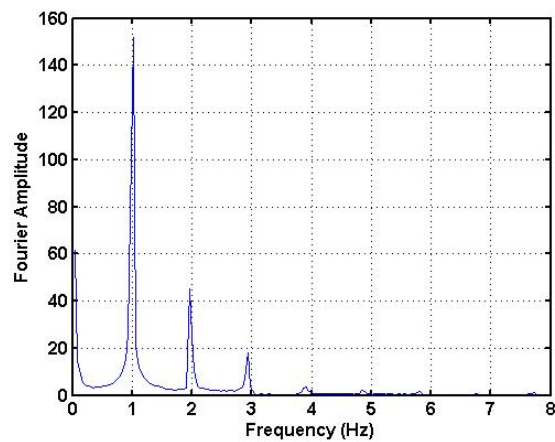


Figure 6.4. The Fourier amplitude spectrum of the free surface wave height of resonant frequency case

## 6.2. Verification for 3D Cylindrical Tank

For the verification of the numerical procedure which will be employed in Chapter 8 for the seismic assessment of real size cylindrical tank models, an existing experimental study carried out on anchored and unanchored tanks by Manos and Clough (1982) are used as reference solution for the tank problem.

In this experimental study, a series of static (tilt test) and dynamic tests were conducted on board tank model and the influence of various parameters such as, base fixity condition, the existence of cone roof at the top, the type and amplitude of ground motion and the stiffness of the foundation material, on the dynamic tank response was investigated. The tank model used in the experiments which is a 1/3 scale model of a steel prototype has a radius of 1.83 m and a total height of 1.83 m. Water ($\rho$ = 1000 kg/m3) is filled up to a height 1.53 m. The tank was made of aluminum with a density of 2700 kg/m3, elastic modulus of 71.0 GPa and yield stress of 100 MPa. The thickness of the aluminum bottom plate and the shell section nearest to the bottom was 0.002 m. The second tank shell course had a thickness of 0.0013 m. L shaped steel wind girder was placed on the top of the second tank shell course. Geometry of the tanks is shown in Figure 6.5. In the experiments, shaking table motion was derived from the horizontal component of the El Centro 1940 Earthquake with 0.50 g peak acceleration, and scaled with regard to time by $1/\sqrt{3}$ to account for similitude requirements. The horizontal earthquake motion in the north-south direction was introduced to the shaking table. The acceleration history and response spectrum of the input motion used in the experiments and numerical simulations are given in Figure 6.6.

### 6.2.1. Finite Element Models of Experimental Tanks

The numerical verifications are carried out for the model tank with open top, anchored and unanchored support condition and resting on rigid foundation. The same tank dimensions and material properties used in the experimental study are employed for the numerical model. For the unanchored tank case, a rigid shell is used to represent the ground underlying the tank and the interaction between ground and the tank base is modeled with the surface to surface contact algorithm. In order to find correct friction

coefficients, several analyses are performed by initially setting frictional coefficients based on code recommendations as a starting point. It is observed that friction coefficient in a range of 0.4-0.6 give almost the same response parameters. Increase the friction coefficient causes a small decrease in uplift displacement of the unanchored tank which leads to negligible decrease in the axial compressive stress in the tank wall which remains in contact with the ground. Therefore, static friction and dynamic friction are taken into account with coefficients of 0.50 and 0.45, respectively.
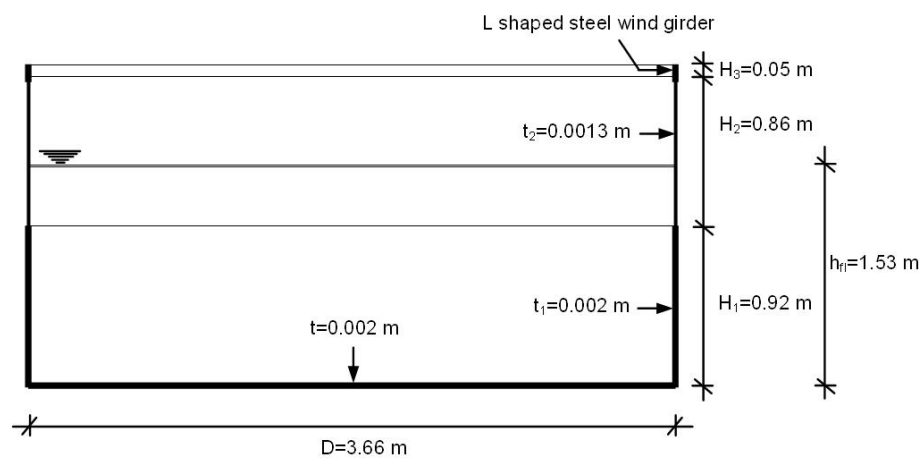


Figure 6.5. Dimensions of experimental cylindrical tank model



|       |       |
| :---: | :---: |
| (a)   | (b)   |
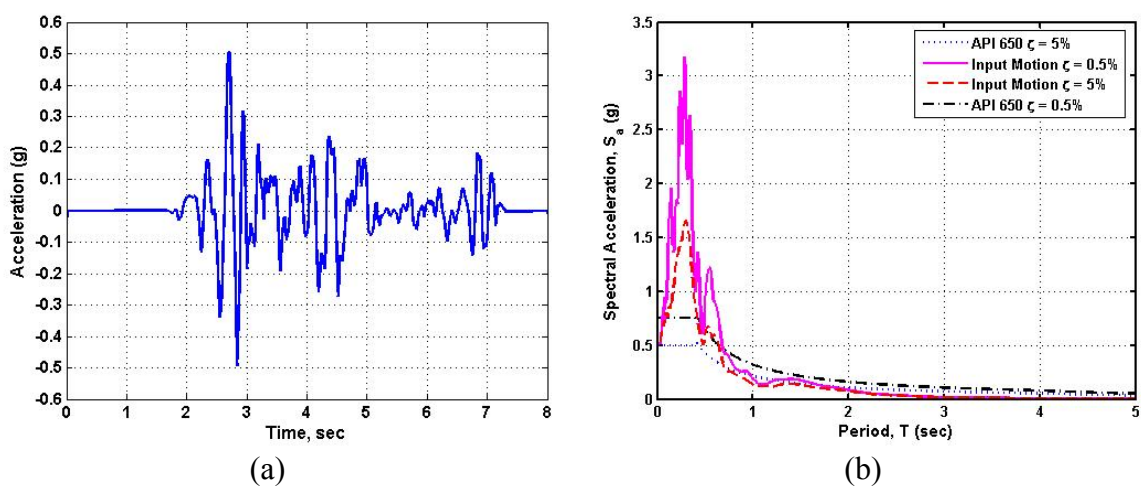
Figure 6.6. Horizontal table acceleration and its response spectra along with API 650 (2005) design spectra for 0.5 per cent and 5 per cent damping

Through the model development process, the effect of the element size and element formulation of both the tank and fluid are investigated and modified to accurately capture the interaction phenomenon between tank and fluid and coupling between tank and soil. Under-integrated shell element formulation causes penetration of tank base plate to the shell which is utilized to represent rigid soil, and fully integrated shell elements are used throughout the model.

Arbitrary Lagrangian Eulerian (ALE) description of the liquid-structure interface is employed in order to enforce compatibility between structure and liquid elements. Four noded fully integrated shell elements with 3 integration points through the thickness are used for the discretization of tank. The resulting finite element model of unanchored tank which has 12526 nodes, 3320 shell elements and 9408 solid elements is given in Figure 6.7. In the simulations, both material and geometric nonlinearities are considered. Since the free surface motion of fluid is nonlinear in reality, single plane of geometric and loading symmetries in the structure are not used in the analyses; the response of the whole system is determined. A vertical acceleration field of a 1 g is applied to give the correct hydrostatic pressure in the fluid.
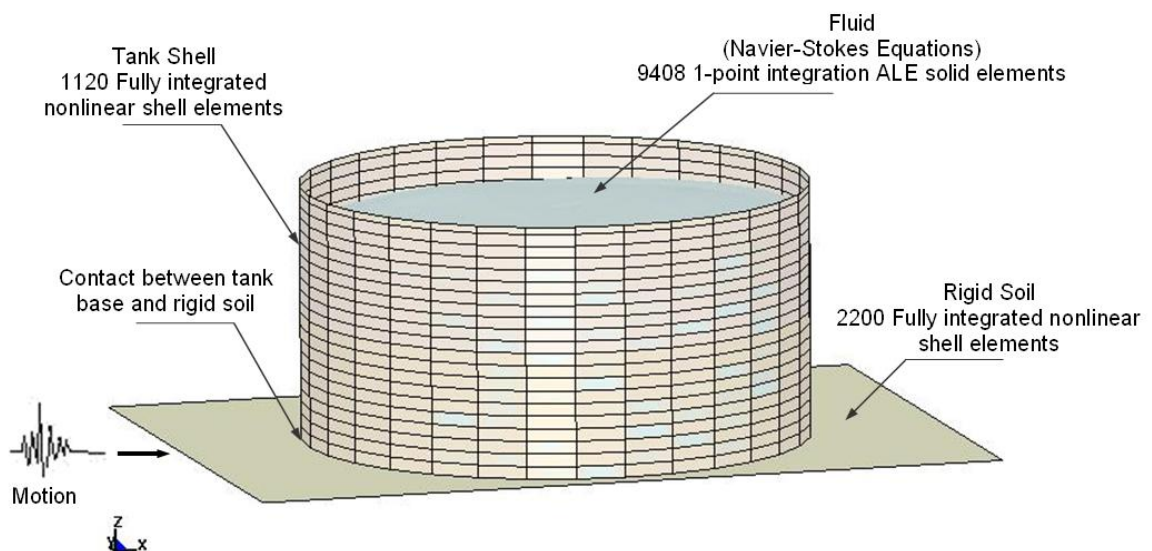


Figure 6.7. Finite element model of the unanchored tank

**6.2.2. Verification of Finite Element Models with Experimental Study**

The experimental study carried out by Manos and Clough (1982) includes a series of measurements of pressure, sloshing wave height, tank base uplift and tank shell stresses extending up to 7 sec. These response parameters are utilized as a reference solution for the numerical algorithm and the consistency of numerical results and experimental findings are assessed in order to evaluate the capability of the finite element method for transient dynamic response of anchored and unanchored liquid containment tanks when subjected to earthquake loads.

The time histories of pressure (excluding hydrostatic pressure) observed at two specific locations (r = 1.83 m with at height of 0.05 m and 0.45 m above the tank base) during the experiments are given in Figure 6.8 and Figure 6.9. Although, the pressure measurements of anchored tank model obtained from experimental and numerical studies represent very small phase differences, all numerical findings match perfectly with the corresponding experimental results. For the anchored tank, the numerical analysis is repeated for rigid tank assumption and it is observed that, tank wall flexibility does not affect the pressure distribution in time but it causes small amplitude high frequency oscillations in the response. The consistency of the experimental and numerical pressure measurements is also observed for the unanchored tank as it is shown in Figure 6.9. Figure 6.10 compares pressure measurements of anchored and unanchored tanks obtained from simulations and clarifies that the amplifications in the pressure response are caused by tank base uplift because this difference appears after tank base plate experiences uplift.

Figure 6.11 compares the base shear and overturning moment time histories of the anchored and unanchored tank models obtained from numerical analysis. According to this figure, both response quantities have similar distribution in time, but for both base shear and overturning moment, the unanchored tank have higher amplitudes than those of anchored tank. The only responsible factor for this amplification is the uplift behavior of the unanchored tank since it is observed during the time period when base plate lifts off from its foundation. Experimental results verify an increase in overturning moment peak response of unanchored tank, but the maximum overturning moment obtained from experiment is higher than that of numerical (Figure 6.11). The general insight in the

literature is that base uplifting reduces the hydrodynamic forces in the tank (Haroun and El Zeiny, 1995, El Zeiny, 1995 and Malhotra *et al.*, 2000). But, for the tank model under consideration, the overturning moment exerted on the unanchored tank is greater than that exerted on the anchored tank for both numerical and experimental studies. This can be attributed that the tank under consideration is a scaled model.

The time history responses of free surface elevation at four measurement locations (*i.e.* r = -1.72, -1.59, 1.59 and 1.72 m) are presented in Figure 6.12 and Figure 6.13. These locations are situated on the loading axis. Although, for some measurement locations, numerical method includes small deviations from experimental results, in general, numerical findings are highly consistent with the reference solution in terms of peak level timing, shape and amplitude of sloshing wave.
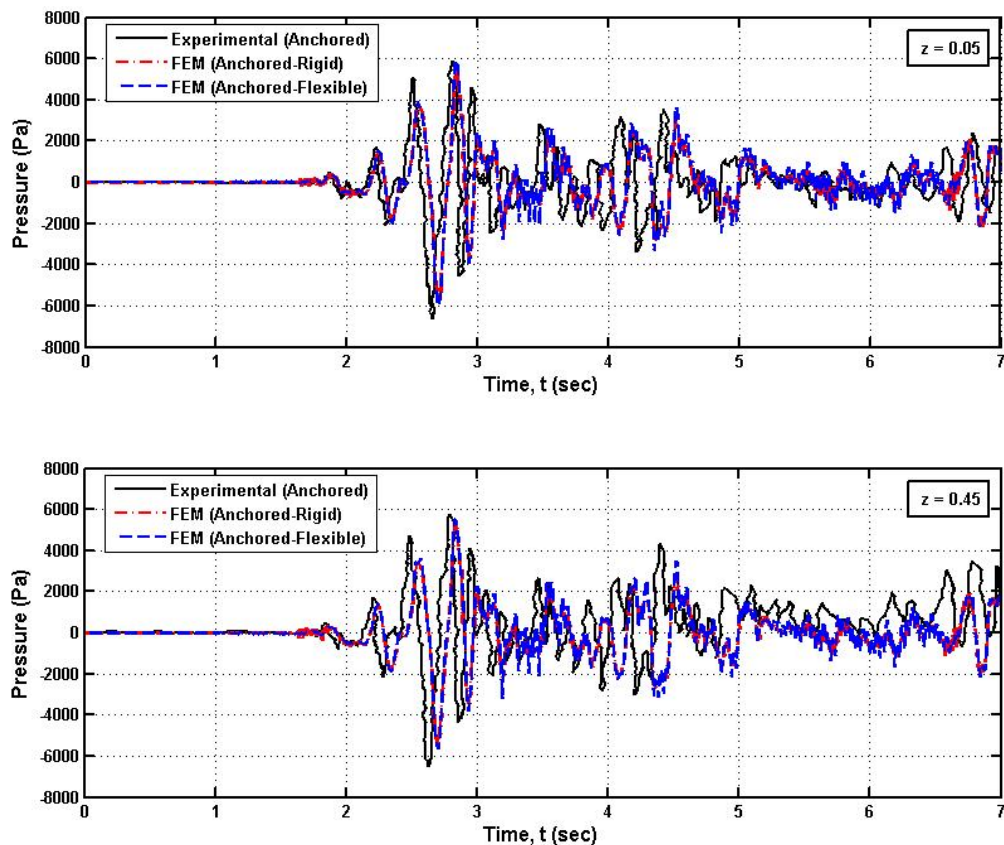


Figure 6.8. Comparison of the pressure time histories of anchored tank for the experimental and the numerical method results
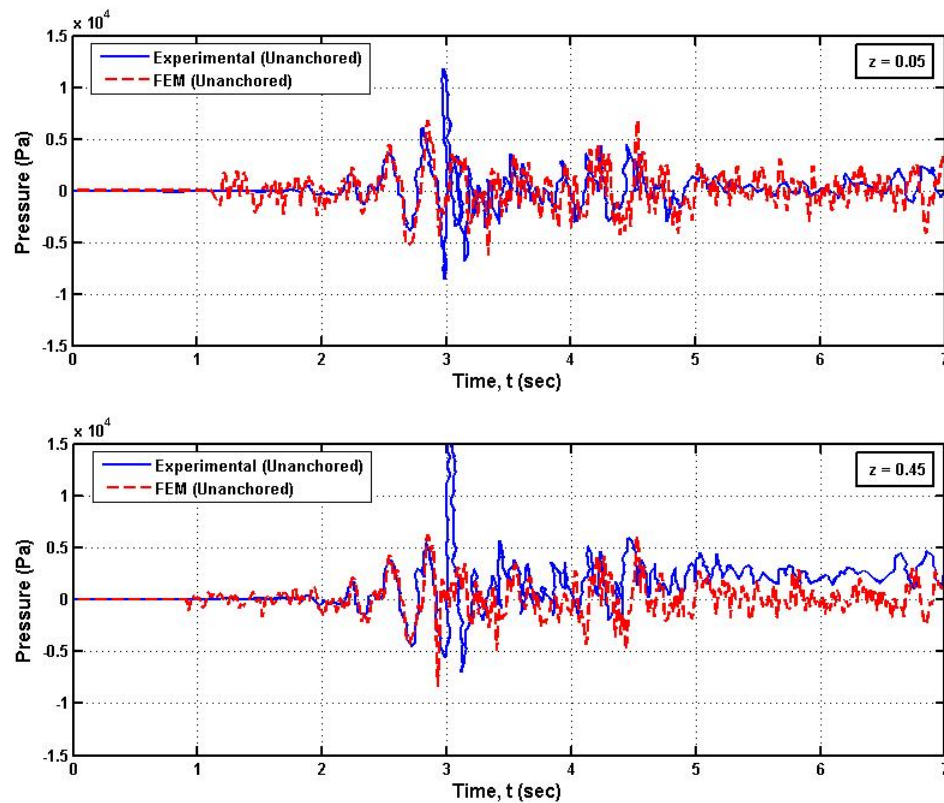
Figure 6.9. Comparison of the pressure time histories of unanchored tank for the experimental and the numerical method results

In order to examine the effect of tank wall flexibility on the sloshing wave height, the numerical analysis is repeated for rigid anchored tank and it is observed that rigid and flexible anchored tanks have exactly identical free surface wave profile (Figure 6.12). The numerical and experimental results for sloshing wave height are provided for both anchored and unanchored tanks in Figure 6.13. Although small oscillations are observed in the sloshing wave shape of the unanchored tank in the numerical results, the experimental study presents almost the same sloshing wave distribution in time for both support conditions. Therefore, analyses results verify that water free surface displacement responses for base free and base fixed cases are virtually identical.

Figure 6.14 presents time history responses of base uplift of the unanchored tank model measured at the left and right ends (r = - 1.83 m and 1.83 m) of the tank base plate. It can be noticed from these figures that the uplift displacements of experimental study include negative values although tank is settled on rigid ground. The numerical and
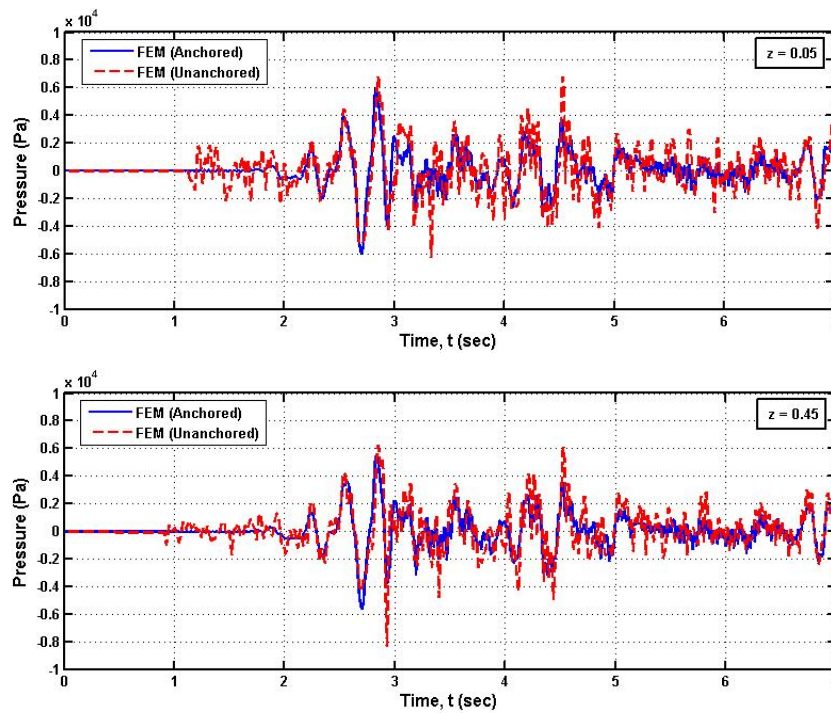
Figure 6.10. Comparison of the pressure time histories of anchored and unanchored tanks for the numerical method results
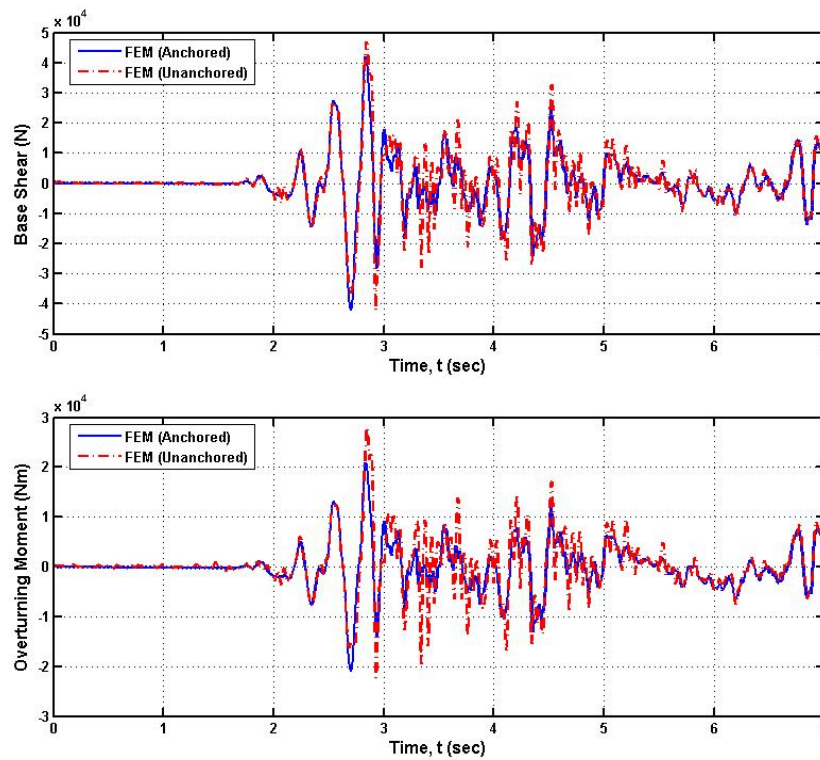


Figure 6.11. Base shear and overturning moment time histories of anchored and unanchored experimental tanks obtained by numerical analyses

experimental models lead to a relatively accurate description of the base uplift displacement for the input earthquake motion and the numerical method captures the amplitude and timing of peak uplift responses of experimental study perfectly.

The numerical analyses and experimental study results verify that the base uplifting completely changes the dynamic characteristics of the system and system response becomes highly non-linear. Uplift triggers out-of-round distortions of the circular tank shell cross-section. When the amplitudes of the motion are very small the out-of-round distortions of the tank shell decreases with the diminishing uplift. Yet, the fixed base tank almost remains its circular cross-section during dynamic response.

These out-of-round distortions have an important influence on tank stresses and pressures developed in the unanchored tank. Coupling between the uplift mechanism and the higher order distortions produces high compressive axial membrane stresses with a narrow distribution along the wall. While the axial stress response, for the fixed base case, is approximately five times smaller than the response of the free base case for the given input motion, hoop stresses magnify two times when the restraints of the tank base plate are released. Hoop stress level in the anchored tank is sensitive to the acceleration amplitude changes. The axial tensile membrane stress has smoother distribution for the fixed than for the free base case. This is attributed to the complicated deformation pattern associated with the uplift mechanism and to the catenary action of the tank bottom plate. Moreover, high compressive hoop membrane and axial bending stresses develop near the bottom of the uplifted part of the wall for the unanchored case.

## 6.2.3. Performances of Experimental Tank Models according to Code Recommendations

The provisions given in API 650 (2005), NZSEE (1986), and Eurocode-8 (2006) standards related to the analysis and modeling of ground supported vertical cylindrical steel tanks are applied to the tank models used in the numerical analyses and results are correlated in Table 6.2. In order to provide consistency between codes, the spectral base shear coefficients are obtained using the design spectra of API 650 (2005) code (Figure 6.6b) with 5 per cent and 0.5  per cent damping for the impulsive and convective

components respectively to evaluate the response parameters of tanks. Moreover, the acceleration response spectrum of the input motion used in the shaking table experiment is also utilized. Therefore, the importance of the consistency between the response spectrum of input motion time history used in the transient analysis and the code design spectrum is assessed. The importance, I, and response modification, R, factors are considered as unity. In order to compute total base shear and overturning moment, combination rules are taken as defined in the corresponding codes. In this section, the comments on the consistency of the experimental, numerical and code results of response parameters are explained in detail along with comparison of code procedures related to the response parameter under consideration.
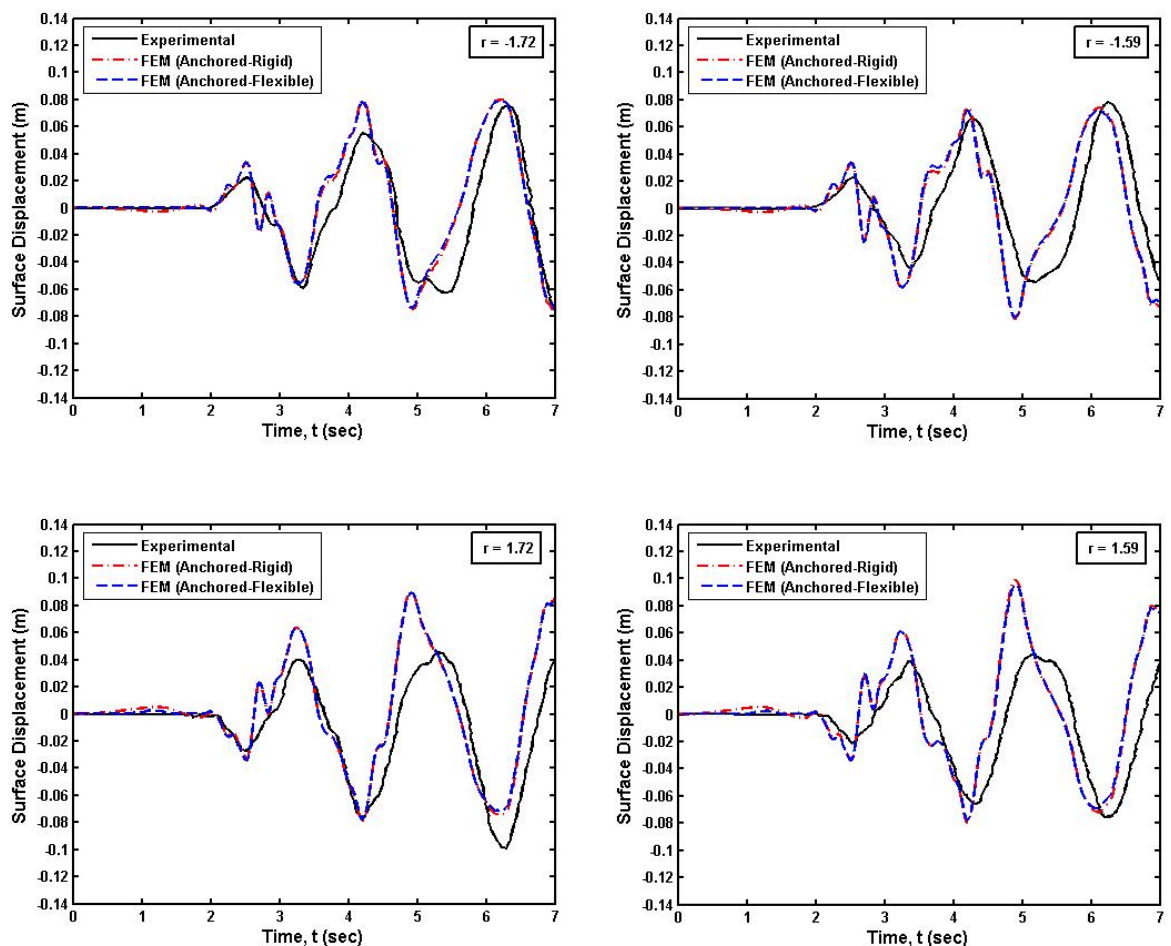


Figure 6.12. Comparisons of the free surface time histories of anchored tank for the experimental and numerical method results
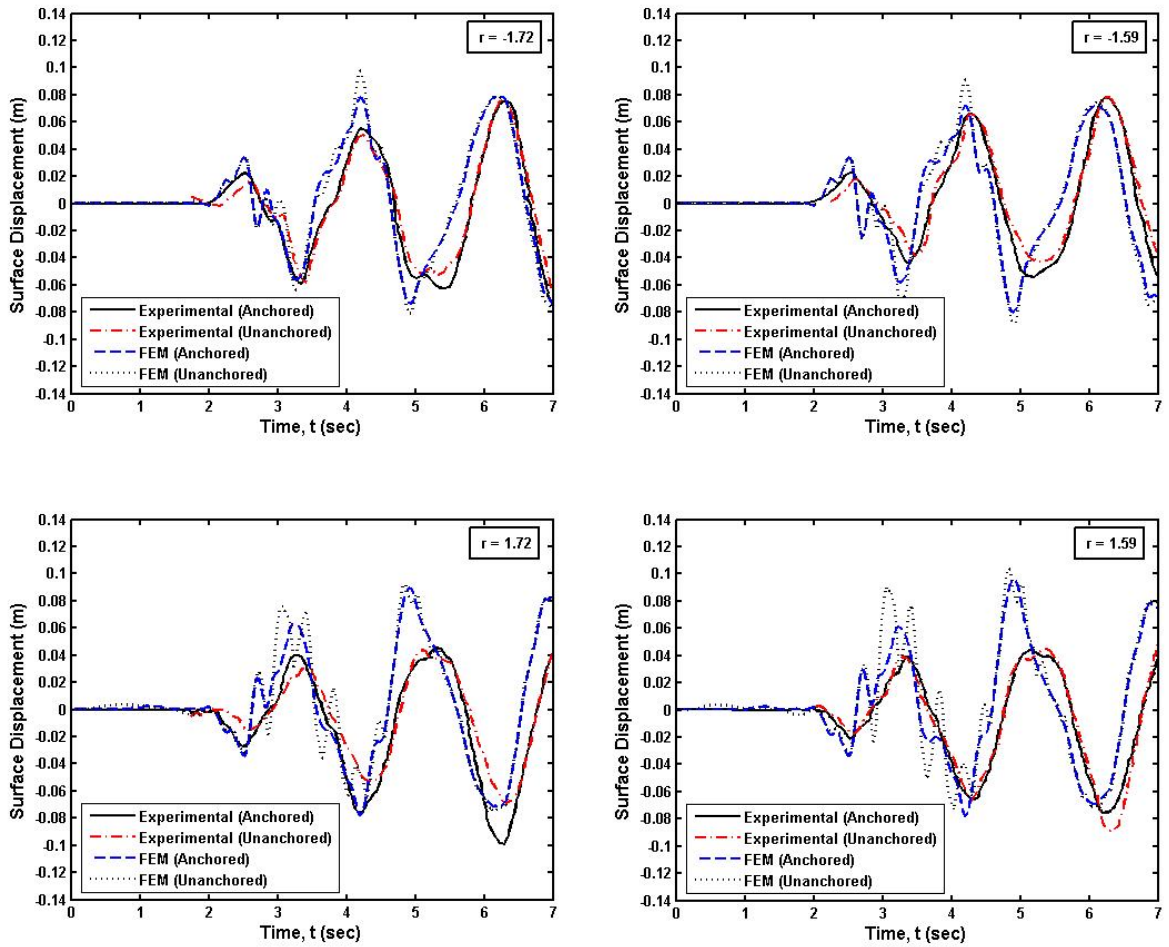
Figure 6.13. Comparisons of the free surface time histories for the experimental and numerical method results
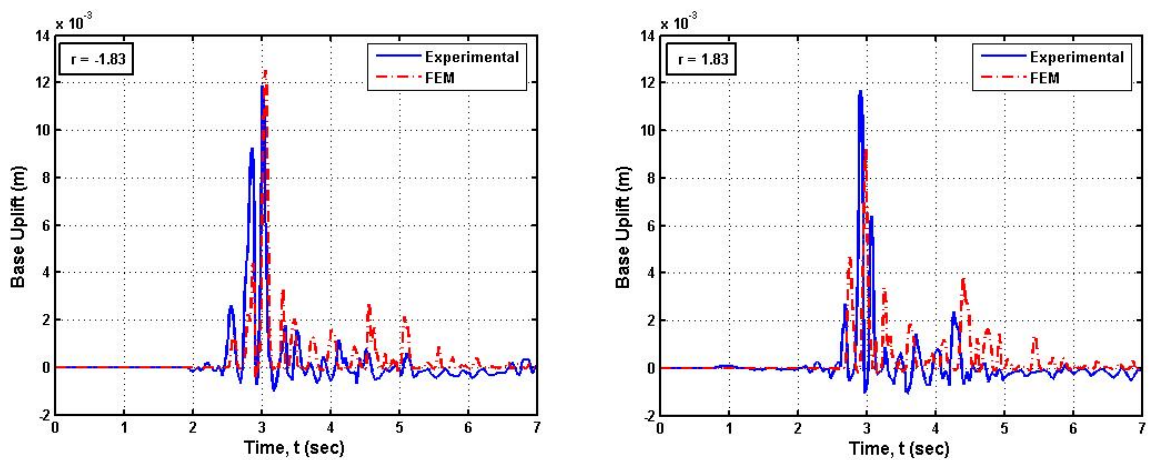


Figure 6.14. Comparisons of the uplift displacement time histories for the experimental and numerical method results

**6.2.3.1. <u>Pressure Distribution, Base Shear and Overturning Moment.</u>** In order to compare experimental and numerical results with code recommendations, the pressure distribution along the rigid anchored tank wall is plotted in Figure 6.15a and Figure 6.15b using design spectral acceleration coefficients of API 650 (2005) and input motion response spectrum, respectively. The combination rule for the impulsive and convective pressure components is applied as defined in the corresponding code. The pressure of 0.05 m above the tank base is obtained as 5940 Pa, 6330 Pa and 6850 Pa from the NZSEE (1986), API 650 (2005) and Eurocode 8 (2006) guidelines, respectively, when the design spectral acceleration values of API 650 (2005) standard is used. Numerical study defines 6000 Pa at the same location. The maximum pressure at $z = 0.45$ m is obtained as 5630 Pa, 5800 Pa and 6610 Pa NZSEE (1986), API 650 (2005) and Eurocode 8 (2006) guidelines, respectively, whereas, it is observed as 5900 Pa from the numerical analysis. Eurocode 8 (2006) predicts the highest value for pressure since it recommends direct sum to combine the impulsive and convective effects. These pressure values slightly reduce if the response spectral acceleration of the input motion is utilized. As can be seen from Figure 6.15, both numerical analysis and code provisions, especially NZSEE (1986) standard, lead close pressure values for the range up to 1.2 m of tank wall from its base, where the impulsive component of hydrodynamic pressure is more effective than the convective component. Near the free surface; where the convective component is dominant because impulsive pressure gradually approaches zero; the pressure values obtained from code provisions deviate from those observed by numerical study. This difference is less for response spectral of input motion than API 650 design spectrum coefficients. One possible reason for this difference is the inconsistency of the design and input motion spectra in the long period region. The second reason is that, during the peak pressure response, the height of free surface waves are less than sloshing wave height expected by code provisions. Therefore, contribution of free surface effects to the pressure response is small.

Overturning moments both above and below the base plate and base shear developed on model tank due to hydrodynamic forces are calculated following the procedures for fixed-base cylindrical tanks recommended by API 650 (2005), Eurocode 8 (2006) and NZSEE (1986) and they are summarized in Table 6.2. These three sources, experimental and numerical studies and code requirements, give very consistent values for overturning moment and base shear values. Utilizing response spectral acceleration of input motion,

both base shear and overturning moment slightly decrease, but the reduction in overturning moment does not significantly affect shell stresses.

**6.2.3.2.  Stress Levels of Tanks and Comparison with Allowable Limits.** As can be seen from Table 6.2, all code provisions predict the axial compressive stress in the anchored tank wall less than the experimental and numerical studies whereas axial compressive stress in the unanchored tank wall can only be evaluated according to NZSEE (1986) guidelines and this stress attenuates 4 times when tank base is fixed. Both API 650 (2005) and NZSEE (2006) methods of stress analysis lead the close hoop stress levels for anchored tank. Although any expression for hoop stress level in the unanchored tank wall is not provided in the seismic tank design codes, numerical study predicts an increase in the hoop stress level when tank base restraints are released.

For the tanks under consideration, the axial compressive and hoop stresses obtained as per minimum requirements of tank design codes are lower than the corresponding code allowable limits and finite element analysis results lie in the range of the code predictions. Therefore, tanks are not prone to buckling as per code requirements. Not only the experimental study but also the numerical findings support this result.

**6.2.3.3.  Sloshing Wave Height.** The maximum free surface displacements for anchored and unanchored tanks obtained from provisions of tank design codes are given in Table 6.2. It can be noticed that the sloshing wave height observed in the experimental study (8 cm) is considerably lower than that computed in accordance with code provisions. Codes predict wave height around 25 and 13 cm using base shear coefficient obtained from design spectrum of API 650 (2005) and response spectrum of input motion, respectively.

In the numerical and experimental results, the amplitude of surface displacement time history shows increasing trend up to 7 sec where experimental study was carried out. Due to the considerable difference in sloshing wave height obtained from provisions of codes and both the numerical approach and experimental results, the numerical analysis for tank model under consideration is extended to 18 sec of the input motion to observe maximum sloshing wave height during the effective duration of the earthquake record. It is observed that the maximum sloshing wave height occurs around 7 sec and after that free

surface oscillates between maximum and minimum limits but never exceeds its value at 7 sec. After the motion subsides, free surface gradually returns its quiescent position.

As a result, for the tank model under consideration, all code provisions overestimate the wave height of free surface and recommend very conservative value, especially when the design spectrum of API 650 (2005) is employed, while numerical method presents very consistent results with the experimental study. This discrepancy is also observed for total hydrodynamic pressure near the free surface of the fluid (Figure 6.15). It is worth to say that, the selected input motion records for the transient analysis should have response spectra consistent with the code design spectrum both in short and long period regions where the fundamental periods of impulsive and convective (sloshing) responses are dominant, respectively. The inconsistency of the design and input motion spectra in the long period region may breed significant difference in maximum free surface wave height and hydrodynamic pressure distribution near the free surface obtained from code provisions and those observed from transient analysis.

**6.2.3.4. <u>Base Uplift.</u>** In Table 6.2, the base uplift displacements obtained from tank design codes are given along with the experimental and numerical results. Maximum base uplift displacements of the unanchored tank predicted by NZSEE (1986) guidelines are significantly less than that of obtained by the experiment whereas API 650 (2005) recommends that tank must be anchored since uplift width exceeds the allowable value. NZSEE (1986) guidelines specifies 0.3 cm of maximum uplift displacement whereas experimental study gives 1.2 cm for the tank under consideration. The base uplift displacement can not be evaluated according to Eurocode 8 (2005) since normalized overturning moment of the examined tank out of range of the graphs given in this code. Numerical study predicts uplift displacement almost perfectly for the two extreme edges of the cylindrical tank on the loading axis (Figure 6.14).
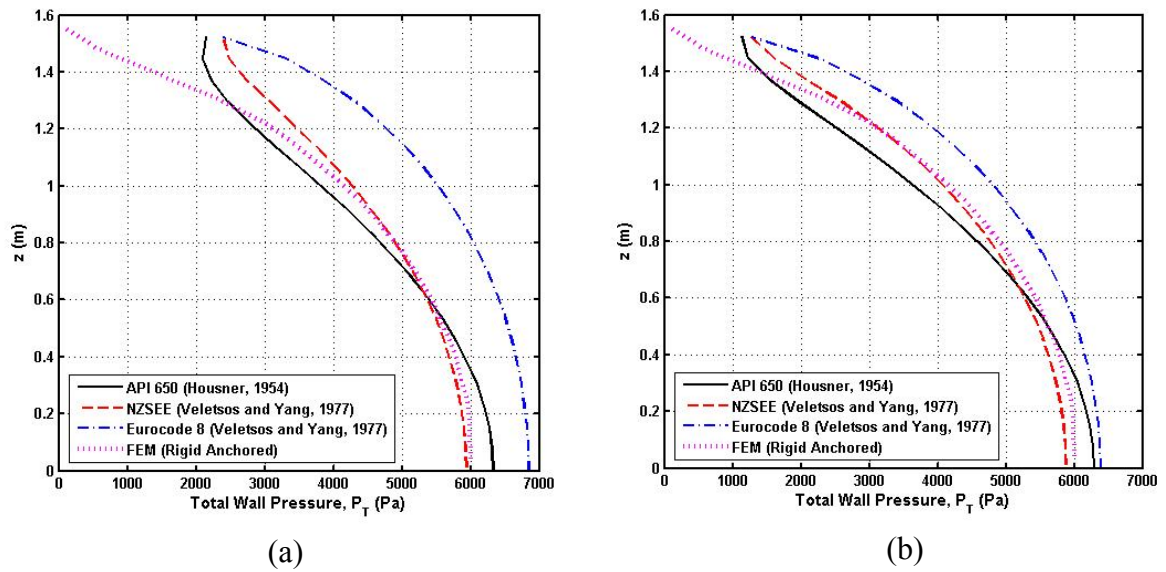
Figure 6.15. Total hydrodynamic pressure distribution on the rigid anchored tank wall obtained using design spectrum of API 650 (2005) and response spectrum of the input motion used in the experiment, respectively

### 6.2.4. Summary of Results

The results of the comparison of the reference experimental study, FEM analyses and code provisions for the response parameters of cylindrical anchored and unanchored tank models used in this section can be summarized as follows:

1. For the experimental tank model under consideration, all code provisions overestimate the maximum free surface displacement and recommend conservative value to provide necessary freeboard in order to prevent spilling of liquid and possible damage to the tank roof due to sloshing. However, numerical results are perfectly compatible with the experimental reference solution in terms of peak level timing, shape and amplitude of sloshing wave. Therefore, it can be justified that the numerical method is reliable for the analysis of sloshing inside a cylindrical tank subjected to earthquake excitation.

Table 6.2. Response parameters of the experimental tank models (units: N, m and sec)

| Parameter | Observed | | API 650 (2005) | Eurocode 8 (2006) | | NZSEE (1986) |
|---|---|---|---|---|---|---|
| | Exp. | FEM | Housner (1954) | Veletsos and Yang (1977) | Malhotra *et al.* (2000) | Veletsos (1984) |
| Impulsive Mode Period | 0.114 | - | - | - | 0.038 | 0.041 |
| Sloshing Mode Period | 2.00 | - | 2.10 | 2.10 / 1.18 | 2.12 | 2.10 / 1.18 |
| Max Sloshing Wave Height | 0.08 (anchored) / 0.08 (unanchored) | 0.09 (anchored) / 0.09 (unanchored) | $0.29^{++}$ {0.16} | 0.25 {0.13} | 0.29 {0.16} | 0.25 {0.14} |
| Base Shear | - | $4.62 \times 10^4$ (anchored) / $5.06 \times 10^4$ (unanchored) | $3.87 \times 10^4$ {$3.72 \times 10^4$} | $5.01 \times 10^4$ {$4.42 \times 10^4$} | $5.31 \times 10^4$ {$4.54 \times 10^4$} | $4.08 \times 10^4$ {$3.94 \times 10^4$} |
| Overturning Moment (excluding base pressure) | $2.75 \times 10^4$ (anchored) / $6.51 \times 10^4$ (unanchored) | $2.20 \times 10^4$ (anchored) / $3.08 \times 10^4$ (unanchored) | $2.38 \times 10^4$ {$2.18 \times 10^4$} | $3.41 \times 10^4$ {$2.89 \times 10^4$} | $3.72 \times 10^4$ {$3.06 \times 10^4$} | $2.67 \times 10^4$ {$2.50 \times 10^4$} |
| Overturning Moment (including base pressure) | | - | $5.54 \times 10^4$ {$5.36 \times 10^4$} | $6.52 \times 10^4$ {$5.74 \times 10^4$} | $7.14 \times 10^4$ {$6.08 \times 10^4$} | $5.00 \times 10^4$ {$4.82 \times 10^4$} |
| Shell Axial Membrane Stress for Anchored Tank | $4.90 \times 10^6$ | $3.30 \times 10^6$ | $1.25 \times 10^{6\,+}$ {$1.15 \times 10^6$} | $1.77 \times 10^6$ {$1.51 \times 10^6$} | $1.93 \times 10^6$ {$1.59 \times 10^6$} | $1.40 \times 10^6$ {$1.31 \times 10^6$} |
| Shell Axial Membrane Stress for Unanchored Tank | $2.57 \times 10^7$ | $2.20 \times 10^7$ | ** | * | * | $5.52 \times 10^6$ {$5.18 \times 10^6$} |
| Allowable Axial Membrane Stress Elastic Buckling | - | - | $2.64 \times 10^7$ | $2.44 \times 10^7$ | $2.45 \times 10^7$ | $2.44 \times 10^7$ |
| Elasto-Plastic Buckling | - | - | - | $2.77 \times 10^7$ | $2.76 \times 10^7$ | $2.77 \times 10^7$ |
| Hoop Stress | - | $1.70 \times 10^7$ (anchored) / $3.30 \times 10^7$ (unanchored) | $2.10 \times 10^7$ {$2.10 \times 10^7$} | - | - | $2.30 \times 10^7$ {$2.27 \times 10^7$} |
| Allowable Hoop Stress | - | - | $9.00 \times 10^7$ | - | - | $1.0 \times 10^8$ |
| Maximum Uplift of Unanchored Tank | 0.012 (left) / 0.012 (right) | 0.0125 (left) / 0.009 (right) | ** | * | * | 0.003 {0.003} |
| Plastic Rotation | - | - | - | *** | *** | 0.042 {0.042} |
| Allowable Plastic Rotation | - | - | - | 0.20 rad (11°) | 0.20 rad (11°) | 0.20 rad (11°) |
| Radial Membrane Stress in the Base Plate | - | - | - | *** | *** | $2.26 \times 10^7$ {$2.16 \times 10^7$} |
| Allowable Radial Membrane Stress in the Base Plate | - | - | - | $1.0 \times 10^8$ $(\sigma_y)$ | - | $1.0 \times 10^8$ $(0.6 \times \sigma_y)$ |

*     The parameter is the out of range of the graphs given in the corresponding code.
**    Tank should be anchored as per minimum API 650 requirements.
***  For the estimation of this quantity, the uplift height is necessary.

+    The shell stresses obtained in accordance with API 650 (2005) is multiply by 1.1 to convert seismic design forces from allowable stress design level to strength design level.
++   The upper and lower (placed in curly brackets) values are computed using design spectral acceleration of API 650 (2005) standard and response spectrum of input motion, respectively.

2. The substantial difference in free surface wave height and total hydrodynamic pressure near the free surface obtained from code provisions and those observed from numerical and experimental studies can be attributed to the inconsistency of the design and input motion spectra in the long period region. The response spectrum of selected input motion for the transient analysis should be consistent with code design spectrum for short and long period regions where the fundamental periods of impulsive and convective (sloshing) responses are dominant respectively.

3. Although small deviations are observed between sloshing wave shapes of anchored and unanchored tanks in the experimental and numerical results, water free surface displacement responses for base free and base fixed cases are virtually identical. Therefore, for the tank cases under consideration, the sloshing response of fluid free surface is almost insensitive to the support condition at the tank base.

4. Time histories of uplift displacement of tank base plate obtained by the finite element method are in a quite acceptable agreement with the experimental reference solution, although code provisions either predict very low value or recommend anchoring of tank or can not provide any value due to the fact that parameters of tank are out of range of the graph given in the corresponding code.

5. Perfect match of pressure time histories of the experimental and finite element method results are obtained for both anchored and unanchored tanks. It is observed that uplift behavior of tank base causes increase in the pressure response.

6. For unanchored tank model, uplift width, uplift height and axial compressive stress in the tank wall could not be evaluated according to Eurocode 8 (2006) since the normalized overturning moment is far outside the range covered by the graphs given in this code. Since plastic rotation of the base plate depends on uplift width and uplift height, this parameter also could not be compared with the other code provisions. The graphs presented in Eurocode 8 (2006) may be extended to cover wider range of the normalized overturning moment.

7. The numerical parameters such as friction coefficients and shell and fluid element formulations calibrated for anchored and unanchored tank models in this chapter is applied to a real size tank problem in Chapter 8 to evaluate its response under three-directional earthquake motion.

8. In tank design codes, the liquid exerted hydrodynamic overturning moments are assumed to be insensitive to the support conditions. For the tank models used in this study, overturning moments developed on the unanchored tank is higher than that of anchored tank for both experimental and numerical studies. Therefore, the effect of support condition on the overturning moment may be examined extensively for different tank proportions and fluid level heights.

9. It can be justified from compatible results of numerical and experimental studies that the finite element method is a reliable tool for the seismic analysis of not only anchored tanks but also unanchored tanks. Sloshing response, overturning moment, shell stresses and base uplift of tanks can be predicted with great accuracy by finite element method.

# 7. SELECTION OF INPUT MOTIONS FOR 3D TRANSIENT ANALYSES OF TANKS

Liquid storage tanks when subjected to intensive ground shaking generally behave beyond the linear elastic range due to nonlinearities associated with fluid-structure interaction, soil-structure interaction and sloshing. Therefore, dynamic tank behavior has to be assessed by transient analyses methods which take into account both material and geometric nonlinearities.

Seismic design codes generally define ground shaking in the form of a response spectrum of acceleration and allow using response spectrum compatible time history records in linear and nonlinear time history analyses. These records can be obtained from natural earthquake records, or can be generated synthetically and artificially. Use of real earthquake records has many advantages over the other record types: Real strong ground motion accelerograms contain wealth of information about the nature of the ground shaking, carry all the ground-motion characteristics (amplitude, frequency, and energy content, duration and phase characteristics), and reflect all the factors that influence accelerograms (characteristics of the source, path, and site). Yet, the input motions used in the transient analyses of tanks should satisfy seismological and geological conditions at a specific site such as, faulting type, magnitude, distance to fault, rupture directivity and site condition, and requirements defined in seismic codes. In many cases, strong motion earthquake records which satisfy these requirements and conditions may not exist. In such cases, the real earthquake records can be modified by spectral matching methods in either the time domain or the frequency domain in three ways: the spectral acceleration values of the selected time history are simply scaled up or down uniformly (time domain scaling); an actual motion is filtered in frequency domain by its spectral ratio with the design target spectrum (frequency domain scaling); elementary wavelets are added or subtracted from the real time history to match a target design spectrum, for example, RSPMATCH developed by Abrahamson (1993).

The difficulty of the spectral matching methods lies in trying to match a single ground motion to a design response spectrum that is not intended to represent the motion

from an individual earthquake (Naeim and Kelly, 1999). The design response spectrum is generally a result of a statistical analysis that considers the influence of several seismic sources simultaneously, whence the response at different periods may be driven by earthquakes in different sources and the spectrum is the envelope of spectra corresponding to scenarios in each of the sources (Reiter, 1990 and Bommer *et al.*, 2000). Therefore, it is expected that the response spectrum of time scaled records will not be consistent with the target spectrum throughout the full spectral range, but only over a portion of a specified range that is of interest to the design. Yet, the natural periods of liquid storage tanks occupy two separated ranges (impulsive modes which include vibrations of flexible tank and contained liquid interacting system have periods less than 1 second, while the typical periods of sloshing are very long, up to 6-10 seconds for very large tanks) and the selected ground motion for the transient analysis of tanks has to have enough energy not only at the lower periods but also at the higher period ranges.

## 7.1. Selection of Time History Records

Real earthquake records are selected to match specific features of the ground motion, generally based on either elastic response spectrum, or an earthquake scenario with the minimum parameters being the magnitude, distance and site classification. Guidance given in seismic design codes on how to select appropriate real records is usually focused on compatibility with the response spectrum rather than seismological parameters. Therefore, records are selected on the basis of strong-motion parameters such as peak ground acceleration, peak ground velocity, and duration to match a design response spectrum.

The ground motion time histories used to represent an intensity measure corresponding to a particular hazard level (or return period) should reflect the magnitude, distance, site condition, and other parameters that control the ground motion characteristics. Selection of records having appropriate magnitudes is important because magnitude strongly influences frequency content and duration of ground motion. It is desirable to use earthquake magnitudes within ± 0.25 magnitude units of the target magnitude (Stewart, 2001). Selection of records having appropriate fault-site distances is important especially for near-fault sites, because the characteristics of near-fault ground motions differ from those of other ground motions. Site conditions have a major effect on

the characteristics and frequency content of the strong ground motion records. Even though the ground motions are amplified in soft soils, the high frequency motions are attenuated. Generally, the ground motions amplification effects can be noticed in spectral acceleration of the records at intermediate to long period. Also, in order to preserve non-stationary characteristics of the initial time history, it is essential to start with an acceleration time history whose spectrum is as close to the target spectrum as possible in the period range of interest. A close initial fit also ensures a speedy convergence to the design values.

## 7.2. Ground Motion Scaling in Time Domain

In this approach, recorded motion is simply scaled up or down uniformly to best match the target spectrum within a period range of interest, without changing the frequency content. When dealing with more than one input time history, one can either use the same procedure to fit each record separately, or try to best-fit the average of the produced spectra to the target spectrum.

The procedure is based on minimizing the differences between the scaled motion's response spectrum and target spectrum in a least-square sense. The methodology proposed herein considers as "Difference" the squared scaled-to-target difference, evaluated by the integral,

$$\left| \text{Difference} \right| = \int_{T_S}^{T_F} \left[ \alpha \ S_a^{actual}(T) - S_a^{target}(T) \right]^2 dT \qquad (7.1)$$

where, $S_a^{target}$ is the target acceleration response spectrum, $S_a^{actual}$ is acceleration spectrum of the given (actual) time history, $\alpha$ is scaling factor, $T$ is period of oscillator, $T_S$ is lower period of scaling, and $T_F$ is upper period of scaling.

In order to minimize the difference, the first derivative of the "Difference" function with respect to the scaling factor has to be zero:

$$min \left| Difference \right| \quad \Rightarrow \quad \frac{d \left| Difference \right|}{d \, \alpha} = 0 \qquad (7.2)$$

By combining Equations 7.1 and 7.2, Equation 7.3 is obtained in a discrete form in terms of initial ($T_S$) and final ($T_F$) periods and step increment ($\Delta T$) of the response spectra range:

$$\alpha = \frac{\sum_{T=T_S}^{T_F} (S_a^{actual} \, S_a^{target})}{\sum_{T=T_S}^{T_F} (S_a^{actual})^2} \qquad (7.3)$$

### 7.3. Criteria for Scaled Records and Limits of Scaling Factors

Turkish Seismic Design Code (2007) provides some restrictions for the scaled real earthquake ground motion records. The peak ground acceleration of the scaled ground motion should not be smaller than zero period spectral acceleration of the target spectrum, $A_o$ g. In the range of periods between 0.2 $T_1$ and 2$T_1$, where $T_1$ is the fundamental period of the structure in the direction earthquake motion, the 5 per cent damped elastic design acceleration spectrum values of the scaled ground motion should not be less than 90 per cent of the corresponding value of the 5 per cent damped elastic design spectrum, $A_o$ I S(T) g. The duration of the strong motion part shall neither be shorter than 5 times the fundamental period of the building nor 15 seconds. Moreover, in transient analyses, a minimum of 3 accelerograms should be used and design is carried out in accordance with the maxima of the results obtained from time history analyses. If at least seven ground motions are used the mean values of the results can be considered for design.

In the literature, there certain limits on the scaling factor depending on the type of problem to which the resulting motion will be applied. For the analysis of linear elastic structures an upper limit of 4 could be accepted (Vanmarcke, 1979 and Krinitzsky and Chang, 1977), for nonlinear analyses, scaling factors ($\alpha_{AT}$) in the range of 0.5 to 2.0 are advised. For liquefaction problems a scaling factor ($\alpha_{AT}$) not greater than 2 should be used.

### 7.4. Target Spectra

Metal cylindrical ground-supported tanks are widely constructed in Turkey especially to store petrochemical products. However, there is no Turkish Design Code (2007) for the seismic analysis of tanks and liquid storage tanks are designed as per minimum requirements of international codes. API 650 (2005), Eurocode 8 (2006) and NZSEE (1986) standards are the most commonly referred ones among the others in current practice. Since this thesis includes the assessment of seismic behavior of liquid containment tanks constructed in Turkey with typical size, the design spectra provided in Turkish Seismic Design Code (2007) are utilized as target spectrum.

The design earthquake considered in the Turkish Seismic Design Code (2007) corresponds to high intensity earthquake for residential buildings where the probability of exceedance of the design earthquake within a period of 50 years is 10 per cent. Seismic zones cited in the specification are considered as first, second, third and fourth seismic zones depicted in Seismic Zoning Map of Turkey (2006) prepared by the Ministry of Public Works and Settlement and issued by the decree of the Council of Ministers. The spectral acceleration coefficient, A(T), to be considered for determining seismic loads is given by following equation:

$$A(T) = A_o \ I \ S(T) \tag{7.4}$$

where, spectrum coefficient curve, S(T), is described in terms of local site classes characterized by spectrum characteristic periods, $T_A$ and $T_B$ for 5 per cent damping. The effective ground acceleration coefficient, $A_o$, introduced to define the peak ground acceleration of the specified seismic zone. The building importance factor, I, is dependent on the purpose of occupancy or type of building and defined in the range of 1.0 to 1.5. The elastic spectral acceleration coefficient curves, A(T), for all the seismic zones and local site classes are shown in Figure 7.1.
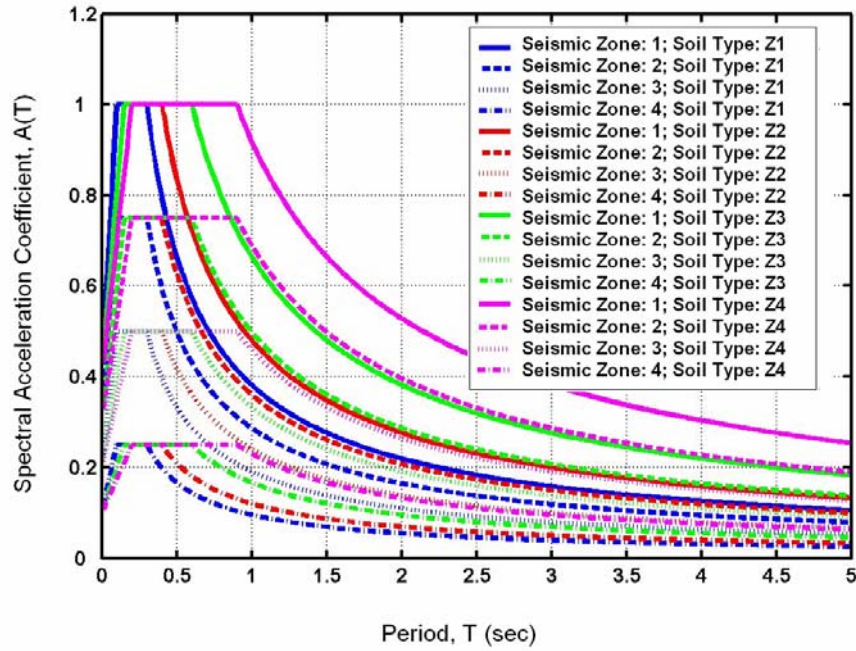
Figure 7.1. Turkish Seismic Design Code (2007) elastic design acceleration spectra for four seismic zones and different local site classes

In Equation 7.3, it can be noticed that the spectral acceleration coefficient curves, $A(T)$, has the same shape of spectrum coefficient curve, $S(T)$, multiplied by a constant factors representing effective ground acceleration, $A_o$, and building importance factor, $I$. Therefore, the scaling factor, $\alpha_{AT}$, for acceleration coefficient, $A(T)$, can be obtain by multiplying the scaling factor, $\alpha_{ST}$, of the corresponding spectrum coefficient, $S(T)$, which is obtained by using Equation 7.3 for the target spectrum by the effective ground acceleration, $A_o$, and building importance factor, $I$:

$$\alpha_{AT} = A_o \; I \; \alpha_{ST} \qquad (7.5)$$

For the transient analysis of tanks supported on rigid ground, Z1 soil class is assumed. In order to take into account the soil effects on tank behavior, Z3 soil type is selected and spring elements are used to represent the soil. In all of the analysis, the tank is assumed to be located at the 1st seismic zone ($A_o = 0.4$) and the importance factor, $I$, is considered as 1.5. Response modification factor, R is taken as 1 for NZSEE (1986) and

Eurocode 8 (2006) code computations. For API 650 (2005), response modification factor is used in accordance with the recommended value in this code.

Due to the fact that the vertical response spectrum is not specified in the Turkish Seismic Code (2007), the two thirds of the horizontal spectrum coefficients are used for those of vertical.

## 7.5. Selection and Scaling of Ground Motion Records for Seismic Analyses of Tanks

Pacific Earthquake Engineering Research (PEER) Center, NGA strong motion data base (2006) is one of the biggest earthquake data base on the world. It includes 4062 records from 92 shallow crustal earthquakes in active tectonic regions around the world. All records in this data base have been processed in a consistent manner and are referenced to specific ground conditions. Since the tank model under consideration is constructed in Turkey, the accelerograms recorded during the major earthquakes occurred in Turkey are selected from the PEER strong motion data base to find the best matched real earthquake records to the target spectrum within the period range of interest. The methodology employed for time domain scaling can be summarized in the following steps:

1. A list of acceleration time histories recorded during the earthquakes occurred in Turkey is prepared using PEER database simply based on magnitude, filtering frequency ranges and site condition. The records which were filtered more than 0.1 Hz with high pass filter are eliminated in order to not to loose the energy required to excite fundamental mode of sloshing. Remaining records are grouped according to site class of the target spectrum.

2. The acceleration response spectra of the each earthquake record including two horizontal and vertical components of the records are computed using MatLab Code for the solution of linear elastic single degree of freedom system of 5 per cent damping ratio using piecewise exact method (Aydınoğlu and Fahjan, 2003).

3.  The scaling factors, $\alpha_{ST}$, of each earthquake record component are individually calculated in accordance with Equation 7.3 for period range ($T_S$=0.01 sec - $T_F$=10 sec).

4.  The records with time duration less than proposed by (TSDC, 2007) and those with scale factors, $\alpha_{AT}$, less than 1/5 or greater than 5 are eliminated.

5.  The absolute summation of relative error for each record is computed for the period range ($T_S$=0.01 sec – $T_F$=10 sec) according to following formulae:

$$\left| \text{Sum Relative Errors} \right| = \sum_{T_S}^{T_F} \left\| (\alpha \, S_a^{actual}(T) - S_a^{target}(T)) / S_a^{target}(T) \right\| \qquad (7.6)$$

6.  The percentage of average relative error are also calculated as follows:

$$\left| \text{Average Relative Error (\%)} \right| = \frac{1}{k} \left| \text{Sum Relative Errors} \right| \times 100 \qquad (7.7)$$

where, k is the number of period steps ($\Delta T$) defined in the period range for the spectra

$$k = (T_F - T_S) / \Delta T \qquad (7.8)$$

7.  The records which have minimum average relative error values and small scale factors are selected.

By applying the procedure summarized above, the first 8 records which have minimum average relative error values and small scale factor are selected. Since period range of interest is so wide, the scaled records are not very consistent with the target design spectrum especially in the long period ranges. A transient analysis is carried out with one of the scaled real earthquake records and it is observed that sloshing wave heights computed in accordance with the provisions of current seismic tank design codes (API 650 (2005), Eurocode 8 (2006) and NZSEE (1986)) are very high in comparison with the transient analysis result. Therefore, it is concluded that the response spectrum of selected

input motion to be used in the transient analysis should be consistent with design spectrum not only in the short period region of the design spectrum where period of impulsive flexible component takes place but also long period region of design spectrum where period of oscillation of convective (sloshing) effects. Hence, time domain scaling procedure should be improved in order to obtain more consistent records not only in the impulsive period range but also in the vicinity of the sloshing period. As a result, in order to obtain the best matched records to the target spectrum throughout the period range of interest, the scaled real earthquake ground motions are reprocessed using time domain spectral matching techniques.

## 7.6. Spectral Matching in Time Domain

One approach for spectral matching is to adjust the original record iteratively in the time domain to achieve compatibility with a specified target acceleration response spectrum by adding wavelets having specified period ranges and limited durations to the input time history. These wave packets are added at times where there is already significant amplitude in that period range in the time history. Although this procedure is more complicated than the frequency domain matching procedure, in most cases it preserves the overall phasing characteristics and as the time varying (*i.e.*, non-stationary) frequency content of the ground motion and introduces less energy into the motion (Somerville, 1998). The resulting records each have an elastic response spectrum that is coincident (within a tolerance) with the target spectrum. Adjusted ground motions possess desired frequency content and peak ground acceleration without significantly altering the time signature of the original ground motion. Wavelet adjustment procedure to recorded accelerograms was first proposed by Kaul (1978) and was extended to simultaneously match spectra at multiple damping values by Lilhanand and Tseng (1987). Abrahamson (1992) modified the Lilhanand and Tseng algorithm and developed the RSPMATCH software.

The input motion used in spectral matching technique should be obtained from earthquakes of similar magnitudes and located at similar distances to those that contribute most significantly to seismic hazard at the site in question. Careful selection of the seed accelerograms is important to minimize the wavelet adjustment required.

The adequacy of the results of the spectral matching methods should be checked by plotting the spectral acceleration, velocity and displacement of the adjusted accelerogram with the target spectra. Although it is desirable to get a good spectral match, it is equally important to check that excessive modification to the original ground motion has not taken place. This should be conducted by comparing plots of the original and adjusted acceleration, velocity and displacement time series. The energy content introduced into the record should also be checked by plotting the build up of the Arias intensity, known as the Husid plot, (Arias 1970) for both the original and adjusted accelerogram.

## 7.7. Input Motions

The time domain scaled records by the time domain scaling procedure presented in preceding sections are reprocessed using RSPMATCH code to improve its compatibility to the target spectra and the best fitted 3 records to the TSDC (2007) design spectra of site class Z1 and the best fitted 3 records for Z3 are selected in order to use for the transient analyses of tank model under consideration. Selected records are presented in Table A.1 and Table A.2 in Appendix A. The acceleration time history plots of original, time domain scaled and RSPMATCH generated records of the selected ground motions are given in Figure A.1 to Figure A.18 in Appendix A. As can be observed from these figures the consistency of the acceleration, velocity and displacement spectra of the real ground motion to the corresponding target spectra is substantially improved by RSPMATCH program.

# 8. NONLINEAR TRANSIENT ANALYSES OF TANKS UNDER MULTI-DIMENSIONAL EARTHQUAKE MOTION

In this chapter, a real tank model with typical proportions and material properties constructed in Turkey are analyzed under different combinations of Turkish Seismic Code (2007) design spectra compatible earthquake records by employing an explicit time integration scheme based on central difference method. Since Arbitrary Lagrangian Eulerian (ALE) formulation permits formation of large structural and fluid deformations without causing mesh distortion problems which occurs for Lagrangian formulation, a Lagrangian mesh system for structure is combined with an ALE mesh for fluid domain by merging nodes at the fluid-structure interface. Analysis results obtained for different ground motion records and loading combinations are evaluated in terms of base shear, overturning moment, free surface wave height, uplift response, shell stresses and plastic strain. The consistency of numerical analyses results with those of simplified methods are assessed for the anchored tank model under consideration when subjected to one horizontal component of earthquake ground motion. In order to clarify the key question of tank problems whether anchoring would prevent earthquake damage to the tank, numerical analyses are carried out on the same tank model having two different support conditions: anchored and unanchored. In addition to two horizontal components of ground motion, the vertical component is also taken into account in order to determine relative importance of vertical ground motion on the behavior of anchored and unanchored tanks. The consistency of provisions presented in current tank seismic design codes and numerical analysis results is assessed.

## 8.1. 3D Cylindrical Tank Model

The tank model under consideration has a radius of 24 m and a total height of 18 m (Figure 8.1). The flat tank roof is constructed on a set of radial beams and rafters which are supported by columns. Tank shell consists of 9 courses which are tapered from bottom to top. The thicknesses of the bottom plate and the first shell course nearest to the bottom are 0.007 m and 0.020 m, respectively. The thickness of the tank shell decreases 0.002 m at each two courses and it reaches 0.012 m at the top course. The steel of cylindrical shell,

roof, base plate, columns and roof rafters has a modulus of elasticity E = 200 GPa, poison's ratio of 0.30, and mass density of 7800 kg/m$^3$. Tank model under consideration is analyzed with three different material types: rigid, linear elastic and elastic-perfectly plastic. For elastic-perfectly plastic steel material, yield stress is assumed to be 3.55x10$^8$ Pa and the reserve strength due to strain hardening is ignored. Water ($\rho$ = 1000 kg/m$^3$) is filled up to a height of 14 m. Bulk modulus and dynamic viscosity of water are considered as 2.2x10$^9$ N/m$^2$ and 10$^{-3}$ Pa.sec, respectively.

The analyses are performed on the same tank model under two support conditions. In one case, all rotational degree of freedom of the tank base nodes are restrained and translational degree of freedom of these nodes only in the loading direction are released (anchored); in the other case, no restraint against translational and rotational degree of freedom are provided at the tank base plate nodes and tank is assumed directly resting on the ground (unanchored). For the unanchored tank case, a shell is used to represent the ground underlying the tank and the interaction between ground and the tank base is modeled with the surface to surface contact algorithm. Anchored tank model is placed on two different soil types: rock and stiff clay, which corresponds to Z1 and Z3 soil types, respectively. Subgrade modulus of stiff clay is taken as 20000 kN/m$^3$ and two noded tensionless spring elements are employed to model stiff clay. For unanchored tank, beneath soil is considered to be rigid.

The determination of analysis parameters such as friction coefficients, shell and fluid element formulations used in the numerical model has a key importance for accurate simulation of the physical phenomenon. In Chapter 6, the parameters for anchored and unanchored tank models are studied and calibrated with existing experimental models. The calibrated parameters are employed to model the real size anchored and unanchored tanks under consideration. Static friction and dynamic friction are taken into account with coefficients of 0.50 and 0.45, respectively. Arbitrary Lagrangian Eulerian (ALE) description is employed for the fluid domain and the nodes at the interface of fluid and structure are merged. Four noded fully integrated shell elements with 3 integration points through the thickness are used for the discretization of tank. In the numerical simulations, both material and geometric nonlinearities are considered in order to accurately determine

stress, strain and strain rate distributions throughout the tank. Initially, a vertical acceleration field of 1 g is applied to give the correct hydrostatic pressure in the fluid.

## 8.2. Ground Motion Combinations

Transient dynamic analyses of tank models described in Section 8.1 are carried out under the ground motion records selected in Chapter 7 by processing time domain matching techniques to be compatible with the Turkish Seismic Code (2007) design spectra. In order to evaluate the relative importance of earthquake ground motion components on anchored and unanchored tank responses, analyses are carried out for different combinations of the selected earthquake record components. These combinations are listed in Table 8.1. Loading 1 represents the horizontal component applied at $\theta=0°$ while the second horizontal component of the selected earthquake motion is applied perpendicular to the $1^{st}$ component ($\theta =90°$). Circumferential angle, ($\theta$), represents the angle from +X axis and it increases counterclockwise. Loading Case 2 includes concurrently application of both of two horizontal components of the selected record. Loading Case 3 consists of simultaneously presence of the horizontal component used in Loading Case 1 and vertical component of ground motion while Loading Case 4 characterizes the three-dimensional nature of the earthquake motion.

## 8.3. Evaluation of Mesh Size Effect

In order to evaluate the effect of mesh size on the response parameters of tanks, two finite element models of tanks with different mesh sizes are prepared. The first model with coarse mesh includes 2880 shell elements, 585 beam elements and 18144 ALE single material fluid elements with a total of 19627 nodes. The number of shell element which represents soil underlying the unanchored tank is 10000. The model with finer mesh has 8256 shell elements. Total number of beam elements which construct the radial beams, rafters and columns is 729. The liquid inside the tanks is discretized into 86400 ALE single material fluid elements with a total of 90613 nodes. Soil under the unanchored tank has 14400 shell elements. The general views of two finite element models are given in Figure 8.2.

The two tank models with different mesh sizes are analyzed under P1087 (ARC000) ground motion record. Analysis results for Mesh Types 1 and 2 are summarized in Table 8.2 in terms of maximum base shear, overturning moment, free surface wave height, plastic strain developed at the tank shell, radial displacements on X and Y axes and uplift displacement of the tank base.
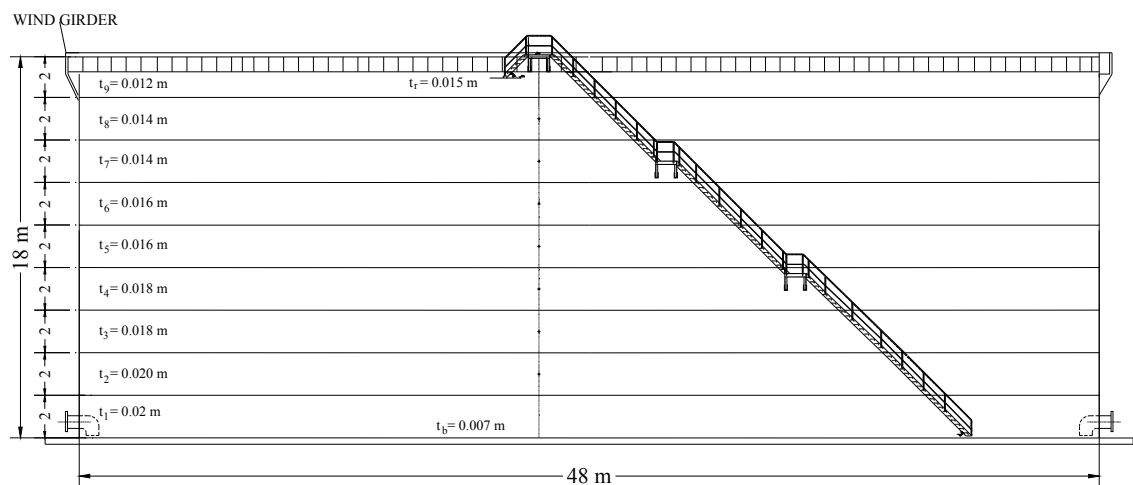


Figure 8.1. Dimensions of the tank model

Table 8.1. Combinations of ground motion components used in the transient analyses

| Loading Name | Record Combinations |
|---|---|
| Loading Case 1 | Horizontal component of the selected earthquake ground motion |
| Loading Case 2 | Concurrently presence of two horizontal components of the selected earthquake ground motion |
| Loading Case 3 | Concurrently presence of one horizontal and vertical components of the selected earthquake ground motion |
| Loading Case 4 | Three components of the selected earthquake ground motion |

(a) Mesh type 1                    (b) Mesh type 2
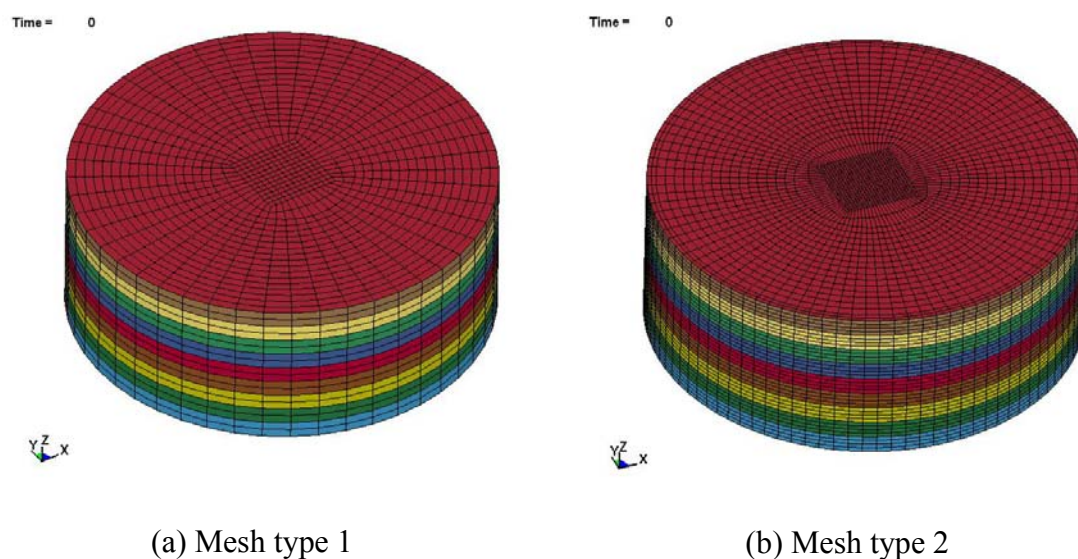
Figure 8.2. Finite element model of tanks with (a) coarse mesh (b) finer mesh

Although maximum base shear and overturning moment developed at anchored and unanchored tank walls are similar for both mesh types, the significant effect of finer mesh is observed on plastic strain, radial displacement of tank wall, base uplift and free surface wave height. Figure 8.3 and Figure 8.4 show base shear and overturning moment time histories of anchored and unanchored tanks. Figure 8.5 shows that uplift displacements amplify approximately 3 times at both sides of the tank base plate on the X axis for finer mesh model. Radial displacements, developed especially on the anchored tank wall, substantially increases with accompanying amplification in plastic strain. The difference in sloshing wave height between two mesh types for both anchored and unanchored tanks is approximately 0.50 m (Figure 8.6). Even though, the fine mesh model's analysis duration increases 5-7 times, the fine mesh type is utilized in this study for more accurate results of base shear, overturning moment, plastic strain and radial displacement. The detailed finite element model of the unanchored tank with fine mesh used in the transient analyses is shown in Figure 8.7.

## 8.4. Analysis of Tank Model with Simplified Methods

In order to assess consistency of numerical analyses results with those of simplified methods that are explained in details in Section 4.1, the methodologies developed by

Housner (1954), Veletsos and Yang (1977), Haroun and Housner (1981a) and Malhotra *et al.* (2000) are applied to the anchored tank model under consideration when subjected to one horizontal component of earthquake ground motion (Loading Case 1). The response parameters evaluated include base shear force, overturning moment and sloshing wave height. Table 8.3 presents the summary of these response parameters including the effect of tank shell and roof inertia obtained from simplified methods using Turkish Seismic Design Code (2007) spectrum for site class Z1, $1^{st}$ degree earthquake zone ($A_o$ = 0.4) and importance factor of 1.5. Damping level is assumed to be 5 per cent for the impulsive modes and 0.5 per cent for the convective modes. The response spectrum values for 0.5 per cent damping for the convective effects are taken as 1.5 (API 650, 2005) times 5 per cent damped spectral values. TSDC (2007) elastic design acceleration spectra with 0.5 per cent and 5 per cent damping are shown in Figure 8.8.

As can be seen from Table 8.3, although Housner (1954) method is based on the approximate solution of fluid flow inside a rigid tank, it presents consistent results for base shear and overturning moment with Yang and Veletsos (1977) method which is based on the mathematical solution of Laplace equation. Methods developed by Haroun and Housner (1981a) and Malhotra *et al.* (2000) which take into account tank wall flexibility provide approximately 2.5 times higher base shear and overturning moment than those based on rigid tank solution. Therefore, the interaction effects between the tank and the contained liquid cause substantial magnification of base shear and overturning moment. For impulsive-flexible and sloshing periods, all methods give consistent results for each parameter. Although, sloshing wave height is obtained as 3.84 m by methods of Housner (1954) and Malhotra *et al.* (2000), other two methods (Veletsos and Yang, 1977 and Haroun and Housner, 1981a) predict 3.21 m of free surface displacement.

In order to compare base shear time histories obtained from simplified methods and FEM model, transient analyses are carried out for mass-spring systems of Housner (1954) and Malhotra *et al.* (2000) using explicit method analysis tool of LS-DYNA. Mechanical analog properties are taken from Table 8.3 and only $1^{st}$ convective mode effect is considered for Housner (1954) method. For both mass-spring systems, convective and impulsive effects are combined with direct superposition method.

Table 8.2. Evaluation of response parameters for mesh types 1 and 2

| | | Anchored Tank Mesh Type 1 | Anchored Tank Mesh Type 2 | Unanchored Tank Mesh Type 1 | Unanchored Tank Mesh Type 2 |
|---|---|---|---|---|---|
| Free Surface Wave Height (m) | max | 3.13 | 3.6 | 3.18 | 3.55 |
| | min | -2.56 | -2.79 | -2.58 | -2.79 |
| Overturning Moment (Nm) | max | $5.71 \times 10^8$ | $5.68 \times 10^8$ | $2.34 \times 10^8$ | $2.63 \times 10^8$ |
| | min | $-5.03 \times 10^8$ | $-5.77 \times 10^8$ | $-3.77 \times 10^8$ | $-3.58 \times 10^8$ |
| Base Shear (N) | max | $1.17 \times 10^8$ | $1.10 \times 10^8$ | $5.65 \times 10^7$ | $5.92 \times 10^7$ |
| | min | $-1.00 \times 10^8$ | $-1.07 \times 10^8$ | $-5.38 \times 10^7$ | $-5.20 \times 10^7$ |
| Uplift (m) | $\theta=0$ $\theta=180$ | - | - | 0.0096 0.013 | 0.034 0.040 |
| Radial Displacement (m) | on the X axis | 0.15 | 0.26 | 0.025 | 0.10 |
| | on the Y axis | 0.11 | 0.23 | 0.001 | 0.09 |
| Plastic Strain | Max | 0.0028 | 0.004 | 0.000025 | 0.0009 |
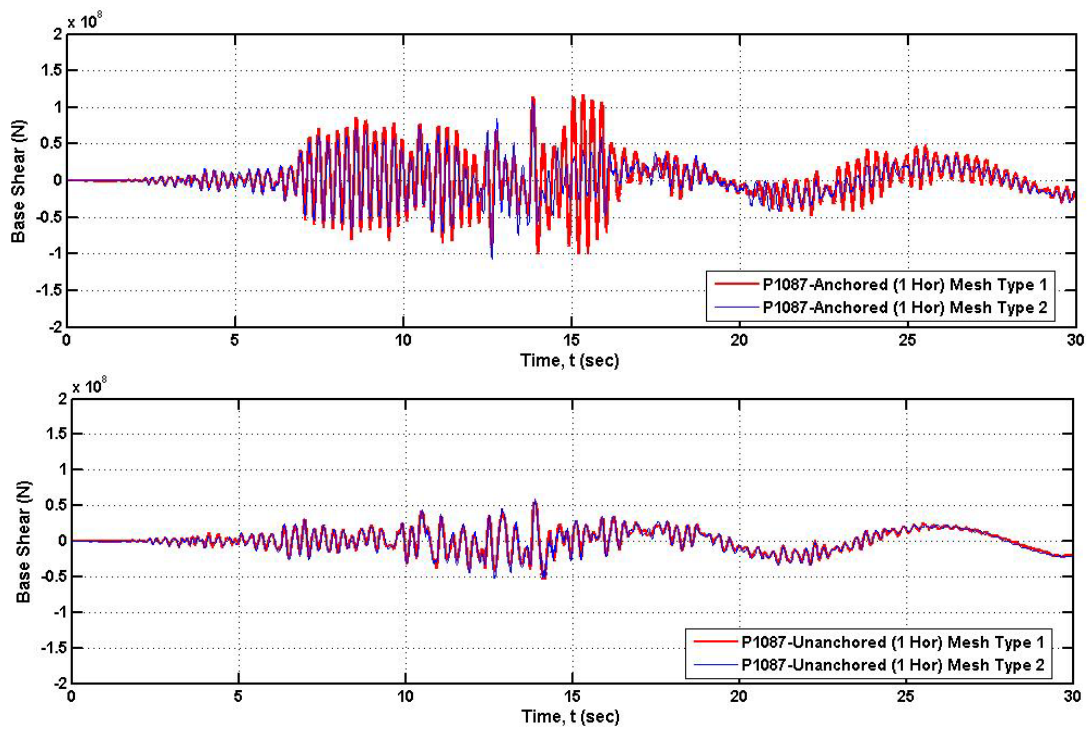
Figure 8.3. Comparison of base shear developed at the base of anchored and unanchored tank walls under modified P1087-ARC000 record for Mesh Types 1 and 2
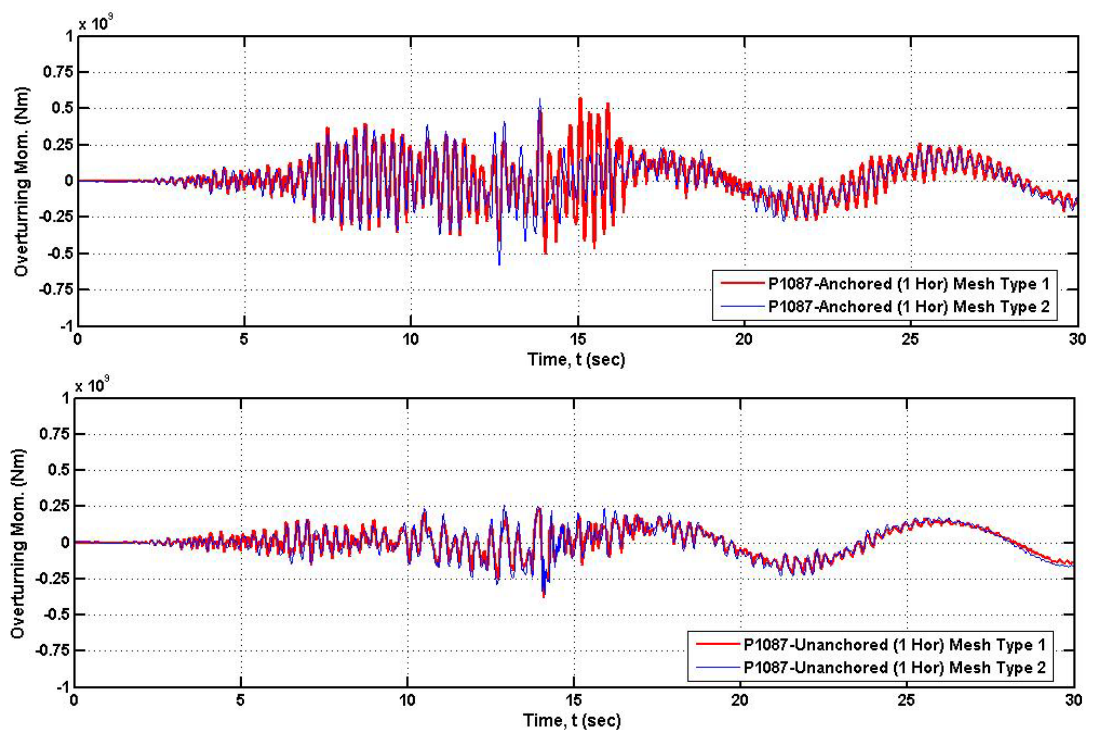


Figure 8.4. Comparison of overturning moment developed at the base of anchored and unanchored tank walls under modified P1087-ARC000 record for Mesh Types 1 and 2

(a)                    (b)
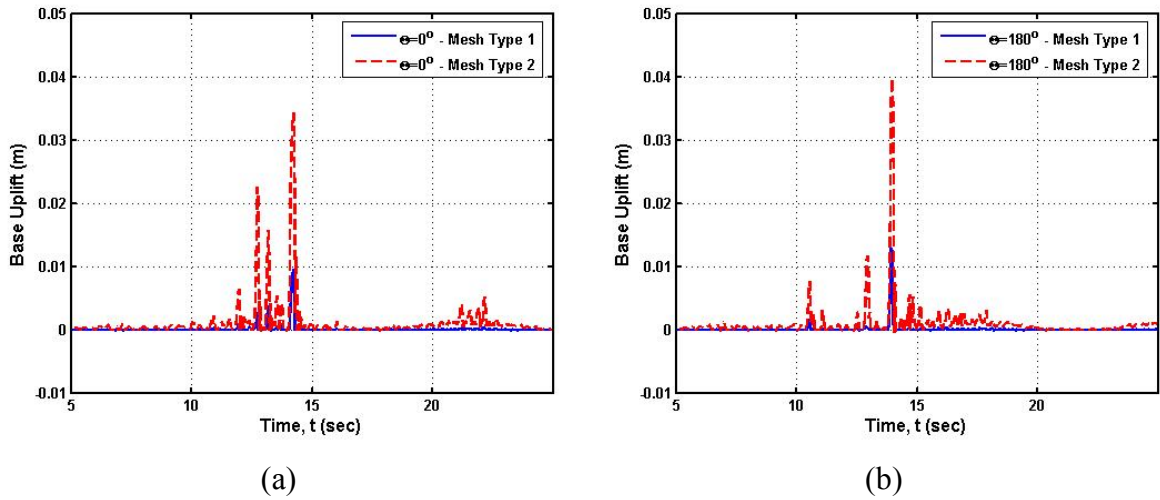
Figure 8.5. Comparisons of the base uplift time histories of unanchored tank under modified P1087-ARC000 record for Mesh Types 1 and 2
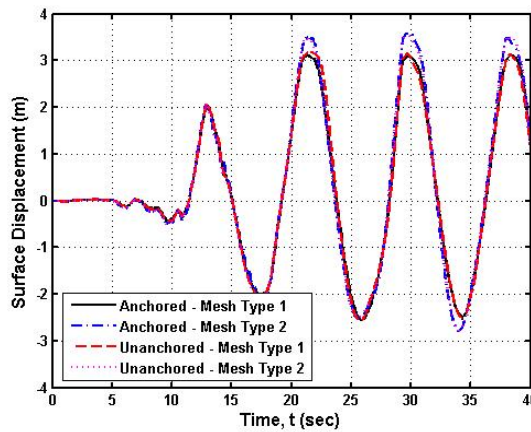


Figure 8.6. Comparisons of sloshing time histories of anchored and unanchored tanks under modified P1087-ARC000 record for Mesh Types 1 and 2
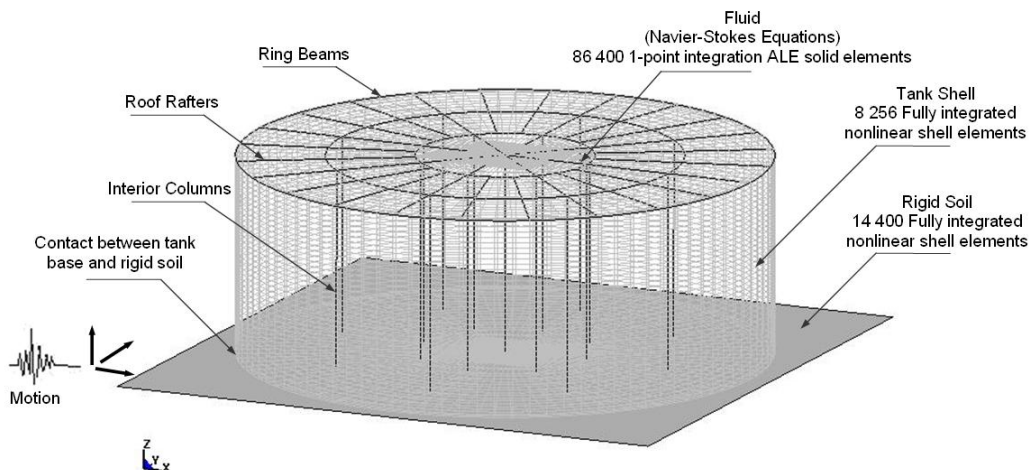


Figure 8.7. Finite element model of the unanchored tank

Table 8.3. Analysis results of tank under consideration with the simplified methods

(units: N, m, sec)

| | Housner (1954) | Yang and Veletsos (1977) | Haroun and Housner (1981) | Malhotra *et al.* (2000) |
|---|---|---|---|---|
| Spectral acceleration imp. rigid | 0.60 g ($1.0 \cdot 0.4g \cdot 1.5$) | 0.60 g ($1.0 \cdot 0.4g \cdot 1.5$) | 0.60 g ($1.0 \cdot 0.4g \cdot 1.5$) | - |
| Spectral acceleration imp. flexible | - | - | 1.5 g ($2.5 \cdot 0.4g \cdot 1.5$) | 1.5 g ($2.5 \cdot 0.4g \cdot 1.5$) |
| Spectral acceleration conv. (first/second mode) | 0.16g /0.27g | 0.16g /0.27g | 0.16g | 0.16g |
| Imp. rigid mass ratio, $m_{impr} / m_{fl}$ | 0.34 | 0.35 | 0.37 | - |
| Imp. flexible mass ratio, $m_{impf} / m_{fl}$ | - | - | 0.36 | 0.35 |
| Conv. mass ratio, $m_{convn} / m_{fl}$ | 0.62 | 0.62 | 0.61 | 0.65 |
| Imp. rigid mass height ratio, $h_{impr} / h$ | 0.38 | 0.40 | 0.40 | - |
| Imp. flexible mass height ratio, $h_{impf} / h$ | - | - | 0.40 | 0.40 |
| Conv. mass height, $h_{convn} / h$ | 0.54 | 0.54 | 0.54 | 0.55 |
| Imp. rigid mass height ratio, $h'_{impr} / h$ (including base pressure) | 1.37 | 1.23 | - | - |
| Imp. flexible mass height ratio, $h'_{impf} / h$ (including base pressure) | - | - | - | 1.27 |
| Conv. mass height, $h'_{convn} / h$ (including base pressure) | 1.22 | 1.26 | - | 1.31 |
| Impulsive Mode Period | - | - | 0.26 | 0.27 |
| Sloshing Mode Period | 8.16 | 8.14 | 8.15 | 8.24 |
| Maximum Sloshing Wave Height | 3.84 | 3.21 | 3.21 | 3.84 |
| Base Shear {Base shear / ($m_{fluid}$*g)} | $5.89 \times 10^7$ {0.24} | $6.08 \times 10^7$ {0.24} | $1.36 \times 10^8$ {0.55} | $1.64 \times 10^8$ {0.66} |
| Overturning Moment (excluding base pressure) {Overturning Moment / ($m_{fluid}$*g*h)} | $3.58 \times 10^8$ {0.10} | $3.82 \times 10^8$ {0.11} | $7.75 \times 10^8$ {0.22} | $1.03 \times 10^9$ {0.30} |
| Overturning Moment (including base pressure) {Overturning Moment / ($m_{fluid}$*g*h)} | $1.09 \times 10^9$ {0.31} | $1.03 \times 10^9$ {0.30} | - | $2.89 \times 10^9$ {0.83} |
| Combination rules (impulsive and convective) | SRSS | SRSS | SRSS | Direct Sum |
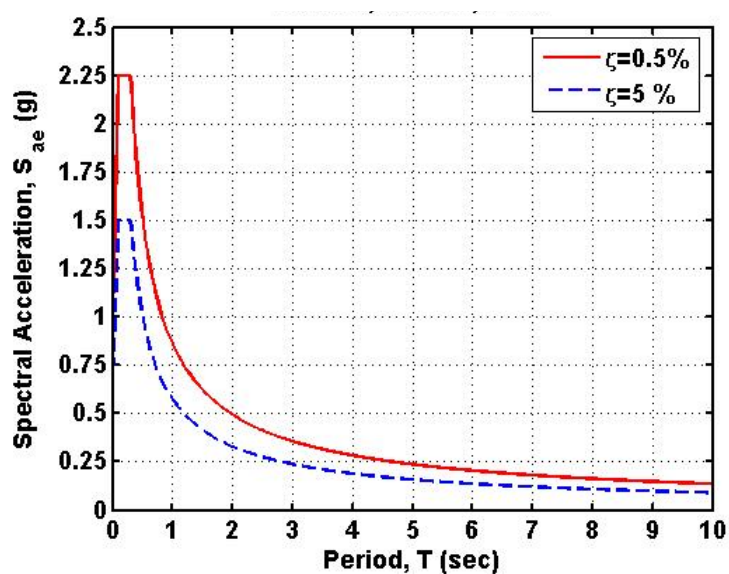
Figure 8.8. Turkish Seismic Design Code (2007) spectra for site class Z1, 1st degree earthquake zone ($A_o = 0.4$) and importance factor of 1.5 with 0.5 per cent and 5 per cent damping

Figure 8.9 to Figure 8.11 present comparisons of base shear time histories of anchored tank obtained from spring-mass models of Housner (1954) and Malhotra *et al.* (2000) and nonlinear FEM for the selected earthquake ground motions. One can observe from these figures that base shear time histories obtained by Housner's method which uses rigid tank assumption perfectly match with base shear response of rigid FEM tank model for all input ground motion records. However, base shear time histories obtained for mechanical analog of Malhotra *et al.* (2000) which takes into account tank wall flexibility and impulsive and convective higher mode effects deviate from FEM results. Especially, spring-mass system of Malhotra *et al.* (2000) when subjected to modified P1558-MDR000 record undergoes large amplitude base shear effects between 10 and 15 sec. In order to find out the reason, Fourier amplitude spectra and Husid plots of records are plotted in Figure 8.12. P1558-MDR000 has high energy content around 3.5 Hz and fundamental frequency of coupled tank-fluid mode is 3.7 Hz (Table 8.3). Resonance between vibrations of input motion and spring-mass system may cause high amplitude base shear effects. Therefore, mechanical simplified analog model, especially developed for flexible tanks, should be used with care for time history analysis since in real tank-fluid system, there are different mechanisms due to fluid-structure interaction.

Maximum base shear values obtained from mechanical analog model of Housner (1954) and Malhotra *et al.* (2000) and finite element method are summarized in Table 8.4. Maximum base shear induced by hydrodynamic effects on rigid tank is approximately 22 per cent and 26 per cent of the fluid weight contained in the tank for analytical and FEM, respectively. When the tank flexibility is taken into account, this ratio increases to 95 per cent and 72 per cent because of the interaction effects between tank and the contained liquid. But, base shear developed on mass-spring system of the flexible anchored tank is very sensitive to input motion and this analog may give 32 per cent higher base shear values than those of obtained by FEM.

As a result, Housner's mechanical analog can accurately predict the response of a rigid tank. However, since rigid tank assumption substantially underestimates the base shear developed at the anchored tank, the application of methods developed for rigid tanks is not appropriate for design of real tanks.
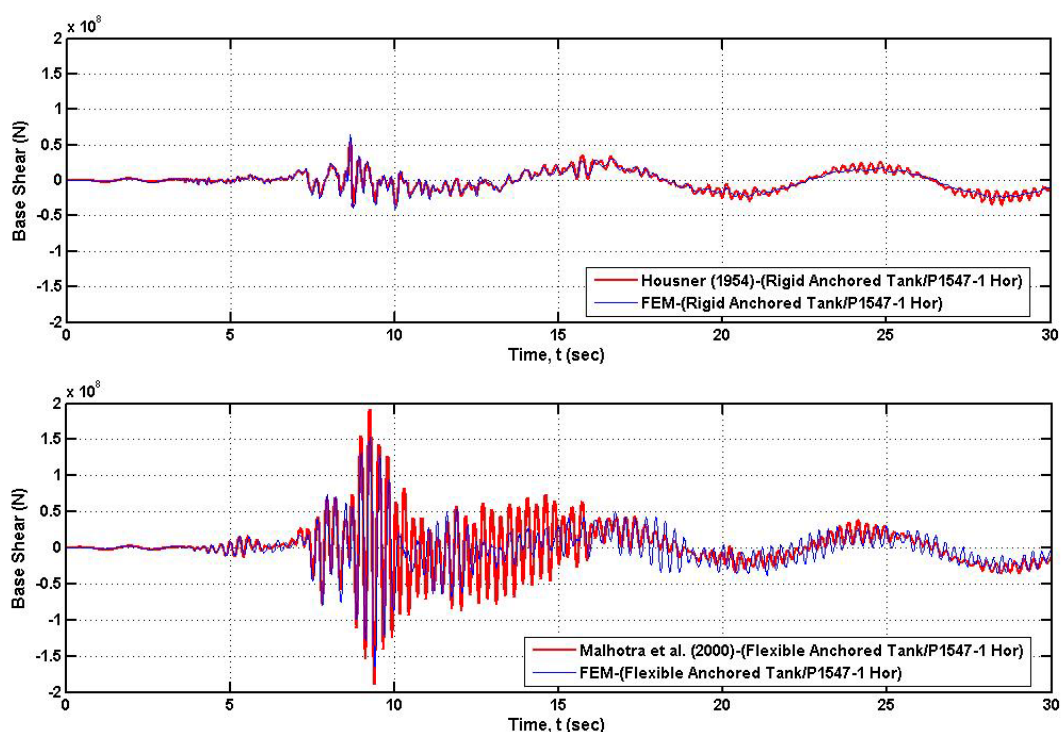


Figure 8.9. Comparisons of base shear time histories of anchored tank obtained from spring-mass models of Housner and Malhotra and nonlinear FEM under P1547 record
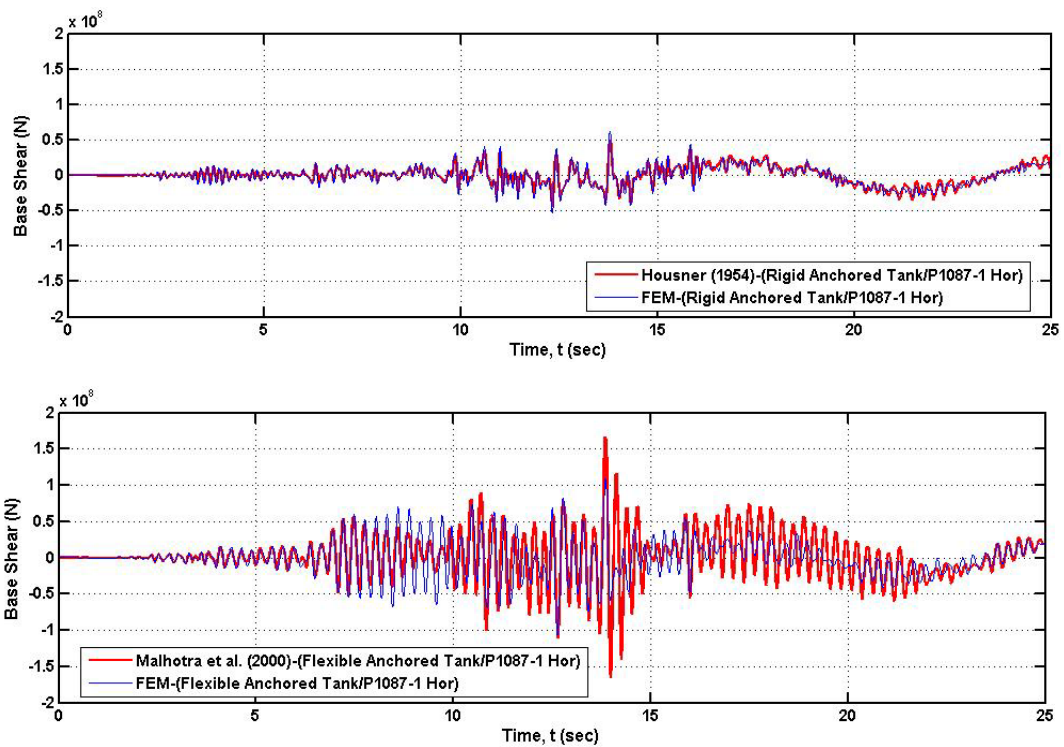
Figure 8.10. Comparisons of base shear time histories of anchored tank obtained from spring-mass models of Housner and Malhotra and nonlinear FEM under P1087 record
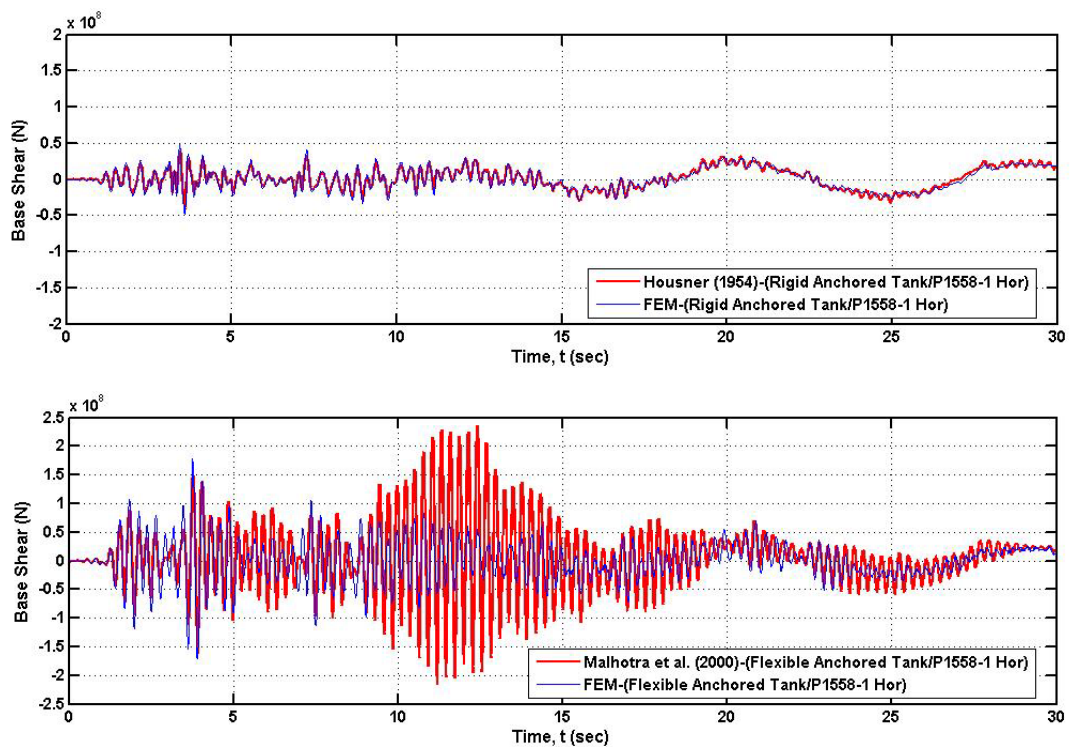


Figure 8.11. Comparisons of base shear time histories of anchored tank obtained from spring-mass models of Housner and Malhotra and nonlinear FEM under P1558 record
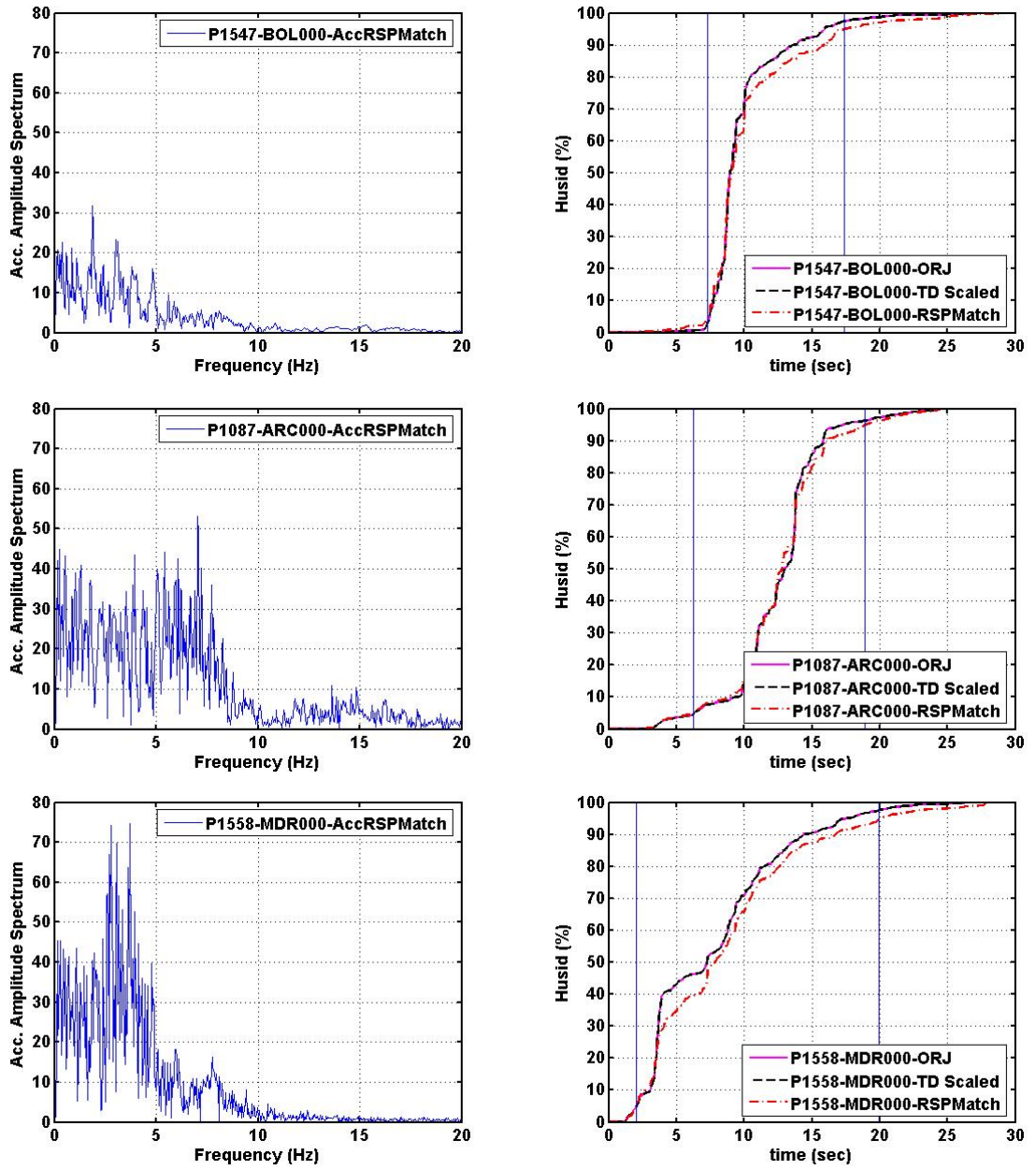
Figure 8.12. Fourier amplitude spectra and Husid plots of records used in the analyses

Table 8.4. Analytical and FEM results for base shear developed on the anchored tank under one horizontal component of selected records

| Loading | Tank Type | Analytical | FEM |
|---|---|---|---|
| P1547-BOL000 (0.64 g) | Rigid Tank (Housner, 1954) | $5.47 \times 10^7$ {0.22}[*] | $6.47 \times 10^7$ {0.26} |
| | Flexible Tank (Malhotra et al., 2000) | $1.91 \times 10^8$ {0.77} | $1.65 \times 10^8$ {0.66} |
| P1087-ARC000 (0.75 g) | Rigid Tank (Housner, 1954) | $4.80 \times 10^7$ {0.19} | $6.22 \times 10^7$ {0.25} |
| | Flexible Tank (Malhotra et al., 2000) | $1.66 \times 10^8$ {0.67} | $1.09 \times 10^8$ {0.44} |
| P1558-MDR000 (0.49 g) | Rigid Tank (Housner, 1954) | $4.12 \times 10^7$ {0.17} | $4.86 \times 10^7$ {0.20} |
| | Flexible Tank (Malhotra et al., 2000) | $2.35 \times 10^8$ {0.95} | $1.78 \times 10^8$ {0.72} |

[*]{Base shear / ($m_{fluid} \cdot g$)}

## 8.5.  Evaluation of Tank Response Parameters Using FEM

The numerical analysis results for anchored and unanchored tank models under consideration are evaluated in terms of response parameters which include base shear, overturning moment, free surface wave height, uplift response, shell stresses and plastic strain.

### 8.5.1.  Base Shear and Overturning Moment

The base shear and overturning moment obtained by numerical method for both anchored and unanchored tanks are summarized in Table 8.5 to Table 8.10. In these tables, the ratio is defined as:

$$Ratio = \frac{Base\ Shear}{liqid\ weight} \tag{8.1}$$

$$Ratio = \frac{Overturning\ Moment}{liqid\ weight \cdot liquid\ depth} \qquad (8.2)$$

for base shear and overturning moment, respectively. X and Y components of the base shear and overturning moment are combined with SRSS rule to obtain maximum response for Loading Cases 2 and 4.

Analysis results verifies that maximum base shear and overturning moment developed on anchored tank supported on rigid foundation generally occur when tank is subjected to one horizontal ground motion component. Concurrently presence of vertical and horizontal ground motion components may decrease base shear and overturning moment developed on the anchored tank while overturning moment and base shear excited on the unanchored tank may increase depending on the input motion characteristics. Simultaneously presence of two horizontal ground motion components and three dimensional seismic loading increase base shear and overturning moment developed on the unanchored tank supported on rigid foundation. Therefore, it is convenient to evaluate tank response considering all components of the ground motion if tank isn't anchored at its base. When the anchored tank is supported on flexible soil, single horizontal ground motion component causes highest base shear response, while three dimensional loading may increase overturning moment. Soil flexibility decreases maximum base shear 12.5 per cent and 9.4 per cent and increases maximum overturning moment 8 per cent and 20 per cent developed on anchored and unanchored tanks, respectively. Both base shear and overturning moment induced at the unanchored tank wall are less than those observed at the anchored tank wall for all ground motion combinations.

Minimum to maximum ranges of base shear and overturning moment are summarized in Table 8.11 for all records used in the analyses. In Table 8.12, maximum base shear and overturning moment developed on the anchored and unanchored tanks under one horizontal component of selected ground motions are summarized along with peak ground acceleration values of these records. Maximum base shear and overturning moment developed on the anchored and unanchored tanks are not directly proportional to peak ground acceleration. In other words, increase in peak ground acceleration may not cause amplification in these two response quantities. The lowest maximum base shear and

overturning moment are observed when the anchored tank is subjected to modified P1087-ARC000 record. If Husid plots of input motions given in Figure 8.12 are compared, it is observed that energy distribution of the modified P1087-ARC000 record is smooth between 3 and 20 sec. The highest base shear and overturning moment develop on anchored tank when subjected to modified P1558-MDR000 record in which energy steeply increases between 3 and 4 sec. But, the lowest base shear and overturning moment are obtained on the unanchored tank under this record.

Maximum base shear developed on rigid anchored tank is 25 per cent of the fluid weight while this ratio may increase 77 per cent when tank is made up of elastic steel material. Overturning moment developed on anchored tank placed on rigid ground may reach as much as 26 per cent of product of tank weight and liquid height. Nonlinearity of the anchored tank decreases base shear around 5 per cent of tank weight, while a decrease in overturning moment is 2 per cent of the product of tank weight and liquid height. Maximum base shear response of rigid and inelastic tanks occur under different earthquake motions. The anchored tank settled on flexible ground undergoes base shear which is around 60 per cent of tank weight and overturning moment which is around 26 per cent of the product of tank weight and liquid height.

Base shear developed on the unanchored tank is around 25 per cent of weight of the contained liquid, while overturning moment is 10 per cent of the product of tank weight and liquid height. If the unanchored tank is founded on flexible foundation base shear is 26 per cent of weight of the contained liquid and overturning moment is 15 per cent of the product of tank weight and liquid height. Base shear and overturning moment developed on the unanchored tank is less than half of those exerted on the anchored tank in average.

Table 8.5. FEM results for base shear and overturning moment developed on anchored and unanchored tanks under modified P1547 record

| Parameter | Loading | Anchored | | | Unanchored | | | |
|---|---|---|---|---|---|---|---|---|
| | | | Ratio | $\frac{\text{Load 2 or 3 or 4}}{\text{Load1}}$ | | Ratio | $\frac{\text{Load 2 or 3 or 4}}{\text{Load1}}$ | $\frac{\text{Unanchored}}{\text{Anchored}}$ |
| $Q$ Base Shear (N) | Load 1 [nonlinear] (Elastic) {Rigid} | [$1.65\times10^8$] ($1.79\times10^8$) {$6.47\times10^7$} | [0.66] (0.72) {0.26} | 100% | $6.13\times10^7$ | 0.25 | 100% | 37% |
| | Load 2 | $1.73\times10^8$ | 0.70 | 105% | $7.11\times10^7$ | 0.29 | 116% | 41% |
| | Load 3 | $1.29\times10^8$ | 0.52 | 78% | $4.88\times10^7$ | 0.20 | 80% | 38% |
| | Load 4 | $1.15\times10^8$ | 0.46 | 70% | $7.92\times10^7$ | 0.32 | 129% | 69% |
| $M$ Overturning Moment (N m) | Load 1 [nonlinear] (Elastic) | [$8.53\times10^8$] ($9.30\times10^8$) | [0.25] (0.27) | 100% | $3.35\times10^8$ | 0.10 | 100% | 39% |
| | Load 2 | $9.15\times10^8$ | 0.26 | 106% | $4.76\times10^8$ | 0.14 | 142% | 52% |
| | Load 3 | $7.11\times10^8$ | 0.20 | 83% | $3.11\times10^8$ | 0.09 | 93% | 44% |
| | Load 4 | $6.55\times10^8$ | 0.19 | 76% | $4.57\times10^8$ | 0.13 | 136% | 70% |

Table 8.6. FEM results for base shear and overturning moment developed on anchored and unanchored tanks under modified P1087 record

| Parameter | Loading | Anchored | | | Unanchored | | | |
|---|---|---|---|---|---|---|---|---|
| | | | Ratio | $\frac{\text{Load 2 or 3 or 4}}{\text{Load1}}$ | | Ratio | $\frac{\text{Load 2 or 3 or 4}}{\text{Load1}}$ | $\frac{\text{Unanchored}}{\text{Anchored}}$ |
| $Q$ Base Shear (N) | Load 1 [nonlinear] (Elastic) {Rigid} | [$1.10\times10^8$] ($1.20\times10^8$) {$6.22\times10^7$} | [0.44] (0.48) {0.25} | 100% | [$5.92\times10^7$] ($5.67\times10^7$) | [0.24] (0.23) | 100% | 54% |
| | Load 2 | $1.06\times10^8$ | 0.43 | 96% | $6.83\times10^7$ | 0.27 | 115% | 64% |
| | Load 3 | $9.30\times10^7$ | 0.37 | 85% | $5.36\times10^7$ | 0.22 | 91% | 58% |
| | Load 4 | $1.13\times10^8$ | 0.45 | 103% | $6.94\times10^7$ | 0.28 | 117% | 61% |
| $M$ Overturning Moment (N m) | Load 1 [nonlinear] (Elastic) | [$5.77\times10^8$] ($6.44\times10^8$) | [0.17] (0.19) | 100% | [$3.58\times10^8$] ($3.47\times10^8$) | [0.10] (0.10) | 100% | 62% |
| | Load 2 | $5.68\times10^8$ | 0.16 | 98% | $4.63\times10^8$ | 0.13 | 129% | 82% |
| | Load 3 | $4.95\times10^8$ | 0.14 | 86% | $4.48\times10^8$ | 0.13 | 125% | 91% |
| | Load 4 | $5.96\times10^8$ | 0.17 | 103% | $5.23\times10^8$ | 0.15 | 146% | 88% |

Table 8.7. FEM results for base shear and overturning moment developed on anchored and unanchored tanks under modified P1558 record

| Parameter | Loading | Anchored | | | | Unanchored | | | |
|---|---|---|---|---|---|---|---|---|---|
| | | | Ratio | $\frac{\text{Load 2 or 3 or 4}}{\text{Load 1}}$ | | | Ratio | $\frac{\text{Load 2 or 3 or 4}}{\text{Load 1}}$ | $\frac{\text{Unanchored}}{\text{Anchored}}$ |
| $Q$ Base Shear (N) | Load 1 [nonlinear] (Elastic) {Rigid} | $[1.78 \times 10^8]$ $(1.95 \times 10^8)$ $\{4.86 \times 10^7\}$ | $[0.72]$ $(0.77)$ $\{0.20\}$ | 100% | | $5.27 \times 10^7$ | 0.21 | 100% | 30% |
| | Load 2 | $1.46 \times 10^8$ | 0.59 | 82% | | $6.25 \times 10^7$ | 0.25 | 119% | 43% |
| | Load 3 | $1.64 \times 10^8$ | 0.66 | 92% | | $5.46 \times 10^7$ | 0.22 | 104% | 33% |
| | Load 4 | $1.37 \times 10^8$ | 0.55 | 77% | | $6.27 \times 10^7$ | 0.25 | 119% | 46% |
| $M$ Overturning Moment (N m) | Load 1 [nonlinear] (Elastic) | $[9.22 \times 10^8]$ $(9.82 \times 10^8)$ | 0.26 (0.28) | 100% | | $2.88 \times 10^8$ | 0.08 | 100% | 31% |
| | Load 2 | $7.58 \times 10^8$ | 0.22 | 82% | | $4.36 \times 10^8$ | 0.13 | 151% | 58% |
| | Load 3 | $8.32 \times 10^8$ | 0.24 | 90% | | $3.62 \times 10^8$ | 0.10 | 126% | 44% |
| | Load 4 | $7.28 \times 10^8$ | 0.21 | 79% | | $4.20 \times 10^8$ | 0.12 | 146% | 58% |

Table 8.8. FEM results for base shear and overturning moment developed on anchored and unanchored tanks under modified P1114 record

| Parameter | Loading | Anchored | | |
|---|---|---|---|---|
| | | | Ratio | $\frac{\text{Load 2 or 3 or 4}}{\text{Load 1}}$ |
| $Q$ Base Shear (N) | Load 1 | $1.40 \times 10^8$ | 0.56 | 100% |
| | Load 2 | $1.28 \times 10^8$ | 0.52 | 91% |
| | Load 3 | $1.23 \times 10^8$ | 0.49 | 88% |
| | Load 4 | $1.27 \times 10^8$ | 0.51 | 91% |
| $M$ Overturning Moment (N m) | Load 1 | $8.81 \times 10^8$ | 0.25 | 100% |
| | Load 2 | $8.33 \times 10^8$ | 0.24 | 95% |
| | Load 3 | $7.50 \times 10^8$ | 0.22 | 85% |
| | Load 4 | $7.85 \times 10^8$ | 0.23 | 89% |

Table 8.9. FEM results for base shear and overturning moment developed on anchored and unanchored tanks under modified P1104 record

| Parameter | Loading | Anchored | | |
|---|---|---|---|---|
| | | | Ratio | $\dfrac{\text{Load 2 or 3 or 4}}{\text{Load1}}$ |
| $Q$ Base Shear (N) | Load 1 | $1.50 \times 10^8$ | 0.60 | 100% |
| | Load 2 | $1.20 \times 10^8$ | 0.48 | 80% |
| | Load 3 | $1.09 \times 10^8$ | 0.44 | 70% |
| | Load 4 | $1.33 \times 10^8$ | 0.54 | 89% |
| $M$ Overturning Moment (N m) | Load 1 | $8.71 \times 10^8$ | 0.25 | 100% |
| | Load 2 | $7.06 \times 10^8$ | 0.20 | 81% |
| | Load 3 | $6.\,69 \times 10^8$ | 0.19 | 77% |
| | Load 4 | $9.\,56 \times 10^8$ | 0.28 | 110% |

Table 8.10. FEM results for base shear and overturning moment developed on anchored and unanchored tanks under modified P1096 record

| Parameter | Loading | Anchored | | | Unanchored | | | |
|---|---|---|---|---|---|---|---|---|
| | | | Ratio | $\dfrac{\text{Load 2 or 3 or 4}}{\text{Load1}}$ | | Ratio | $\dfrac{\text{Load 2 or 3 or 4}}{\text{Load1}}$ | $\dfrac{\text{Unanchored}}{\text{Anchored}}$ |
| $Q$ Base Shear (N) | Load 1 [nonlinear] (Elastic) {Rigid} | $1.56 \times 10^8$ | 0.63 | 100 % | $6.53 \times 10^7$ | 0.26 | 100 % | 42 % |
| | Load 2 | $1.30 \times 10^8$ | 0.53 | 84 % | - | - | - | - |
| | Load 3 | $1.08 \times 10^8$ | 0.44 | 69 % | $6.79 \times 10^7$ | 0.27 | 104 % | 63 % |
| | Load 4 | $1.13 \times 10^8$ | 0.45 | 72 % | $7.11 \times 10^7$ | 0.29 | 109 % | 63 % |
| $M$ Overturning Moment (N m) | Load 1 [nonlinear] (Elastic) | $9.12 \times 10^8$ | 0.26 | 100 % | $5.22 \times 10^8$ | 0.15 | 100 % | 57 % |
| | Load 2 | $7.85 \times 10^8$ | 0.23 | 86 % | - | - | - | - |
| | Load 3 | $6.24 \times 10^8$ | 0.18 | 68 % | $6.21 \times 10^8$ | 0.18 | 119% | 100 % |
| | Load 4 | $6.15 \times 10^8$ | 0.18 | 67 % | $5.78 \times 10^8$ | 0.17 | 111% | 94 % |

**8.5.2. Pressure Distribution**

Pressure distributions on the anchored tank wall during maximum pressure response along with those of obtained from Housner (1954) and Veletsos and Yang (1977) methods are plotted in Figure 8.13 to Figure 8.15 for 1 horizontal ground motion component of selected earthquake records. Pressure values for the rigid anchored tank are very close for both analytical methods (Figure 8.13). Numerical method provides very regular distribution for pressure along the rigid tank height and peak pressure response always occurs in response to peak ground acceleration for rigid tank. P1558-MDR000 record provides lowest pressure values as similar to base shear. The pressure developed on rigid anchored tank especially under modified P1547-BOL000 record represents very similar distribution to those predicted by simplified methods up to 11 m. However, near the free surface; where the convective component is dominant; the pressure values obtained from simplified methods deviate from those observed by numerical method. The reason for this is that, during the peak pressure response, the height of the surface waves does not reach maximum free surface wave height (only 1.8 m) as predicted by simplified methods. Free surface height reaches its maximum value close to the end of effective ground motion duration. This also verifies that SRSS combination rule is more appropriate to combine impulsive and convective effects.

Figure 8.14 shows pressure distribution on the anchored tank with inelastic material settled on rigid soil along with the results of analytical methods. Veletsos and Yang (1977) proposed two different methods to evaluate hydrodynamic pressure response in a flexible tank. The first method assumes that flexible tank deforms in a prescribed form without cross sectional distortions and pressure distribution is obtained by solving Laplace equation under boundary conditions specified for flexible tanks. In the other method, the impulsive effects are determined similarly as the rigid tank solution by replacing the ground acceleration in the relevant expressions of this solution by the pseudo acceleration function corresponding to the natural frequency of the tank-liquid system (Veletsos, 1984). In both methods, convective effects are evaluated considering the tank to be rigid. The second method provides higher pressure values than the first method (Figure 8.14) for the tank model under consideration. Pressure distribution obtained from numerical method along the tank height is not smooth and it fluctuates. Pressure values for P1087 record are

smaller than those for other records as is the case for base shear and overturning moment obtained from this record. Pressure distributions for modified P1547 and P1558 records are higher than those predicted by analytical methods.

Pressure distributions on the anchored tank wall settled on flexible foundation are given in Figure 8.15 for different earthquake ground motions. For modified P1114 and P1096 records, numerical method provides higher pressure values than those obtained by analytical methods between 0-6 m.

Table 8.11. Base shear and overturning moment ranges for anchored and unanchored tanks

| | | Rigid Soil | | | | Flexible Soil | |
|---|---|---|---|---|---|---|---|
| | | Anchored | | Unanchored | | Anchored | |
| Parameter | Loading | | Ratio [*] | | Ratio [*] | | Ratio [*] |
| Base Shear (N) | Load 1 [nonlinear] | $[1.10 \times 10^8 \text{-} 1.78 \times 10^8]$ | 0.44-0.72 | $[5.27 \times 10^7 \text{-} 6.13 \times 10^7]$ | [0.21-0.25] | $1.40 \times 10^8 \text{-} 1.56 \times 10^8$ | 0.56-0.63 |
| | (Elastic) | $(1.20 \times 10^8 \text{-} 1.95 \times 10^8)$ | 0.48-0.77 | $(5.67 \times 10^7)$ | (0.23) | | |
| | {Rigid} | $\{4.86 \times 10^7 \text{-} 6.47 \times 10^7\}$ | 0.20-0.26 | | | | |
| | Load 2 | $1.06 \times 10^8 \text{-} 1.73 \times 10^8$ | 0.43-0.70 | $6.25 \times 10^7 \text{-} 7.11 \times 10^7$ | 0.25-0.29 | $1.20 \times 10^8 \text{-} 1.30 \times 10^8$ | 0.48-0.53 |
| | Load 3 | $9.30 \times 10^7 \text{-} 1.64 \times 10^8$ | 0.37-0.66 | $4.88 \times 10^7 \text{-} 5.46 \times 10^7$ | 0.20-0.22 | $1.08 \times 10^8 \text{-} 1.23 \times 10^8$ | 0.44-0.49 |
| | Load 4 | $1.13 \times 10^8 \text{-} 1.37 \times 10^8$ | 0.45-0.55 | $6.27 \times 10^7 \text{-} 7.92 \times 10^7$ | 0.25-0.32 | $1.13 \times 10^8 \text{-} 1.33 \times 10^8$ | 0.45-0.54 |
| Overturning Moment (N m) | Load 1 [nonlinear] | $[5.77 \times 10^8 \text{-} 9.22 \times 10^8]$ | [0.17-0.26] | $[2.88 \times 10^8 \text{-} 3.58 \times 10^8]$ | [0.08-0.10] | $8.71 \times 10^8 \text{-} 9.12 \times 10^8$ | 0.25-0.26 |
| | (Elastic) | $(6.44 \times 10^8 \text{-} 9.82 \times 10^8)$ | 0.19-0.28 | $(3.47 \times 10^8)$ | (0.10) | | |
| | Load 2 | $5.68 \times 10^8 \text{-} 9.15 \times 10^8$ | 0.16-0.26 | $4.36 \times 10^8 \text{-} 4.76 \times 10^8$ | 0.13-0.14 | $7.06 \times 10^8 \text{-} 8.33 \times 10^8$ | 0.20-0.24 |
| | Load 3 | $4.95 \times 10^8 \text{-} 8.32 \times 10^8$ | 0.14-0.24 | $3.11 \times 10^8 \text{-} 4.48 \times 10^8$ | 0.09-0.13 | $6.24 \times 10^8 \text{-} 7.50 \times 10^8$ | 0.18-0.22 |
| | Load 4 | $5.96 \times 10^8 \text{-} 7.28 \times 10^8$ | 0.17-0.21 | $4.20 \times 10^8 \text{-} 5.23 \times 10^8$ | 0.12-0.15 | $6.15 \times 10^8 \text{-} 9.56 \times 10^8$ | 0.18-0.28 |

[*] Ratio is defined in Equations 8.1 and 8.2 for base shear and overturning moment, respectively.

Table 8.12. Base shear and overturning moment developed on anchored and unanchored tanks under 1 horizontal component of modified earthquake records

| Parameter | Loading | PGA (g) | Anchored | | Unanchored | | $\dfrac{\text{Unanchored}}{\text{Anchored}}$ |
|---|---|---|---|---|---|---|---|
| | | | | Ratio | | Ratio | |
| $Q$ Base Shear (N) | P1547-BOL000 [nonlinear] (Elastic) {Rigid} | 0.64 | [1.65x10^8] (1.79x10^8) {6.47x10^7} | [0.66] (0.72) {0.26} | 6.13x10^7 | 0.25 | 37% |
| | P1087-ARC000 [nonlinear] (Elastic) {Rigid} | 0.75 | [1.10x10^8] (1.20x10^8) {6.22x10^7} | [0.44] (0.48) {0.25} | [5.92x10^7] (5.67x10^7) | [0.24] (0.23) | 54% |
| | P1558-MDR000 [nonlinear] (Elastic) {Rigid} | 0.49 | [1.78x10^8] (1.95x10^8) {4.86x10^7} | [0.72] (0.77) {0.20} | 5.27x10^7 | 0.21 | 30% |
| | P1114-YPT330 | 0.84 | 1.40x10^8 | 0.56 | - | - | - |
| | P1104-IZN090 | 0.59 | 1.50x10^8 | 0.60 | - | - | - |
| | P1096-DZC180 | 0.77 | 1.56x10^8 | 0.63 | 6.53x10^7 | 0.26 | 42% |
| $M$ Overturning Moment (N m) | P1547-BOL000 [nonlinear] (Elastic) | 0.64 | [8.53x10^8] (9.30x10^8) | [0.25] (0.27) | 3.35x10^8 | 0.10 | 39% |
| | P1087-ARC000 [nonlinear] (Elastic) | 0.75 | [5.77x10^8] (6.44x10^8) | [0.17] (0.19) | [3.58x10^8] (3.47x10^8) | [0.10] (0.10) | 62% |
| | P1558-MDR000 [nonlinear] (Elastic) | 0.49 | [9.22x10^8] (9.82x10^8) | [0.26] (0.28) | 2.88x10^8 | 0.08 | 31% |
| | P1114-YPT330 | 0.84 | 8.81x10^8 | 0.25 | - | - | - |
| | P1104-IZN090 | 0.59 | 8.71x10^8 | 0.25 | - | - | - |
| | P1096-DZC180 | 0.77 | 9.12x10^8 | 0.26 | 5.22x10^8 | 0.15 | 57% |
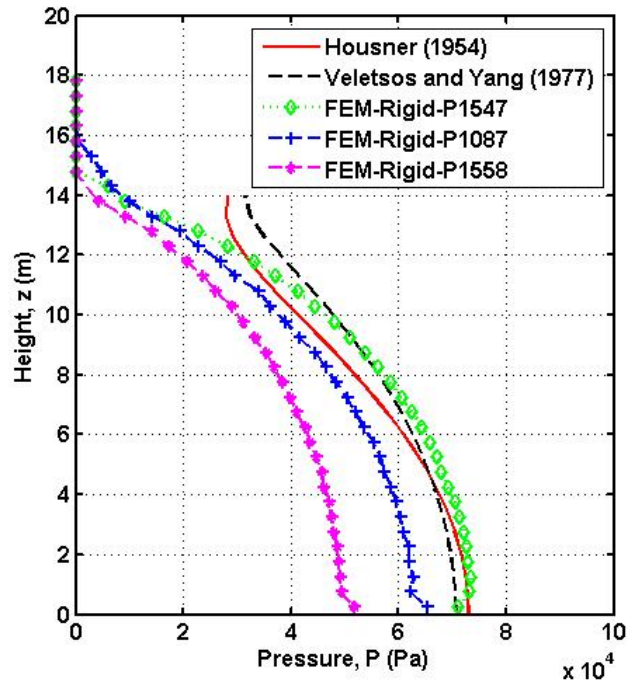
Figure 8.13. Pressure distribution on the rigid anchored tank wall
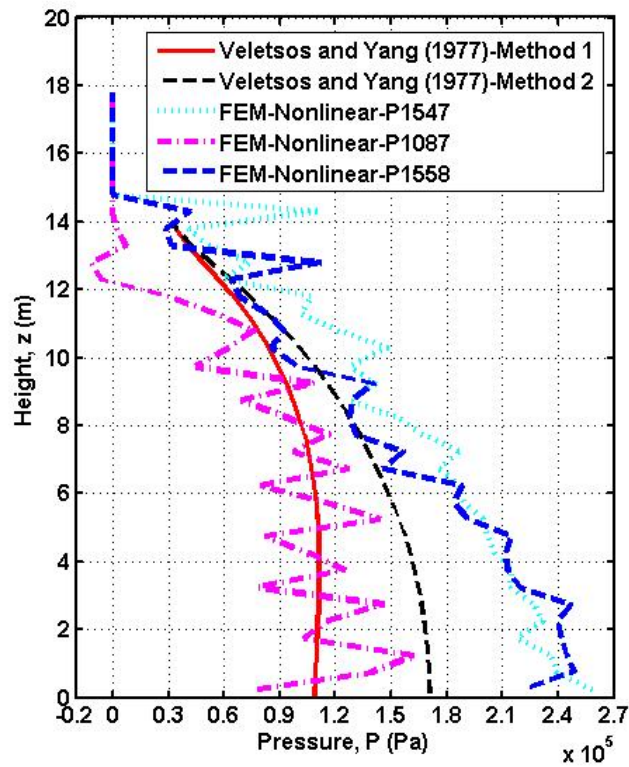
(rigid foundation)



Figure 8.14. Pressure distribution on the non-linear anchored tank wall

(rigid foundation)
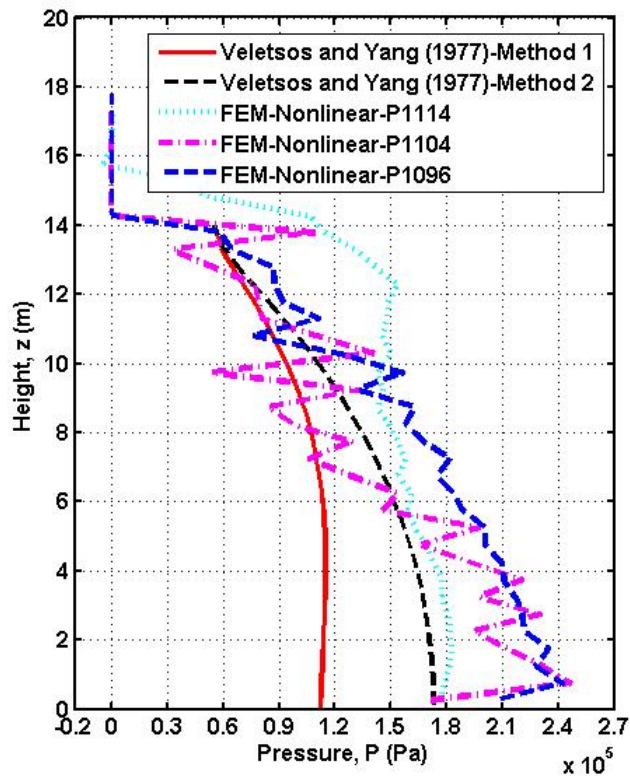
Figure 8.15. Pressure distribution on the non-linear anchored tank wall
(flexible foundation)

### 8.5.3. Free Surface Wave Height

In Figure 8.16, the elevation of the free surface in the anchored tank for Loading Cases 1 and 2 of modified P1547 record is represented by plotting iso-surface of element volume fraction ratio. These plots correspond to the occurrence of peak free surface displacement for Loading Cases 1 and 2 at 28.3 sec and 17.3 sec, respectively. The same surface shape of Loading Case 1 can be obtained for Loading Case 3. Loading Case 4 matches very well with Loading Case 2 as well. Therefore, Loading Cases 1 and 3 have almost the same sloshing response while both Loading Cases 1 and 4 deviate from them. For Loading Cases 2 and 4, even though the maximum wave height does not occur on the X axis, it is only slightly higher than that observed on the X axis. The maximum displacement occurs at $\theta=0°$ and $r =\pm R$, while the free surface displacement is negligible at $\theta=90°$ and $270°$, when tank is subjected to one horizontal ground motion component (Loading Case 1). The sloshing response is symmetric about the X axis. The symmetry of the free surface is preserved when tank is subjected to 1 horizontal and 1 vertical ground

motion components (Loading Case 3). However, when two horizontal components or 3 dimensional earthquake loading is considered the free surface displacement loses its symmetric behavior and the maximum value of the displacements does not occur at r = ±R. Free surface displacement observed at its maximum location is slightly higher than its value at r = ±R. As a result, the presence of the second horizontal motion component is responsible for these changes in the sloshing response. It affects temporal and spatial distributions of free surface wave height, while the vertical component of the earthquake motion has a negligible effect on the sloshing response. These observations are valid for all of selected records.

Figure 8.18 to Figure 8.22 show time history plots of the free surface elevation at X=-R (θ=180.0°) when anchored and unanchored tanks are subjected to different earthquake ground motion records and different combinations of record components. It can be seen from these figures that the sloshing response is almost identical for anchored and unanchored tanks. Hence, the general acceptance in the literature regarding the insensitivity of sloshing response to the tank base support conditions is validated by using the fully nonlinear algorithm. Sloshing response does not change for different ground motion components as well.

Figure 8.23 to Figure 8.25 show free surface time history at X=-R and θ=180.0° when anchored tank are founded on Z3 soil type. In this case, sloshing response is different than that when tank is settled on rigid foundation. Maximum free surface wave height for anchored tank supported on Z3 soil type exceeds 4 m. Sloshing waves in the anchored tank impact to the roof of the tank and cause high joint stresses at the junction between tank wall and tank roof and sloshing damage at the tank roof. Therefore, regular harmonic behavior of sloshing waves is disturbed.

Maximum sloshing wave height observed for all selected earthquake ground motion records and combinations are summarized in Table 8.13. Average maximum sloshing wave height is around 3.60 m for tanks supported on rigid foundation. Numerical analyses are extended up to 40 sec in order to observe the variation of sloshing wave height after motion subsides. It is figured out that free surface height decreases slowly and never exceeds its maximum value observed during the effective duration of the earthquake.

Anchored - P1547-BOL  (Loading 1)          Anchored - P1547-BOL (Loading 2)
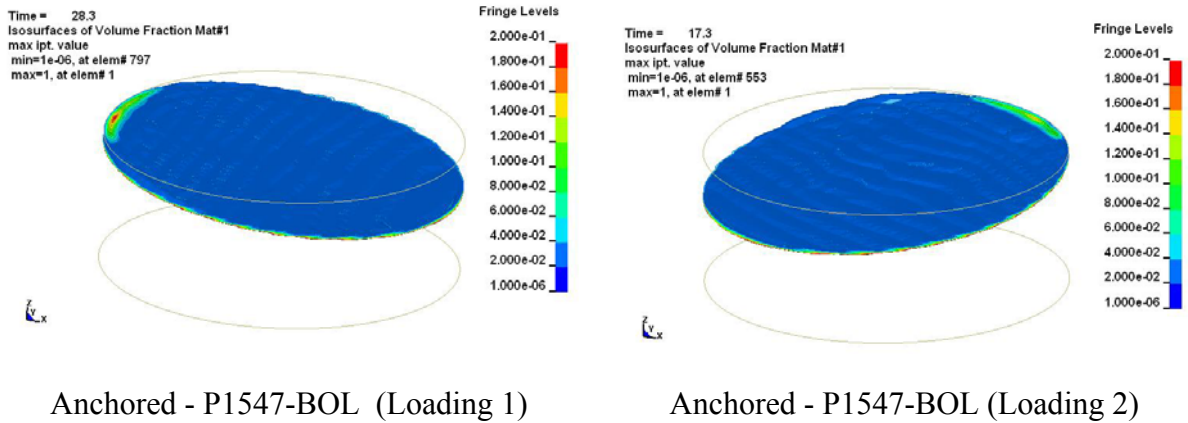
Figure 8.16. Contours of free surface elevation
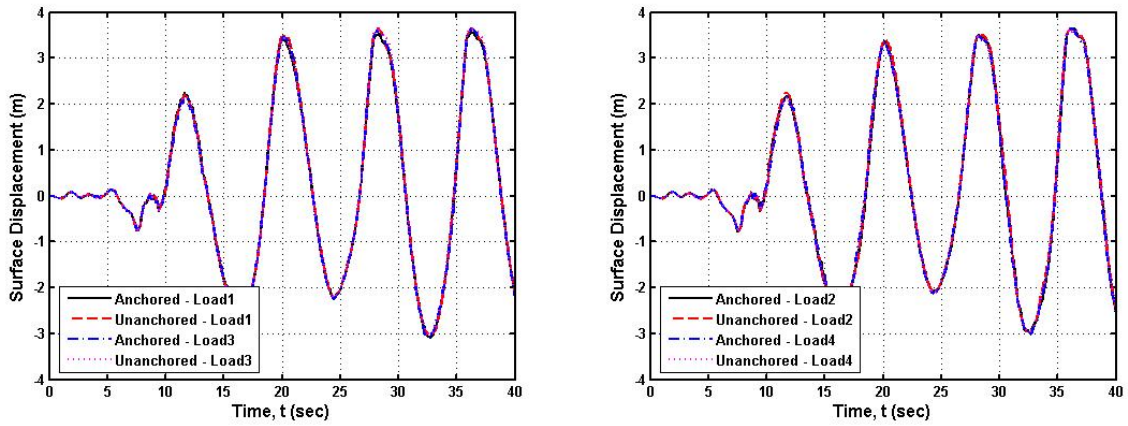


Figure 8.17. Comparisons of the free surface time histories of tanks under different combinations of earthquake ground motion components of P1547 BOL record (θ=180.0°)
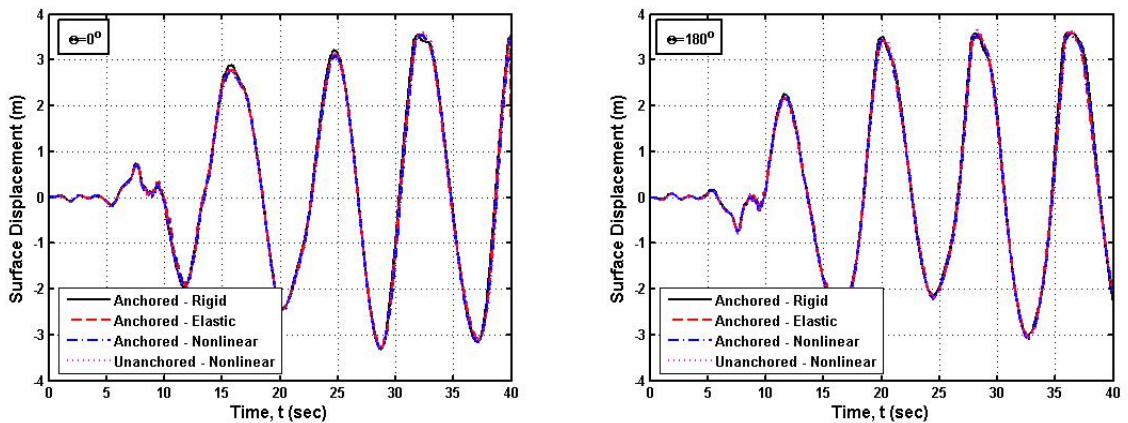


Figure 8.18. Comparisons of the free surface time histories of tanks with different tank materials and support conditions under P1547 BOL000 record
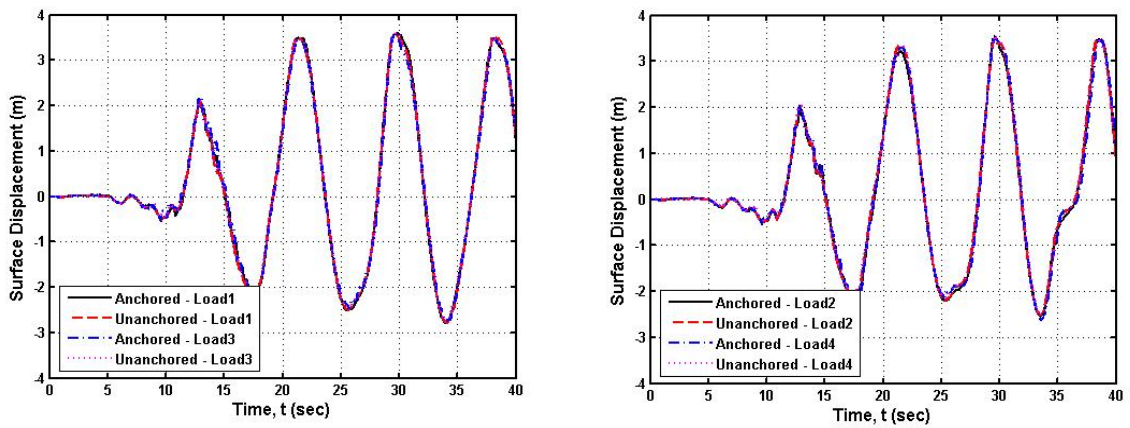
Figure 8.19. Comparisons of the free surface time histories of tanks under different combinations of earthquake ground motion components of P1087-ARC record (θ=180.0°)
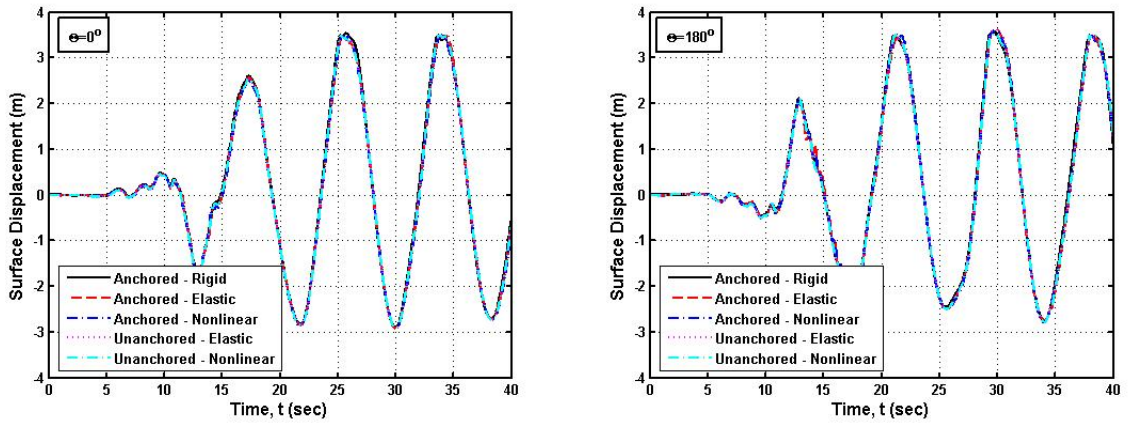


Figure 8.20. Comparisons of the free surface time histories of tanks with different tank materials and support conditions under P1087-ARC000 record
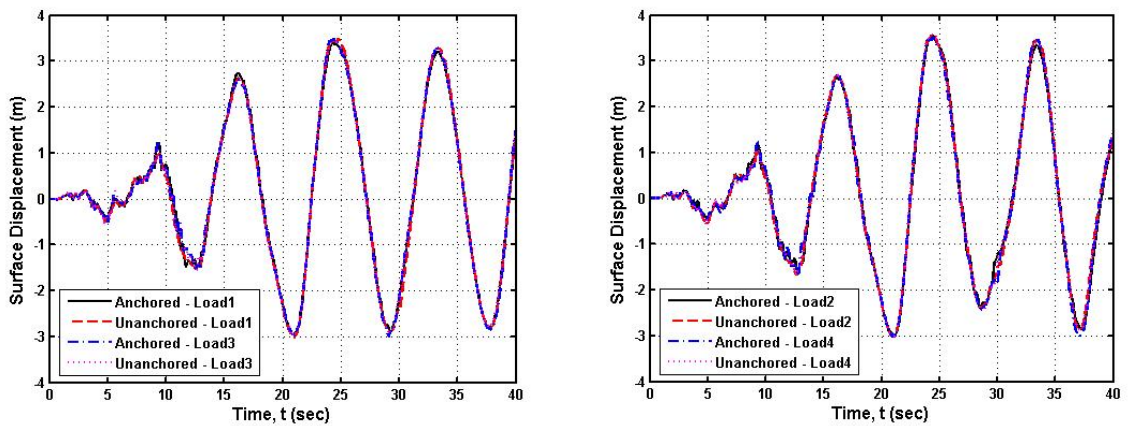


Figure 8.21. Comparisons of free surface time histories of tanks under different combinations of earthquake ground motion components of P1558-MDR record (θ=180°)
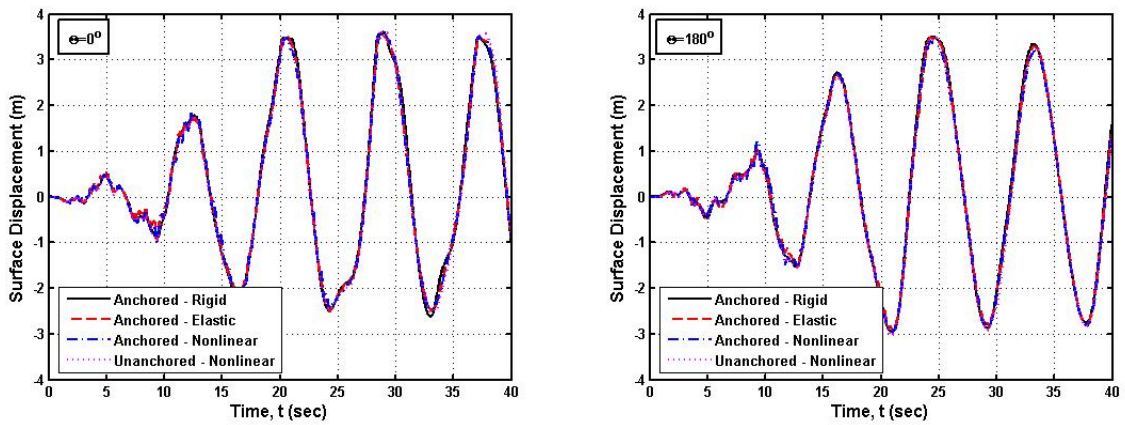
Figure 8.22. Comparisons of the free surface time histories of tanks with different tank materials and support conditions under P1558-MDR000 record
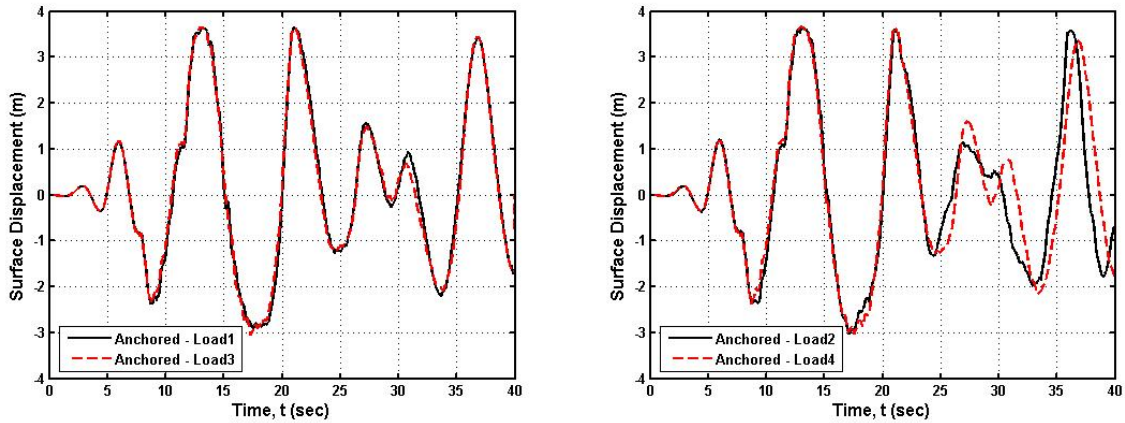


Figure 8.23. Comparisons of the free surface time histories of tanks under different combinations of earthquake ground motion components of P1114-YPT record (θ=180.0°)
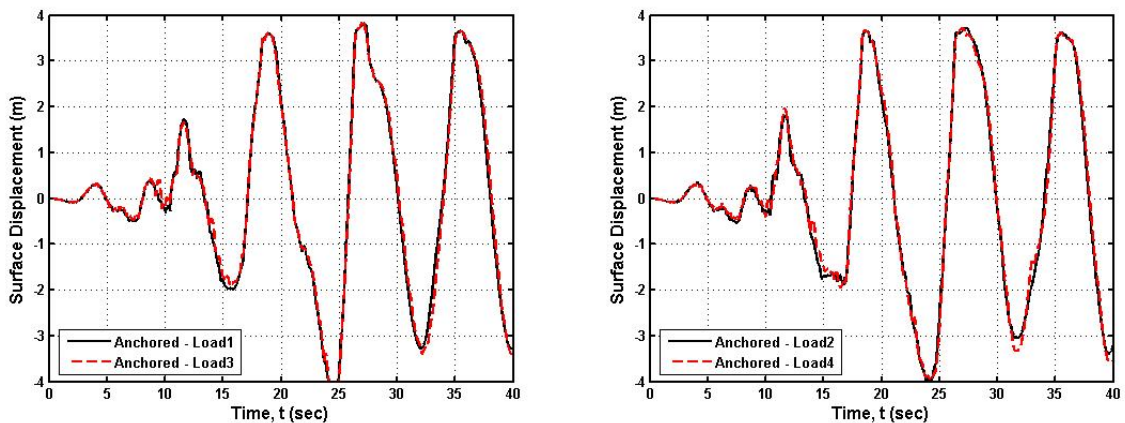


Figure 8.24. Comparisons of the free surface time histories of tanks under different combinations of earthquake ground motion components of P1104-IZN record (θ=180.0°)
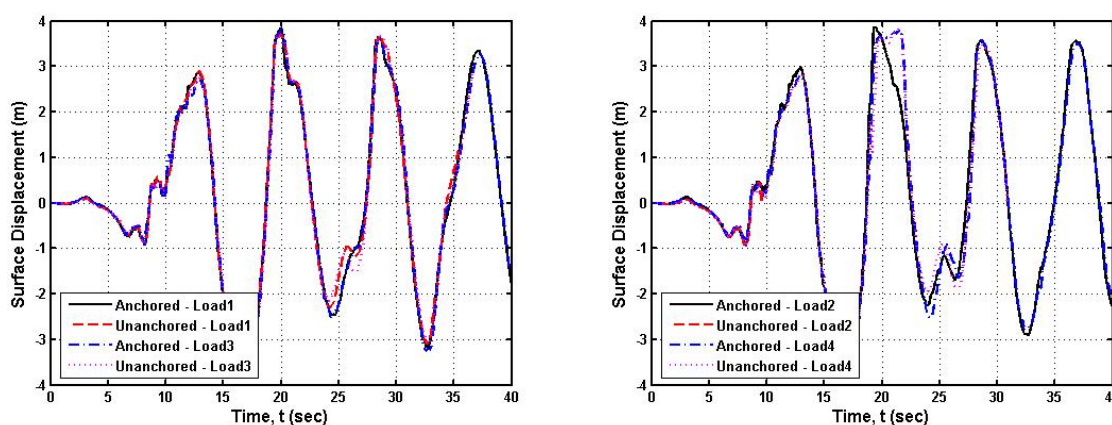
Figure 8.25. Comparisons of the free surface time histories of tanks under different combinations of earthquake ground motion components of P1096-DZC record (θ=180.0°)

### 8.5.4. Uplift Response of the Unanchored Tank

Figure 8.26 to Figure 8.29 show uplift response of the unanchored tank for different loading conditions of 3 earthquake ground motions between 5 and 25 sec of the analysis which coincides with the intensive ground shaking portion of both horizontal components. The maximum uplift displacements of the tank base nodes during seismic motion are illustrated in Figure 8.30 to Figure 8.33. According to these graphs uplift is observed at all nodes around the circumference of the base plate for all loading case. Maximum uplift occurs at θ=0° or θ=180° for Loading Case 1. Uplift displacements slightly increase when vertical ground motion component combined with horizontal component (Loading Case 3). The second horizontal ground motion component substantially amplifies the uplift displacements. Presence of vertical component simultaneously with the two horizontal components (Loading Case 4) slightly influences maximum base uplift. As a summary, the concurrent presence of both two horizontal components causes considerable amplification in the uplift response, while vertical component slightly affects the uplift. Unlike Loading Cases 1 and 3, maximum uplift is not observed at the nodes on the X axis for Loading Cases 2 and 4. Figure 8.29 shows the base uplift displacement of the unanchored tank subjected to modified P1096 record and founded on flexible soil. Soil flexibility increases the uplift displacement almost 4 times when the unanchored tank is subjected to Loading Cases 1 and 3, while uplift displacement almost reached almost 0.30 m under three-dimensional motion. The variation of uplift displacement of the unanchored tank base around the tank circumference is given in Figure 8.33. For the Loading Cases 1 and 3,

uplift displacement is symmetric about the X axis while the nodes around the circumference of the tank base between θ=0° or θ=202.5° experience base uplift displacement of approximately 0.28 m under Loading Case 4.

In Figure 8.34, the base uplift displacements of the unanchored tank with elastic and nonlinear material properties are compared when unanchored tank is subjected to P1087 record. Maximum base displacement at θ=180° is 0.038 m for elastic tank material while it slightly increases to 0.04 m for nonlinear tank material. For θ=0°, base displacement is 0.031 m and 0.043 m for elastic and inelastic tank materials, respectively. Figure 8.35 shows the variation of base uplift around the elastic and nonlinear unanchored tank circumference. As can be seen from this figure, base uplift all around the tank circumference is slightly affected by tank material nonlinearity.

Figure 8.36 to Figure 8.38 show overturning moment developed at the base of the unanchored tank wall due to Loading Case 1. Uplift displacements of the two extreme points of the tank on the X axis are scaled with an arbitrary factor and are plotted on this graph in order to examine the relation between uplift displacement and overturning moment. As can be seen from this graph, the peak values of the overturning moment are accompanied by uplift of the base plate. But, uplift occurs when the overturning moment exceeds a threshold value (approximately $1.5 \times 10^8$ Nm) and continues increasing in the same direction. In other words, although the overturning moment that is developed may exceed the resisting moment temporarily, the uplift may be not observed due to the cyclic reversal of the acceleration that stops the uplift tendency.

Maximum uplift displacements of unanchored tank along with maximum overturning moment values and peak ground accelerations are summarized in Table 8.14. Increase in peak ground acceleration accompanies slight amplification of overturning moment that lead to slight uplift displacement of unanchored tank base.

Table 8.13. Maximum free Surface wave height on the X axis, θ=180.0°, r =-R (unit: m)

| | Loading | Anchored | Unanchored |
|---|---|---|---|
| P1547 | Load 1 [Nonlinear] (Elastic) {Rigid} | [3.58] (3.61) {3.60} | [3.65] |
| | Load 2 | 3.66 | 3.65 |
| | Load 3 | 3.65 | 3.65 |
| | Load 4 | 3.65 | 3.61 |
| P1087 | Load 1 [Nonlinear] (Elastic) {Rigid} | [3.60] (3.62) {3.60} | [3.55] (3.63) |
| | Load 2 | 3.54 | 3.50 |
| | Load 3 | 3.59 | 3.60 |
| | Load 4 | 3.50 | 3.56 |
| P1558 | Load 1 [Nonlinear] (Elastic) {Rigid} | [3.41] (3.48) {3.51} | [3.48] |
| | Load 2 | 3.54 | 3.58 |
| | Load 3 | 3.48 | 3.43 |
| | Load 4 | 3.51 | 3.60 |
| P1114 | Load 1 | > 4.00 | - |
| | Load 2 | > 4.00 | - |
| | Load 3 | > 4.00 | - |
| | Load 4 | > 4.00 | - |
| P1096 | Load 1 | > 4.00 | > 4.00 |
| | Load 2 | > 4.00 | - |
| | Load 3 | > 4.00 | > 4.00 |
| | Load 4 | > 4.00 | > 4.00 |
| P1104 | Load 1 | > 4.00 | - |
| | Load 2 | > 4.00 | - |
| | Load 3 | > 4.00 | - |
| | Load 4 | > 4.00 | - |
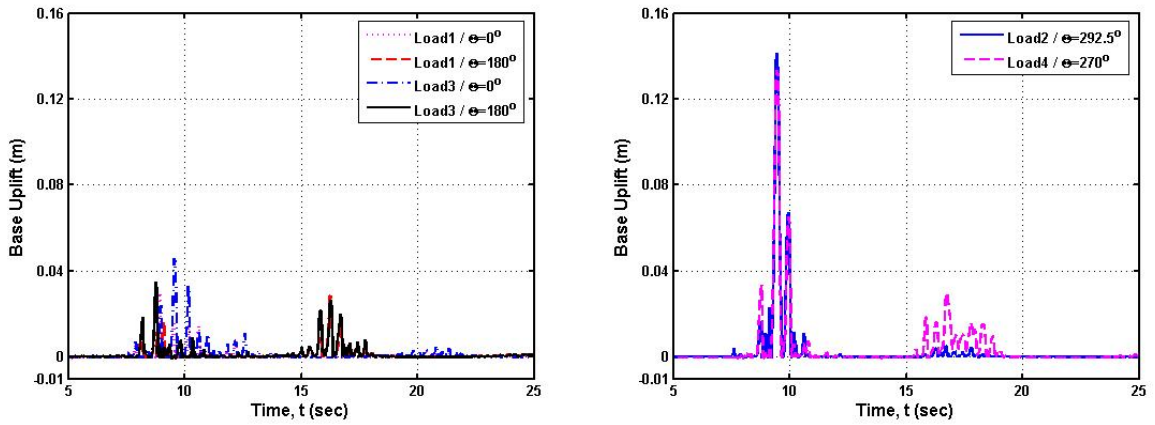
Figure 8.26. Comparisons of the base uplift time histories of unanchored tanks under different combinations of earthquake components (P1547-BOL)
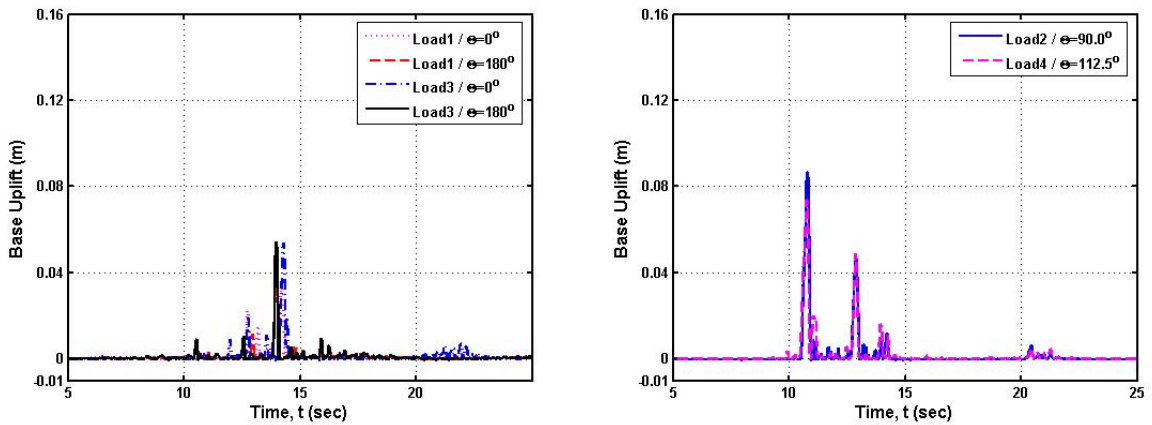


Figure 8.27. Comparisons of the base uplift time histories of unanchored tanks under different combinations of earthquake components (P1087-ARC)
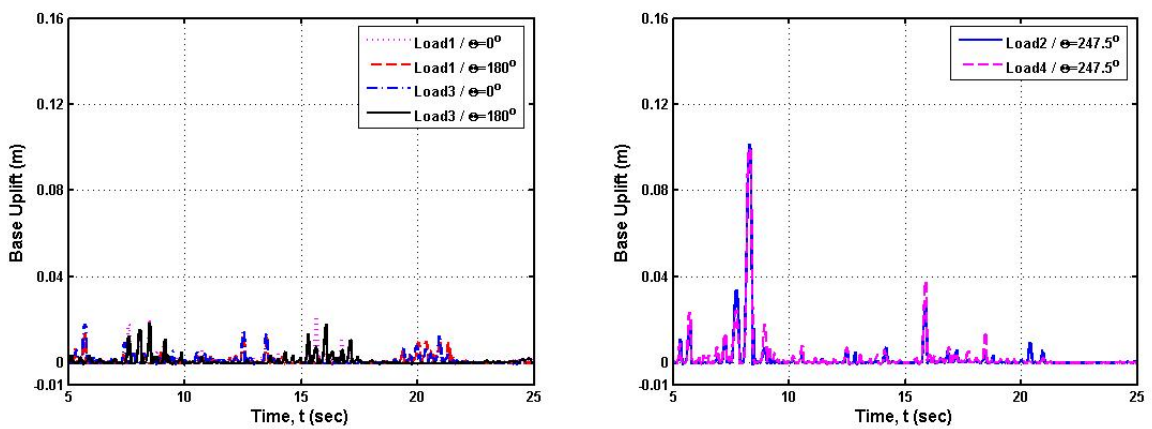


Figure 8.28. Comparisons of the base uplift time histories of unanchored tanks under different combinations of earthquake components (P1558-MDR)
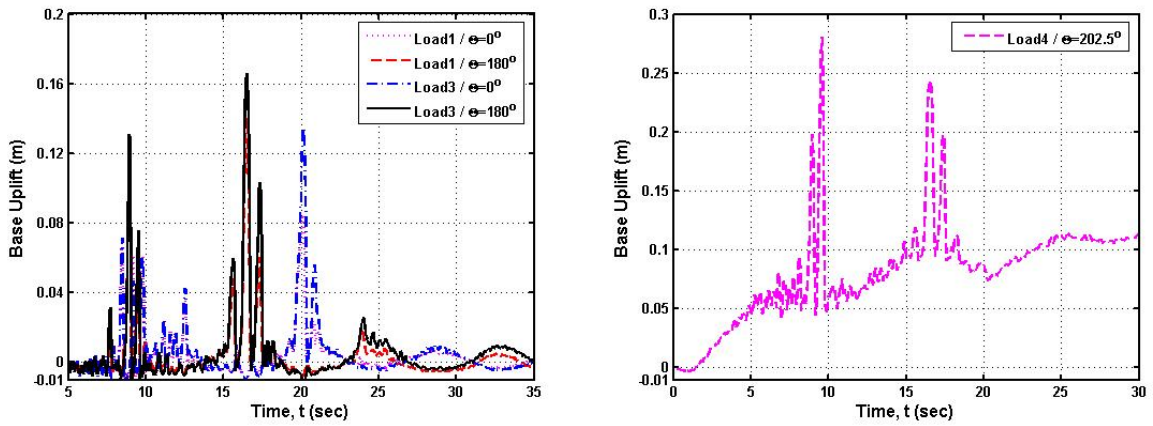
Figure 8.29. Comparisons of the base uplift time histories of unanchored tanks under different combinations of earthquake components (P1096-DZC)
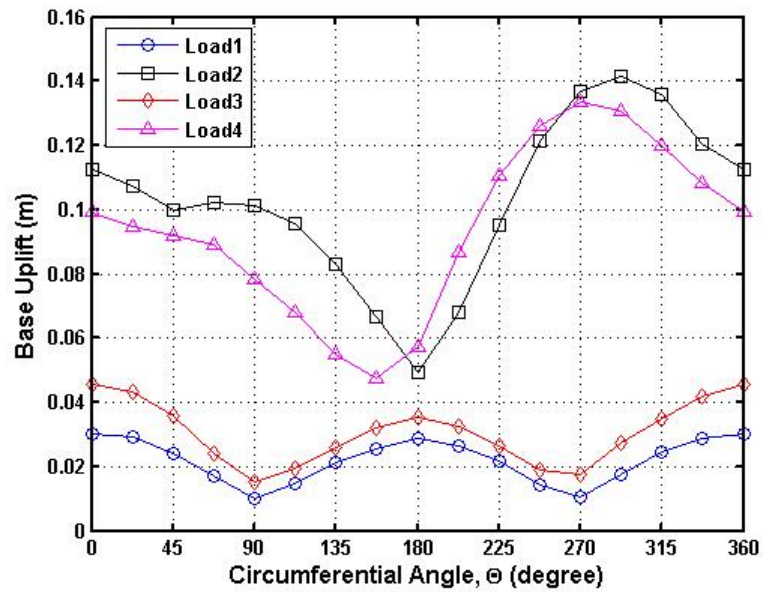


Figure 8.30. Uplift displacement around the unanchored tank circumference for different record combinations (P1547-BOL)
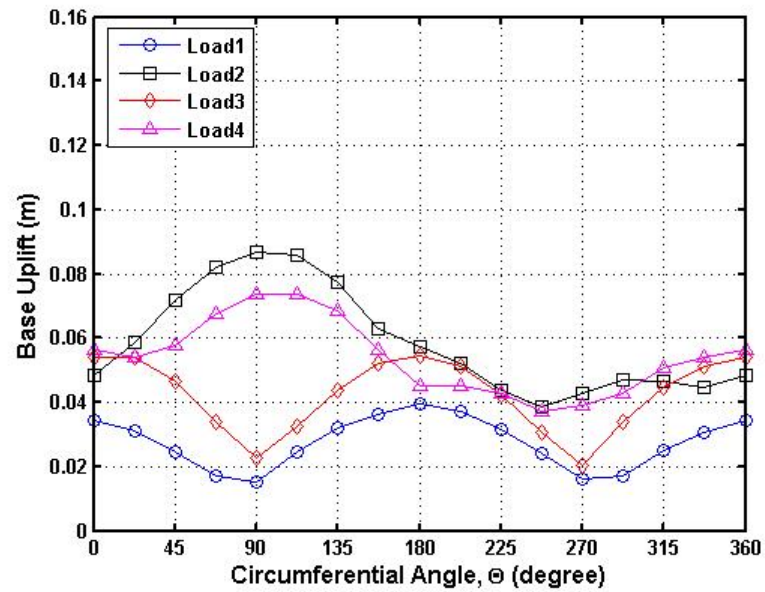
Figure 8.31. Uplift displacement around the unanchored tank circumference for different record combinations (P1087-ARC)
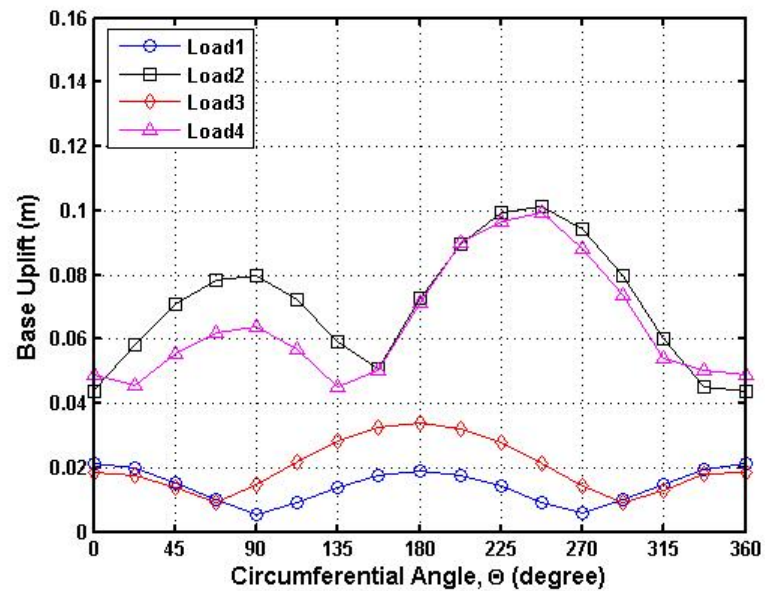


Figure 8.32. Uplift displacement around the unanchored tank circumference for different record combinations (P1558-MDR)
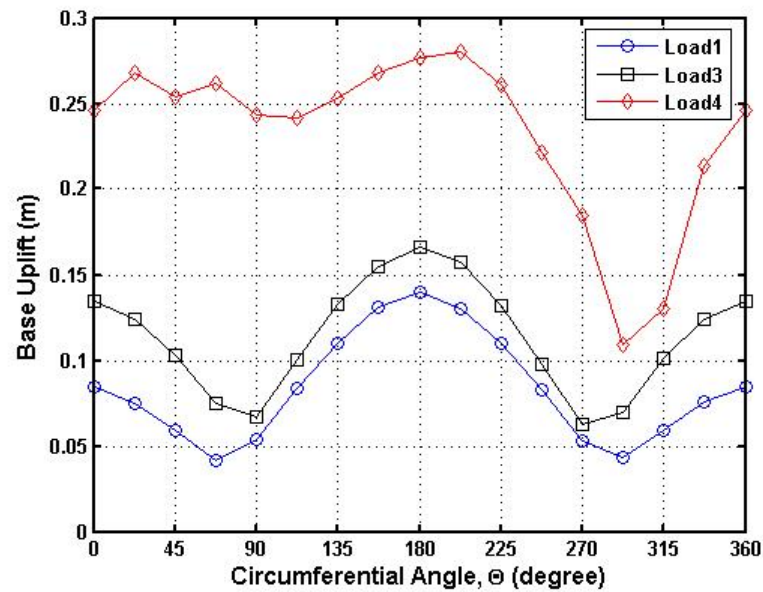
Figure 8.33. Uplift displacement around the unanchored tank circumference for different record combinations (P1096-DZC)
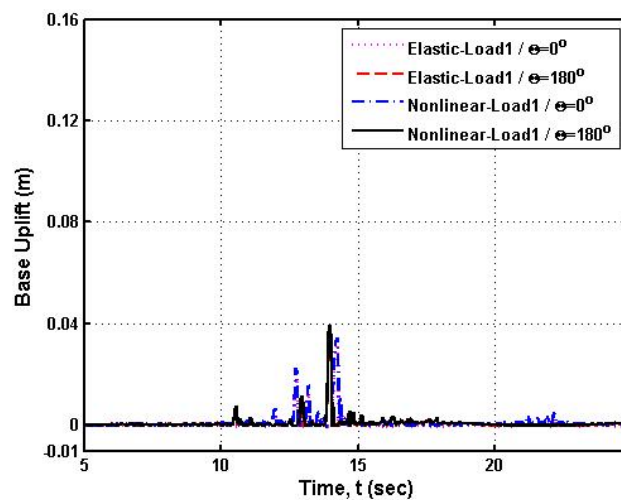


Figure 8.34. Comparisons of the base uplift time histories of unanchored tanks with elastic and inelastic material properties under P1087-ARC000 record
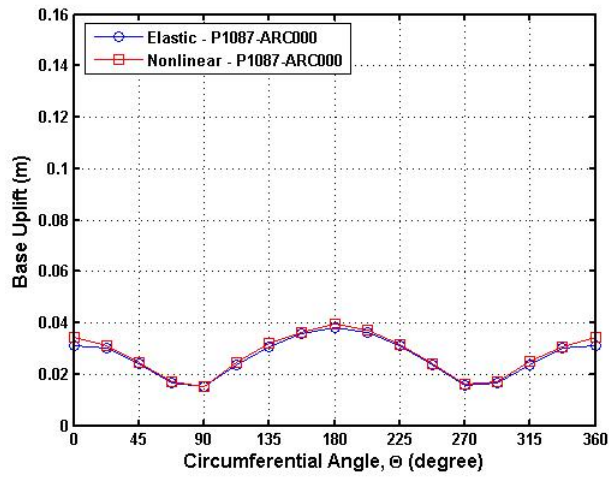
Figure 8.35. Uplift displacement around the unanchored tank circumference for elastic and inelastic tank materials under P1087-ARC000 record
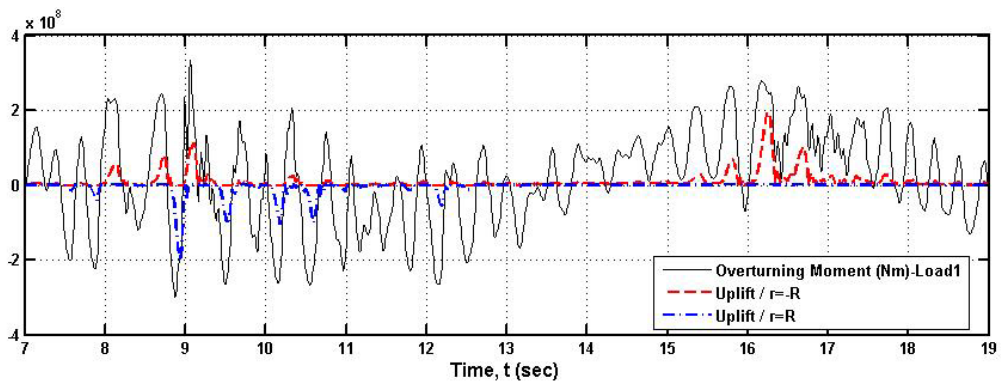


Figure 8.36. Overturning moment-uplift relation for P1547-BOL000 record
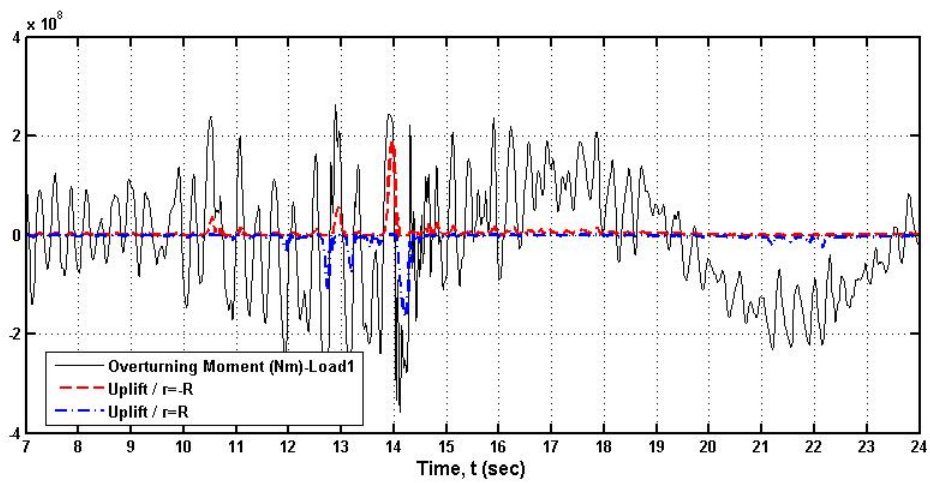


Figure 8.37. Overturning moment-uplift relation for P1087-ARC000 record
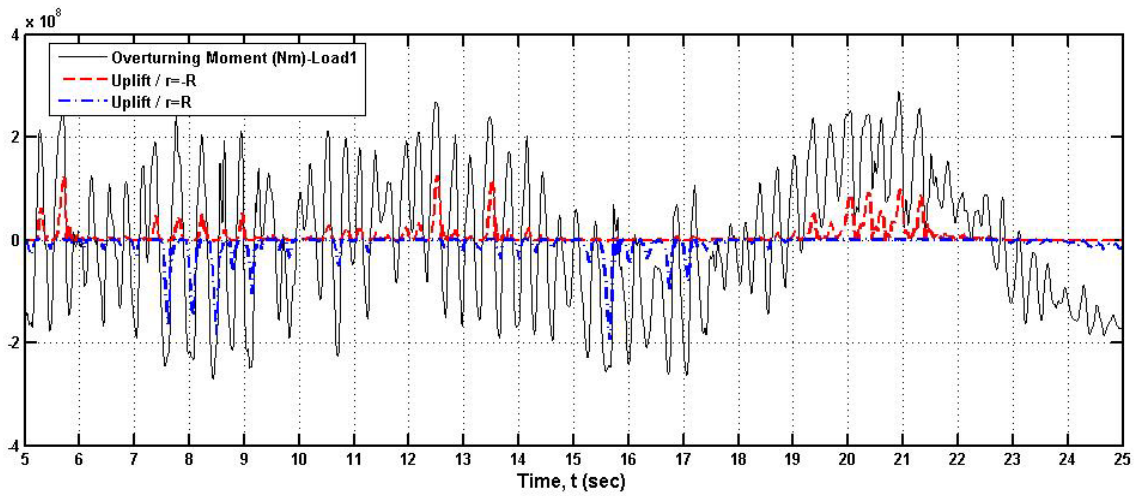
Figure 8.38. Overturning moment-uplift relation for P1558-MDR000 record

Table 8.14. Overturning moment and uplift displacement

| | Loading | PGA (g) | Max Overturning Moment (Nm) | Max Uplift (m) |
|---|---|---|---|---|
| P1547 | Load 1 | 0.64 | $3.35 \times 10^8$ | 0.03 |
| | Load 2 | 0.64 / 0.91 | $4.76 \times 10^8$ | 0.14 |
| | Load 3 | 0.64 / 0.43 | $3.11 \times 10^8$ | 0.05 |
| | Load 4 | 0.64 / 0.91 / 0.43 | $4.57 \times 10^8$ | 0.13 |
| P1087 | Load 1 (Elastic) | 0.75 | $3.58 \times 10^8$ ($3.47 \times 10^8$) | 0.04 (0.038) |
| | Load 2 | 0.75 / 0.56 | $4.63 \times 10^8$ | 0.09 |
| | Load 3 | 0.75 / 0.49 | $4.48 \times 10^8$ | 0.05 |
| | Load 4 | 0.75 / 0.56 / 0.49 | $5.23 \times 10^8$ | 0.07 |
| P1558 | Load 1 | 0.49 | $2.88 \times 10^8$ | 0.02 |
| | Load 2 | 0.49 / 0.46 | $4.36 \times 10^8$ | 0.11 |
| | Load 3 | 0.49 / 0.36 | $3.62 \times 10^8$ | 0.03 |
| | Load 4 | 0.49 / 0.46 / 0.36 | $4.20 \times 10^8$ | 0.09 |

### 8.5.5. Shell Stresses

Axial compressive and hoop stresses developed on anchored and unanchored tanks when subjected to selected earthquake ground motions are summarized in Table 8.15. Maximum axial compressive stresses developed in the anchored tank wall concentrate just above the base plate due to the restraint action of the tank base and in regions where out-of-round distortions occur. The numerical analysis results verify that the base uplifting changes the dynamic characteristics such as stiffness and energy dissipation capacity of the system. High axial compressive stresses in the unanchored tank wall concentrates at the regions where bulging formation develops and tank base remains in contact with the ground while the opposite edge of the base plate experiences uplift. Uplift triggers small amplitude local out-of-round distortions of the circular tank shell cross-section however anchored tank has slightly larger radial deformations than unanchored tank. When the amplitude of ground motion is small, the out-of-round distortions of the tank shell decreases. These out-of-round distortions influence stresses developed in the anchored and unanchored tanks. Coupling of the uplift mechanism and out-of round distortions produces high axial compressive membrane stresses with a narrow distribution along the wall of the unanchored tank which remains contact with the ground. Also, the vertical component of ground motion increases out-of round distortions of the tank shell. Out-of round distortions of the anchored tank are always greater than those of the unanchored tank due to restraint action of the tank base support condition.

For P1547 record, the maximum axial compressive stress developed at the anchored tank shell is around $3-4\times10^8$ Pa for all loading cases, while that exerted on the unanchored tank wall is $1.5\times10^8$ Pa for Loading Case 1, $2.5\times10^8$ Pa for Loading Cases 2 and 3 and $3.0\times10^8$ Pa for Loading Case 4. For both anchored and unanchored tanks, hoop stresses are close to yield limit.

The maximum axial compressive stress developed on the anchored tank under different combinations of the P1087-ARC record is around $3.6-3.8\times10^8$ Pa while this stress is between $1.7\times10^8$ Pa and $2.9\times10^8$ Pa in the unanchored tank wall for different loading conditions. Elastic anchored and unanchored tanks material plasticity undergoes axial compressive stress of $4.7\times10^8$ Pa and $1.7\times10^8$ Pa under Loading Case 1. Hoop stresses in

anchored and unanchored tank walls with elastic material under 1 horizontal ground motion component are $4.7 \times 10^8$ and $3.6 \times 10^8$ Pa, respectively, while hoop stress developed in tank with elasto-plastic material is close to yield limit.

Table 8.15. Shell stresses of anchored and unanchored tanks under different earthquake records (unit: Pa)

| | | Anchored | | Unanchored | |
|---|---|---|---|---|---|
| | Loading | Axial | Hoop | Axial | Hoop |
| P1547 | Load 1 | $3.0 \times 10^8$ | $2.5 \times 10^8$ | $1.5 \times 10^8$ | $3.0 \times 10^8$ |
| | Load 2 | $4.0 \times 10^8$ | $> \sigma_{yield}$ | $2.5 \times 10^8$ | $3.5 \times 10^8$ |
| | Load 3 | $3.6 \times 10^8$ | $3.5 \times 10^8$ | $2.5 \times 10^8$ | $> \sigma_{yield}$ |
| | Load 4 | $3.5 \times 10^8$ | $> \sigma_{yield}$ | $3.0 \times 10^8$ | $> \sigma_{yield}$ |
| P1087 | Load 1 inelastic (elastic) | $3.8 \times 10^8$ $(4.70 \times 10^8)$ | $3.4 \times 10^8$ $(4.70 \times 10^8)$ | $2.0 \times 10^8$ $(1.7 \times 10^8)$ | $3.0 \times 10^8$ $(3.6 \times 10^8)$ |
| | Load 2 | $3.7 \times 10^8$ | $3.5 \times 10^8$ | $1.7 \times 10^8$ | $> \sigma_{yield}$ |
| | Load 3 | $3.6 \times 10^8$ | $3.5 \times 10^8$ | $2.4 \times 10^8$ | $> \sigma_{yield}$ |
| | Load 4 | $3.8 \times 10^8$ | $> \sigma_{yield}$ | $2.9 \times 10^8$ | $> \sigma_{yield}$ |
| P1558 | Load 1 | $3.5 \times 10^8$ | $> \sigma_{yield}$ | $1.7 \times 10^8$ | $3.4 \times 10^8$ |
| | Load 2 | $3.5 \times 10^8$ | $> \sigma_{yield}$ | $1.9 \times 10^8$ | $3.2 \times 10^8$ |
| | Load 3 | $3.5 \times 10^8$ | $> \sigma_{yield}$ | $2.2 \times 10^8$ | $> \sigma_{yield}$ |
| | Load 4 | $3.5 \times 10^8$ | $> \sigma_{yield}$ | $3.0 \times 10^8$ | $> \sigma_{yield}$ |
| P1114 | Load 1 inelastic (elastic) | $3.6 \times 10^8$ $(5.0 \times 10^8)$ | $> \sigma_{yield}$ $(6.0\ 10^8)$ | - | - |
| | Load 2 | $3.7 \times 10^8$ | $> \sigma_{yield}$ | - | - |
| | Load 3 | $3.7 \times 10^8$ | $2.5\ 10^8$ | - | - |
| | Load 4 | $3.7 \times 10^8$ | $> \sigma_{yield}$ | - | - |
| P1096 | Load 1 | $3.8 \times 10^8$ | $> \sigma_{yield}$ | $2.5 \times 10^8$ | $\approx \sigma_{yield}$ |
| | Load 2 | $3.9 \times 10^8$ | $> \sigma_{yield}$ | - | - |
| | Load 3 | $3.8 \times 10^8$ | $> \sigma_{yield}$ | $2.0 \times 10^8$ | $> \sigma_{yield}$ |
| | Load 4 | $3.8 \times 10^8$ | $> \sigma_{yield}$ | $3.1 \times 10^8$ | $> \sigma_{yield}$ |
| P1104 | Load 1 | $3.6 \times 10^8$ | $> \sigma_{yield}$ | - | - |
| | Load 2 | $3.6 \times 10^8$ | $> \sigma_{yield}$ | - | - |
| | Load 3 | $3.6 \times 10^8$ | $> \sigma_{yield}$ | - | - |
| | Load 4 | $3.7 \times 10^8$ | $> \sigma_{yield}$ | - | - |

For P1558 record, maximum axial compressive stress developed in the anchored tank wall is around $3.5 \times 10^8$ Pa for all loading cases. Axial compressive stress developed on the unanchored tank wall is between $1.7 \times 10^8$ and $3.0 \times 10^8$ Pa for different loading cases while hoop stresses are close to yield limit for all loading cases.

Soil flexibility increases axial compressive stresses developed in the anchored and unanchored tank walls and hoop stresses exceed yield limit for both support conditions. For the anchored tank founded on flexible foundation, axial compressive stress is between $3.6 \times 10^8$ and $3.9 \times 10^8$ Pa.

## 8.5.6. Plastic Deformations and Radial Displacements

Maximum radial deformations on the X axis and plastic strain developed at the anchored and unanchored tank walls are given in Table 8.16. Fringe plots of plastic strain developed on anchored and unanchored tanks for all loading conditions are illustrated in Figure 8.39 to Figure 8.44. The most critical loading condition is the 3 dimensional loading for both radial shell displacements and plastic strain developed on the anchored and unanchored tank walls. For the same loading conditions, anchored tank always undergoes higher plastic deformation and radial displacements than unanchored tank due to the restraints at the anchored tank base. Presence of second horizontal or vertical ground motion component in addition to one horizontal component causes increase in plastic strain.

For all loading and support conditions, hoop stress developed in the tank shell close to yield limit or in some cases it exceeds yield stress of the tank material and axial compressive stress exceeds theoretical buckling stress of the tank shell. This stress state causes plasticity at the lower part of the tank wall in the form of elephant foot buckling. Therefore, anchoring does not prevent occurrence of elasto-plastic instability at the tank wall just above the tank base.

For tanks settled on rigid ground, hydrodynamic pressure generated by sloshing waves cause increase in the joint stresses at the junction of the tank wall and roof. Sloshing damage at the tank roof is only observed when tank is placed on stiff clay. Maximum

plastic strain reaches 0.015 at the connection between tank roof and wall under P1114 record. Flexible soil increases radial deformation and plastic strain developed on the anchored and unanchored tanks and causes roof damage.

Table 8.16. Maximum radial displacement on the X axis and plastic strain developed on anchored and unanchored tanks (unit: m)

| | | Anchored | | Unanchored | |
|---|---|---|---|---|---|
| | Loading | Radial Displacement | Plastic Strain | Radial Displacement | Plastic Strain |
| P1547 | Load 1 | 0.25 | 0.004 | 0.11 | 0.001 |
| | Load 2 | 0.18 | 0.005 | 0.10 | 0.0015 |
| | Load 3 | 0.23 | 0.005 | 0.15 | 0.003 |
| | Load 4 | 0.25 | 0.005 | 0.13 | 0.005 |
| P1087 | Load 1 | 0.26 | 0.004 | 0.10 | 0.0009 |
| | Load 2 | 0.21 | 0.004 | 0.12 | 0.0012 |
| | Load 3 | 0.21 | 0.0042 | 0.12 | 0.0015 |
| | Load 4 | 0.36 | 0.0053 | 0.10 | 0.0015 |
| P1558 | Load 1 | 0.20 | 0.0045 | 0.12 | 0.0011 |
| | Load 2 | 0.21 | 0.0045 | 0.10 | 0.0012 |
| | Load 3 | 0.23 | 0.0052 | 0.10 | 0.0023 |
| | Load 4 | 0.29 | 0.007 | 0.12 | 0.0025 |
| P1114 | Load 1 | 0.24 | 0.015 | - | - |
| | Load 2 | 0.20 | 0.015 | - | - |
| | Load 3 | 0.39 | 0.015 | - | - |
| | Load 4 | 0.39 | 0.015 | - | - |
| P1104 | Load 1 | 0.25 | 0.011 | - | - |
| | Load 2 | 0.32 | 0.009 | - | - |
| | Load 3 | 0.36 | 0.01 | - | - |
| | Load 4 | 0.35 | 0.008 | - | - |
| P1096 | Load 1 | 0.26 | 0.012 | 0.14 | 0.008 |
| | Load 2 | 0.22 | 0.006 | - | - |
| | Load 3 | 0.32 | 0.011 | 0.18 | 0.009 |
| | Load 4 | 0.34 | 0.006 | 0.35 | 0.008 |

Anchored (Loading 1)

Anchored (Loading 2)

Anchored (Loading 3)

Anchored (Loading 4)

Unanchored (Loading 1)

Unanchored (Loading 2)

Unanchored (Loading 3)

Unanchored (Loading 4)
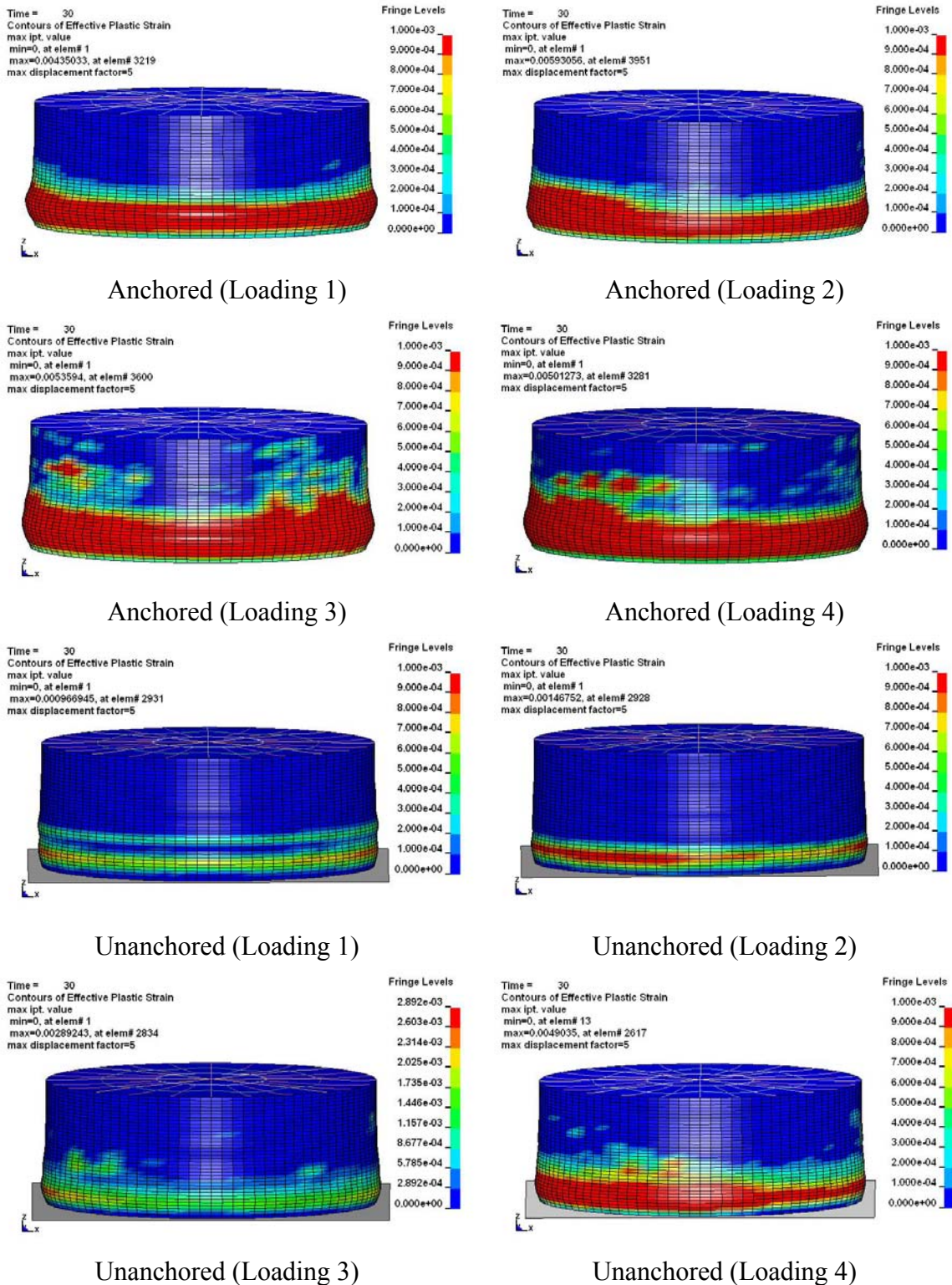
Figure 8.39. Plastic deformations and deflections of the anchored and unanchored tank

models subjected to different combinations of P1547 earthquake record
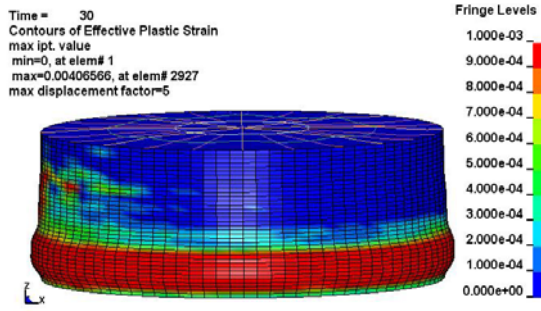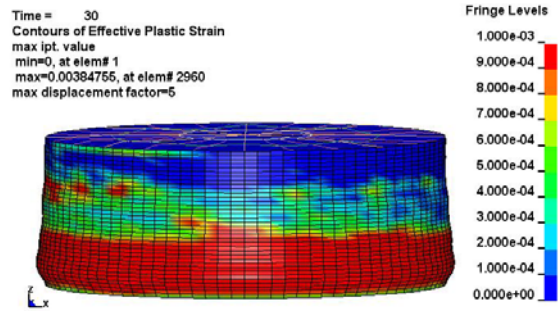
(displacements magnified 5 times)

Anchored (Loading 1)
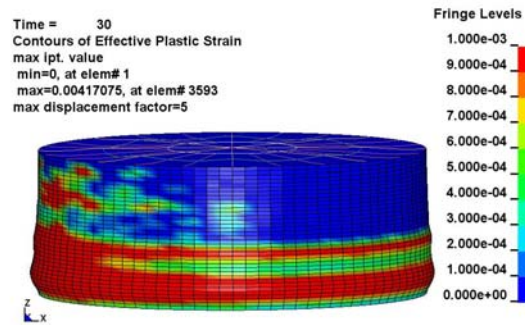
Anchored (Loading 2)
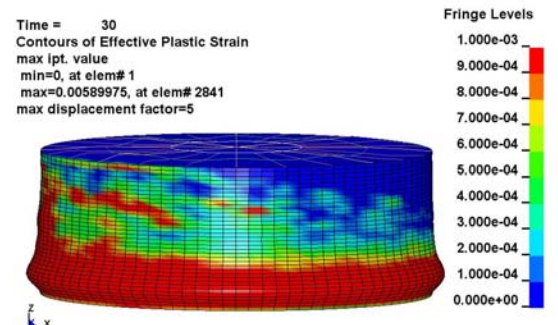
Anchored (Loading 3)
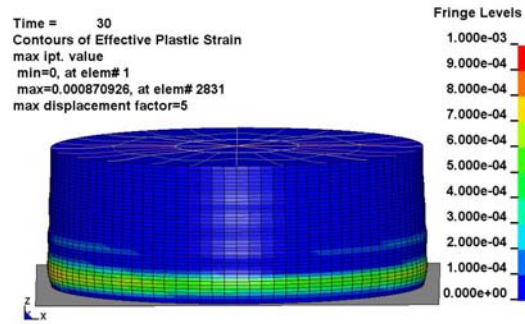
Anchored (Loading 4)

Unanchored (Loading 1)
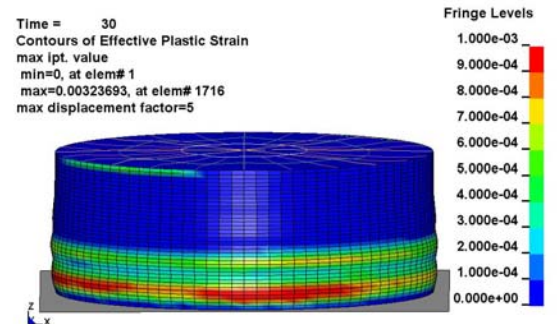
Unanchored (Loading 2)
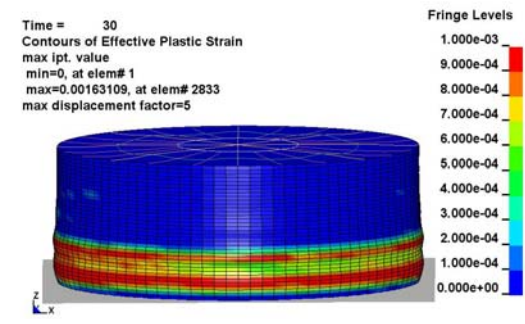
Unanchored (Loading 3)
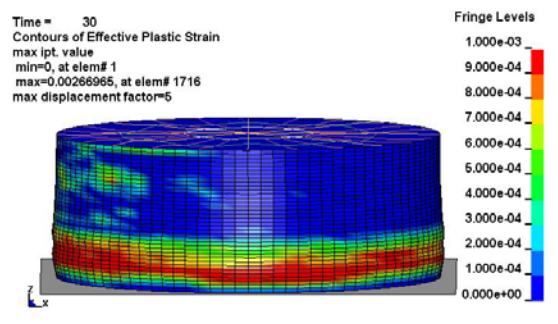
Unanchored (Loading 4)

Figure 8.40. Plastic deformations and deflections of the anchored and unanchored tank

models subjected to different combinations of P1087 earthquake record

(displacements magnified 5 times)
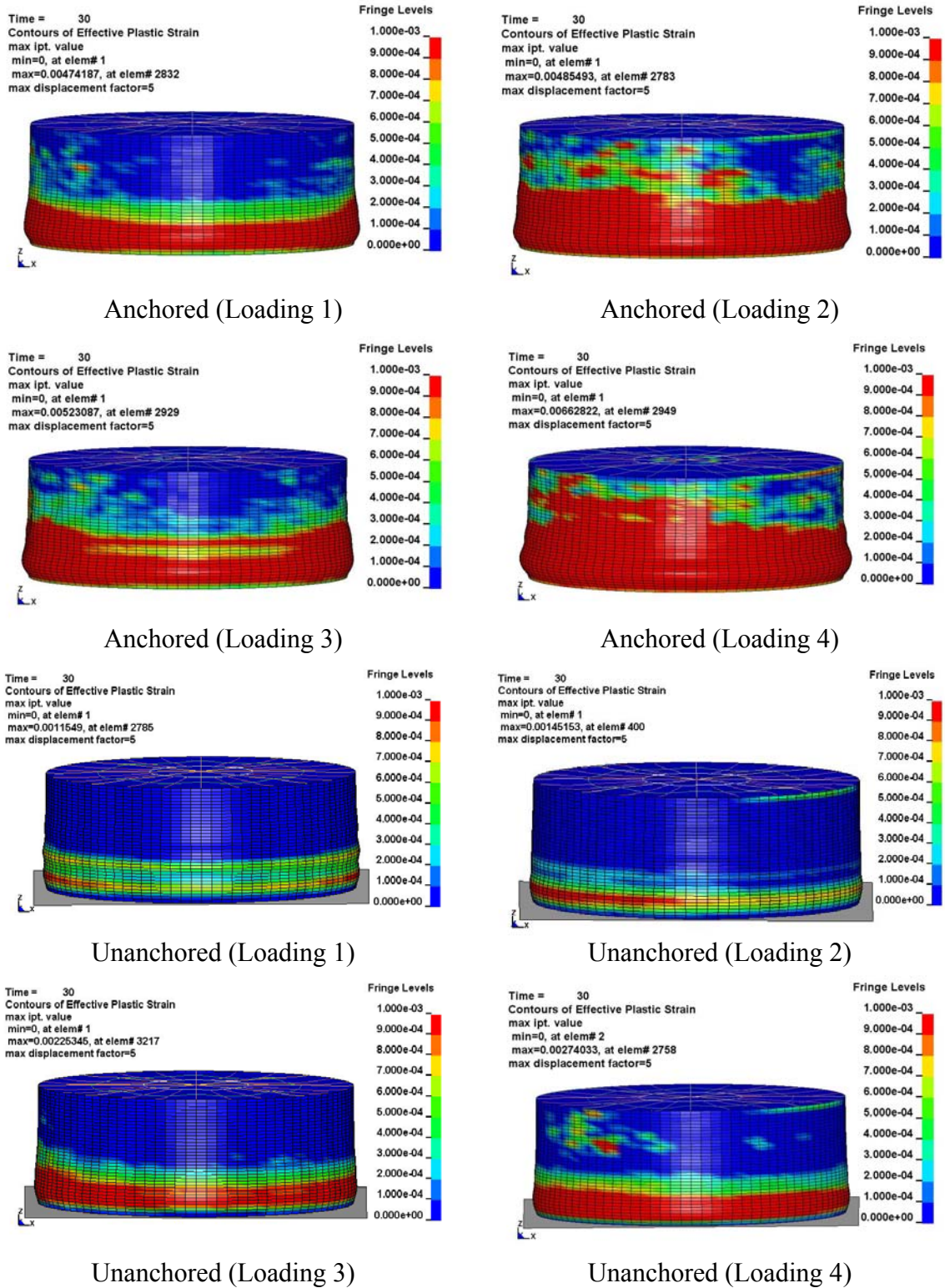
Figure 8.41. Plastic deformations and deflections of the anchored and unanchored tank models subjected to different combinations of P1558 earthquake record (displacements magnified 5 times)

Anchored (Loading 1)

Anchored (Loading 2)

Anchored (Loading 3)

Anchored (Loading 4)
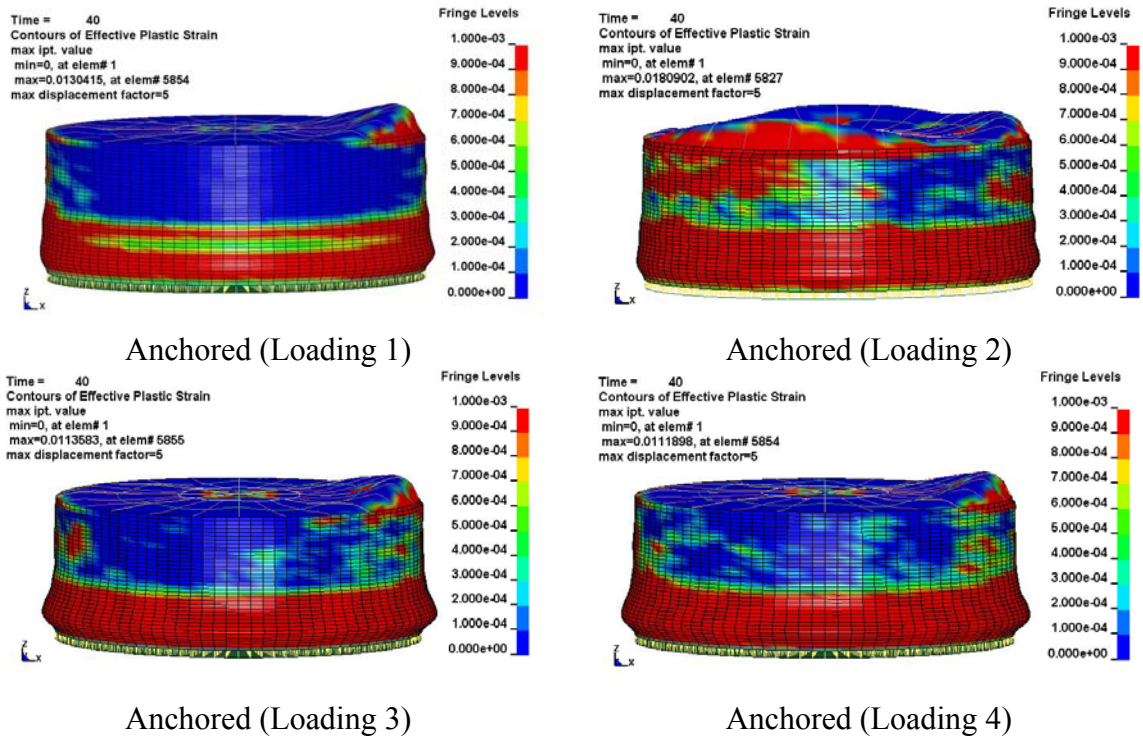
Figure 8.42. Plastic deformations and deflections of the anchored tank subjected to different combinations of P1114 earthquake record (displacements magnified 5 times)



Anchored (Loading 1)

Anchored (Loading 2)

Anchored (Loading 3)
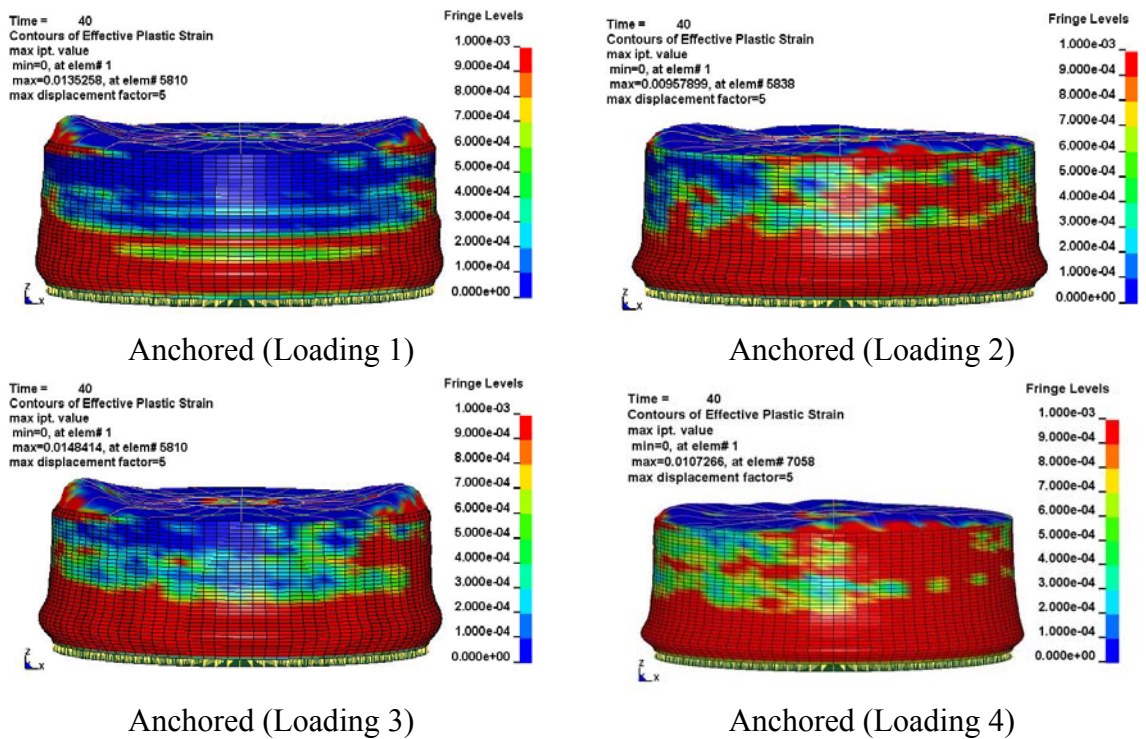
Anchored (Loading 4)

Figure 8.43. Plastic deformations and deflections of the anchored tank subjected to different combinations of P1104 earthquake record (displacements magnified 5 times)
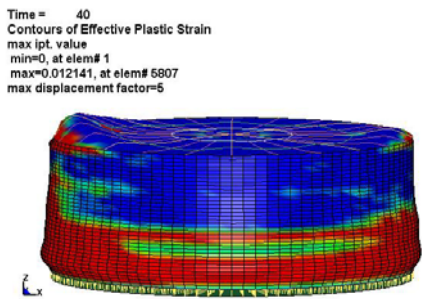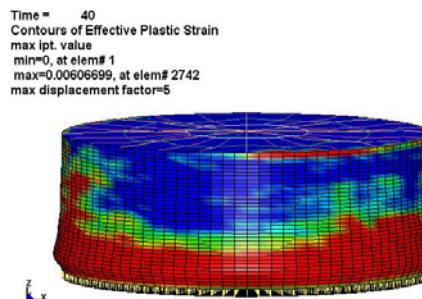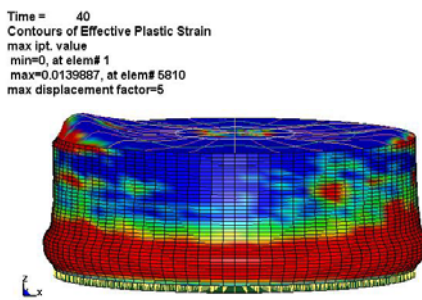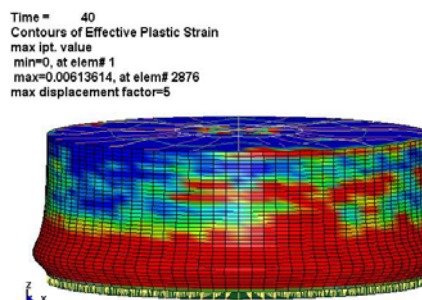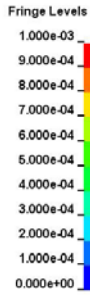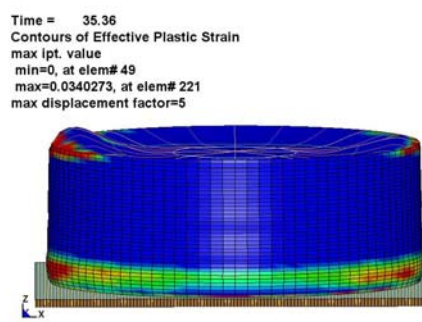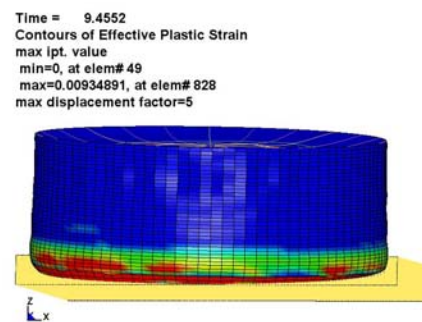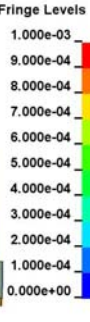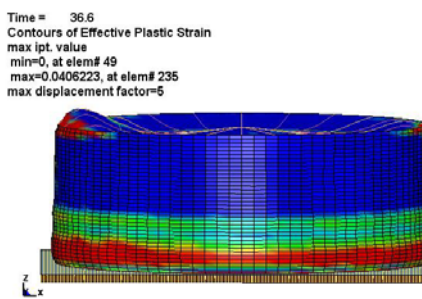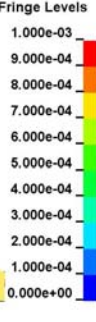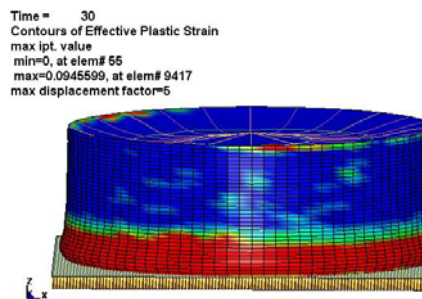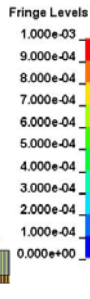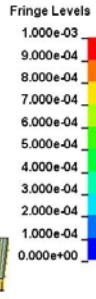
Figure 8.44. Plastic deformations and deflections of the anchored tank subjected to different combinations of P1096 earthquake record (displacements magnified 5 times)

## 8.6. Top Displacement and Fluid-Tank System Period

Fourier spectrum of the radial displacement of a node at the top of the tank on the loading axis may be used to evaluate the period of the coupled liquid- tank system. For this purpose, a node at the connection between tank wall and roof is selected and its Fourier spectrum is plotted in Figure 8.45 for P1558-MDR000 record. Peaks of the Fourier amplitude spectrum can be clearly observed from this figure. The frequency of first peak in the FFT spectra coincides for both tank types and corresponds to sloshing frequency.

The second peak of the Fourier amplitude spectrum of the anchored tank is 3.60 Hz. In Table 8.3, coupled anchored tank-fluid system frequency is obtained as 3.70 Hz. Therefore, analytical and FEM models give close results for frequency of anchored tank-fluid system. However, the natural frequency of an unanchored tank cannot be computed analytically since stiffness of an unanchored tank changes time to time depending on the contact area between tank base and ground. In Figure 8.45, the first mode frequency of the unanchored tank coincides 2.72 Hz which is higher than natural frequency of anchored tank. The unanchored tank has shorter period because the motion of unanchored tank is governed by rocking motion.

## 8.7. Relationship between Response Parameters

In order to evaluate the relationship between input motion and tank response, earthquake record and the corresponding response parameters of tank models under 1 horizontal component of P1087 record are presented in Figure 8.46 to Figure 8.50. These plots clearly show that the maximum base shear, overturning moment, radial displacement and base uplift occur in response to peak ground acceleration. Hydrodynamic base shear and overturning moment are directly influenced by the input motion and by free surface wave action. After motion subsides, the main response occurs due to sloshing action of the free surface and the fluid-structure interaction generates small amplitude oscillations on base shear and overturning moment. Thus, the validity of Housner's (1954) concept of the combination of impulsive plus convective pressure effects is verified by fully nonlinear fluid-structure interaction algorithm. For the unanchored tank, uplift primarily develops due to base acceleration. The wave action causes uplifting of the tank base, but only at

times when the base acceleration contributes to uplift. The sole sloshing motion does not induce considerable uplift displacement of the tank base. Unanchored tank has smaller radial displacements than anchored tank, top displacement of the unanchored tank reaches 3 cm, while top displacement of anchored tank less than 2 cm. Radial displacements of both anchored and unanchored tanks increase with intensive ground shaking. Similar observations can be made for other ground motion records.

Modified records for site class Z3 and response parameters of anchored tank analyzed under these ground motions are given in Figure 8.51. In this case, sloshing response is different than previous cases. Sloshing waves exceed the free board between fluid free surface and tank top and impact tank roof. Time histories of base shear and overturning moment are affected by changes in free surface motion.
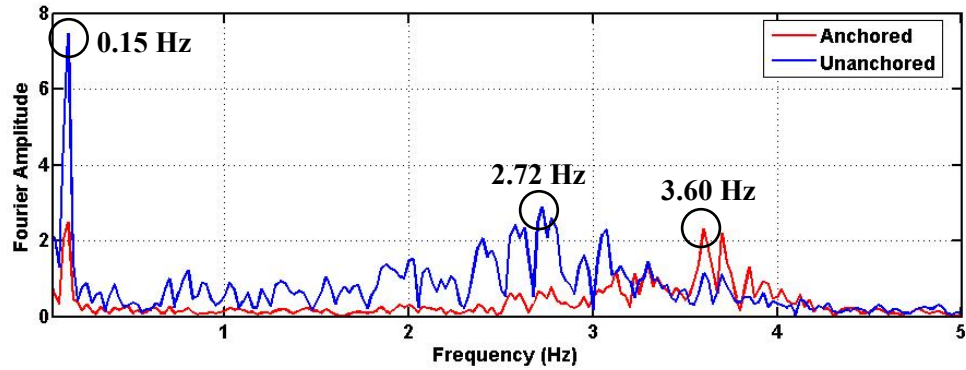
Figure 8.45. Fourier amplitude spectra of radial top displacement of tank models subjected to modified P1558-MDR000 record
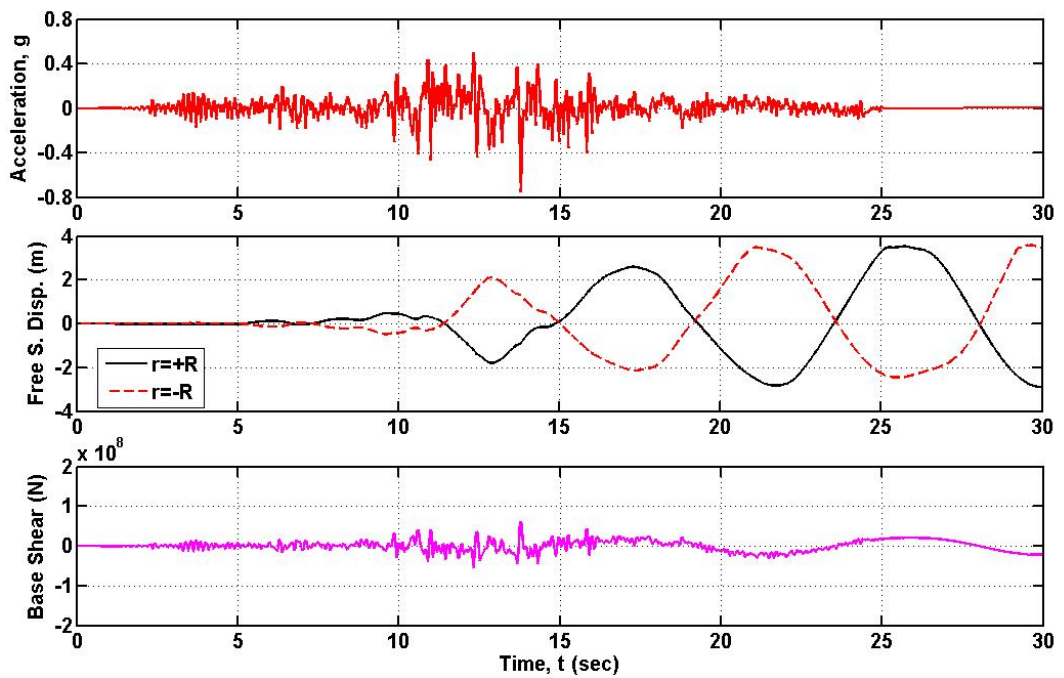


Figure 8.46. Acceleration history of modified P1087-ARC000 record and response parameters of anchored tank model with rigid material
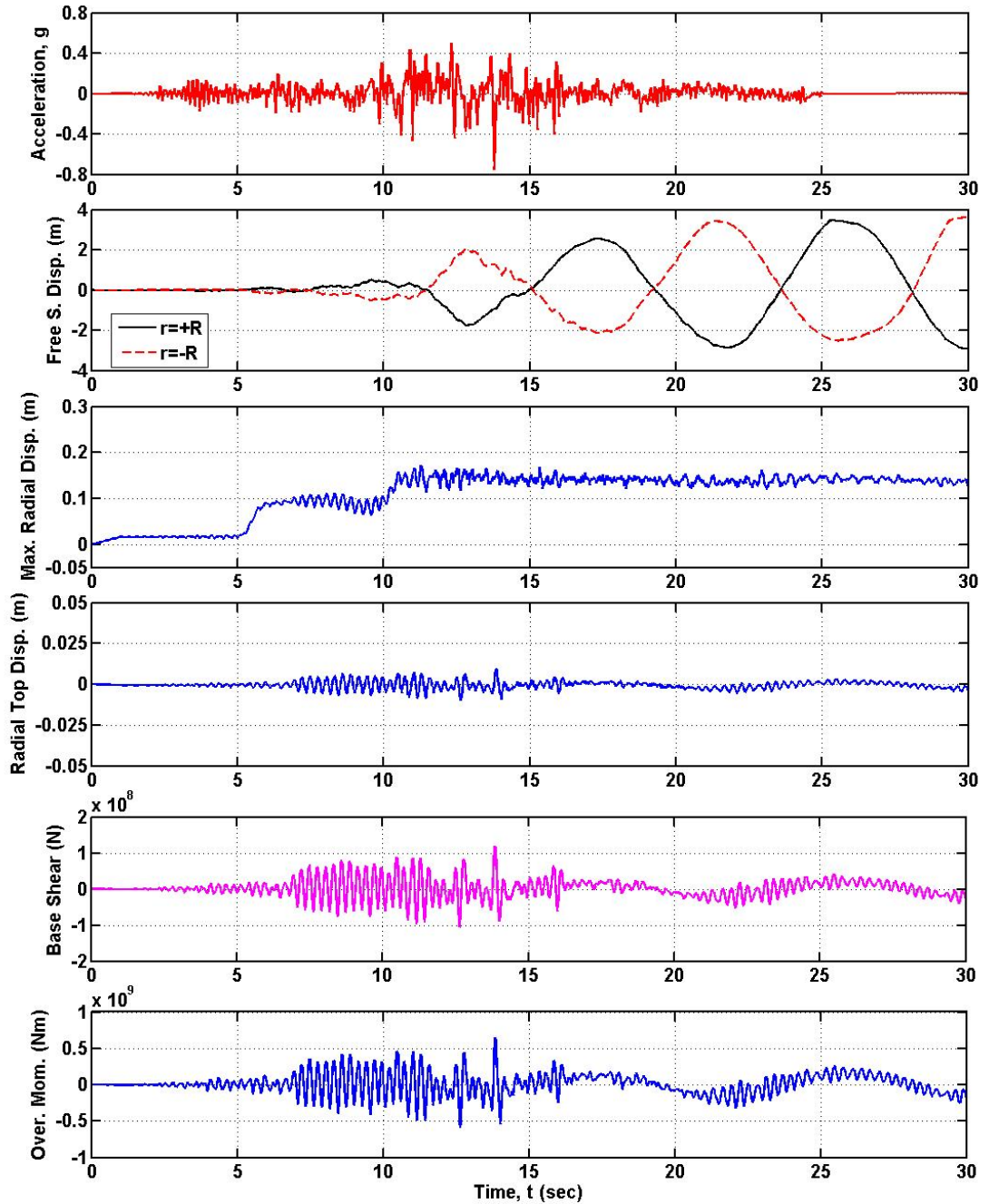
Figure 8.47. Acceleration history of modified P1087-ARC000 record and response parameters of anchored tank model with elastic material
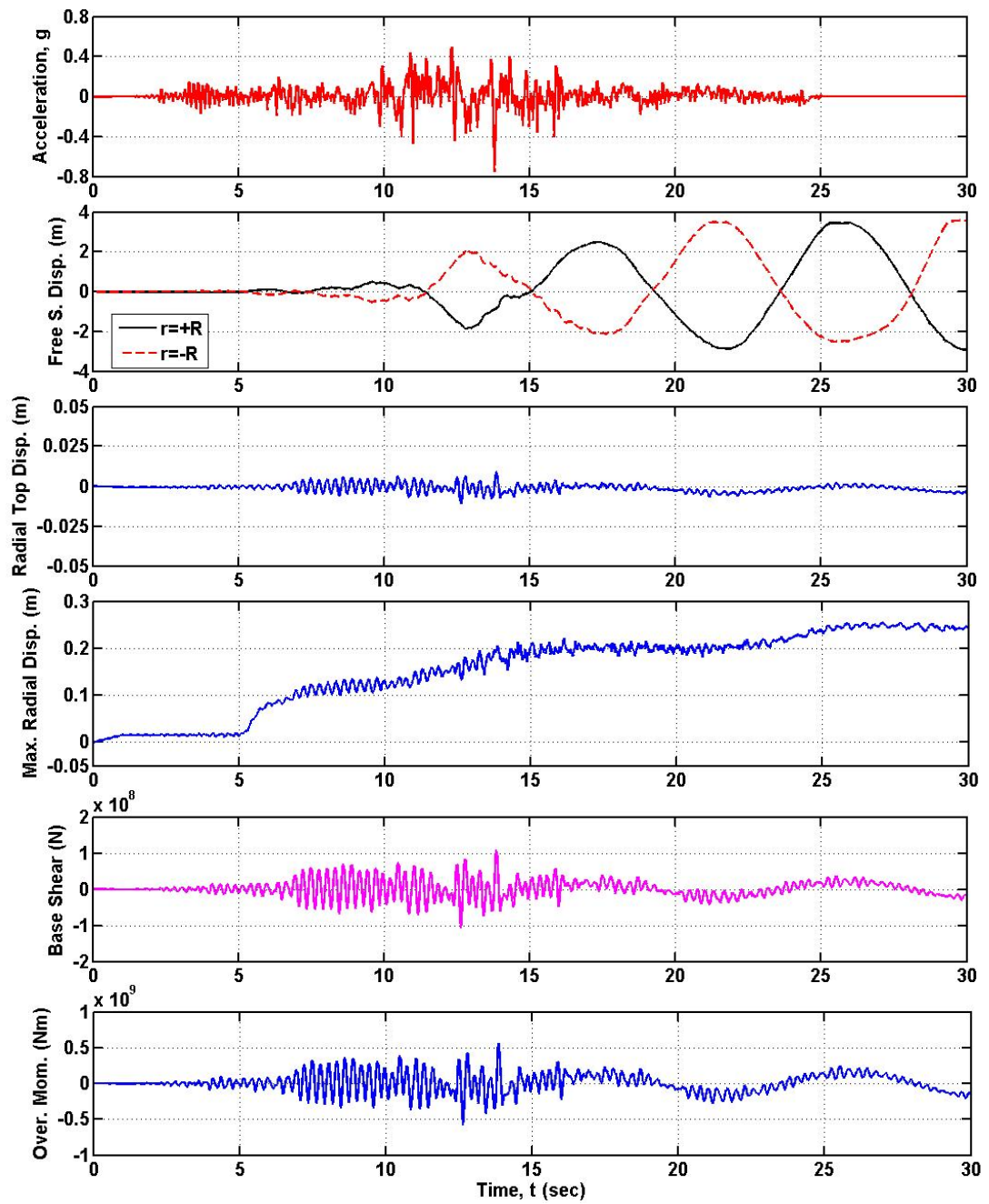
Figure 8.48. Acceleration history of modified P1087-ARC000 record and response
parameters of anchored tank model with elastic perfectly plastic material
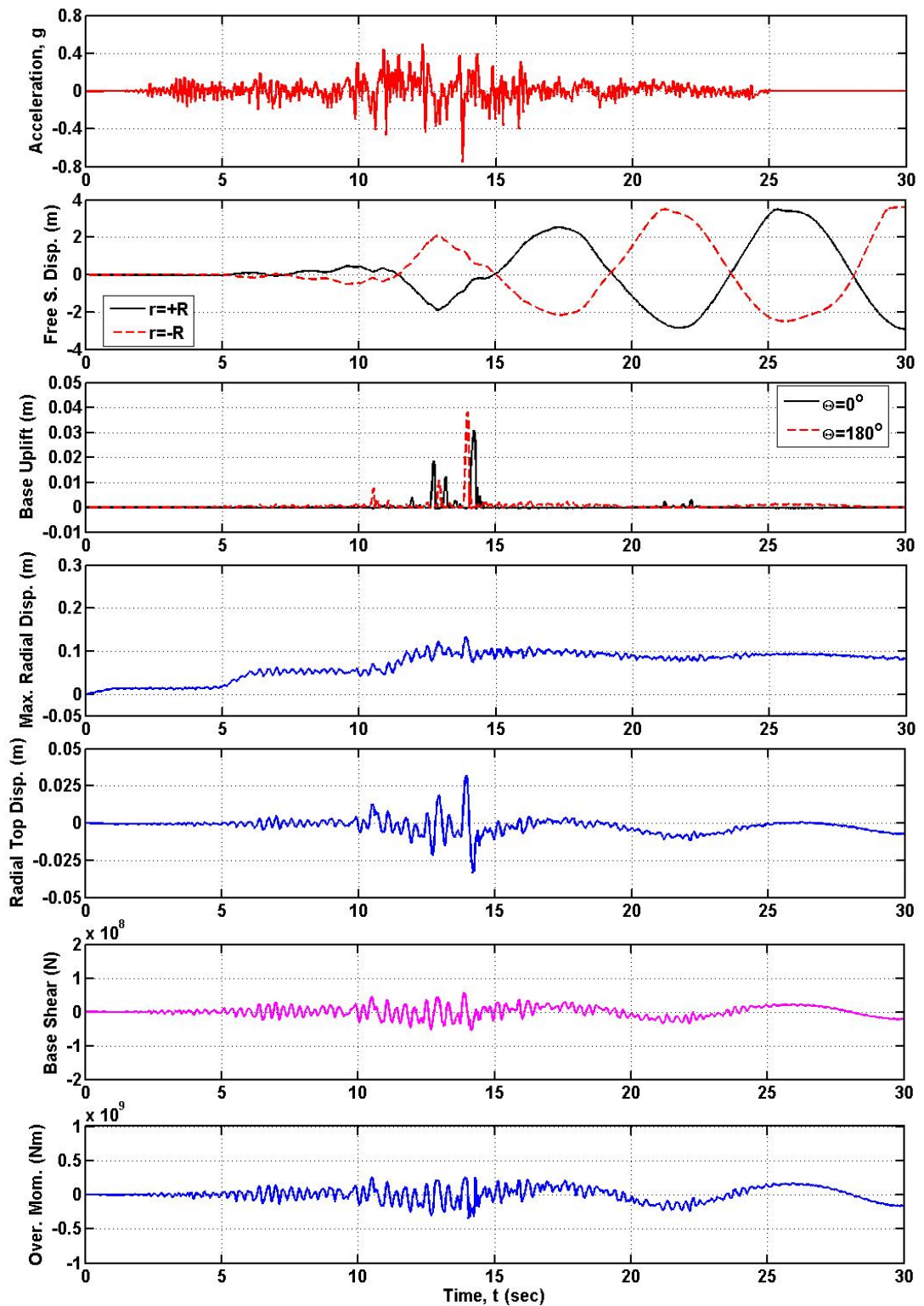
Figure 8.49. Acceleration history of modified P1087-ARC000 record and response

parameters of unanchored tank model with elastic material
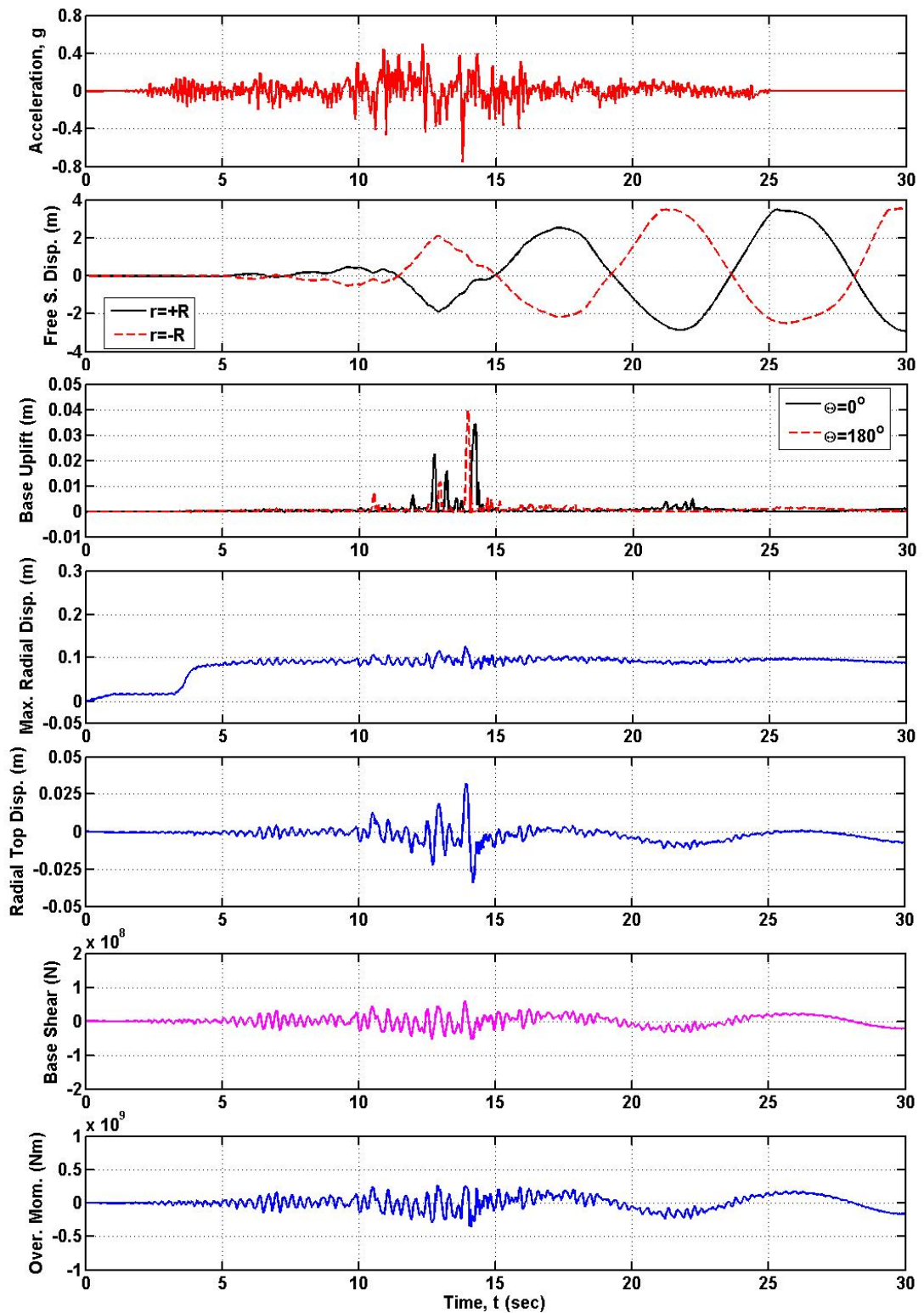
Figure 8.50. Acceleration history of modified P1087-ARC000 record and response

parameters of unanchored tank model with elastic perfectly plastic material
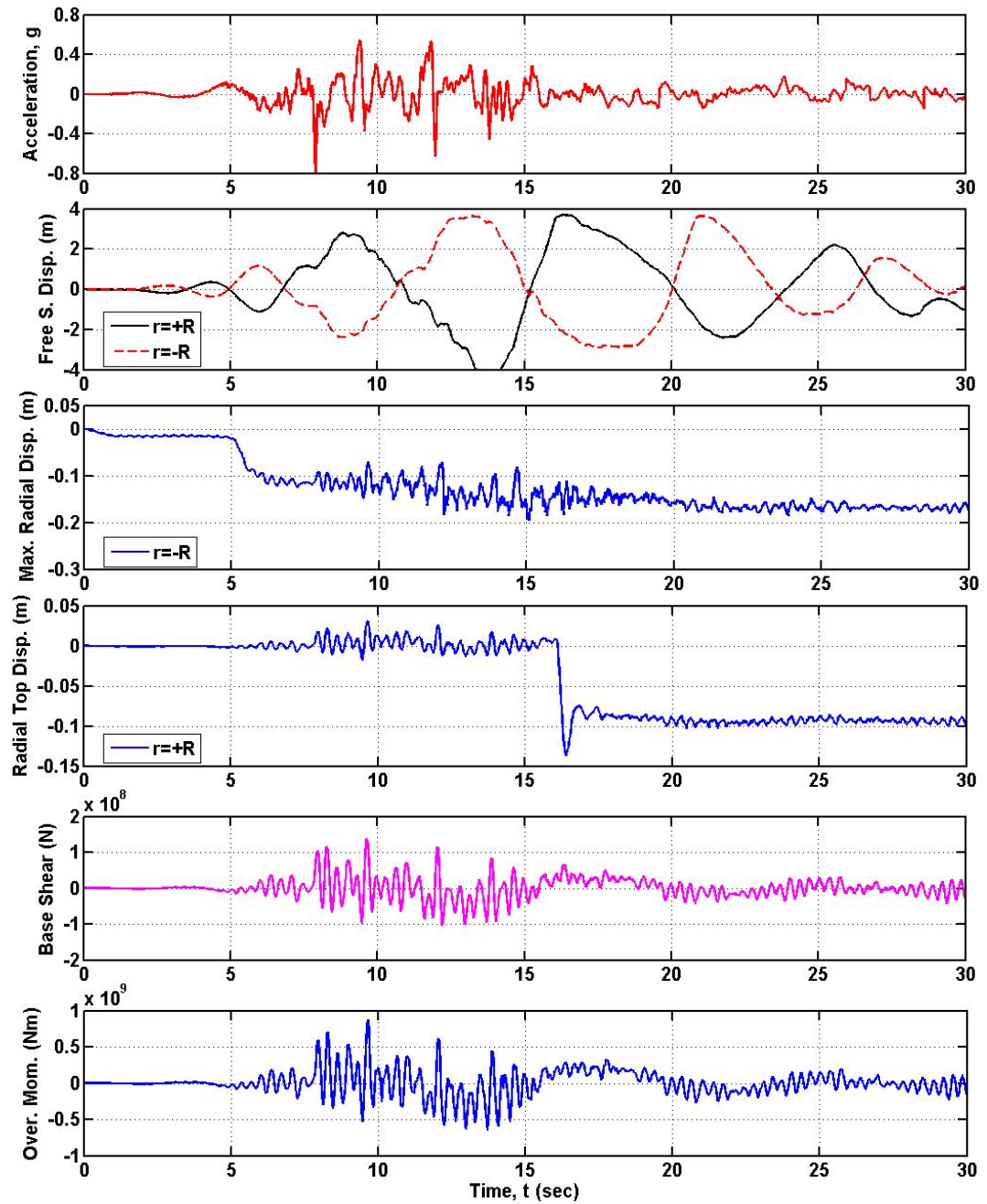
Figure 8.51. Acceleration history of modified P1114-YPT330 record and response

parameters of anchored tank model with elastic perfectly plastic material

### 8.8. Assessment of the Provisions Provided in Current Seismic Tank Design Codes

The response parameters of the anchored and unanchored tanks obtained from numerical analyses are compared with the predictions of API 650 (2005), Eurocode 8 (2006) and NZSEE (1986) standards in order to check consistency of the results. Maximum FEM results obtained from 3 different earthquake records with code computations are presented in Table 8.17. Since tank seismic design codes recommend the consideration of simultaneous effect of one horizontal and vertical earthquake components in the analysis, numerical analysis results of Loading Case 3 of modified records are used for comparison purpose. The impulsive and convective effects are combined with SRSS rule for API 650 (2005) and NZSEE (1986) code computations.

Although base shear and overturning moment have a critical importance for the evaluation of seismic performance of tanks, provisions presented in the seismic tank design codes do not take into account the effect of support condition on both response quantities and the tank is fixed at its base to a rigid foundation. Eurocode 8 (2006) code with Malhotra *et al.* (2000) method gives the same result with FEM solution for base shear. NZSEE (1986) provisions provide the most consistent results with numerical method for overturning moment among tank design codes.

The hoop stresses developed at the anchored tank wall predicted by NZSEE (1986) guidelines and obtained by numerical simulations exceed yield limit. But, hoop stresses obtained by API 650 (2005) provisions are less than yield stress. For the anchored tank case, axial compressive stress obtained from code provisions is almost ten times less than that obtained by numerical results. The reasons for this difference are that codes assume tanks deform like a cantilever beam preserving its cross-sectional shape and high axial compressive stresses developed at short distance to tank base plate due to restraint action of the anchors. Actually, tanks undergo out-of-round distortions during intensive ground shaking. All axial stress values obtained by code provisions are under critical axial compressive stress which causes elastic (diamond shape) buckling. In the numerical simulations, the axial stress developed at the unanchored tank wall which remains in contact with the ground reaches a maximum value of $2.5 \times 10^8$ Pa which is higher than the critical theoretical buckling stress (Table 8.17). Only NZSEE (1986) standard predicts

axial compressive stress developed at the unanchored tank wall that is higher than the allowable value defined in this code. Therefore, high axial compressive stresses may cause elastic buckling of the unanchored tank shell according to NZSEE (1986) code provision. However, simulation results show that these stresses do not cause elastic buckling of the tank shell. Instead, they affect the development of the small amplitude outward bulging of the lower part of the unanchored tank. Due to the fact that hoop stresses exceed the yield limit of the tank material, the tank model under consideration is susceptible to elephant foot buckling in accordance with provisions provided in NZSEE (1986) and Eurocode 8 (2006).

Sloshing wave height observed from numerical simulations is very close to the values obtained by code provisions (Table 8.17). NZSEE (1996) and API 650 (2005) give 3.26 m and 3.84 m, respectively, while maximum sloshing wave height is obtained as 3.65 m for both anchored and unanchored tanks by the numerical method. Two methods of Eurocode 8 (2006) predict this displacement as 3.21 m and 3.84 m. Therefore, numerical results for free surface wave height lies in between the values obtained by code provisions.

According to NZSEE (1986) provisions plastic rotation of the unanchored tank base plate is lower than the allowable value of 0.20 rad, but radial membrane stress in the base exceeds yield limit of the base material. Base uplift displacement of the unanchored tank predicted by NZSEE (1986) guidelines is higher than that obtained by the numerical analysis. Yet, if tank base uplift is evaluated under two horizontal component of ground motion or 3 dimensional earthquake loading, numerical analysis results for uplift exceed NZSEE (1986) code provisions. For unanchored tank model, uplift width, uplift height and axial compressive stress in the unanchored tank wall could not be evaluated according to Eurocode 8 (2006) since the normalized overturning moment is far outside the range covered by the graphs given in this code.

Soil-structure interaction effects are evaluated in accordance with the procedure provided in Eurocode 8 (2006) and API 650 (2005) provisions. In this procedure, the convective periods and pressures are assumed not to be affected by soil-structure interaction and the fundamental period and the damping of rigid and flexible impulsive components of hydrodynamic effects are modified. The modified system response is

computed considering that tank rests on a rigid soil and is subjected to the free-field motion. According to this procedure, periods of rigid and flexible fluid-tank systems increase to 0.23 and 0.35 sec, respectively due to soil-structure interaction effects. Since dampers are not placed to represent soil damping effects, change in damping response due to soil effects are not take into account. Therefore, spectral acceleration values do not change, because these periods fall within plateau region of the spectrum for Z3 soil type. But, spectral acceleration of convective response increases from 0.16g to 0.28g for first sloshing mode and 0.28g to 0.47g for second sloshing mode when tank is founded on flexible soil. Since the convective effects are a small portion of the overturning moment and hydrodynamic pressure, tank shell stresses slightly increase. The most important effect of soil effects on the tank response is the increase in free surface wave height. The height of sloshing waves reach 6.72 m for API 650 (2005) and for the second method of Eurocode 8 (2006) (Malhotra *et al.*, 2000) and 5.70 m for NZSEE (1986) and 5.65 m for the first method of Eurocode 8 (2006) (Veletsos and Yang, 1977).

Table 8.17. Response parameters of the tank models as per code requirements

(units: N, m and sec)

| | Numerical | API 650 (2005)[+] | Eurocode 8 (2006) | | NZSEE (1986) |
|---|---|---|---|---|---|
| | | | 1st Method | 2nd Method | |
| Impulsive Hor. Mode Period | - | - | - | 0.27 | 0.27 |
| Impulsive Ver. Mode Period | - | - | - | - | 0.26 |
| Sloshing Mode Period | - | 8.16 | 8.14 / 4.27 | 8.24 | 8.14 / 4.27 |
| Sloshing Wave Height | 3.65 (anchored) / 3.65 (unanchored) | 3.84 | 3.21 | 3.84 | 3.26 |
| Base Shear | $1.64 \times 10^8$ (anchored) / $5.46 \times 10^7$ (unanchored) | $4.99 \times 10^7$ | $8.01 \times 10^7$ | $1.64 \times 10^8$ | $1.36 \times 10^8$ |
| Overturning Moment (excluding base pressure) | $8.32 \times 10^8$ (anchored) / $4.48 \times 10^8$ (unanchored) | $2.98 \times 10^8$ | $5.20 \times 10^8$ | $1.03 \times 10^9$ | $7.77 \times 10^8$ |
| Overturning Moment (including base pressure) | - | $9.23 \times 10^8$ | $1.37 \times 10^9$ | $2.89 \times 10^9$ | $2.21 \times 10^9$ |
| Shell Axial Membrane Stress for Anchored Tank | $3.60 \times 10^8$ | $1.05 \times 10^7$ | $1.81 \times 10^7$ | $3.37 \times 10^7$ | $2.59 \times 10^7$ |
| Shell Axial Membrane Stress for Unanchored Tank | $2.50 \times 10^8$ | * | ** | ** | $1.03 \times 10^8$ |
| Allowable Axial Membrane Stress | | | | | |
| Elastic Buckling | - | $3.12 \times 10^7$ | $8.12 \times 10^7$ | $8.16 \times 10^7$ | $8.16 \times 10^7$ |
| Elasto-Plastic Buckling | - | - | Susceptible to EFB | Susceptible to EFB | Susceptible to EFB |
| Hoop Stress | $> \sigma_{yield}$ (anchored) / $> \sigma_{yield}$ (unanchored) | $2.97 \times 10^8$ | - | - | $4.50\ 10^8$ |
| Allowable Hoop Stress | - | $3.20 \times 10^8$ | $3.55 \times 10^8$ | $3.55 \times 10^8$ | $3.55 \times 10^8$ |
| Uplift for Unanchored Tank | 0.05 | * | ** | ** | 0.11 |
| Plastic Rotation | - | - | *** | *** | 0.10 |
| Allowable Plastic Rotation | - | - | 0.20 rad (11°) | 0.20 rad (11°) | 0.20 rad (11°) |
| Radial Membrane Stresses in the Base Plate | - | - | *** | *** | $3.98 \times 10^8$ |

According to classical buckling theory $\sigma_{cl} = \dfrac{1}{\sqrt{3(1-\nu^2)}} \dfrac{E\,t}{R} = 9.20 \, x \, 10^7 \ Pa$

\*     Tank should be anchored as per minimum API 650 requirements.
\*\*    The parameter is the out of range of the graphs given in the corresponding code.
\*\*\* For the estimation of this quantity, the uplift height is necessary.

    Method 1: Veletsos and Yang (1977)     Method 2 : Malhotra *et al.* (2000)

\+   The response parameters obtained according to API 650 (2005) is multiply by a factor of 1.4 to convert seismic design forces from allowable stress design level to strength design level (Jaiswal *et al.*, 2007).

EFB : Elephant foot buckling

# 9. CONCLUSIONS

This dissertation aims to assess the seismic behavior of steel cylindrical ground supported anchored and unanchored liquid storage tanks under different combinations of earthquake ground motion components by employing fluid-structure algorithm of finite element method which takes into account large amplitude nonlinear sloshing, material and geometrical nonlinearities of tank, nonlinear behavior of contained liquid and their interaction effects. A real size typical tank model with two different support conditions as anchored and unanchored is analyzed under Turkish Seismic Design Code (2007) spectra compatible real earthquake records by employing an explicit time integration scheme based on central difference method. Since Arbitrary Lagrangian Eulerian (ALE) formulation permits formation of large structural and fluid deformations without causing mesh distortion problems, a Lagrangian mesh system for structure is combined with an ALE mesh for fluid domain by merging nodes at the fluid-structure interface. Analysis results obtained for different ground motion records and loading combinations are evaluated in terms of base shear, overturning moment, free surface wave height, uplift response, shell stresses, plastic strain and radial shell deformations. The consistency of numerical analyses results with those of simplified methods that are based on simple mass-spring representation of hydrodynamic effects developed on the tank are assessed for the anchored tank model under consideration when subjected to one horizontal component of earthquake ground motion. A comparison between the earthquake response of anchored and unanchored tanks is presented along with the relative importance of the second horizontal and vertical components of ground motion. The consistency of provisions presented in current tank seismic design codes and numerical analysis results is evaluated.

The key conclusions of the research work described in this thesis can be summarized as follows:

- It can be justified from consistent results of numerical and experimental studies presented in Chapter 6 that the finite element method is a reliable tool for the seismic analysis of not only anchored tanks but also unanchored tanks. Sloshing response,

overturning moment, shell stresses and base uplift of tanks can be predicted with great accuracy.

- The inconsistency of the design and input motion spectra in the long period region may lead substantial difference in free surface wave height obtained from code provisions and those observed from numerical time history analyses. The response spectrum of selected input motion for the transient analysis should be consistent with code design spectrum for both short and long period regions where the fundamental periods of impulsive and convective (sloshing) responses are dominant, respectively.

- The nonlinear finite element analyses carried out on a typical tank model show that Housner's mechanical analog can accurately predict the response of a rigid anchored tank. In reality, the rigid tank assumption is not appropriate for the design of a real size tank, since it substantially underestimates the forces developed on an anchored tank. On the other hand, mechanical analog models developed for flexible tanks may give inaccurate results in time history analysis. Better results with simplified mechanical analog developed for flexible tanks can be obtained for spectrum analysis.

- Mesh size has a substantial effect on plastic strain and radial displacement of tank wall, base uplift and free surface wave height of tanks.

- The nonlinear finite element analyses carried out on the typical tank model show that base shear developed on rigid anchored tank is 25 per cent of the tank weight under one horizontal ground motion component while this ratio may increase up to 77 per cent when tank is made up of elastic steel material. Overturning moment developed on anchored tank placed on rigid ground may reach as much as 26 per cent of the product of tank weight and liquid height. Nonlinearity of the anchored tank decreases base shear around 5 per cent of tank weight, while this decrease in overturning moment is 2 per cent of the product of tank weight and liquid height when anchored tank is subjected to one horizontal ground motion component. Base shear developed on the unanchored tank is around 25 per cent of weight of the contained liquid, while overturning moment is 10 per cent of the product of tank weight and liquid height.

The anchored tank settled on flexible ground undergoes base shear which is around 60 per cent of tank weight and overturning moment which is around 26 per cent of the product of tank weight and liquid height.  In average, base shear and overturning moment developed on the unanchored tank is less than half of those exerted on the anchored tank for all ground motion combinations. In tank design codes, the liquid exerted hydrodynamic overturning moments are assumed to be insensitive to the support conditions.

- For anchored tank, single horizontal component generally provides the highest response for base shear and overturning moment. On the other hand, it is convenient to evaluate base shear and overturning moment of the tank considering all components of the ground motion if tank isn't anchored at its base. When the anchored tank is supported on flexible soil, single horizontal ground motion component causes highest base shear response, while three dimensional loading may increase overturning moment.

- Dynamic behavior of the unanchored tank is different from that of anchored tank. Numerical analysis results show that anchored tank undergoes higher axial compressive stresses than unanchored tank due to the restraint action of the base plate. The change in axial compressive stress due to tank support condition is accounted for in design codes, while the redistribution of the hoop stress due to uplift of the base of the tank is not considered.

- The concurrently presence of both two horizontal components causes considerable amplification in the uplift response of the unanchored tank, while vertical component slightly affects the uplift. Maximum uplift is not observed at the nodes on the X axis when unanchored tank is subjected to concurrently presence of two horizontal components and three dimensional earthquake ground motion.

- Free surface wave responses of free and fixed base cases are virtually identical. Sloshing response is not affected by the flexibility of the tank material. Moreover, presence of other ground motion components in addition to one horizontal component has ignorable importance on the sloshing response. Second horizontal

component affects temporal and spatial distributions of free surface wave height, but it does not substantially affect maximum response. The vertical component of the earthquake motion has a negligible effect on the sloshing response.

- Radial displacements and plastic deformations developed at the anchored tank wall are higher than those of observed at the unanchored tank wall for all combinations of ground motion components due to the restrictive action of the fixed tank base. Flexibility of soil further amplifies radial displacements and plastic deformations developed on the anchored tank.

- The nonlinear finite element analyses results reveal that both anchored and unanchored tank models suffer elephant foot buckling at a small distance above tank base plate due to hoop stresses exceeding yield limit. Therefore, anchoring does not prevent development of elasto-plastic instability. Anchored tank is also susceptible to elephant foot buckling according to both NZSEE (1986) and Eurocode 8 (2006) provisions while API 650 (2005) does not take into account elastic-plastic buckling. Elastic-plastic buckling criterion may be adapted to API (650) code in order to minimize the occurrence of such damage in future seismic events.

- The maximum base shear and overturning moment and base uplifting occur in response to peak ground acceleration, while free surface waves reach their maximum value close to end of the effective earthquake duration.

- Comparison of acceleration time history of the input motion, free surface sloshing wave height and base uplift time histories showed that uplift at the base of the unanchored tank primarily develops due to base acceleration. The wave action also causes uplifting of the tank base, but only at times when the base acceleration contributes to uplift. The sole sloshing motion does not induce considerable uplift displacement of the tank base.

- Maximum axial compressive stresses developed in the anchored tank wall concentrate short distance above the base plate due to the restraint action of the tank base and in the regions where out-of-round distortions occur in response to intensive

ground shaking. High axial compressive stresses in the unanchored tank wall occur at the regions where tank base remains in contact with the ground while the opposite edge of the base plate experiences uplift.

- Out-of round distortions of the anchored tank are always greater than those of the unanchored tank due to restraint action of the tank base support condition. Vertical and second horizontal ground motion components increase out-of round distortions of the tank wall.

- Soil flexibility increases axial compressive stresses, radial deformations and plastic strain developed at the anchored tank wall.

- For unanchored tank model, uplift width, uplift height and axial compressive stress in the tank wall could not be evaluated according to Eurocode 8 (2006) since the normalized overturning moment is far outside the range covered by the graphs given in this code. Since plastic rotation of the base plate depends on uplift width and uplift height, this parameter also could not be compared with the other code provisions.

- Code provisions predict approximately 10 times lower axial compression stresses in the anchored tank wall than that observed by FEM due to the fact that codes presume anchored tanks deform like a cantilever beam preserving its perfect circular cross-sectional shape. However, not only anchored tank wall but also unanchored tank shell undergoes out-of-round distortions during strong ground shaking.

**APPENDIX A**

Earthquake records processed with time domain matching techniques as explained in Chapter 7 are presented in Appendix A.
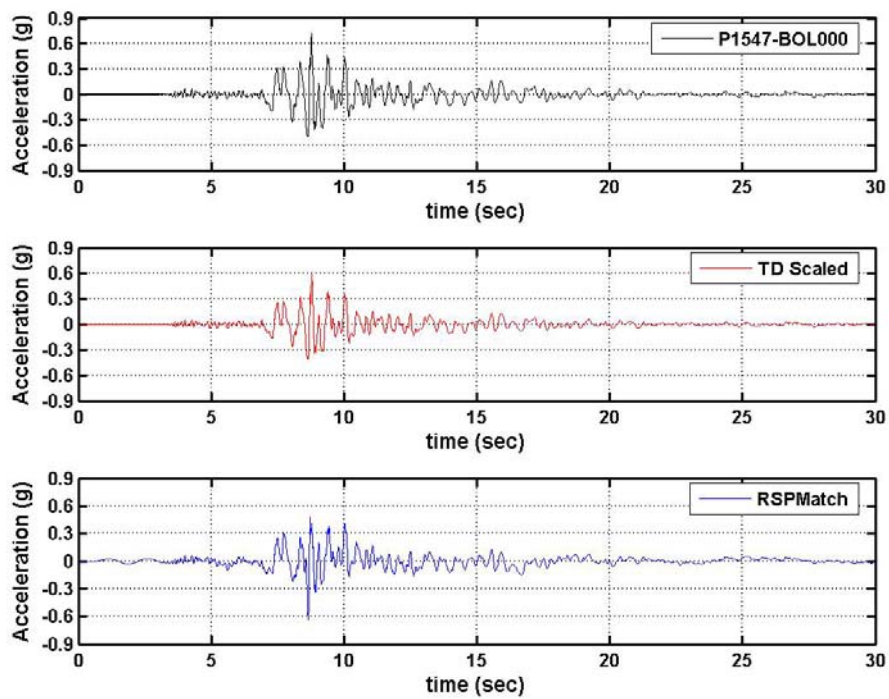


Figure A.1. Acceleration time histories of the first horizontal component of the real (P1547-BOL000), time domain scaled and RSPMATCH generated records, respectively
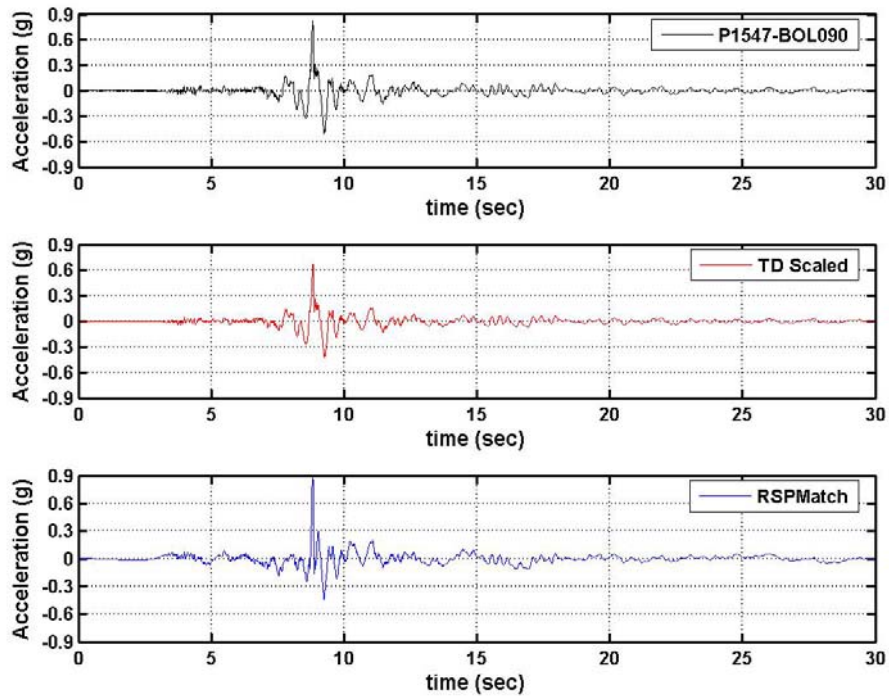
Figure A.2. Acceleration time histories of the second horizontal component of the real (P1547-BOL090), time domain scaled and RSPMATCH generated records, respectively
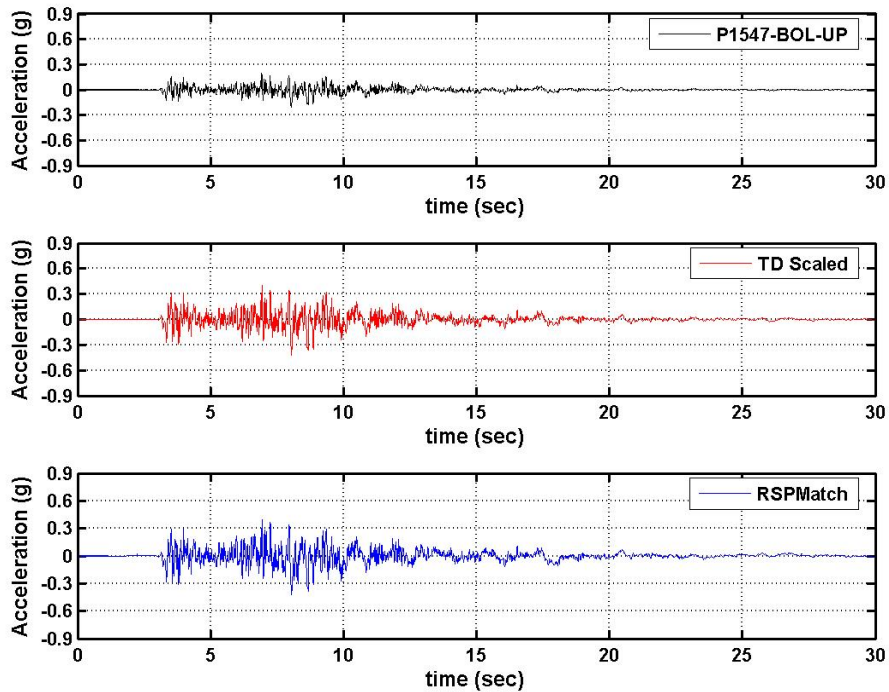


Figure A.3. Acceleration time histories of the vertical component of the real (P1547-BOL-UP), time domain scaled and RSPMATCH generated records, respectively
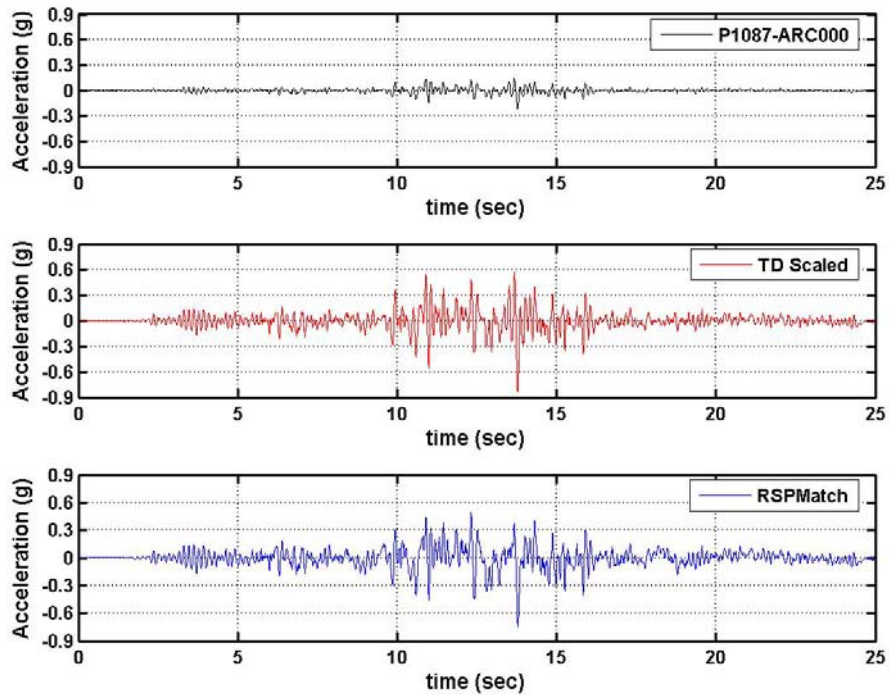
Figure A.4. Acceleration time histories of the first horizontal component of the real (P1087-ARC000), time domain scaled and RSPMATCH generated records, respectively
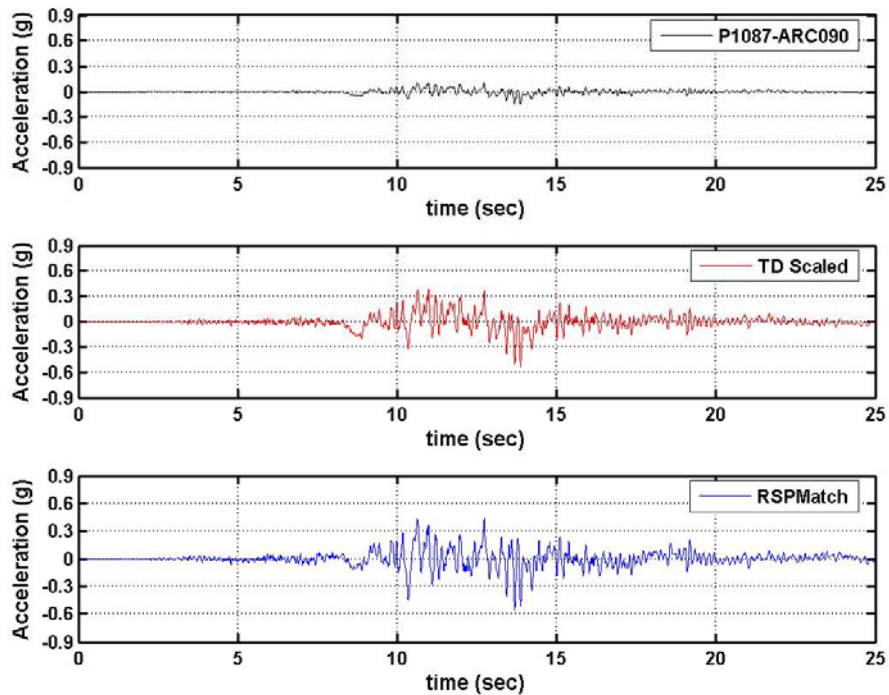


Figure A.5. Acceleration time histories of the first horizontal component of the real (P1087-ARC090), time domain scaled and RSPMATCH generated records, respectively
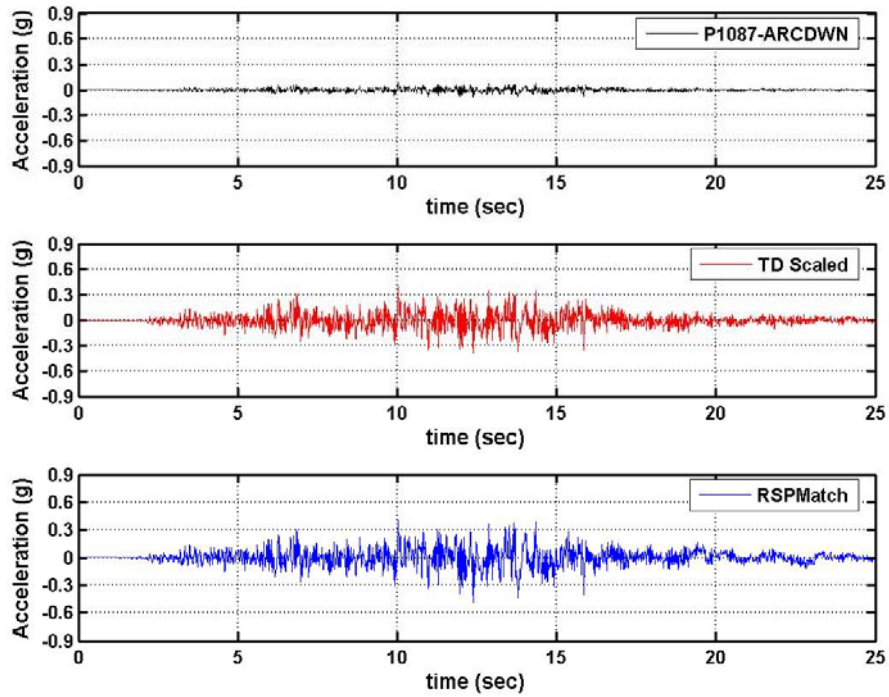
Figure A.6. Acceleration time histories of the first horizontal component of the real (P1087-ARCDWN), time domain scaled and RSPMATCH generated records, respectively
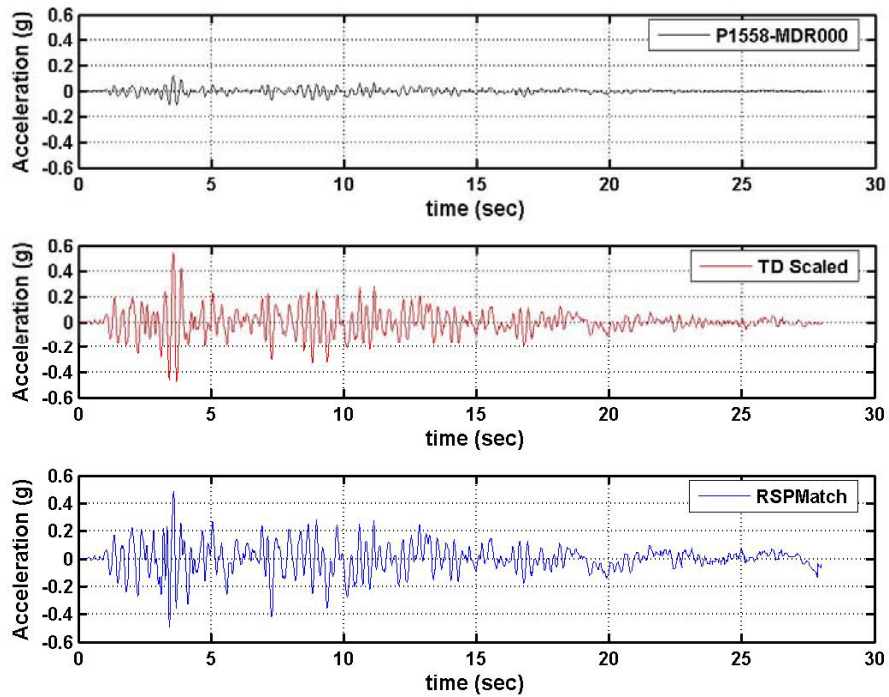


Figure A.7. Acceleration time histories of the first horizontal component of the real (P1558-MDR000), time domain scaled and RSPMATCH generated records, respectively
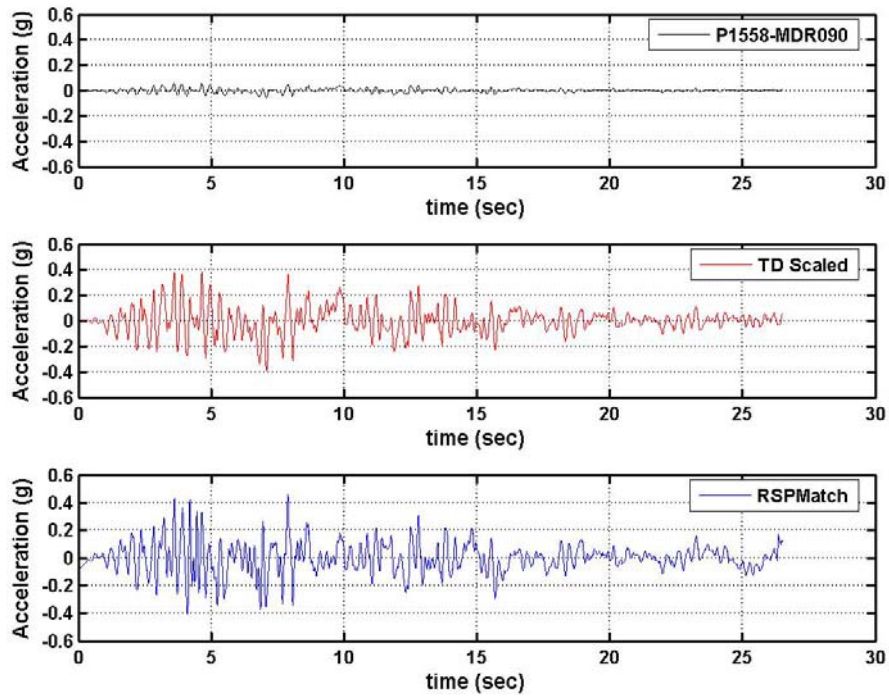
Figure A.8. Acceleration time histories of the first horizontal component of the real (P1558-MDR090), time domain scaled and RSPMATCH generated records, respectively
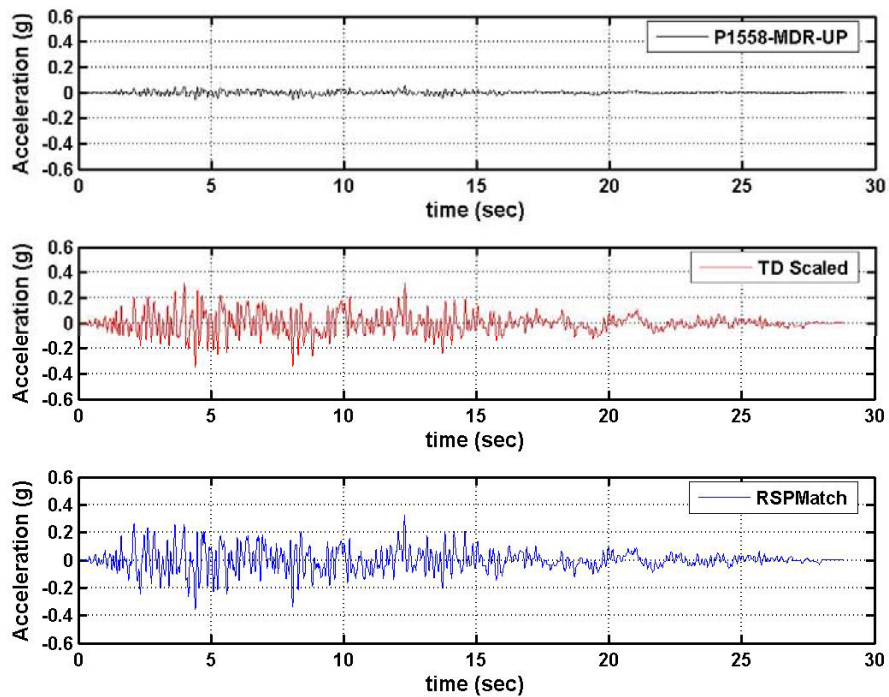


Figure A.9. Acceleration time histories of the first horizontal component of the real (P1558-MDR-UP), time domain scaled and RSPMATCH generated records, respectively
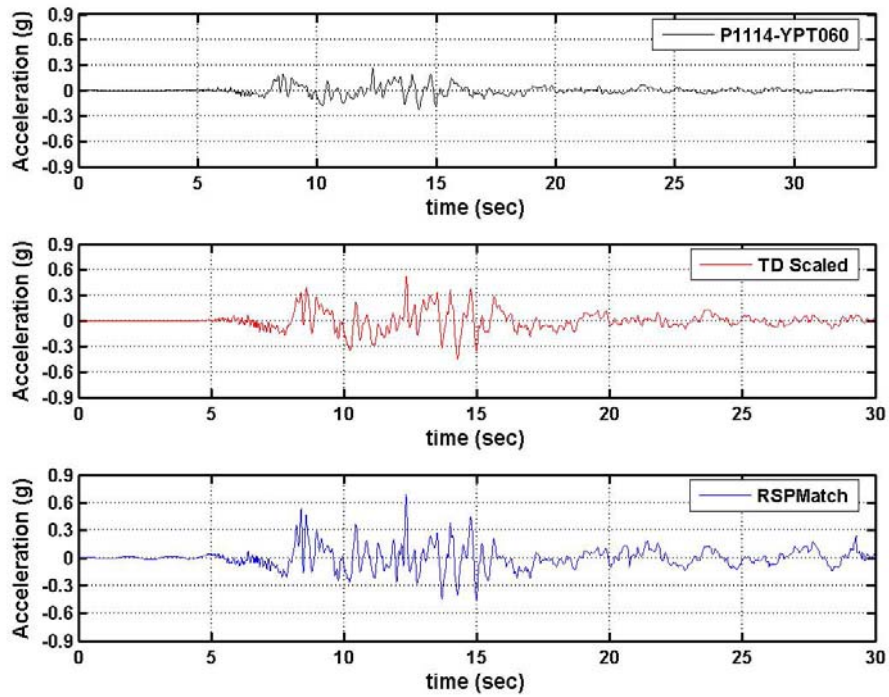
Figure A.10. Acceleration time histories of the first horizontal component of the real (P1114-YPT060), time domain scaled and RSPMATCH generated records, respectively
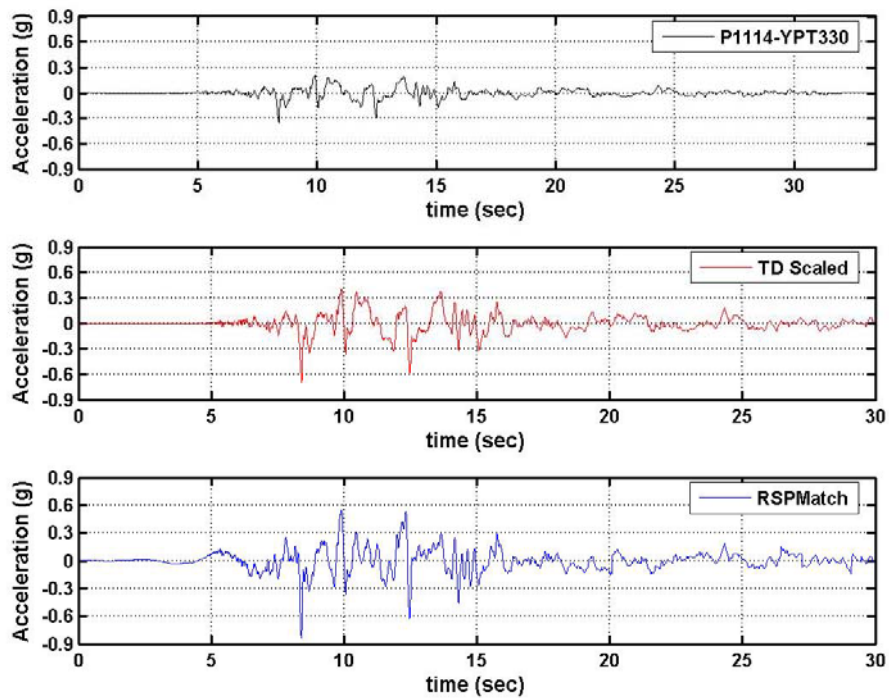


Figure A.11. Acceleration time histories of the first horizontal component of the real (P1114-YPT330), time domain scaled and RSPMATCH generated records, respectively
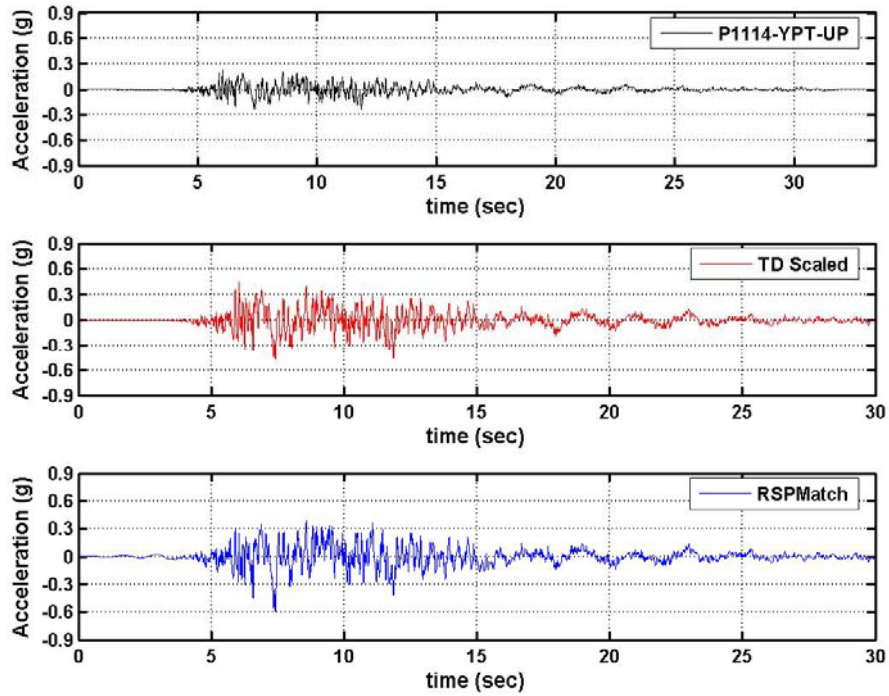
Figure A.12. Acceleration time histories of the first horizontal component of the real (P1114-YPT-UP), time domain scaled and RSPMATCH generated records, respectively
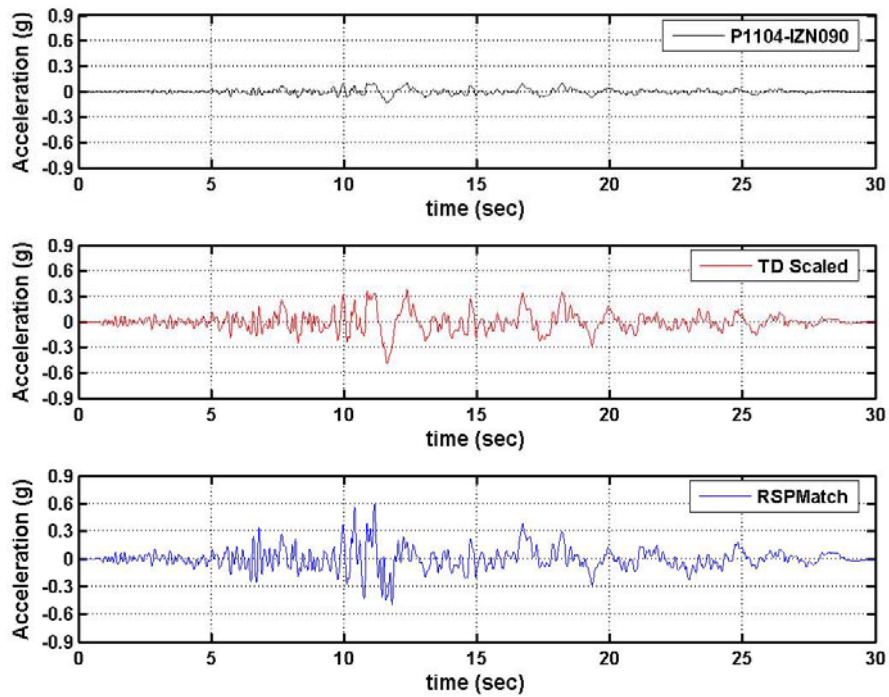


Figure A.13. Acceleration time histories of the first horizontal component of the real (P1104-IZN090), time domain scaled and RSPMATCH generated records, respectively
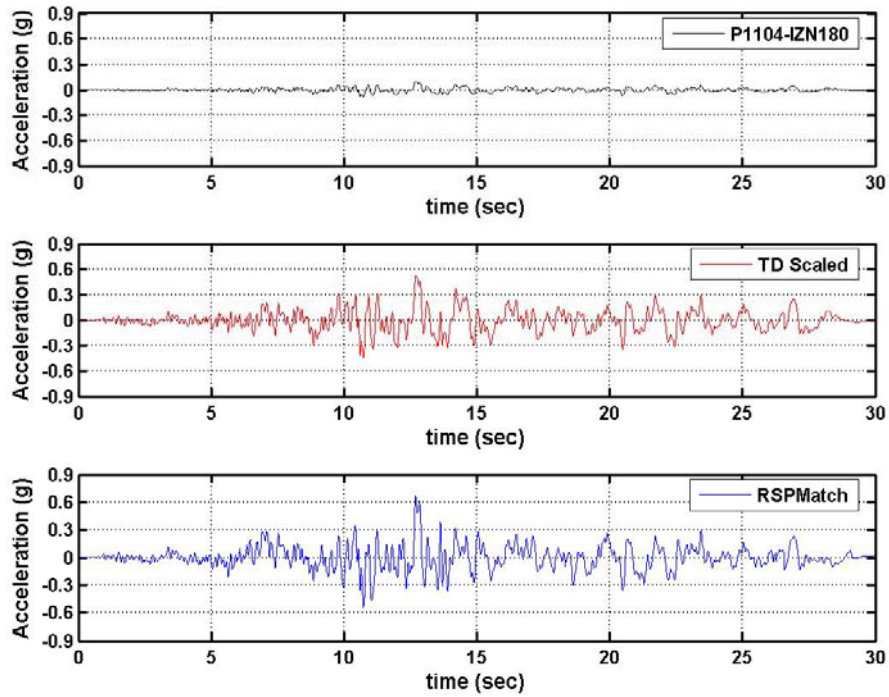
Figure A.14. Acceleration time histories of the first horizontal component of the real (P1104-IZN180), time domain scaled and RSPMATCH generated records, respectively
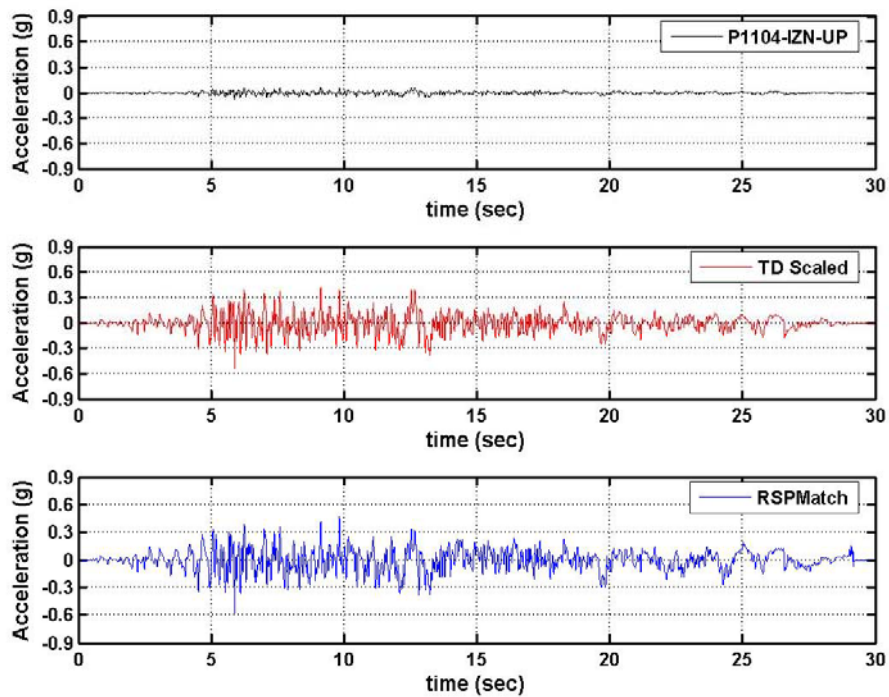


Figure A.15. Acceleration time histories of the first horizontal component of the real (P1104-IZN-UP), time domain scaled and RSPMATCH generated records, respectively
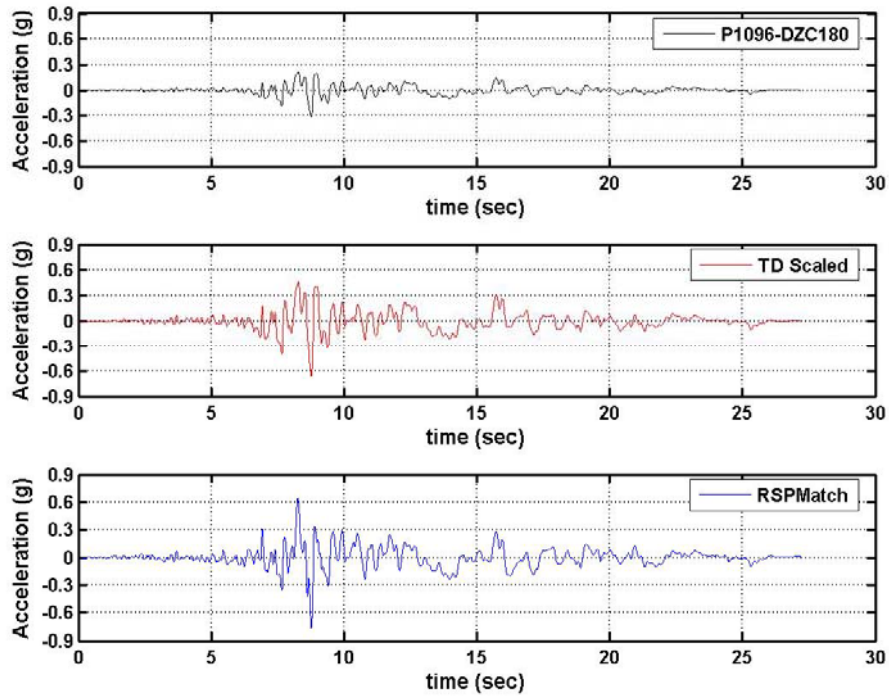
Figure A.16. Acceleration time histories of the first horizontal component of the real (P1096-DZC180), time domain scaled and RSPMATCH generated records, respectively
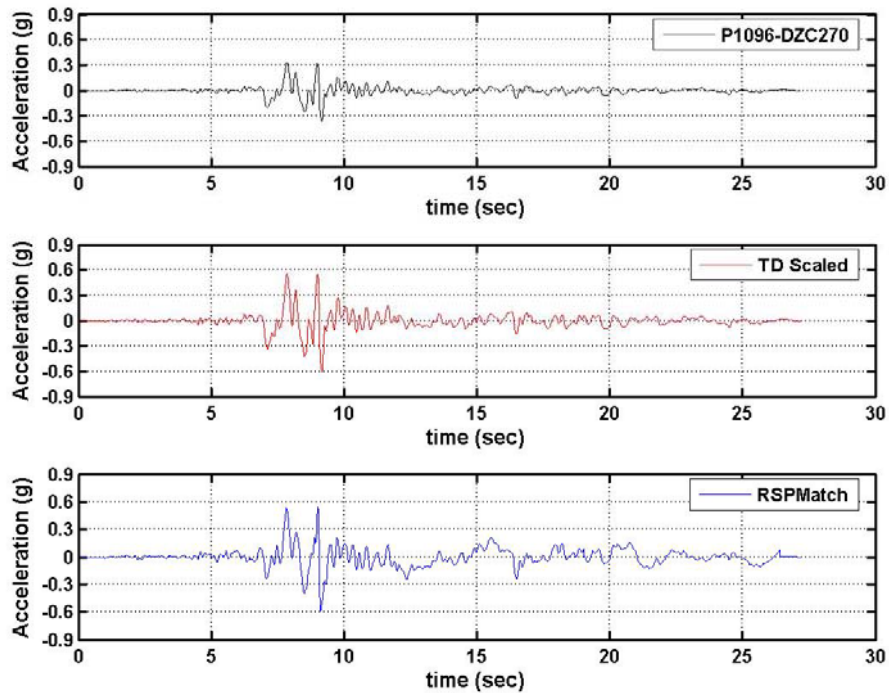


Figure A.17. Acceleration time histories of the first horizontal component of the real (P1096-DZC270), time domain scaled and RSPMATCH generated records, respectively
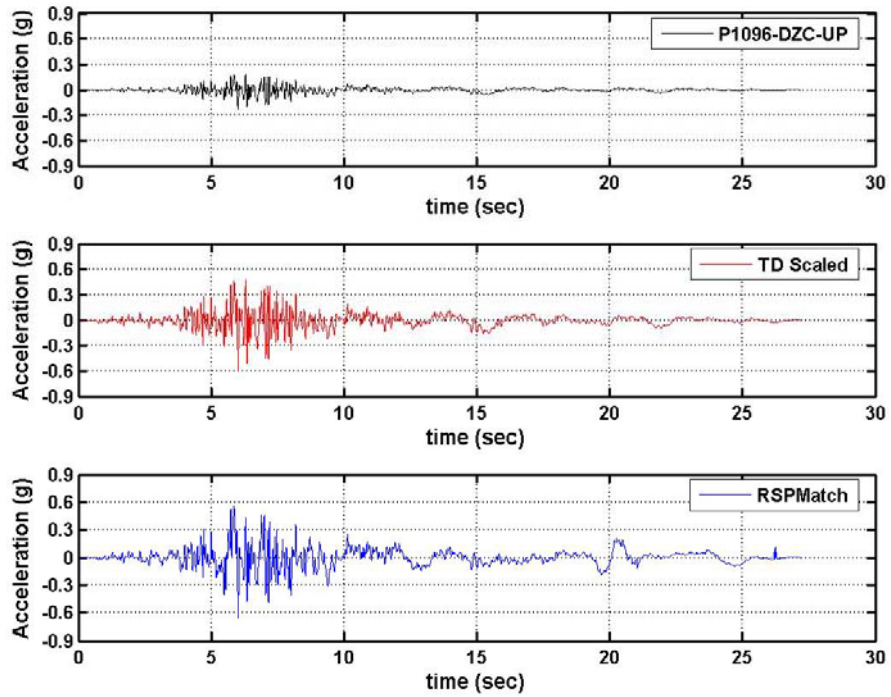
Figure A.18. Acceleration time histories of the first horizontal component of the real (P1096-DZC-UP), time domain scaled and RSPMATCH generated records, respectively

Table A.1. Selected earthquake records and scaling factors ($\alpha_{AT}$) for local site class Z1

| Local Site Class: Z1 | | | | | | | | | | | | | | | | |
|---|---|---|---|---|---|---|---|---|---|---|---|---|---|---|---|---|
| Record No | Earthquake | Date | Station | Record 1 | Record 2 | Record 3 | Closest to Fault Rupture | Record Duration | Significant Duration | Bracketed Duration | Fault Type | Scaling Factor 1 ($\alpha_{AT}$) | Scaling Factor 2 ($\alpha_{AT}$) | Scaling Factor 3 ($\alpha_{AT}$) | Sum Relative Error 1 | Sum Relative Error 2 | Sum Relative Error 3 |
| P1547 | Düzce, Turkey | 12.11.1999 | Bolu | BOL000 | BOL090 | BOL-UP | 17.6 | 55.9 | 12.5 | 14.2 | SS | 0.82 | 0.82 | 2.07 | 194.14 | 238.59 | 117.44 |
| P1087 | Kocaeli, Turkey | 17.08.1999 | Arcelik | ARC000 | ARC090 | ARCDWN | 17 | 30.0 | 11.0 | 9.7 | SS | 3.82 | 3.53 | 4.70 | 117.64 | 193.81 | 101.18 |
| P1558 | Düzce, Turkey | 12.11.1999 | Mudurnu | MDR000 | MDR090 | MDR-UP | 33.6 | 28.8 | 15.5 | 8.9 | SS | 4.49 | 6.84 | 5.85 | 126.39 | 169.82 | 120.88 |

Table A.2. Selected earthquake records and scaling factors ($\alpha_{AT}$) for local site class Z3

| Local Site Class: Z3 | | | | | | | | | | | | | | | | |
|---|---|---|---|---|---|---|---|---|---|---|---|---|---|---|---|---|
| Record No | Earthquake | Date | Station | Record 1 | Record 2 | Record 3 | Closest to Fault Rupture | Record Duration | Significant Duration | Bracketed Duration | Fault Type | Scaling Factor 1 ($\alpha_{AT}$) | Scaling Factor 2 ($\alpha_{AT}$) | Scaling Factor 3 ($\alpha_{AT}$) | Sum Relative Error 1 | Sum Relative Error 2 | Sum Relative Error 3 |
| P1114 | Kocaeli, Turkey | 17.08.1999 | Yarimca | YPT060 | YPT330 | YPT-UP | 2.6 | 35 | 15.34 | 17.00 | SS | 1.95 | 1.98 | 1.94 | 334.19 | 329.17 | 341.13 |
| P1104 | Kocaeli, Turkey | 17.08.1999 | Iznik | IZN090 | IZN180 | IZN-UP | 31.8 | 30 | 16.91 | 14.21 | SS | 3.65 | 5.35 | 6.81 | 458.95 | 532.66 | 510.26 |
| P1096 | Kocaeli, Turkey | 17.08.1999 | Duzce | DZC180 | DZC270 | DZC-UP | 12.7 | 27.2 | 11.79 | 14.74 | SS | 2.14 | 1.68 | 2.57 | 204.75 | 537.44 | 443.65 |

# REFERENCES

Abrahamson, N. A., 1992, "Non-stationary Spectral Matching", *Seismological Research Letters*, Vol. 63, Issue 1, 30.

Abrahamson, N. A., 1993, *Non-Stationary Spectral Matching Program RSPMATCH*, User Manual.

Ahari, M. N., S. Eshghi and M. G. Ashtiany, 2009, "The Tapered Beam Model for Bottom Plate Uplift Analysis of Unanchored Cylindrical Steel Storage Tanks", *Engineering Structures*, Vol. 31, pp. 623-632.

American Society of Civil Engineers (ASCE), 2005, *Minimum Design Loads for Buildings and Other Structures*, ASCE 7, ASCE Standard, SEI/ASCE 7-02, Reston, VA.

American Water Works Association (AWWA), 2005, *Welded Steel Tanks for Water Storage*, AWWA D-100, Denver, CO.

API 650, 2005, *Welded Steel Tanks for Oil Storage*, American Petroleum Institute Standard, Washington D. C., Addendum 4, December.

Aquelet, N., M. Souli, J. Gabrys and L. Olovsson, 2003, "A New ALE Formulation for Sloshing Analysis", *Structural Engineering and Mechanics*, Vol. 16, Issue 4, pp. 423-440.

Aquelet, N., M. Souli, and L. Olovson, 2005, "Euler Lagrange Coupling with Damping Effects: Application to Slamming Problems", *Computer Methods in Applied Mechanics and Engineering*, Vol. 195, pp 110-132.

Arias, A., 1970, "A Measure of Earthquake Intensity", *Seismic Design of Nuclear Power Plants, MIT Press*, Cambridge Massachusetts, pp. 438-489.

ASCE, 1987, "The Effects of Earthquakes on Power and Industrial Facilities and Implications for Nuclear Power Plant Design" *Working Group on Past Behavior of the Committee on Dynamic Analysis of the Committee on Nuclear Structures and Materials of the Structural Division of ASCE*, Robert C. Murray, chairman, New York, pp. 232.

Aydınoğlu, M. N. and Y. M. Fahjan, 2003, "A Unified Formulation of the Piecewise Exact Method for Inelastic Seismic Demand Analysis including the P-Delta Effect", *Earthquake Engineering and Structural Dynamics*, Vol. 32, Issue 6, pp. 871-890.

Barton, D. C., and J. V. Parker, 1987, "Finite Element Analysis of the Seismic Response of Anchored and Unanchored Liquid Storage Tanks", *Earthquake Engineering and Structural Dynamics*, Vol. 15, pp. 299–322.

Belytschko, T, W. K. Liu, and B. Moran, 2000, *Nonlinear Finite Elements for Continua and Structures*, Wiley, New York, p. 300.

Benson, D., 1992, "Computational Methods in Lagrangian and Eulerian Hydrocodes", *Computer Methods in Applied Mechanics and Engineering*, Vol. 99, pp. 235-394.

Benson, D., 1997, "A Mixture Theory for Contact in Multi-Material Eulerian Formulations", *Computer Methods in Applied Mechanics and Engineering*, Vol. 140, pp. 59-86.

Bommer, J. J., S. G. Scott and S. K. Sarma, 2000, "Hazard-Consistent Earthquake Scenarios", *Soil Dynamics and Earthquake Engineering*, Vol. 19, pp. 219-231.

Cambra, F. J., 1982, *Earthquake Response Considerations of Broad Liquid Storage Tanks*, Earthquake Engineering Research Center Report, UCB/EERC 82-25, November.

Chen, B. F. and H. W. Chiang, 1999, "Complete 2D and Fully Nonlinear Analysis of Ideal Fluid in Tanks", *Journal of Engineering Mechanics*, ASCE, Vol. 125, No. 1, pp. 70-78, January.

Chen, B. F., 2005, "Viscous Fluid in Tank under Coupled Surge, Heave, and Pitch Motions", *Journal of Waterway, Port, Coastal, and Ocean Engineering*, ASCE, Vol. 131, No. 5, pp. 239-256, September.

Chen, Y. H., W. S. Hwang, and C. H. Ko, 2007, "Sloshing Behaviors of Rectangular and Cylindrical Liquid Tanks Subjected to Harmonic and Seismic Excitations", *Earthquake Engineering and Structural Dynamics*, Vol. 36, pp.1701–1717.

Cimellaro, G. P., I. P. Christovasilis , and P. K. Malhotra, 2007, "Roof Pressures Due To Sloshing Loads in Rectangular Tanks with Insufficient Freeboard", *Rethymno, ECCOMAS Thematic Conference on Computational Methods in Structural Dynamics and Earthquake Engineering*, COMPDYN 2007, Paper No.1170, Crete, Greece, 13–16 June.

Clough, D. P., 1977, *Experimental Evaluation of Seismic Design Methods for Broad Cylindrical Tanks*, Earthquake Engineering Research Center Report, UCB/EERC 77-10, May.

Clough, R. W., and A. Niwa, 1979, *Static Tilt Tests of a Tall Cylindrical Liquid Storage Tank*, Earthquake Engineering Research Center, Reports UCB/EERC 79-06, February.

Colella, P. and P. Woodward, 1994, "The Piecewise Parabolic Method (PPM) for Gas Dynamical Simulations", *Journal of Computational Physics*, Vol. 54, pp. 174-201.

Cooper, T. W. and T. P. Wachholz, 1999, "Performance of Petroleum Storage Tanks during Earthquakes 1933-1995", *Proceedings of the 5th US Conference on Lifeline Earthquake Engineering*, ASCE, Seattle, Washington.

Costley, A.C., S. A. Mourad, R. P. Kazanji, and G. C. Pardoen, 1991, "Determination of critical Buckling Load of Thin- Walled Cylinders Using Modal Analysis", *Proceedings of the 9th International Modal Analysis Conference*, Florence, Italy, April.

Czygan, O., and O. Von Estorff, 2002, "Fluid-Structure Interaction by Coupling BEM and Nonlinear FEM", *Engineering Analysis with Boundary Elements*, Vol. 26, pp. 773–779.

Donea, J., 1983, "Arbitrary Lagrangian-Eulerian Finite Element Methods", *Computational Methods for Transient Analysis*, Editors T. Belytschko and T.J.R. Hughes, Elsevier Sciences Publishers, B.V., pp. 473–513.

Earthquake Engineering Research Institute (EERI), 1995, *The Hyogoken-nambu Earth quake Preliminary Reconnaissance Report*.

Edwards, N. W., 1969, *A Procedure for Dynamic Analysis of Thin Wailed cylindrical Liquid Storage Tanks subjected to Lateral Ground Motions*, Ph.D. Thesis, University of Michigan, Ann Arbor.

EERI (Earthquake Engineering Research Institute), 1986, *Reducing Earthquake Hazards: Lessons Learned From Earthquakes*, National Science Foundation (U.S.) El Cerrito, California, No. 86-02, November.

El-Zeiny, A., 1995, *Nonlinear Time-Dependent Seismic Response of Unanchored Liquid Storage Tanks*, PhD. Dissertation, Department of Civil and Environmental Engineering, University of California, Irvine.

El-Zeiny, A., 2002, "Study of Factors Affecting the Seismic Response of Unanchored Tanks", *15th ASCE Engineering Mechanics Conference*, Columbia University, New York, NY.

Eurocode 8, 2006, *Design of Structures for Earthquake Resistance, Part 4-Silos, Tanks and Pipelines*, European Committee for Standardization, Brussels, BS EN 1998-4: 2006.

Faltinsen, O. M., 1978, "A Numerical Nonlinear Method of Sloshing in Tanks with Two-Dimensional Flow", *Journal of Ship Research*, Vol. 22, pp. 193–202.

Fischer, F. D. and F. G. Rammerstorfer, 1999, "A Refined Analysis of Sloshing Effects in Seismically Excited Tanks", *International Journal of Pressure Vessels and Piping*, Vol. 76, pp. 693–709.

Fischer, F. D., and R. Seeber, 1988, "Dynamic Response of Vertically Excited Liquid Storage Tanks Considering Liquid-Soil-Interaction", *Earthquake Engineering and Structural Dynamics*, Vol. 16, pp. 329-342.

Flanagan, D. P. and T. Belytschko, 1981, "A Uniform Strain Hexahedron and Quadrilateral and Orthogonal Hourglass Control", *International Journal of Numerical Methods in Engineering*, Vol. 17, pp. 679-706.

Ghosh, S. and N. Kikuchi, 1991, "An arbitrary Lagrangian-Eulerian Finite Element Method for Large Deformation Analysis of Elastic-Viscoplastic Solid", *Computational Methods in Applied Mechanics and Engineering*, Vol. 86, pp. 127-188.

Graham, E. W. and A. M. Rodriguez, 1952, "The Characteristics of Fuel Motion Which Affect Airplane Dynamics", *Journal of Applied Mechanics*, pp 381–388, September.

Grilli, S. T., J. Skourup, and I. A. Svendsen, 1988, "The Modeling of Highly Nonlinear Water- Waves - A Step Toward a Numerical Wave Tank", *Proceedings of the Tenth International Conference on Boundary Element Methods*, Southampton, England, pp. 549-566.

Hamdan, F. H., 2000, "Seismic Behavior of Cylindrical Steel Liquid Storage Tanks", *Journal of Constructional Steel Research*, Vol. 53, pp. 307–333.

Hanson, R. D., 1973, "Behavior of Liquid Storage Tanks, the Great Alaska Earthquake of 1964", *Proceedings of the National Academy of Sciences*, Washington,. DC, 7, 331-339.

Haroun, M. A. and A. A. El-Zeiny, 1995, "Simulation of Dynamic Behavior of Unanchored Tanks", *Simulation of Transactions of the Thirteenth Conference on Structural Mechanics in Reactor Technology*, August 13-18, Brazil, Volume III, pp. 341-346.

Haroun, M. A. and G. W. Housner, 1981a, "Seismic Design of Liquid Storage Tanks", *Journal of the Technical Councils of ASCE*, Vol. 107, No. TC1, April.

Haroun, M. A. and G. W. Housner, 1981b, "Earthquake Response of Deformable Liquid Storage Tanks", *Journal of Applied Mechanics*, ASME, Vol. 48, pp. 411-418., June.

Haroun, M. A. and G. W. Housner, 1982b, "Complications in Free Vibration Analysis of Tanks", *Journal of Engineering Mechnics*, ASCE, Vol. 108, pp. 801-818, October.

Haroun, M. A. and H. A. Bhatia, 1995, "Analysis of Tank Damage during the 1994 Northridge Earthquake", *Proceedings of the Fourth US Conference on Lifeline Earthquake Engineering*, San Francisco, August, pp. 763-770.

Haroun, M. A. and H. M. Ellaithy, 1985, "Model for Flexible Tanks Undergoing Rocking", *Journal of Engineering Mechanics*, ASCE, Vol. 111, No. 2, pp. 143-157, February.

Haroun, M. A. and M. A. Tayel, 1985a, "Axisymmetrical Vibrations of Tanks-Numerical", *Journal of Engineering Mechanics*, ASCE, Vol. 111, No. 3, pp. 329-345, March.

Haroun, M. A. and M. A. Tayel, 1985b, "Axisymmetrical Vibrations of Tanks-Analytical", *Journal of Engineering Mechanics*, ASCE, Vol. 111, No. 3, pp. 346-358, March.

Haroun, M. A. and M. A. Tayel, 1985c, "Response of Tanks to Vertical Seismic Excitations", *Earthquake Engineering and Structural Dynamics*, Vol. 13, pp. 583-595.

Haroun, M. A. and W. Abou-Izzeddine, 1992a, "Parametric Study of Seismic Soil-Tank Interaction. I: Horizontal Excitation", *Journal of Structural Engineering*, ASCE, Vol. 118, No. 3, pp. 783-797, March.

Haroun, M. A. and W. Abou-Izzeddine, 1992b, "Parametric Study of Seismic Soil-Tank Interaction. II: Vertical Excitation", *Journal of Structural Engineering*, ASCE, Vol. 118, No. 3, pp. 798-812, March.

Haroun, M. A., 1980, *Dynamic Analyses of Liquid Storage Tanks*, Earthquake Engineering Research Laboratory Report, EERL 80-04, California Institute of Technology, February.

Haroun, M. A., 1983, "Vibration Studies and Tests of Liquid Storage Tanks", *Earthquake Engineering and Structural Dynamics*, Vol. 11, pp. 179-206.

Haroun, M. A., and A. Zeiny, 1995a, "Nonlinear Transient Response of Unanchored Liquid Storage Tanks", *Proceedings of the PVP Conference*, ASME, Hawaii, pp. 35-41, July.

Haroun, M. A., and A. Zeiny, 1995b, "Simulation of Dynamic Behavior of Unanchored Tanks", *Proceedings of the 13th International Conference on Structural Mechanics in Reactor Technology*, Porto Alegre, Brazil, pp. 341-346, August.

Haroun, M. A., H. A. Bhatia, and A. Zeiny, 1997, "Characterization of Observed Uplift and Buckling of an Unanchored Tank during the Northridge Earthquake", *The Northridge Earthquake Research Conference*, Los Angeles, CA, August.

Haroun, M. A., S. A. Mourad, and W. Abou-Izzeddine, 1991, "Performance of Liquid Storage Tanks during the 1989 Loma Prieta Earthquake", *Proceedings of The Third U.S. Conference in Lifeline Earthquake Engineering*, Los Angeles, August 22-23, pp. 1152-1161.

Haroun, M. A. and G. W. Housner, 1982a, "Dynamic Characteristics of Liquid Storage Tanks", *Journal of Engineering Mechnics*, ASCE, Vol. 108, pp. 783-800, October.

Haroun, M. A., 1983, "Behavior of Unanchored Oil Storage Tanks: Imperial Valley Earthquake", *Journal of Technical Topics in Civil Engineering*, Vol. 109, April, pp. 23-40.

Harten, A., 1989, "ENO Schemes with Subcell Resolution", *Journal of Computational Physics*, Vol. 83, pp. 148-184.

Harten, A., B. Engquist and S. Osher, 1997, "Uniformly High Order Accurate Essentially Non-Oscillatory Schemes", *Journal of Computational Physics*, Vol. 131, No. 1, pp. 3-47.

Hirt, C. W. and B. D. Nichols, 1981, "Volume of Fluid (VOF) Method for the Dynamics of Free Boundaries", *Journal of Computational Physics*, Vol. 39, pp. 201-225.

Housner, G. W., 1963, "The Dynamic Behavior of Water Tanks", *Bulletin of the Seismological Society of America*, Vol. 53, No. 2, pp. 381-387, February.

Housner, G. W., 1954, "Earthquake Pressures on Fluid Containers", *The Eighth Technical Report under Office of Naval Research*, California Institute of Technology, Pasadena, California, August.

Housner, G. W., 1957, "Dynamic Pressures on Accelerated Fluid Containers", *Bulletin of the Seismological Society of America*, Vol. 47, No. 1, pp. 15-35, January.

Huang, Y.Y., S. K. Wang, and W. M. Cheng, 1988, "Fluid-Structure Coupling Boundary Element Method for Analyzing Free-Vibration of Axisymmetric Thick-Walled Tanks", *Proceedings of the 10th International Conference on Boundary Element Methods*, Southampton, England, pp. 521-534.

Hughes, T. J. R., W. K. Liu and T. K. Zimmerman, 1981, "Lagrangian Eulerian Finite Element Formulation for Viscous Flows", *Journal of Computer Methods in Applied Mechanics and Engineering*, Vol. 29, pp. 329-349.

Hwang, I. T., and K. Ting, 1987, "Dynamic Analysis of Liquid Storage Tanks Including Hydrodynamic Interaction Boundary Element Method", *Proceedings of the Ninth International Conference on Structural Mechanics in Reactor Technology* (SMIRT-9), Lausanne, Switzerland, August, pp. 429-434.

Hwang, I. T., and K. Ting, 1989, "Boundary Element Method for Fluid-Structure Interaction Problems in Liquid Storage Tanks", *Journal of Pressure Vessels Technology*, Vol. III, No. 4, November, pp. 435-440.

Jacobsen, L.S., 1949, "Impulsive Hydrodynamics of Fluid inside a Cylindrical Tank and of Fluid Surrounding a Cylindrical Pier", *Bulletin of the Seismological Society of America*, Vol. 39, No. 3, pp. 189-204, July.

Jaiswal, O. R., D. C. Rai and S. K. Jain, 2007, "Review of Seismic Codes on Liquid-Containing Tanks", *Earthquake Spectra*, Vol. 23, No. 1, pp. 239–260.

Johnson, G. S., 2002, *Refinery Damage and Emergency Response in the 1999 Izmit, Turkey Earthquake*, The California State Lands Commission, http://www.slc.ca.gov/Division_pages/MFD/Prevention_First/Documents/2002/Paper%20by%20Gayle%20Johnson.pdf.

Kana, D. D., 1979, "Seismic Response of Flexible Cylindrical Liquid Storage Tanks", *Nuclear Engineering and Design*, Vol. 52, pp. 185-199.

Kaul, M. K., 1978, "Spectrum Consistent Time History Generation", *ASCE Journal of Engeering Mechanics*, EM4, pp. 781-788.

Kock, E. and L. Olson, 1991, "Fluid-Structure Interaction Analysis by the Finite Element Method-A Variational Approach", *International Journal for Numerical Methods in Engineering*, Vol. 31, pp. 463-491.

Koh, H. M., J. K. Kim, and , J. H. Park, 1998, "Fluid-Structure Interaction Analysis of 3-D Rectangular Tanks by a Variationally Coupled BEM-FEM and Comparison with Test Results", *Earthquake Engineering and Structural Dynamics*, Vol. 27, pp.109-124.

Koller, M. G. and P. K. Malhotra, 2004, "Seismic Evaluation of Unanchored Cylindrical Tanks", *Thirteenth World Conference on Earthquake Engineering*, Vancouver, B.C., Canada, August 1-6.

Kondo, H., S. Yamamoto, and Y. Sasaki, 1990, "Fluid-Structure Interaction Analysis Program for Axisymmetric Structures", *JSME International Journal, Series III - Vibration Control Engineering for Industry*, Vol. 33, No. 3, September, pp. 315-322.

Krinitzsky, E. L. and F. K. Chang , 1977, *Specifying Peak Motions for Design Earthquakes, State-of the-Art for Assessing Earthquake Hazards in the United States*, Report No. 7, Miscellaneous Paper S-73-1, US Army Corps of Engineers.

Kumar, A., 1981, *Studies of Dynamic and Static Response of Cylindrical Liquid Storage Tanks*, Ph.D. Thesis, Rice University, Houston, Texas.

Lau, D. T., and X. Zeng, 1992, "Simplified Uplift Analysis of Unanchored Cylindrical Tanks", *Proceedings of the Conference on Lifeline Earthquake Engineering*, Vol. 33, pp. 975-985.

Lau, D. T., and Zeng, X., 1991, "Hydrodynamic Forces in Uplifting Cylindrical Tanks", *Proceedings of the Fluid-Structure Vibration and Sloshing*, ASME, PVP, Vol. 237, California, pp. 39-44.

Lay, K. S., 1993, "Seismic Coupled Modeling of Axisymmetric Tanks Containing Liquid", *Journal of Engineering Mechanics*, Vol. 119, No. 9, September, pp. 1747-1761.

Le Tallec, P. J. and Mourob, 2001, "Fluid Structure Interaction with Large Structural Displacements", *Computer Methods in Applied Mechanics and Engineering*, Vol. 190, Issue 24-25, pp. 3039-3067.

Leon, O. S., and E. A. Kausel, 1986, "Seismic Analysis of Fluid Storage Tanks", *Journal of Structural Engineering*, ASCE, Vol. 112, No. 1, January.

Lilhanand, K. and W. S. Tseng, 1987, "Generation of Synthetic Time Histories Compatible with Multiple Damping Response Spectra", SMIRT-9, Lausanne, K2-10.

Liu D. and P. Lin, 2008, "A Numerical Study of Three-Dimensional Liquid Sloshing in Tanks", *Journal of Computational Physics*, Vol. 227, pp. 3921-3939.

Lubkowski, Z. A., J. W. Pappin, and M. R. Willford, 2000, "The Influence of Dynamic Soil-Structure Interaction on the Seismic Design and Performance of an Ethylene Tank", *12th World Conference on Earthquake Engineering*.

Lysmer, J., F. Ostadan, M. Tabatabaie, F. Tajirian, S. Vahdani, 1999, *A System for Analysis of Soil-Structure Interaction (SASSI2000)* – User's and Theoretical Manual, Department of Civil and Environmental Engineering, University of California, Berkeley.

Malhotra, P. K. and A. S. Veletsos, 1994a, "Beam Model for Base-Uplifting Analysis of Cylindrical Tanks", *Journal of Structural Engineering*, ASCE, Vol. 120, No. 12, pp. 3471-3488, December.

Malhotra, P. K. and A. S. Veletsos, 1994b, "Uplifting Analysis of Base Plates in Cylindrical Tanks", *Journal of Structural Engineering*, ASCE, Vol. 120, No. 12, pp. 3489-3505, December.

Malhotra, P. K. and A. S. Veletsos, 1994c, "Uplifting Response of Unanchored Liquid-Storage Tanks", *Journal of Structural Engineering*, ASCE, Vol. 120, No. 12, pp. 3525- 3547, December.

Malhotra, P. K., 1995, "Base Uplifting Analysis of Flexibly Supported Liquid-Storage Tanks", *Earthquake Engineering and Structural Dynamics*, Vol. 24, Issue 12, pp. 1591-1607.

Malhotra, P. K., T. Wenk, and M. Weiland, 2000, "Simple Procedure of Seismic Analysis of Liquid Storage Tanks", *Structural Engineering International*, Vol. 10, Issue 3, pp. 197–201.

Malhotra, P. K., 2001, *Industrial Facilities*, EERI Special Reconnaissance Report.

Malhotra, P. K., 2005, "Sloshing Loads in Liquid-Storage Tanks with Insufficient Freeboard", Technical Note, *Earthquake Spectra*, Volume 21, No. 4, pp. 1185–1192, November.

Manos, G. C. and R. W. Clough, 1985, "Tank Damage during the May 1983 Coalinga Earthquake", *Earthquake Engineering and Structural Dynamics*, Vol. 13, No. 4, pp. 449-466.

Manos, G. C., 1986, "Earthquake Tank Wall Stability of Unanchored Tanks", *Journal of Structural Engineering*, ASCE, Vol. 112, No. 8, pp. 1863-1880.

Manos, G.C., and R.W. Clough, 1982, *Further Study of the Earthquake Response of a Broad Cylindrical Liquid Storage Tank*, Earthquake Engineering Research Center, Report UCB/EERC 82-07, July.

Marchaj, T. J., 1979, "Importance of Vertical Acceleration in the Design of Liquid Containing Tanks", *Proceedings of the Second U.S. National Conference on Earthquake Engineering*, Stanford, California, August, pp. 146-155.

Mathon, C. and A. Limam, 2006, "Experimental Collapse of Thin Cylindrical Shells Submitted to Internal Pressure and Pure Bending", *Thin-Walled Structures*, Vol. 44, Issue 1, pp. 39-50, January.

Mitra, S., P. P. Upadhyay, and K. P. Sinhamahapatra, 2008, "Slosh Dynamics of Inviscid Fluids in Two-Dimensional Tanks of Various Geometry Using Finite Element Method", *International Journal for Numerical Methods in Fluids*, Vol. 56, pp.1625–1651.

Mourad, S.A., 1991, *Modal Analysis and Buckling Effects on Steel Structures Under Dynamic Loading*, PhD. Dissertation, Civil Engineering Department., University of California, Irvine, 1991.

Naeim, F. and J. M. Kelly, 1999, *Design of Seismic Isolated Structures: From Theory to Practice*, John Wiley & Sons.

Nakayama, T., and H. Tanaka, 1990, "A Numerical Method for the Analysis of Nonlinear Sloshing in Circular Cylindrical Containers", In Morino L. and R. Piva, editors *Boundary Integral Methods, Theory and Applications*, Proceedings of the lst ABEM Symposium, Rome, Italy.

NASA SP-8007, 1968, *Buckling of Thin-walled Circular Cylinders*, 47 p.

National Board of Fire Underwriters, 1933, *Committee on Fire Prevention and Engineering Standards, Report on the Southern California Earthquake of March 10, 1933*, New York.

Niwa, A., and R.W. Clough, 1982, "Buckling of cylindrical Liquid Storage Tanks Under Earthquake Loading", *Journal of Earthquake Engineering and Structural Dynamics*, Vol. 10, pp. 107-122, January.

NZSEE (New Zealand National Society for Earthquake Engineering), 1986, *Seismic Design of Storage Tanks, Recommendations of a Study Group of the New Zealand*

*National Society for Earthquake Engineering*, Editors: M. J. N. Priestley, B. J. Davidson, G. D. Honey, D. C. Hopkins, R. J. Martin, G. Ramsey, J. V. Vessey and J. H. Wood, Wellington, New Zealand.

O'Rouke, M. J. and P. So, 2000, "Seismic Fragility Curves for On-grade Steel Tanks, *Earthquake Spectra*, Vol. 16, Issue 4, pp. 801-815.

Pacific Earthquake Engineering Research (PEER) Center, 2006, *PEER Strong Motion Database*, http://peer.berkeley.edu/smcat/.

Rammerstorfer, F. G., K. Scharf and F. D. Fisher, 1990, "Storage Tanks under Earthquake Loading", *ASME Applied Mechanics Review*, Vol. 43 (11), pp. 261–82.

Rammerstorfer, F. G., H. J., Holl, F. D. Fischer, and R. Seeber, 1987, "Influence of the Vertical Motion Component on the Plastic Collapse of Earthquake Excited Tanks", *Proceedings of the 9th International Conference on Structural Mechanics in Reactor Technology (SMIRT-9)*, Lausanne, Switzerland, August, pp. 793-798.

Razzaghi, M. S. and S. Eshghi, 2004, "Behavior of Steel Oil Tanks due to Near-Fault Ground Motion", *13th World Conference on Earthquake Engineering*, Vancouver, B.C., Canada, August 1-6.

Reiter, L., 1990, *Earthquake Hazard Analysis: Issues and Insights*, Columbia University Press.

Richter, C. F., 1958, *Elementary Seismology*, Freeman and Co., pp. 488.

Rinne, J. E., 1967, *The Prince William Sound, Alaska, Earthquake of 1964 and Aftershocks*, U.S. Department of Commerce, Volume II, Part: A, Oil Storage Tanks, Environmental Sciences Services Administration, Washington: Government Printing OffIce, pp. 245-252.

Rinne, J. E., 1967, *The Prince William Sound. Alaska, Earthquake of 1964 and After Shocks*, Vol. II, Part A, U.S. Coast and Geodetic Survey, pp. 245-252.

Rotter, J. M., 1985, "Buckling of Ground-Supported Cylindrical Steel Bins under Vertical Compressive Wall Loads", *Proceedings of Metal Structures Conference*, Institution of Engineers of Australia, Melbourne, pp. 112-127.

Sakai, F., A. Isoe, H. Hirakawa, and Y. Montani, 1987, "Experimental Study on Uplift Behavior of Large-sized Cylindrical Liquid Storage Tanks", *Pressure Vessels and Piping Conference*, ASME, PVP, San Diego, pp. 349-355, June.

Scharf, K., 1990, *Beiträge zur Erfassung des Verhaltens von Erdbebenerregten, Oberirdischen Tankbauwerken*, Fortschritt-Berichte VDI, Reihe 4, Bauingenieurwesen, Nr. 97, VDI, Verlag, Düsseldorf.

Seismic Zoning Map of Turkey, 2006, Ministry of Public Works and Settlement, Earthquake Research Department, http://www.deprem.gov.tr.

Sezen, H. and A. S. Whittaker, 2004, "Performance of Industrial Facilities during the 1999 Kocaeli, Turkey Earthquake", *13th World Conference on Earthquake Engineering, Conference Proceedings*, Vancouver, British Columbia, Canada, August 1-6, Paper No. 282.

Shaaban, S. H., and W. A. Nash, 1975, *Finite Element Analysis of a Seismically Excited cylindrical Storage Tank, Ground Supported and Partially Filled with Liquid*, Report, University of Massachusetts, Amherst, August.

Shu, C. W. and S. Osher, 1988, "Efficient Implementation of Essentially Non-Oscillatory Shock-Capturing Schemes", *Journal of Computational Physics*, Vol. 77, No. 2, pp. 439-471.

Somerville, P. G., 1998, "Emerging Art: Earthquake Ground Motion. Geotechnical Earthquake Engineerng and Soil Dynamics III", *ASCE Geotechnical Special Publication*, No. 75, Vol. 1, pp.1-38.

Souli, M. and J. P. Zolesio, 2001, "Arbitrary Lagrangian-Eulerian and Free Surface Methods in Fluids Mechanics", *Computational Methods in Applied Mechanics and Engineering*, Vol. 191, pp. 451–466.

Souli, M., A. Ouahsine, and L. Lewin, 2000, "ALE Formulation for Fluid-Structure Interaction Problems", *Computer Methods in Applied Mechanics and Engineering*, Vol. 190, pp.659-675.

Steinbrugge, K. V. and D. F. Moran, 1954, "An Engineering Study of the Southern California Earthquake of July 21, 1952, and its aftershocks", *Bulletin of Seismological Society of America*, Vol. 44. No. 2B, pp. 201-462.

Stewart, J. P., S. J. ChiouBray, R. W. Graves, P. G. Somerville and N. A. Abrahamson, 2001, *Ground Motion Evaluation Procedures for Performance-Based Design*, PEER Report 2001/09, Pacific Earthquake Engineering Research Center, University of California, Berkeley.

Suzuki, K., 2002, "Report on Damage to Industrial Facilities in the 1999 Kocaeli Earthquake, Turkey", *Journal of Earthquake Engineering*, Vol. 6, No. 2, pp. 275-296.

Tanaka, M., T. Sakurai, K. Ishida, H. Tazuke, H. Akiyama, N. Kobayashi and T. Chiba, 2000, "Proving Test of Analysis Method on Nonlinear Response of Cylindrical Storage Tank Under Severe Earthquakes", *Proceedings of 12th World Conference on Earthquake Engineering (12 WCEE)*, Auckland, New Zealand.

Timoshenko, S. P. and J. M. Gere, 1961, *Theory of Elastic Stability*, McGraw-Hill, New York.

Tosaka, N., R. Sugino, and H. Kawabata, 1989, "Boundary Element-Lagrangian Solution Method for Nonlinear Free Surface Problems", In B. S. Annigeri and K. Tseng, editors, *Proceedings of the Intl. Symposium on BEM: Advances in Solid and Fluid Mechanics*, East Hartford, Connecticut.

Turkish Seismic Design Code (TSDC), 2007, *Specification for Buildings to be Built in Seismic Zones (TSC)*, Ministry of Public Works and Settlement Government of Republic of Turkey, Earthquake Research Department, http://www.deprem.gov.tr, 2007 (in Turkish).

Van Leer, B., 1977, "Towards the Ultimate Conservative Difference Scheme. IV. A New Approach to Numerical Convection", *Journal of Computational Physics*, Vol. 23, pp. 276-299.

Vanmarcke, E. H., 1979, *State-of-the-Art for Assessing Earthquake Hazards in the United States: Representation of Earthquake Ground Motions – Scaled Accelerograms and Equivalent Response Spectra*, Miscellaneous Paper S-73-1, Report 14, US Army Corps of Engineers Waterways Experiment Station, Vicksburg, Mississippi.

Veletsos, A. S. and J. Y. Yang, 1977, "Earthquake Response of Liquid Storage Tanks", *Advances in Civil Engineering through Engineering Mechanics*, *Proceedings of the Engineering Mechanics Division Specialty Conferences*, ASCE, Raleigh, North Carolina, pp. 1-24, May.

Veletsos, A. S., 1974, "Seismic Effects in Flexible Liquid Storage Tanks", *Proceedings of the Fifth World Conference on Earthquake Engineering*, Rome, Italy, Vol. 1, pp. 630-639.

Veletsos, A. S., 1984, *Seismic Response and Design of Liquid Storage Tanks, in Guidelines for the Seismic Design of Oil and Gas Pipeline Systems*, ASCE, pp. 255-370 and pp. 443-460.

Veletsos, A. S., and A. Kumar, 1984, "Dynamic Response of Vertically Excited Liquid Storage Tanks", *Proceedings of the Eighth World Conference on Earthquake Engineering*, California, Vol. VII, July, pp. 453-459.

Veletsos, A. S., and Y. Tang, 1986, "Dynamic of Vertically Excited Liquid Storage Tanks", *Journal of Structural Engineering*, ASCE, Vol. 112, No. 6, pp. 1229-1246.

Veletsos, A. S., and Y. Tang, 1987, "Rocking Response of Liquid Storage Tanks", *Journal of Engineering Mechanics*, Vol. 113, No. 11, November, pp. 1774-1792.

Virella, J. C., L. A. Godoy and L. E. Suarez, 2003, "Influence of the Roof on the Natural Periods of Empty Steel Tanks", *Engineering Structures*, Vol. 25, pp. 877–887.

Westergaard, H. M., 1933, "Water Pressures on Dams during Earthquakes", *Transactions American Society of Civil Engineers*, Vol. 98, 1835, pp. 418-472, November.

Whittaker, D., and D. Saunders, 2008, "Revised NZSEE Recommendations for Seismic Design of Storage Tanks", *NZSEE Conference*, Paper Number 04.

Woodward, P. R., and P. Collela, 1982, *The Numerical Simulation of Two-Dimensional Fluid Flow with Strong Shocks*, Lawrence Livermore National Laboratory, UCRL-86952.

Wozniak, R.S., and W. W. Mitchell, 1978, "Basis of Seismic Design Provisions for Welded Steel Oil Storage Tanks", *Proceedings of the Session on Advances in Storage Tank Design*, API, Toronto, Canada, May.

Xu, J., C. Costantino, and C. Hofmayer, 2007, "Overview on BNL Assessment of Seismic Analysis Methods for Deeply Embedded NPP Structures", *19th International Conference on Structural Mechanics In Reactor Technology (SMiRT 19)*, August 12-17, Toronto, Canada.

Xu, J., C. Costantino, C. Hofmayer, and H. Graves, 2006, "Finite Element Models for Computing Seismic Induced Soil Pressures on Deeply Embedded Nuclear Power Plant Structures", *ASME Pressure Vessels and Piping Division Conference*, July 23–27, Vancouver, BC, Canada.

Young, D. L., 1982, "Time-dependent Multi-Material Flow with Large Fluid Distortion", *Numerical Methods for Fluids Dynamics*, Editors K. W. Morton and M. J. Baines, Academic Press, New-York.